The American Mineralogist

Journal of the Mineralogical Society of America

VOL. 43 SEPTEMBER–OCTOBER 1958 Nos. 9 and 10

UNIVERSITY OF
1958

Contents

Synthesis and properties of carnotite and its alkali analogues . . . . Paul B. Barton, Jr. 799
Calcium analogue of chondrodite . . . . E. R. Buckle and H. F. W. Taylor 818
Beryllium content of roscherite from the Sapucaia pegmatite mine, Minas Gerais, Brazil . . . . Marie L. Lindberg 824
Effects of geologic significance of potassium "fixation" by expandable clay minerals derived from muscovite, biotite, chlorite and volcanic material . . . . Charles E. Weaver 839
Calcium-bearing magnesium-iron olivines . . . . Th. G. Sahama and Kai Hytönen 862
Alkali feldspars: IV. The cooling history of high-temperature sodium-rich feldspars . . . . J. V. Smith and W. S. MacKenzie 872
Significance of amphibole paragenesis in the Bidwell Bar region, California . . . . Robert R. Compton 890
Some observations on the crystallization of amorphous silica . . . . R. M. Carr and W. S. Fyfe 908
Characterization of serpentine minerals . . . . E. J. W. Whittaker and J. Zussman 917
Structural and chemical variation in chromium chlorite . . . . Davis M. Lapham 921
Study of the directional hardness in silicon . . . . A. A. Giardini 957
The structure of leached gillespite, a sheet silicate . . . . A. Pabst 970
Notes and News: Holmquistite as a rhombic amphibole . . . . Thorolf Vogt, Otto Bastiansen and Per Skancke 981
  Crandallite (pseudowavellite) from Gardner Mine Ridge, Lawrence County, Indiana . . . . S. S. Greenberg and W. T. Elberty 983
  Relation of ionic radius to structures of rare-earth phosphates, arsenates and vanadates . . . . M. K. Carron, M. E. Mrose and K. J. Murata 985

(*Continued on Cover 2*)

EDITOR: LEWIS S. RAMSDELL

BOARD OF ASSOCIATE EDITORS:

CHARLES L. CHRIST
ROBERT GARRELS
D. JEROME FISHER
E. WM. HEINRICH (1957–58)
JOSEPH MURDOCH (1957–59)
GEORGE T. FAUST (1958–60)

Published bi-monthly by the Society

(Contents continued)

Goethite-hematite relation . . . . Mihir Kumar Bose 989
Yttrium-bearing pegmatite body near Lake George, Park County, Colorado . . . . J. J. Glass, H. J. Rose, Jr., and E. Over 991
Earthy monazite at Magnet Cove, Arkansas . . . . H. J. Rose, Jr., L. V. Blade and Malcolm Ross 995
Low magnification thin-section photography . . . . Frank W. Atchley 997
Stage for macro point counting . . . . Donald O. Emerson 1000
Book Reviews 1004
New Mineral Names 1006

Mineralogical Society of America

ASSOCIATED WITH THE GEOLOGICAL SOCIETY OF AMERICA

President: George E. Goodspeed, University of Washington, Seattle 5, Washington.
Vice-President: Ralph E. Grim, University of Illinois, Urbana, Illinois.
Secretary: C. S. Hurlbut, Jr., Harvard University, Cambridge 38, Massachusetts.
Treasurer: Earl Ingerson, U. S. Geological Survey, Washington 25, D. C.
Editor: Lewis S. Ramsdell, University of Michigan, Ann Arbor, Michigan.
Councilors: Leonard G. Berry, Queen's University, Kingston, Ontario, Canada.
Chester B. Slawson, University of Michigan, Ann Arbor, Michigan.
Alfred O. Woodford, Pomona College, Claremont, California.
Samuel S. Goldich, University of Minnesota, Minneapolis 14, Minnesota.
Brian H. Mason, American Museum of Natural History, New York 24, New York.
Richard H. Jahns, California Institute of Technology, Pasadena, California.
Charles Milton, U. S. Geological Survey, Washington 25, D. C.
D. Jerome Fisher, University of Chicago, Chicago 37, Illinois.

The enlarged issues of this journal for 1958 are made possible by a grant from the Penrose Fund of the Geological Society of America.

The American Mineralogist—Journal of the Mineralogical Society of America

The journal, containing articles on mineralogy, crystallography, and allied sciences, is issued every two months. Contributions are invited.

The general conduct of the journal is in the hands of the editor, Lewis S. Ramsdell, Department of Mineralogy, University of Michigan, to whom all manuscripts should be submitted. To assist the editor, the Council of the Society has appointed the following Board of Associate Editors:

Charles L. Christ, U. S. Geological Survey, Washington 25, D. C.
E. Wm. Heinrich, Department of Mineralogy, University of Michigan, Ann Arbor, Michigan.
Robert M. Garrels, Harvard University, Cambridge 38, Massachusetts.
Joseph Murdoch, University of California at Los Angeles, Los Angeles, California.
D. Jerome Fisher, University of Chicago, Chicago 37, Illinois..
George T. Faust, U. S. Geological Survey, Washington 25, D. C.

Authors are requested to submit two copies of each manuscript, typewritten on standard size paper, 8½×11 inches. Photographs submitted for cuts should be glossy prints.

Beginning with Vol. 43, 1958, authors are entitled to 50 free reprints, without covers, of each article published.

Sent to all members and fellows of the Mineralogical Society of America. Membership dues $4.00 annually, fellowship dues $5.00 annually, which includes receipt of the American Mineralogist and GeoTimes, which is published by the American Geological Institute. Subscriptions for libraries, colleges, institutions, companies and similar organizations $6.00 annually.

Entered as second class matter at the post office at Menasha, Wis., under Act of March 3, 1879. Acceptance for mailing at the special rate of postage provided for in section 1103, Act of Oct. 3, 1917, paragraph 4 section 429 P. L. & R. authorized March 13, 1922.

Notice of change of address, orders, and remittances should be sent to Mineralogical Society of America, Dr. Earl Ingerson, Treasurer, U. S. Geological Survey, Washington 25, D.C.

Printed by the George Banta Company, Inc., Menasha, Wisconsin
Printed in the United States of America

Leitz®

first in precision optics

NEW POLARIZING MICROSCOPE SM-pol

21158

Leitz sets a new standard with this student polarizing and chemical microscope of modern design, with dual, low-position focusing controls and large field of view. A reasonably priced polarizing microscope, the model SM-pol, has rugged, one-piece construction with Bertrand lens and pinhole diaphragm built into the tube. Inclined monocular tube will accommodate wide-field eyepieces and the microscope can be used faced away from the observer, permitting easy accessibility to the stage.

A reputation for integrity and a tradition of service have led thousands of scientific workers to bring their optical problems to Leitz. If you have problems in this field, why not let us help you with them?

See your Leitz dealer and examine these Leitz instruments soon. Write for information.

E. LEITZ, INC., Dept. AM-10
468 Fourth Avenue, New York 16, N. Y.

Please send me the Leitz__________brochure.

NAME__________

STREET__________

CITY__________ZONE______STATE______

E. LEITZ, INC., 468 FOURTH AVENUE, NEW YORK 16, N. Y.
Distributors of the world-famous products of
Ernst Leitz G. m. b. H., Wetzlar, Germany—Ernst Leitz Canada Ltd.
LEICA CAMERAS · LENSES · MICROSCOPES · BINOCULARS

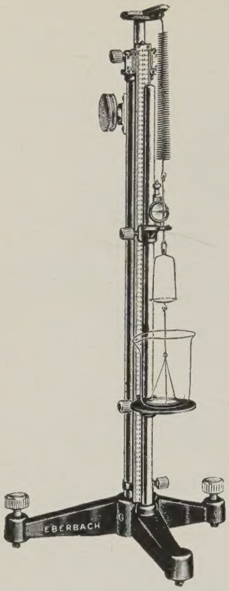

KRAUS JOLLY BALANCE

For Speedier Specific Gravities

This professional model is mentioned in *Mineralogy* by Kraus, Hunt and Ramsdell, in *Dana's Manual of Mineralogy* by Hurlbut and *Elements of Mineralogy* by Winchell.

The Kraus Jolly balance simplifies the determination of specific gravity; only two readings and a division are necessary; older forms of the balance require more extensive computation. The balance is especially well adapted for the rapid and accurate determination of specific gravity of solids, such as minerals, rocks, coal, precious stones, etc.

Send for our bulletin.

Eberbach CORPORATION
SCIENTIFIC INSTRUMENTS & APPARATUS
ANN ARBOR, MICH.
ESTABLISHED 1843

MINERAL SPECIMENS

Large variety of crystals, crystal groups, rare minerals, and ore minerals for collectors, universities and museums.

1958 Mineral Catalog 25¢, or sent free when requested on official letterhead.

Filer's are interested in buying or exchanging for good quality minerals, especially from foreign countries. Correspondence is invited.

FILER'S
P. O. Box 372, Redlands, California

Our Specialty is

SELECTED MINERAL SPECIMENS
FROM WORLD-WIDE LOCALITIES FOR COLLECTORS AND MUSEUMS

we also carry a complete line of
MINERALIGHTS, DETECTRON GEIGER COUNTERS, ESTWING PROSPECTOR PICKS, MINERALOGICAL BOOKS, ETC.

Send for free current bulletin

SCHORTMANN'S MINERALS
6 McKinley Avenue **Easthampton, Massachusetts**

For Mineralogists:

Index of Refraction Liquids

Range: 1.35 to 2.11 index; available in sets of limited range, or in sets with various intervals, or in any selection. Note that liquids 2.01 to 2.11 are now available.

See detailed price list of index liquids in our three-page advertisement in the July-August and September-October issues of the American Mineralogist. Or, write for Price List Nd-AM

Allen Reference Sets for Microscopical Studies in Mineralogy and Petrology

Six sets of Authentic materials for use as standards for refractive index, for standard materials mounted in balsam to be compared with unknowns, and for demonstration of typical optical characteristics under microscopical study.

Write for descriptive material A-AM

Text: Practical Refractometry by Means of the Microscope

By ROY M. ALLEN, D.SC.

Describes the technique of the immersion method of microscopy, with particular reference to the identification of minerals. Written primarily for elementary instruction, but this text will be very useful also to advanced workers. Price $1.00. Copy will be sent on approval.

Heavy Liquids

Formulated especially for determination of specific gravity of minerals, but special formulations are being made to order for various procedures. If you have any special problem in this field of separation of minerals or other materials by differences in specific gravity, please write us about your problem. Or, just write for leaflet HL-AM.

Lovins Field Finder

For re-locating any point of interest on microscope slide. Same size as a 3″ x 1″ microscope slide; has 1012 1mm. squares, each square numbered and lettered, with sides graduated into tenths. A beautiful example of micro-photography.

Write for Leaflet LFF-AM

Gems, Testing For Identity and For Defects

The CARGILLE-ALLEN GEM TESTING SET is the title of our new book describing the properties of gems and also the equipment for certain identification of gems by a new simple procedure. Price $1.00; this amount applicable to purchase price of any of the items listed in the book.

R. P. Cargille Laboratories, Inc.
117 Liberty St., New York 6, N.Y.

SCOTT J. WILLIAMS
Mineralogist
offers
NEW MINERAL CATALOG 25¢

Specializing in Specimens for
Collections, Museums, Research and Teaching Purposes

Specimens for Sale or Exchange

2346 S. Scottsdale Road
Scottsdale, Arizona, U.S.A.

ULTRA VIOLET LAMPS FOR QUALITY FLUORESCENCE

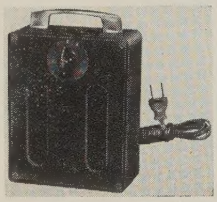

"Most powerful small lamps available"—Dr. H. C. Dake.
For the mineralogist, laboratory or school.
Compact—Rugged—Versatile
7 models available, priced from $14.50
(Model SL-1, combination sw-lw dual unit, illustrated, only $47.50) Write for brochure.

Radiant Ultra Violet Products-Manufacturers
Cambria Heights 11, L.I., New York

AMERICAN MINERALOGIST BACK VOLUMES

We urgently require for purchase the following volumes of the American Mineralogist to complete our files:

Volumes 1-5, 7, 9-11, and 25-32 incl.

Please send your list of complete volumes and single issues to:

Pergamon Institute
122 East 55th Street, New York 22, New York

d. m. organist
PETROGRAPHIC
LABORATORY
BOX 176 • NEWARK, DELAWARE

THIN SECTIONS OF
ROCKS, MINERALS, ORES, CERAMICS

PREPARED ROCK SECTIONS FOR STUDENT USE

GRAIN COUNTS • PETROGRAPHIC ANALYSIS

WILEY BOOKS

PRINCIPLES OF GEOCHEMISTRY

Second Edition

By BRIAN MASON, *The American Museum of Natural History.* A summary of the significant data concerning the chemistry of the earth, this book provides a coherent account of the physical and chemical evolution of our planet.

Some of the new material in this revision includes discussions on electronegativity as a geochemical factor, isotope fractionation in geological processes, minor and trace elements in metamorphic rocks, and energy changes in the geochemical cycle. Rewritten material covers the origin of the elements, isomorphism, atomic substitution, polymorphism, clay materials, composition and origin of petroleum, metamorphism and metamorphic rocks.

Data tables incorporate the most recent information available. The annotated bibliographies are valuable guides to the latest literature. *1958. 310 pages. $8.50.*

ELEMENTS OF GEOLOGY

By JAMES H. ZUMBERGE, *University of Michigan.* In this work historical and physical geology receive equal emphasis. It treats the earth's dimensions, composition, origin and the major forces active to keep the earth in a dynamic condition. Descriptions are given of how geologic forces alter the face of the earth, and how these processes may be studied to best advantage. Included is a journey through the geologic past, covering the several billion years of existence, and highlighting the prominent geologic changes. *1958. Approx. 368 pages. Prob. $5.50.*

Write today for examination copies.

JOHN WILEY & SONS, Inc.

440 Fourth Avenue **New York 16, N. Y.**

The New 282 Page Decennial Author-Subject

INDEX TO VOLUMES 31-40, 1946-1955, of

THE AMERICAN MINERALOGIST

by Earl Ingerson, U. S. Geological Survey

Over 21,000 entries provide comprehensive coverage of the 9564 text pages in the last 10 volumes of the Journal. The price is $3.00 to members and fellows; $5.00 to non-members and subscribers, postpaid. Orders, with remittance, should be sent to the Treasurer, Dr. Earl Ingerson, U. S. Geological Survey, Washington 25, D.C.

Previous indexes are still available at their original prices:

Index to volumes 21-30, $2.00 and $3.00
Index to volumes 1-20, $1.00 and $2.00

THE AMERICAN MINERALOGIST

JOURNAL OF THE MINERALOGICAL SOCIETY OF AMERICA

Vol. 43 SEPTEMBER-OCTOBER, 1958 Nos. 9 and 10

SYNTHESIS AND PROPERTIES OF CARNOTITE AND ITS ALKALI ANALOGUES*

PAUL B. BARTON, JR., *U. S. Geological Survey, Washington 25, D. C.*

ABSTRACT

Carnotite and its Na, Rb, Tl, Cs, and H_3O(?) analogues have been synthesized in several different ways in attempts to obtain crystals suitable for single crystal structural investigations. Aqueous methods failed to produce usable crystals, but a simple fusion technique using metavanadate fluxes proved highly satisfactory. Work in progress by D. E. Appleman has shown that carnotite is composed of $[(UO_2)_2V_2O_8]_n^{-2n}$ layers bound together by alkali ions with or without water. Studies of the rate of precipitation of carnotite from aqueous solution as a function of pH suggest that the reaction involves interaction between uranyl, alkali, and metavanadate ($V_4O_{12}^{-4}$) ions, though this is not the only possible interpretation of the data. The x-ray and optical properties of the synthetic compounds are presented. The similarity of the a and b dimensions in metatyuyamunite, sengierite, and the alkali analogues of carnotite shows that the same $[(UO_2)_2V_2O_8]_n^{-2n}$ layer is present in all of these compounds. The Na analogue of carnotite is less stable than the other carnotites, and it is not expected that the pure Na variety would occur in nature.

INTRODUCTION

This report records the results of experiments dealing with the synthesis of carnotite and its alkali analogues. The work was primarily concerned with the preparation of single crystals suitable for detailed structural analysis, though some insight into the chemistry of the precipitation of carnotite was obtained.

PREVIOUS WORK ON SYNTHESIS

Carnotite is named for M. Adolphe Carnot, French chemist and mining engineer. Carnot (1887) unknowingly synthesized the ammonium analogue of carnotite when he noted that uranyl salts quantitatively precipitate vanadate from aqueous solution as ammonium uranyl vanadate. The mineral was not described until 1899.

Canneri and Pestelli (1924) synthesized anhydrous carnotite, $K_2(UO_2)_2V_2O_8$, and anhydrous sodium carnotite, $Na_2(UO_2)_2V_2O_8$, by fusing a uranyl salt with an excess of the appropriate alkali metavanadate. Their chemical analyses show that the compound is equivalent to anhydrous carnotite. Canneri and Pestilli obtained well developed, diamond-shaped, platy crystals which they reported to be fluorescent. It was suggested that the crystals were orthorhombic, but no *x*-ray or morphological work was done. They proposed that the crystals were salts of a uranovanadic anion, $(UO_2VO_4)^{-1}$.

---

* Publication authorized by the Director, U. S. Geological Survey.

Hillebrand (1924) formed carnotite by exchanging the calcium in tyuyamunite, $Ca(UO_2)_2V_2O_8 \cdot nH_2O$, for potassium in a potassium-mercuric iodide solution.

Sundberg and Sillén (1949) followed the vanadate fusion procedure of Canneri and Pestelli, but because Sundberg and Sillén were unable to obtain sufficiently large crystals by this method they fused a mixture of potassium carbonate, vanadium pentoxide and ammonium uranate (diuranate?) in an excess of potassium carbonate. After slow cooling the resulting crystals were washed free of the flux with water and dilute nitric acid and were then used for the determination of the preliminary structure of KUO_2VO_4. Sundberg and Sillén also recorded the formation of at least one other potassium-uranium-vanadium phase, but they did not define it.

Murata, Cisney, Steiff, and Zworykin (1950) studied base exchange among the potassium, barium, calcium, strontium and sodium analogues of carnotite and tyuyamunite. They mixed solutions of alkali or alkaline earth pyrovanadates with solutions of uranyl nitrate; the pH was adjusted to 6 with varying amounts of the oxide or hydroxide of the alkali or alkaline earth used. Following the development of the precipitate the pH was lowered to 3 and the preparation was digested for two weeks on a steam bath. Platy crystals of the calcium preparation, that is, tyuyamunite, were visible under the optical microscope; the other preparations showed crystals only under the electron microscope.

Morachevskii and Belyaeva (1956) revived the idea of Canneri and Pestelli (1924) of a uranovanadic anion. By spectrophotometric methods in the 250–400 mu region Morachevskii and Belyaeva noted that dilute solutions (less than 5×10^{-5} *M* in uranovanadate) had a much higher optical density than either the uranyl or the vanadate solutions alone, and from this they concluded the existence of some complex ion. They cited no evidence that the uranovanadate solution was not colloidal. Insoluble salts formed by the reaction of the uranovanadic anion with the divalent cations Pb^{+2}, Ba^{+2}, and UO_2^{+2} contained 6 to 8 per cent H_2O (they also made a Mg^{+2} compound but gave no analysis). They assigned to these salts the structural formula $Me[UO_2(OH)_2VO_3]_2 \cdot nH_2O$. By analogy they give the same general formula to carnotite, tyuyamunite, and sengierite. Morachevskii and Belyaeva give no *x*-ray data, but it seems much more likely that they prepared the Pb^{+2}, Ba^{+2}, and UO_2^{+2} analogues of metatyuyamunite which would also contain about 6 to 8 per cent H_2O but whose general structural formula would be $Me[(UO_2)_2V_2O_8]\cdot 3H_2O$.

Recently R. F. Marvin, U. S. Geological Survey, (personal communication, 1956) has synthesized carnotite and rauvite (a poorly defined hydrous uranyl vanadate having V:U greater than 1:1) in aqueous solution; the rauvite formed in the pH range from approximately 1.5 to 2.0. The products were very fine grained.

Because carnotite is very easily prepared, it is probable that many other investigators have also created this compound; but to my knowledge, there is no procedure described to form carnotite crystals satisfactory for single-crystal *x*-ray work from aqueous solution.

Precipitation of Carnotite from Aqueous Solutions

Carnotite usually occurs in nature as a microcrystalline yellow powder impregnating sandstones or coating joints and fractures. Crystals of suitable size for single-crystal *x*-ray work (largest dimension greater than 0.1 mm.) are extremely rare. This is due, at least in part, to the very low solubility of carnotite, less than 1 ppm in pure water at pH 7 (R. F. Marvin, personal communication), which causes it to precipitate in a very fine grained or colloidal state. As shown below, the reactions involved in the precipitation of carnotite are very complicated, and this fact, also, may contribute to the very fine grain size in most natural carnotites.

At room temperature carnotite is precipitated from aqueous solutions as the stable phase when stoichiometric proportions of potassium, uranyl, and vanadate ions are mixed in the pH range from 2 to 9.5. Above pH 9.5 another phase of unknown composition precipitates at a more rapid rate than does carnotite, but the unknown compound apparently converts to carnotite on standing. In the pH range from 1.5 to 2 a brown phase, identified through its comparatively diffuse *x*-ray powder pattern as rauvite, precipitates from solutions greater than about 0.01 *M* in uranyl and vanadate ions. It is not known whether rauvite is metastable with respect to carnotite. Below pH 1.5 the uranium is not precipitated, but $V_2O_5\cdot nH_2O$ may form if the vanadate concentration exceeds 0.001 *M*. The pH ranges and concentrations given above are only approximate as the attainment of equilibrium is extremely slow at 25° C.

The uranyl ion, UO_2^{+2}, exists as the predominant uranium species in aqueous solution below pH 3.5 (Miller, 1955). Above this pH various hydrolysis products become predominant, eventually leading to the precipitation of uranyl hydroxides at about pH 4.5. In the presence of anions such as sulfate, acetate, and especially carbonate, the degree of hydrolysis is reduced through the formation of complex ions, and uranium-bearing solutions are stable at higher pH values (up to 11 or 12 with the carbonate). These complexes must be destroyed to precipitate carnotite, but even the very stable carbonate complexes seem to have little effect in retarding precipitation (though they undoubtedly increase the solubility of carnotite to some extent).

H. T. Evans, Jr., and R. M. Garrels (U. S. Geological Survey, personal communication, 1956) have summarized the available chemical and thermodynamic data on vanadium in aqueous solution. On acidification, an alkaline aqueous solution on pentavalent vanadium goes through a complex series of polymerization reactions which are shown in the lower two-thirds of Fig. 1. The lower part of the diagram illustrates approximately how the concentrations of the different vanadate species vary with pH, the central part shows the predominant ion at any given pH. The formulas assigned to the various vanadate species are believed by Evans and Garrels to give the best agreement with the diffusion, cryoscopic and titration studies recorded in the literature, but these data merely reflect the average degree of polymerization and other, undefined, ionic species may be present in significant amounts. Likewise, the coordination of the vanadium by oxygen, a factor which is reflected in the ratio of vanadium to oxygen in the various ions, may reasonably be assumed to be 4, or 5, or possibly even some intermediate values in the cases of ions having vanadium in both degrees of coordination. Because the ionization constants are not known, all of the anionic species with the exception of the polyvanadates are written without attached hydrogen ions. Thus Fig. 1 presents a gross simplification of the aqueous chemistry of pentavalent vanadium. The chemical formula for carnotite, $KUO_2VO_4 \cdot nH_2O$, suggests that it is an orthovanadate, but new *x*-ray diffraction studies clearly show that it is not.

D. E. Appleman (U. S. Geological Survey, personal communication, 1957) has done preliminary work on the structure of carnotite, using material synthesized in the course of the investigation described by this report, and has shown that the structure proposed by Sundberg and Sillén (1949) is in error so far as the coordination and position of the oxygen and vanadium atoms are concerned. The new work on the structure of carnotite has shown that the vanadium occurs in "divanadate" groups, $V_2O_8^{-6}$. The vanadium is in fivefold coordination with oxygen, so that the resulting polyhedra are distorted trigonal bipyramids; two such bipyramids share an edge to form the $V_2O_8^{-6}$ ion. This ion is similar in structure to two links from the five-coordinated $V_nO_{3n}^{-n}$ chains found in the compound potassium metavanadate monohydrate, $KVO_3 \cdot H_2O$

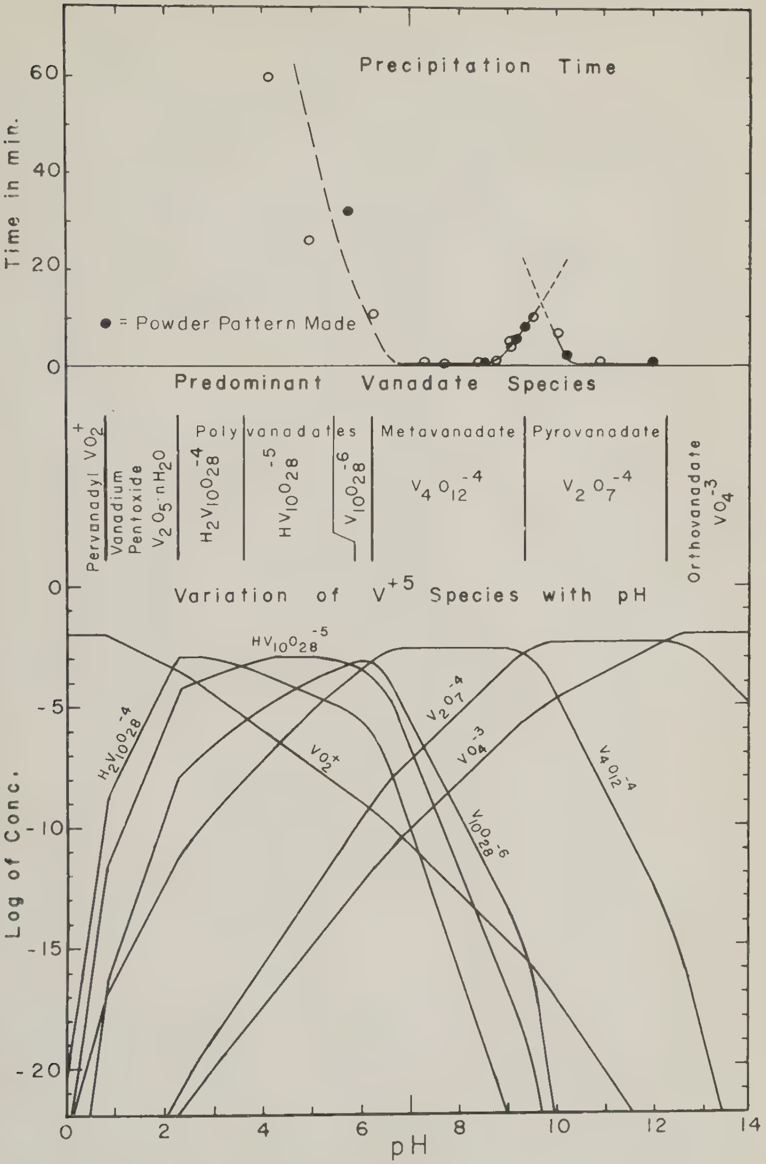

FIG. 1. Relation of rate of precipitation of carnotite to concentration of various pentavalent vanadium species.

(Christ, Clark, and Evans, 1954). The linear uranyl ion is coordinated in a fairly regular way by five oxygens from three $V_2O_8^{-6}$ groups, forming $[(UO_2)_2V_2O_8]_n^{-2n}$ sheets, with the axes of the uranyl ions nearly normal to the sheets. The alkali ions fit between the sheets as in the case of the micas. As will be discussed later, water molecules may also fit between the sheets, but they are not essential to the structure nor do they greatly affect the cell dimensions except for the interlayer spacing. The structural formula is $K_2(UO_2)_2V_2O_8 \cdot nH_2O$ with 2 formula units per unit cell.

The rate of precipitation of carnotite as a function of pH was determined, and the results are plotted in the upper part of Fig. 1. In the rate experiments 20 ml. aliquots of 0.01 *M* $NaVO_3$ were mixed with 20 ml. portions of a solution 0.009 *M* in $Na_4UO_2(CO_3)_3$ and 0.5 *M* in K_2SO_4. Before mixing, the pH of each portion was adjusted to the desired value with KOH or HNO_3. The solutions were well mixed and the pH recorded. The time for precipitation was defined as the time required to obtain the first noticeable cloudiness in the solution. Obviously, refinements could be made in the experimental techniques, but the present results are satisfactory for this study. The scatter of points in the acid range (Fig. 1) is due in part to difficulty in detecting the beginning of precipitation; however, disequilibrium is a more important factor. Because adjusting the acidity upsets the equilibrium between the various condensed vanadate species and because the depolymerization reactions are sluggish in the pH range 4 to 8, the measured pH values do not necessarily reflect the concentrations of the various vanadate species. Due to the presence of considerable amounts of Na^+, it is probable that the carnotite contained at least a small amount of sodium although the powder patterns of the precipitates have spacings very similar to those of the pure potassium carnotite.

The rapid increase in rate of precipitation up to pH 7 shows that precipitation involves reaction with a species of ion that increases in concentration with pH. The decrease in rate from pH 9 to 9.5 suggests that the reaction involves the ionic species predominant in the pH range 7 to 9, that is the metavanadates. The return to instantaneous precipitation at the highest pH values suggests that another compound may be forming instead of carnotite above pH 9.5. Powder patterns of the low pH precipitates (below 9.5) show diffuse but definite carnotite lines, whereas precipitates from the high pH region (above 9.5) show weaker carnotite lines plus a faint, fuzzy line at about 11 Å. One precipitate that formed at pH 7.4 also had the line at 11 Å, but this line was weak compared to the carnotite lines. The differences between the powder patterns are not pronounced, and the high pH phase cannot be characterized with certainty from the powder patterns; but the *x*-ray diffraction work does lend permissive support to the interpretation that a poorly crystallized uranyl vanadate of uncertain composition precipitates more rapidly than does carnotite at pH above 9.5 and that this phase converts to carnotite on standing. At lower pH carnotite precipitates directly from solution.

There are several possible reactions by which carnotite can be precipitated while fulfilling the restrictions placed upon the precipitation by the rate study. The upper part of Fig. 1 shows that the rate-determining reaction is controlled by a species that has its maximum abundance in the pH range 7.0 to 9.5. The work of Evans and Garrels shows that metavanadate, perhaps $V_4O_{12}^{-4}$, is predominant in the pH range 7.0 to 9.5; thus there is a strong possibility that the precipitation reaction is of the sort:

$$4K^+ + 4UO_2^{+2} + V_4O_{12}^{-4} + 6H_2O = 2K_2(UO_2)_2V_2O_8 \cdot H_2O + 8H^+.$$

However, this is not the only possible reaction. Simple calculations show that any ion of the type $(H_{2n}V_mO_{3m+n})^{-m}$, which includes $H_2VO_4^-$, $H_2V_2O_7^{-2}$, $H_4V_2O_8^{-2}$, and others, will have its maximum concentration in exactly the same region as the metavanadate plateau because the formula $(H_{2n}V_mO_{3m+n})^{-m}$ is merely the general formula for hydrated metavanadate ion, $(H_{2n}V_4O_{12+n})^{-4}$. There are no experimental data to indicate which of the possible ionic species determines the rate of reaction. Whatever the formula of the metavanadate, there will be other possible ions corresponding to the hydrated metavanadates discussed above so that we cannot be certain of the identity of the ionic species that reacts to precipitate carnotite. The rapidity of the precipitation in the metavanadate region suggests, but certainly does not prove, that the metavanadate ion contains at least some 5-coordinated vanadium atoms. The available data are too poor to permit evaluation of the order of the rate-determining reaction in terms of metavanadate concentration.

It may be noted that the metavanadate ($V_4O_{12}^{-4}$) plateau in the lower part of Fig. 1 is slightly broader than the region of rapid precipitation of carnotite shown at the top of this diagram. Although the metavanadate plateau is plotted as if it represents only one species, it probably represents several species such as $V_4O_{12}^{-4}$, $HV_4O_{12}^{-3}$, $H_2V_4O_{12}^{-2}$, and $H_3V_4O_{12}^{-1}$; and possibly several $V_3O_9^{-3}$, $V_2O_6^{-2}$, or other species. This situation is parallel to that in the polyvanadates, except that some of the ionization constants are known for the polyvanadates and therefore they may be plotted as separate ions. It seems likely that the rate-determining reaction for the formation of carnotite does not involve all of the possible metavanadate species; thus the composite metavanadate pH range is wider than the pH range of rapid precipitation.

If the reaction does involve metavanadate ion, there must be some sort of interaction at the crystal-solution interface by which metavanadate is depolymerized to divanadate, $V_2O_8^{-6}$, because the crystal structure contains $V_2O_8^{-6}$ ions. Under these circumstances the problem arises of how the initial carnotite nuclei originate. It is possible that the initial carnotite nuclei may form from a small amount of aqueous divanadate ion (if it exists in appreciable concentration in aqueous solution), or perhaps some other vanadate species may provide a transient seed phase on which the carnotite crystallizes. The line at 11 Å in the powder pattern of the precipitate obtained at pH 7.4 suggests that this transient phase may be the same one that precipitates at a high pH, but there are few data at present to justify such a conclusion.

CRYSTAL CHEMISTRY

The composition of carnotite reflects the unique crystal structure of the $[(UO_2)_2V_2O_8]_n^{-2n}$ layers. Because of its coordination in the dumbbell-shaped uranyl ion, UO_2^{+2}, the uranium is not likely to be replaced by any other ion. The asymmetric, fivefold coordination of the vanadium is not similar to that found in any other ion; therefore, elements such as phosphorous and arsenic, which sometimes form isomorphous series with tetrahedrally coordinated vanadate compounds (pyromorphite-mimetite-vanadinite), will not proxy for vanadium in the carnotite structure. The tendency for vanadium to occur in peculiar coordination may also explain the absence of naturally occurring vanadium analogues to torbernite, autunite, zeunerite, and abernathyite. Isomorphous substitution in the carnotite-type structure is very likely limited to the interlayer sites, that are occupied by potassium in carnotite and by calcium in tyuyamunite.

Natural carnotite contains from 1 to 3 moles of water per formula weight (Palache, Berman, and Frondel, 1951). The synthetic material on which the present structural work was done was originally entirely anhydrous (see description of synthesis below), yet this synthetic material, when kept anhydrous by immersion in mineral oil, gave an x-ray powder pattern practically identical to that of natural carnotite. Luedemann and Bates (1957) show that the curve for weight loss versus temperature for natural carnotite is smooth, with no sharp breaks, and their differential thermal analysis curve shows no pronounced endothermic or exothermic peaks. If carnotite is heated to 1100° to 1200° C. it will melt and recrystallize as carnotite (unless held at the high temperature for several days, in which case it decomposes through loss of oxygen to U_3O_8 and other as yet unidentified compounds). Therefore, none of the water in natural carnotite is essential to the structure. Under normal laboratory humidity the amount of water in carnotite is sufficiently low so that there is little variation in the cell dimensions, although Donnay and Donnay (1955) have shown that some natural material (Table 2) may show a considerable range in the *c* dimension, presumably due to variation in water content. Carnotite does not seem to hydrate in a stepwise fashion as do autunite and tyuyamunite. *X*-ray diffraction examination shows that the natural carnotite crystals are noticeably disordered, especially in the *c* direction, as would be expected if there is disorder in stacking of the layers or variation in water content.

SYNTHESIS

In this work several techniques were used in attempts to obtain well-crystallized carnotite. Aqueous systems from room temperature to 200° C. were tried without success, and therefore it was necessary to resort to fusion methods.

Aqueous methods

In aqueous systems at low temperatures it is difficult, if not impossible, to avoid the precipitation of carnotite from a solution containing appreciable amounts of potassium, hexavalent uranium, and pentavalent vanadium from pH 2 to pH 9.5. Beyond these pH limits other phases precipitate. (See discussion of precipitation from aqueous solution above.) The rapid precipitation from cold aqueous solution produces a carnotite which is very poorly crystallized, as is indicated by its diffuse *x*-ray powder pattern. Sharp powder patterns, but no crystals distinguishable at 500× magnification, are obtained by prolonged digestion of the precipitate on the steambath or by placing it for a few days in a closed tube with water at temperatures as high as 200° C. Variations in pH, concentration, and relative proportions of reagents seemed to make little improvement in the crystallization of the carnotite. A single experiment in which fine-grained carnotite was aged in an approximately neutral solution in an autoclave at 150° C. and about 35 atmospheres CO_2 pressure failed to improve the crystallinity of the carnotite measureably.

It was thought that perhaps the very slow mixing of uranyl and vanadate solutions might permit the growth of single crystals. Excellent crystals of many insoluble compounds can be grown by slow mixing of reactants by diffusion through silica jelly. When uranyl (or uranyl carbonate) and vanadate solutions containing potassium are introduced into the opposite sides of a U-tube partly filled with silica jelly a precipitate forms at the contact of the diffusing ions. The precipitates develop in 2 to 20 days and often show rhythmic Liesegang banding but, unfortunately, no visible crystals. When the solutions have a low pH (about

2) two distinctly different phases result. On the uranium side is a bright yellow precipitate of carnotite which gives a sharp x-ray pattern, while on the vanadium side there is a brown cryptocrystalline material identified as rauvite through its relatively diffuse pattern. At the higher pH (about 8) investigated by this method only carnotite appears. Because of the buffering action of the silica jelly (prepared by mixing 5 volumes of 2 per cent H_2SO_4 with 8 volumes of 1:6 sodium silicate) the exact hydrogen ion concentration at the point of precipitation is unknown. At the lower pH the predominant ions are UO_2^{+2}, $V_{10}O_{28}^{-6}$, K^+, Na^+, H^+, and SO_4^{-2}; at the higher pH they are $UO_2(CO_3)_3^{-4}$, $V_4O_{12}^{-4}$, K^+, Na^+, and SO_4^{-2}.

Most natural carnotite was apparently precipitated from solutions derived from sources containing tetravalent uranium and tri- and tetravalent vanadium compounds; this suggests another method of precipitation in which vanadate and uranyl solutions could be combined very slowly. Tetravalent vanadium and hexavalent uranium do not precipitate each other from solution. Tetravalent vanadium is amphoteric; the vanadyl ion, VO^{+2}, is stable in solutions up to about pH 3 where V_2O_4 hydrate precipitates; above a pH of about 8.2 the V_2O_4 redissolves as the vanadite ion, possibly $V_4O_9^{-4}$.

Two types of experiment were set up in an attempt to duplicate the natural method of crystal growth. In the first, sulfur dioxide was bubbled through a solution of potassium sulfate and sodium vanadate so that the vanadium was reduced to the tetravalent state. Hexavalent uranium in molecular excess of the vanadium was then added to the vanadite solution and the mixture was permitted to drip at the rate of about one drop per hour on a sloping piece of filter paper where the sulfur dioxide either escaped as a gas or was converted to sulfate by air oxidation. The vanadium slowly oxidized to the pentavalent state. The pH of the solution before loss of sulfur dioxide was about 3. A yellow film of carnotite developed in a few days but even after two months there were no crystals visible under 80 power magnification.

The second experiment involved diffusion of ions through U-tubes. A silica jelly containing sodium, potassium, and hexavalent uranium was prepared. Vanadyl sulfate was introduced into one limb of the tube and potassium peroxydisulfate (a strong oxidizing agent) was placed in the other. Small, well formed, yellow crystals in the shape of roughly equant plates developed after a few days, especially along the glass-jelly contact. These were at first thought to be carnotite which had had its tendency to form diamond-shaped plates suppressed by the interference of the jelly. But the appearance of penetration twinning and the fact that the crystals later redissolved proved that the crystals were not carnotite. X-ray data suggest that the crystals are a potassium uranyl sulfate. Later, the usual bands of cryptocrystalline rauvite and carnotite appeared.

There is another mechanism through which the well crystallized natural carnotites may have been formed, but this has not been tried in the laboratory because of the success of the fusion techniques which are described later. Tyuyamunite (or metatyuyamunite), being considerably more soluble than carnotite, occurs in nature as visible crystals much more frequently than does carnotite. It is also possible to synthesize suitable crystals of tyuyamunite (Murata et al., 1950). Such crystals could then be converted to carnotite by treatment with a solution containing a high concentration of K^+ relative to Ca^{++} (Hillebrand, 1924). A possible drawback to this method is that the base exchange process might well result in random stacking of the layers. As is discussed later, the natural carnotite crystals commonly exhibit stacking disorder.

Fusion methods

By following the procedure developed by Canneri and Pestelli (1924) carnotite crystals up to a centimeter across were obtained. The same technique also provided the Na, Rb, Tl, and Cs analogues of carnotite as crystals which were suitable for single crystal *x*-ray work. The crystals of the K and Cs compounds were also sufficiently well developed for goniometric work (D. E. Appleman, personal communication).

The procedure used to crystallize carnotite and its alkali analogues is very simple, although the size to which the individual crystals grow is, as yet, controlled more by luck than science. Ammonium metavanadate, NH_4VO_3, and an alkali hydroxide, chloride, carbonate or nitrate were fused together in a platinum crucible to give the alkali metavanadate. The reactions were quite rapid, especially with the hydroxides. Usually one or two per cent NH_4VO_3 in excess of the stoichiometric amount was used in order to prevent the possibility of excess hydroxide which might react with the crucible. Then a small amount of uranyl nitrate or acetate, or uranium trioxide hydrate was added to the alkali metavanadate and the mixture was fused. On cooling, beautiful, yellow, rhombic plates could be seen to grow rapidly at the surface of the melt just before the main mass of the metavanadate crystallized. The crystals were then separated by handpicking, or the flux was dissolved away with water or dilute nitric acid. If the acid used was too strong, V_2O_5 hydrate precipitated and was then redissolved in a solution of the appropriate alkali.

In an attempt to perform the synthesis in the manner of Sundberg and Sillén (1949), stoichiometric amounts of uranyl nitrate and potassium metavanadate were fused in a great excess of potassium carbonate.

This technique gave orange, tabular, pseudotetragonal (orthorhombic) crystals with three mutually perpendicular cleavages. The (001) cleavage is micaceous, the other two are good. The unit-cell dimensions, determined by Joan R. Clark, U. S. Geological Survey, are 4.33, 4.33, and 13.21 Å, or possibly some multiples thereof. The intensity distribution on *x*-ray patterns of the compound shows that the two short axes are not equivalent. The crystals break down rapidly in contact with atmospheric moisture, but they can be preserved under mineral oil or toluene. The optical character of the crystals changes with hydration from sensibly uniaxial to biaxial with 2V of 10° to 15°, and the crystals soon become disordered. The powder patterns of the hydrated material show some carnotite lines; the other lines present cannot be indexed on either the carnotite or the above-mentioned pseudotetragonal cell. A more detailed study of this very interesting phase has thus far been prevented by its instability. Similar sodium and rubidium compounds have been prepared using melts of the appropriate alkali carbonate, but no *x*-ray work has been done on these. Attempts to make the thallium member have been unsuccessful, presumably due to the difficulty of preventing the thermal decomposition of the thallous carbonate.

Besides the carbonate and vanadate fluxes some other types of flux were tried. As described above, uranyl salt was added to the vanadate fluxes; to the other fluxes (Table 1) a small amount of the appropriate alkali analogue of previously prepared synthetic carnotite was added. The mixtures were fused and allowed to cool slowly. In general, there were only two types of uranium-bearing crystals formed: carnotite, and the previously described orange, orthorhombic compound. Table 1 summarizes the results of the fluxing experiments.

In the course of the fusion synthesis experiments the preparation of the lithium analogue was tried. An insoluble compound with a greenish-yellow sheen, too fine grained to be resolved under the microscope, was retained after the leaching away with water of the lithium metavanadate flux. The compound gave a powder pattern that was practically identical to that of carnotite. This was tentatively explained as due to the base exchange of Li^+ by H_3O during the washing, so as to yield a hydronium carnotite practically identical to the natural carnotite in cell dimensions ($r_{K^+}=1.33$ Å; $r_{H_3O^+} \approx r_{O^{-2}} = 1.40$ Å). It is unlikely in terms of modern crystal chemical theory to find the small Li^+ ion ($r_{Li^+}=0.68$ Å) in the same structural position as K^+ or Cs^+. The $[(UO_2)_2V_2O_8]_n{}^{-2n}$ layers may exist in the Li compound, but the Li^+ would not occupy the same position as does the H_3O^+ which replaces it.

It was not possible to make the ammonium analogue of carnotite by the fusion technique because the ammonia was lost on heating. Fine-

TABLE 1.—SUMMARY OF FUSION EXPERIMENTS

Flux	Melting point ° C. of pure flux	Nature of uranium-bearing phase
KVO_3	650 (estimated)	yellow carnotite crystals
K_2CO_3	891	orange orthorhombic crystals
$K_2CO_3:KVO_3$ 2:1	600 (estimated)	orange orthorhombic crystals
K_2CO_3KF 5:1	750 (estimated)	orange orthorhombic crystals
K_2SO_4	1076	orange, poor crystals
KCl	776	orange pseudomorphs of original yellow carnotite crystals
KNO_3	334	yellow, no recrystallization
$UO_2(NO_3)_2\cdot 6H_2O$	60	yellow, no recrystallization
V_2O_5	690	no micaceous uranium-bearing phase (carnotite requires alkali)
$KHSO_4$	210	orange melt turns yellow on cooling; no crystals, too acid
$NaVO_3$	630	yellow Na carnotite crystals
Na_2CO_3	851	orange orthorhombic(?) crystals
$TlVO_3$	424	yellow Tl carnotite crystals
Tl_2SO_4	632	yellow Tl carnotite crystals
Tl_2CO_3	273	unsuccessful due to oxidation of Tl; requires further work
$RbVO_3$	500 (estimated)	yellow Rb carnotite crystals
Rb_2CO_3	837	orange orthorhombic(?) crystals
$CsVO_3$	500 (estimated)	yellow Cs carnotite crystals
$LiVO_3$	600 (estimated)	very fine grained insoluble greenish yellow material that gives carnotite-like pattern after washing with water

grained ammonium carnotite prepared by K. J. Murata by aqueous methods gave a powder pattern very similar to that of natural carnotite $(r_{NH_4^+}=1.43\ \text{Å})$.

The synthesis of the Na carnotite from the $NaVO_3$ melts could not be repeated at will as some as yet undetermined factor often prevented the formation of visible crystals. Murata and others (1950) record a peculiar formula, in which there is an excess of V_2O_5, for their Na "carnotite," and they suggest that further investigation on the nature of this compound be carried out. They report that the Na compound is also readily base exchanged in K^+ bearing solutions with the formation of K carnotite. In addition, the present study showed that Na carnotite dissolves in acid much more rapidly, and at a slightly higher pH than the other carnotites. These observations indicate that Na carnotite is relatively unstable compared to the carnotites which contain larger alkali cations. It seems unlikely that pure Na carnotite would occur in nature because

TABLE 2.—UNIT-CELL DATA FOR CARNOTITE AND RELATED COMPOUNDS

Material	a (in Å)	b (in Å)	c (in Å)	β	Specific gravity	
					Calculated	Observed
$Na_2(UO_2)_2V_2O_8$	10.39±0.03	8.39±0.03	6.14±0.10	100°10′±30′	5.16	
$K_2(UO_2)_2V_2O_8$	10.47±0.02	8.41±0.01	6.59±0.01	103°50′±05′	4.99	4.95±0.05
$Tl_2(UO_2)_2V_2O_8$	10.48±0.02	8.41±0.02	6.82±0.01	105°15′±10′	6.76	6.58±0.05
$Rb_2(UO_2)_2V_2O_8$	10.49±0.02	8.43±0.02	6.93±0.02	105°25′±10′	5.29	5.14±0.05
$Cs_2(UO_2)_2V_2O_8$	10.51±0.02	8.45±0.01	7.32±0.01	106°05′±05′	5.52	5.48±0.05
Carnotite[1]	10.48±0.03	8.37±0.02	6.75±0.05	104°20′± 1°		
Carnotite[2]	10.47±0.03	8.39±0.02	6.63±0.03	103°50′±15′		
Carnotite[3]	10.47	8.41	6.91	103°40′±10′	4.91	4.70±0.05
$K_2(UO_2)_2V_2O_8 \cdot nH_2O$[4]	10.46	8.40	6.59	103°40′±20′	5.00	4.80±0.05
$K_2(UO_2)_2V_2O_8$[5]	10.43	8.40	6.59	104°12′	5.03	
Sengierite[6]	10.62	8.10	10.11	103°36′±10′	3.99	4.41
Metatyuyamunite[7]	10.63	8.36	16.96	orthorhombic	4.04	3.92±0.05
Metatyuyamunite[8]	10.54	8.49	17.34	orthorhombic		3.61±0.05
$Ca(UO_2)_2V_2O_8 \cdot 3\text{-}5H_2O$[9]	10.38	8.46	17.02	orthorhombic		

[1] Carnotite from Cane Springs Pass, Utah.
[2] Carnotite from Congress Junction, Arizona.
[3] Carnotite from Cane Springs Pass, Utah, fully hydrated (Donnay and Donnay, 1955).
[4] Synthetic hydrated carnotite prepared by K. J. Murata (Donnay and Donnay, 1955).
[5] Synthetic anhydrous carnotite (Sundberg and Sillén, 1949).
[6] Sengierite from Haut-Katanga, Belgian Congo (Donnay and Donnay, 1955).
[7] Metatyuyamunite from May Day mine, Mesa County, Colorado (Donnay and Donnay, 1955).
[8] Metatyuyamunite from Small Spot mine, Mesa County, Colorado (Donnay and Donnay, 1955).
[9] Synthetic metatyuyamunite prepared by K. J. Murata (Donnay and Donnay, 1955).

sufficient amounts of K^+ are present in most natural solutions to base exchange the Na^+ by K^+. Apparently the decrease in stability of Na carnotite relative to K carnotite is related to the decrease in ionic size of Na^+ relative to K^+ ($r_{Na^+}=0.97$ A; $r_{K^+}=1.33$ A).

PROPERTIES OF CARNOTITE AND RELATED COMPOUNDS

Table 2 presents the unit-cell data for natural and synthetic carnotite, its alkali analogues, and some related natural compounds. The new data were obtained using filtered molybdenum radiation ($\lambda K\alpha=0.7107$ Å) with a precession camera; corrections were made for film shrinkage. The cell dimensions of the synthetic compounds show systematic variation with the ionic radius of the alkali cation. The similarity of the a and b dimensions of carnotite, sengierite, and metatyuyamunite (and tyuyamunite) suggests that all have essentially the same $[(UO_2)_2V_2O_8]_n^{-2n}$ layer structure with only the interlayer cations and the degree of hydration accounting for the differences. Tyuyamunite and metatyuyamunite contain $2[(UO_2)_2V_2O_8]_n^{-2n}$ layers per unit cell and are orthorhombic; whereas carnotite and sengierite have only one such layer and are monoclinic. Further evidence for the similarity of the layers in these minerals is furnished by the similarity in physical properties (Palache, Berman, and Frondel, 1951) and by the ability of these compounds to convert to one another through base exchange (Hillebrand, 1924; Murata et al., 1950; and Donnay and Donnay, 1955).

The indexed powder patterns for the synthetic carnotites are shown in Table 3. These data were calculated from measurements taken from powder patterns obtained using CuKα radiation ($\lambda = 1.5418$ Å). Corrections for film shrinkage have been made. Because of the platy nature of the carnotite, it was almost impossible to avoid alignment of crystals in the spindle, thus the relative intensities of the various reflections were influenced by this preferred orientation. Intensities were visually estimated. The reflections were indexed on the basis of the unit cells of the synthetic crystals. The NH_4 and H_3O(?) carnotites were indexed on the basis of the K carnotite cell. Lines with *d* values of less than 2.0 Å were not indexed.

Single crystals of the natural carnotite commonly exhibit very diffuse, streaky spots in the *h*0*l* and 0*kl* precession photographs, although the the *hk*0 patterns have fairly well defined spots. This indicates that the crystals are relatively disordered in the *c* direction, presumably due to disorder in the stacking of the layers or random variation in the water content so that the 00*l* spacings are nonuniform.

The carnotite crystals are brilliant canary yellow to greenish yellow. Although most vanadates do not fluoresce, the Cs carnotite and a K carnotite that had been held at 1000° C. for three hours fluoresced yellow-green under ultraviolet light.

Twinning by reticular pseudomerohedry, as described (and erroneously recorded as reticular merohedry) by Donnay and Donnay (1955), was noted in the precession patterns from the K, Cs, Rb, and Tl carnotites.

The micaceous (001) cleavage of carnotite is well developed in all of the synthetic and natural carnotites examined. A good cleavage parallel to (100) is seen in the larger crystals of the natural carnotite and in most of the synthetic crystals. Less frequently (010) and (110) cleavages appear. The diamond-shaped platy crystals are commonly bounded by {110} faces in addition to the (001) cleavage planes. The Cs carnotite also shows {010} and {100} faces. In the natural carnotite from Congress Junction, Arizona, the {110} faces are so well developed that the crystals are almost equant rather than tabular; however, there is much disorder in the *c** direction in these crystals.

The optical data for various synthetic carnotites are presented in Table 4. The crystals are biaxial (−), and the micaceous cleavage flakes give centered optic axis figures. The optic angles were measured on a universal stage using optic axis figures; the values are reproducible to within 0.5° or less. The optic angle of the thallium carnotite is too large

TABLE 3.—*X*-RAY POWDER DATA FOR CARNOTITE AND ITS ALKALI ANALOGUES (*d* in angstroms). Cu$K\alpha$; $\lambda = 1.5418$ Å

Na Carnotite

hkl	*d*(calc.)	*d*(obs.)	*I*
110	6.49	6.47	W
001	6.04	6.04	VS
200	5.11	5.12	M
$\bar{2}01$	4.30	4.29	VW
111	4.19	4.16	S
201	3.603	3.579	VW
021	3.447	3.437	M
220	3.243	3.222	W
310	3.159	3.140	M
002	3.022	3.015	M
$\bar{2}21$	3.001	3.000	M
$\bar{2}12$	2.681	2.680	W
311	2.628	2.612	M
410	2.445	2.437	M
$\bar{3}12$	2.387	2.387	VW
$\bar{4}02$	2.148	2.150	W
222	2.097	2.104	VW

NH_4 Carnotite

hkl	*d*(calc.)	*d*(obs.)	*I*
110 001	6.48 6.40	6.61	VS
111 020	4.24 4.20	4.19	M
201 021	3.585 3.514	3.534	M
211	3.297	3.314	W
220 002	3.240 3.199	3.220	W

K Carnotite

hkl	*d*(calc.)	*d*(obs.)	*I*
110	6.48	6.46	W
001	6.40	6.36	VS
200	5.08	5.06	W
111 020	4.24 4.20	4.22	M
201 021	3.585 3.514	3.530	S
220 002	3.240 3.199	3.207	S
310	3.143	3.140	M
311 $\bar{2}21$	3.107 3.086	3.100	M
112	2.709	2.705	W
311	2.602	2.600	VW
131 $\bar{3}12$ 400	2.549 2.542 2.542	2.544	M
202 230	2.456 2.455	2.453	VW
330 $\bar{2}03$	2.160 2.160	2.156	VW
003	2.133	2.140	W
312	2.028	2.031	VW

Tl Carnotite

hkl	*d*(calc.)	*d*(obs.)	*I*
001	6.58	6.56	M
200	5.06	5.05	M
210	4.33	4.33	M
111	4.27	4.29	M
020	4.21	4.23	W

VS very strong
S strong
M moderate
W weak
VW very weak

TABLE 3 (*continued*)

NH_4 Carnotite

hkl	*d*(calc.)	*d*(obs.)	*I*
310	3.140	3.132	M
$\bar{3}11$	3.107	3.115	M

H_3O(?) Carnotite

110	6.48	6.48	M
001	6.40	6.37	VS
200	5.08	5.05	VW
111 020	4.24 4.20	4.20	M
021	3.514	3.507	M
$\bar{1}21$	3.464	3.453	W
220 002	3.240 3.199	3.215	M
121	3.194	3.193	W
310	3.143	3.126	M
$\bar{3}11$ $\bar{2}21$	3.107 3.086	3.095	W
112	2.709	2.698	VW
311	2.602	2.589	W
$\bar{3}12$ 400	2.542 2.542	2.543	VW

Rb Carnotite

hkl	*d*(calc.)	*d*(obs.)	*I*
001	6.68	6.70	VS
110	6.45	6.46	W
200	5.06	5.08	M
$\bar{2}01$	4.67	4.68	W
111	4.30	4.30	M
020	4.21	4.21	M
211	4.09	4.10	M
120	3.891	3.883	W

Tl Carnotite

hkl	*d*(calc.)	*d*(obs.)	*I*
$\bar{2}11$	4.06	4.06	M
021	3.543	3.535	S
002	3.289	3.285	VS
$\bar{3}11$ 310 $\bar{2}21$	3.136 3.128 3.116	3.128	M
012	3.064	3.054	VW
$\bar{2}12$	2.961	2.956	VW
130	2.701	2.705	W
031	2.579	2.579	W
401	2.176	2.179	VW
330	2.155	2.154	W
222 032	2.133 2.133	2.130	VW
$\bar{2}32$	2.098	2.098	W
312	2.032	2.032	W

Cs Carnotite

hkl	*d*(calc.)	*d*(obs.)	*I*
001	7.03	7.02	S
110	6.48	6.50	VW
200	5.05	5.04	W
111 210	4.39 4.33	4.37	M
$\bar{2}11$	4.16	4.13	M
$\bar{1}21$	3.575	3.591	M
002	3.517	3.482	VS
$\bar{2}02$ 211 $\bar{1}12$	3.354 3.351 3.351	3.339	M
220	3.240	3.220	M

TABLE 3 (*continued*)

Rb Carnotite			
hkl	*d*(calc.)	*d*(obs.)	*I*
021	3.565	3.562	S
002	3.341	3.339	S
220	3.237	3.231	M
310	3.130	3.137	S
212	2.997	2.988	W
221	2.736	2.726	VW
130	2.707	2.702	M
$\bar{3}12$	2.631	2.625	M
$\bar{4}01$	2.605	2.603	M
222	2.552	2.543	VW
$\bar{4}11$	2.489	2.488	VW
230 131	2.457 2.449	2.452	M
322 321	2.314 2.292	2.230	M
013	2.153	2.154	M
040	2.107	2.108	W
140	2.064	2.067	W
132	2.034	2.036	W

Cs Carnotite			
hkl	*d*(calc.)	*d*(obs.)	*I*
$\bar{3}11$ $\bar{2}21$	3.176 3.165	3.170	M
$\bar{2}12$	3.118	3.102	M
112	2.884	2.867	W
$\bar{3}12$	2.708	2.706	M
031	2.614	2.614	M
230 212	2.460 2.460	2.458	M
003 $\bar{1}13$	2.344 2.342	2.331	M
$\bar{4}12$	2.298	2.294	VW
013	2.268	2.262	VW
222 401	2.196 2.191	2.193	VW
232	2.157	2.153	M
$\bar{4}22$ 132	2.078 2.075	2.077	M
023 041	2.052 2.023	2.037	M

TABLE 4.—OPTICAL DATA FOR SYNTHETIC COMPOUNDS RELATED TO CARNOTITE[1]

Material	α[2]	β	γ	2V (Na light)
$Na_2(UO_2)_2V_2O_8$		2.21 ±0.01	2.21 ±0.01	13° ±1°
$K_2(UO_2)_2V_2O_8$	1.77±0.04	2.010±0.005	2.090±0.005	53°30′±1°
$Tl_2(UO_2)_2V_2O_8$		>2.70	>2.70	>64°40′
$Rb_2(UO_2)_2V_2O_8$	1.86±0.04	2.125±0.005	2.205±0.005	51°30′±1°
$Cs_2(UO_2)_2V_2O_8$	<1.83	2.49 ±0.01	>2.70	45°30′±1°

---

[1] The indices of refraction were determined by C. S. Ross, U. S. Geological Survey, using sulfur-selenium mixtures.

[2] Calculated values.

to obtain a centered figure, but it was measured using a ruled eyepiece which was calibrated at lower angles. The optic plane is parallel to *b* and, so far as can be determined (within a degree), lies in the *bc** plane.

ACKNOWLEDGMENTS

I wish to thank many of my coworkers in the U. S. Geological Survey, especially D. E. Appleman, C. L. Christ, H. T. Evans, Jr., R. M. Garrels, R. F. Marvin, K. J. Murata, A. M. Pommer, and E. W. Roedder for discussion and suggestions throughout the study. Joan R. Clark measured the cell dimensions of the synthetic K carnotite and the orange orthorhombic phase. C. S. Ross measured the indices of refraction of the synthetic materials. Mary Mrose, Daphne Riska Ross, and Evelyn Cisney identified fine-grained materials by means of *x*-ray powder patterns.

This work was done by the U. S. Geological Survey on behalf of the Division of Raw Materials of the U. S. Atomic Energy Commission.

REFERENCES

CANNERI, G., AND PESTELLI, V., (1924), La sintesi della carnotite: *Gazz. chim. italiana*, **54,** 641–646.

CARNOT, M. ADOLPHE, (1887), Etude sur les reactions des vanadates au point de vue de l'analyse chimique: *Acad. Sci. Paris Comptes Rendus*, **104,** 1850–1853.

CHRIST, C. L., CLARK, JOAN R., AND EVANS, H. T., JR., (1954), The crystal structure of potassium metavanadate monohydrate, $KVO_3 \cdot H_2O$: *Acta Cryst.*, **7,** 801–807.

DONNAY, GABRIELLE, AND DONNAY, J. D. H., (1955), Contribution to the crystallography of uranium minerals: *U. S. Geol. Survey* **TEI-507,** 42 p., issued by U. S. Atomic Energy Comm., Tech. Inf. Service Extension, Oak Ridge, Tenn.

HILLEBRAND, W. F., (1924), Carnotite and tyuyamunite and their ores in Colorado and Utah: *Am. Jour. Sci.*, 5th ser., **8,** 201–216.

LEUDEMAN, LOIS, AND BATES, T. F., (1957), Mineralogical study of several hydrous vanadates: Pennsylvania State Univ., College of Mineral Industries, Tech. report no. 8 to Office of Naval Research. Available as microfilm or photocopy, Library of Congress, Washington, D. C.

MILLER, LEO J., (1955), Annual report for June 30, 1954 to April 1, 1955, Part 1. The chemical environment of pitchblende: U. S. Atomic Energy Comm. RME-3110 (Pt. 1), 49 p., issued by U. S. Atomic Energy Comm. Tech. Inf. Service Extension, Oak Ridge, Tenn.

MORACHEVSKII, YU. V., AND BELYAEVA, L. I., (1956), O sostave uranovanadatov [On the composition of the uranovanadates]: *Geokhimiya*, no. 7, 20–24.

MURATA, K. J., CISNEY, E. A., STIEFF, L. R., AND ZWORYKIN, E. V., (1950), Hydration and base-exchange properties of carnotite, tyuyamunite, and related compounds (abs.): *Geol. Soc. America Bull.*, **61,** no. 12, pt. 2, 1489.

PALACHE, C., BERMAN, H., AND FRONDEL, C., (1951), Dana's system of Mineralogy, 7th ed., v. 2, New York, John Wiley and Sons, Inc.

SUNDBERG, I., AND SILLÉN, L. G., (1949), The crystal structure of KUO_2VO_4: *Arkiv for Kemi*, **1,** 337–351.

Manuscript received January 24, 1958

THE AMERICAN MINERALOGIST, VOL. 43, SEPTEMBER–OCTOBER, 1958

A CALCIUM ANALOGUE OF CHONDRODITE

E. R. BUCKLE AND H. F. W. TAYLOR, *University of Aberdeen, Scotland.*

ABSTRACT

A calcium analogue of chondrodite, of composition $Ca_5(SiO_4)_2(OH)_2$, has been prepared hydrothermally from tricalcium silicate at 600–700° C. The unit-cell is monoclinic with *a* 11.42, *b* 5.05, *c* 8.94 Å, β 109.3°, space-group $P2_1/a$, $Z=2$. The crystals are prisms with length *b*, very low birefringence, positive elongation, and mean refractive index 1.630. Dehydration occurs at 650–700° C. The name calcio-chondrodite is suggested.

INTRODUCTION

In an earlier paper on tricalcium silicate hydrate (Buckle, Gard, and Taylor, 1958), mention was made of a synthetic silicate mineral or mixture of minerals loosely termed "gamma-hydrate(s)." The name was chosen because the *x*-ray powder pattern closely resembled that of dicalcium silicate γ-hydrate or dicalcium silicate hydrate (C) (Heller and Taylor, 1956). The substance was found as an impurity in tricalcium silicate hydrate preparations made hydrothermally at 350–500° C. It has now been prepared in a purer state and its composition and crystallographic properties determined. These show that it is a calcium analogue of chondrodite ($(Mg,Fe)_5(SiO_4)_2(OH,F)_2$), and the name calcio-chondrodite will be used.

PREPARATION AND OPTICAL EXAMINATION

Pastes of anhydrous tricalcium silicate ($Ca_3O(SiO_4)$; 0.5 gm.) and water (0.3–0.5 ml.) were autoclaved in closed bombs of 7 ml. capacity at 600–700° C.; the pressures developed were not known accurately but were estimated from the degree of filling of the bombs to be between 3000 and 5000 p.s.i. The technique was similar to that already described (Buckle, Gard, and Taylor, 1958). Below 600° C., tricalcium silicate hydrate was also formed, and above 700° C. other, as yet unidentified phases, appeared. Times of autoclaving varied from one to three days, the longer times giving better crystallized products.

A typical photomicrograph of one of the preparations (Fig. 1) shows, chiefly, prismatic crystals up to 70μ long. These appear pseudohexagonal in the most commonly observed orientation and somewhat resemble olivine crystals. They had positive elongation, very low birefringence, and mean refractive index 1.630 ± 0.003. Many showed either simple or multiple twinning across a plane parallel to the prism axis. A little calcite was also observed.

X-RAY INVESTIGATION

Rotation and *h*0*l*, *h*1*l*, and *h*2*l* Weissenberg photographs were taken

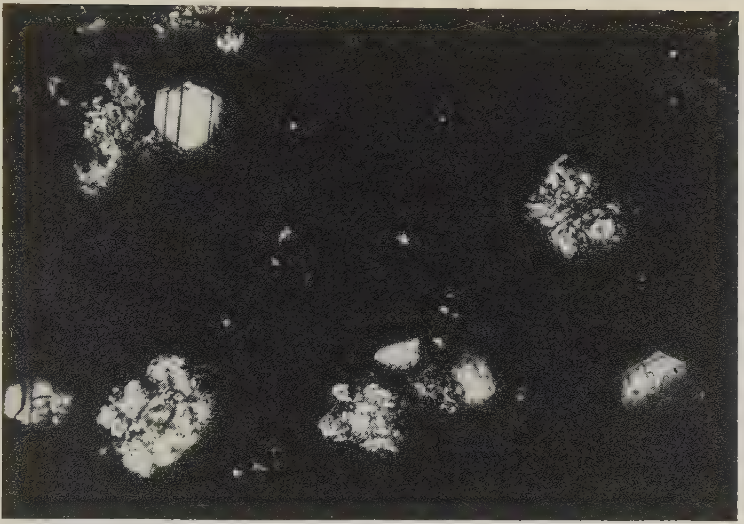

FIG. 1. Photomicrograph of a typical preparation, showing simple and twinned prismatic crystals of calcio-chondrodite. Crossed nicols, ×300.

about the prism axis (*b*), and rotation and equatorial Weissenberg photographs were taken about the axis normal to (001). Filtered copper radiation was used for all exposures. The unit-cell was found to be monoclinic with a 11.4, b 5.05, c 9.0 Å, β 108.4°. $0k0$ reflections were absent for k odd, and $h0l$ for h odd; the space-group is thus $P2_1/a$. The parameters a, c, and β are related by the equation $a=-4c\cos\beta$, and all reflections are therefore indexable in terms of an orthorhombic cell with a 11.4, b 5.05, c 34.2 Å. The crystal used was twinned across (001), which enhanced the pseudo-orthorhombic character.

X-ray powder data for a typical preparation are given in Table 1. Spacings larger than 1.8 Å were indexed, chiefly by superposition of powder and rotation photographs. A few weak lines (marked *) could not be indexed and are probably due to impurities; some can be attributed to calcite. From the indexing of the powder data, the monoclinic cell parameters were refined to a 11.42, b 5.05, c 8.94 Å, all ± 0.05 Å, β 109.3° ± 0.5°.

THERMAL DECOMPOSITION, ANALYSIS, AND CELL CONTENTS

A dehydration isobar (Fig. 2) was obtained at $p_{H_2O}=6$ mm., using the procedure already described (Buckle, Gard, and Taylor, 1958). Loss of weight occurred in three stages. Comparison with reference data showed that the first, at 380° C., could be attributed to calcium hydrox-

TABLE 1. *X*-RAY POWDER DATA FOR CALCIO-CHONDRODITE
Obtained using 6 cm. and 11.46 cm. diameter cameras with CuK$_\alpha$ radiation.

Observed (spacings (Å), intensities, and indices)			Calculated spacings (Å)	Observed (spacing (Å), intensities, and indices			Calculated spacings (Å)
8.45	vw	001	8.45	2.54	ms	$11\bar{3}$	2.55
5.42	s	200, $20\bar{1}$	5.40	2.51	m	212, $21\bar{3}$	2.52
4.24	w	002	4.23	2.48	m†	$41\bar{1}$	2.49
3.98	mw	201, $20\bar{2}$	3.99	2.46	vw	120, $12\bar{1}$	2.46
3.79	ms	111	3.81	2.41	vvw*		
3.67	w	210, $21\bar{1}$	3.69	2.36	vw	401, $40\bar{3}$	2.37
3.31	s	$11\bar{2}$	3.33	2.27	w*		
3.23	vvw*			2.02	w	402, $40\bar{4}$	2.00
3.11	vvw*			1.914	vvw*		
3.02	vs†	$31\bar{1}$	3.03	1.903	vs	222, $22\bar{3}$	1.905
2.92	s	310	2.94	1.898	mw	$42\bar{1}$	1.897
2.89	s	202, $20\bar{3}$	2.91	1.870	vvw*		
2.84	vvw	$40\bar{1}$	2.85	1.846	mw	420, $42\bar{2}$	1.845
2.76	s	$31\bar{2}$	2.78	1.820	mw	511	1.818
2.69	m	400, $40\bar{2}$	2.70	1.801	ms	600, $60\bar{3}$	1.805
2.57	ms	311	2.58				

Observed spacings (Å.) and intensities (continued)

1.775	w	1.504	vvw	1.292	vvw	1.145	w
1.724	m	1.494	vvw	1.277	w	1.12	w
1.695	w	1.469	vw	1.266	vw	1.105	vw
1.682	ms	1.459	w	1.261	w	1.09	w
1.657	s	1.433	vw	1.242	vw	1.075	mw
1.619	vw	1.418	vw	1.232	w	1.065	vw
1.599	vvw	1.405	vw	1.218	vvw	1.04	vw
1.575	vvw	1.388	vvw	1.207	vw	1.02	m
1.552	m	1.376	vvw	1.196	vw	0.981	mw
1.540	vvw	1.352	vw	1.173	m	0.862	w
1.523	vvw	1.331	vvw	1.160	m	0.813	ms

* Lines probably due to impurity.
† Lines probably partly due to calcite.

ide, and the second, at 530–600° C., to calcite. The final stage, at 650–750° C., therefore represents decomposition of the silicate mineral. From the heights of the steps attributed to calcium hydroxide and calcite, the phase composition was estimated to be calcium hydroxide, 3%; calcite, 11%; silicate (by difference), 86%. *X*-ray powder photographs of the residue after heating at 750° C. gave a slightly modified pattern of γ-dicalcium silicate.

Chemical analysis of the specimen used for the dehydration work gave

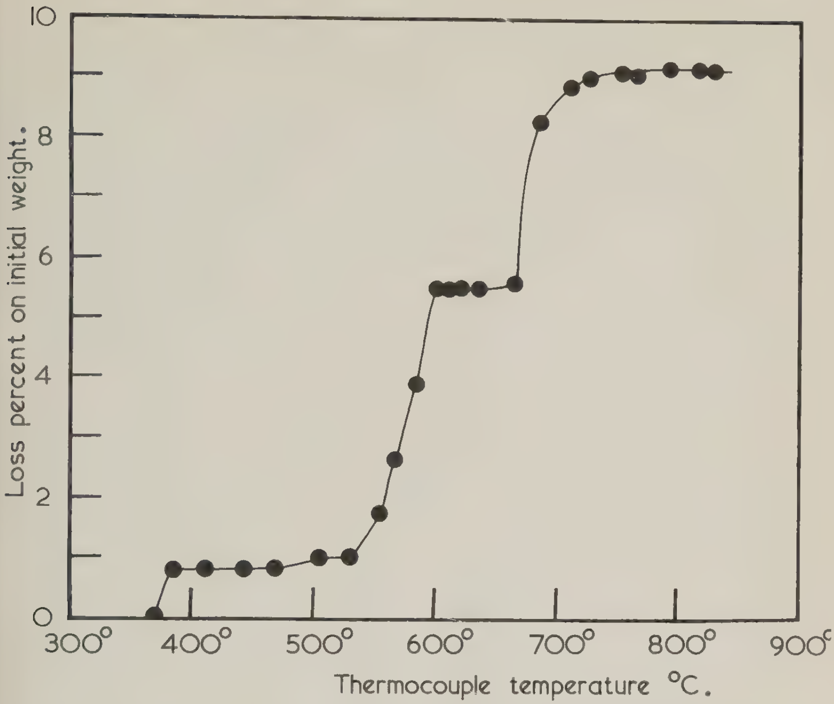

FIG. 2. Dehydration isobar of a typical preparation. The steps at 380°, 530–600°, and 650–750° C. represent decomposition of calcium hydroxide, calcite, and calcio chondrodite respectively.

Ca: Si = 2.88. In conjunction with the evidence from the dehydration isobar, this leads to the composition $5CaO \cdot 2SiO_2 \cdot H_2O$ for the silicate mineral. The density of this specimen, determined by suspension of compressed pellets in bromoform-benzene mixtures after degassing under reduced pressure, was 2.80 $gm.cm.^{-3}$. Correction for calcium hydroxide and calcite gives the value 2.84 $gm.cm.^{-3}$. This agrees well with the theoretical value of 2.85 $gm.cm.^{-3}$ calculated for the cell contents $2[5CaO \cdot 2SiO_2 \cdot H_2O]$.

DISCUSSION

The present results show that the substance previously called "gamma-hydrate(s)" is in fact a single phase of composition $5CaO \cdot 2SiO_2 \cdot H_2O$. In Table 2, some properties of olivine, γ-dicalcium silicate, chondrodite, and the new compound are compared. γ-dicalcium silicate is known to have a structure resembling that of olivine (O'Daniel and Tscheischwili, 1942), and the relation of the new compound to γ-dicalcium silicate is analogous to that of chondrodite to olivine. It seems reasonable to con-

TABLE 2. COMPARISON OF PROPERTIES OF OLIVINE, CHONDRODITE, γ-DICALCIUM SILICATE, AND CALCIO-CHONDRODITE

Composition	Olivine $(Mg,Fe)_2SiO_4$	Chondrodite $(Mg,Fe)_5(SiO_4)(F,OH)_2$	γ-dicalcium silicate Ca_2SiO_4	Calcio-chondrodite $Ca_5(SiO_4)_2(OH)_2$
Crystal system	Orthorhombic	Monoclinic	Orthorhombic	Monoclinic
Unit cell	b 10.21 Å a 4.755 Å c 5.985 Å —	a 10.27 Å b 4.733 Å c 7.87 Å β 109°2′	b 11.28 Å a 5.06 Å c 6.78 Å —	a 11.42 Å b 5.05 Å c 8.94 Å β 109°18′
$-a/4c \cos\beta$	—	1.06	—	1.00
Space group	*Pbnm*	$P\,2_1/a$	*Pbnm*	$P\,2_1/a$
Z	4	2	4	2
Habit	Prisms often elongated ‖c	Often (010) tablets	Prisms	Prisms elongated ‖b
Twinning	Rare	Multiple on (001)	?	Single or multiple across a plane ‖b
Principal source of data	Bragg and Brown (1926)	Taylor and West (1928)	O'Daniel and Tscheischwili (1942)	This investigation

clude that it is a calcium analogue of chondrodite, with the ionic constitution $(Ca_5(SiO_4)_2(OH)_2$.

Chondrodite belongs to a series of minerals structurally derived from olivine, which also includes clinohumite, humite, and norbergite. Taylor and West (1928, 1929), who determined the crystal structures of the minerals in this series, showed that their cell parameters could be calculated from those of olivine. Analogous calculations for the calcium series give the results:

Calcium analogue of:	Formula	Cell parameters			Z
			c (Å)	β	
Clinohumite	$Ca_9(SiO_4)_4(OH)_2$	$a=5.05$ Å	15.52	100.5°	2
Humite	$Ca_7(SiO_4)_3(OH)_2$		23.73	90°	4
Chondrodite	$Ca_5(SiO_4)_2(OH)_2$	$b=11.28$ Å	8.94	108.4°	2
Norbergite	$Ca_3(SiO_4)\,(OH)_2$		10.17	90°	4

The predicted values for calcio-chondrodite agree well with those actually found. Calcium analogues of the other three minerals are so far unknown; the resemblance between the x-ray powder patterns of calcio-chondrodite and dicalcium silicate hydrate (C) suggests a near relationship, which is being further investigated.

Calcio-chondrodite apparently differs from the magnesian or iron-containing minerals in that no isomorphous replacement of hydroxyl by fluorine is essential to its composition. All natural specimens of chondrodite appear to contain fluorine, and attempts to synthesize it have been successful only when fluorine was present (Van Valkenburg, 1957).

The *x*-ray powder data given by Keevil and Thorvaldson (1936) for tricalcium silicate hydrate suggest that their product contained calcio-chondrodite as an unsuspected impurity. More recently, Roy (1958) has mentioned a "Phase X" formed under conditions comparable with those used to prepare calcio-chondrodite in the present investigation. Comparison of her optical and *x*-ray powder data for this phase with those of our calcio-chondrodite[1] suggest that the two are probably identical.

ACKNOWLEDGMENTS

We thank the Johns-Manville Corporation for their generous financial support which has made this work possible, and for permission to publish it. We thank also Dr. D. M. Roy and Dr. A. Van Valkenburg for allowing references to unpublished work.

REFERENCES

BRAGG, W. L., AND BROWN, G. B. (1926): *Zeit. Krist.*, **63,** 538.

BUCKLE, E. R., GARD, J. A., AND TAYLOR, H. F. W. (1958): *J. Chem. Soc.* (*London*), 1351.

HELLER, L., AND TAYLOR, H. F. W. (1956): "Crystallographic Data for the Calcium Silicates." H.M.S.O., London. pp. 79.

KEEVIL, N. B., AND THORVALDSON, T. (1936): *Canad. J. Res.*, **14B,** 20.

O'DANIEL, H., AND TSCHEISCHWILI, L. (1942): *Zeit. Krist.*, **104,** 124.

ROY, D. M. (1958): *Am. Mineral.*, in press.

TAYLOR, W. H., AND WEST, J. (1928): *Proc. Roy. Soc. London*, **117A,** 517; (1929); *Zeit. Krist.*, **70,** 461.

VAN VALKENBURG, A. (1957): Private communication.

Manuscript received January 4, 1958

---

[1] Private discussion, September 1957.

THE AMERICAN MINERALOGIST, VOL. 43, SEPTEMBER-OCTOBER, 1958

THE BERYLLIUM CONTENT OF ROSCHERITE FROM THE SAPUCAIA PEGMATITE MINE, MINAS GERAIS, BRAZIL, AND FROM OTHER LOCALITIES*

MARIE LOUISE LINDBERG, *U. S. Geological Survey, Washington 25, D. C.*

ABSTRACT

New spectrographic and chemical data for roscherite from the Sapucaia pegmatite mine, Minas Gerais, Brazil, from the Nevel Quarry at Newry, Maine, and from the type locality at Greifenstein, Saxony, show that roscherite is a beryllium mineral with formula $(Ca, Mn, Fe)_3Be_3(PO_4)_3(OH)_3 \cdot 2H_2O$. The known range in substitution varies from $Ca_{4.45}Mn_{4.45}Fe_{3.1}$ (Greifenstein) to $Ca_{4.0}Mn_{2.7}Fe_{5.3}$ (Newry) and to $Ca_{3.0}Mn_{3.2}Fe_{5.8}$ (Sapucaia pegmatite mine). The unit-cell dimensions derived from x-ray data are $a=15.95$ Å, $b=11.95$ Å, and $c=6.62$ Å; $\beta=94°50'$ (Sapucaia pegmatite mine) and $a=15.88$ Å, $b=11.90$ Å, $c=6.66$ Å, $\beta=94°42'$ (Greifenstein); Z=4. The new $a{:}c$ ratio is equivalent to the ratio $2a{:}c$ previously derived from the morphology of the crystals, and the β angle is here refined. Apparently the (110) face from which the $a{:}b$ ratio originally was determined was misidentified and completely new $a{:}b$ and $b{:}c$ ratios are here recorded. The indices of refraction for roscherite from the Sapucaia pegmatite mine are $\alpha=1.636$, $\beta=1.641$, $\gamma=1.651$, biaxial +, dispersion $r>v$, strong.

Roscherite from the Sapucaia pegmatite mine occurs as single crystals, crystal aggregates, and granular crusts in vugs in muscovite. It is associated with faheyite, variscite, frondelite, beryl, and euhedral crystals of quartz.

INTRODUCTION

In the period 1943 to 1945, William T. Pecora, of the U. S. Geological Survey, and A. L. de M. Barbosa, of the Departamento Nacional da Produção Mineral, Brazil, made several examinations of the Sapucaia pegmatite mine, near Conselheiro Pena, Minas Gerais, Brazil, and collected a representative suite of minerals for later study. This paper presents a detailed mineralogical description of roscherite, $(Ca,Mn,Fe)_3Be_3(PO_4)_3(OH)_3 \cdot 2H_2O$, from the Sapucaia pegmatite mine and new data are given for roscherite from the type locality at Greifenstein, Saxony and from the Nevel Quarry, Newry, Maine. The beryllium content of roscherite has not been previously recognized. Roscherite was first described as a hydrous calcium iron manganese aluminum phosphate mineral by Slavík (1914). New spectrographic and chemical analyses confirm that beryllium occurs in roscherite as a major constituent and aluminum only in traces.

OCCURRENCE

Roscherite occurs disseminated in the smaller interstices between books of muscovite, as individual measurable crystals, approximately 1 mm. in size, as crystal aggregates, or as fine-grained sericitic-like powdery masses. With increasing mineralization, in the larger vugs, the roscherite forms a structureless granular groundmass in which grow euhedral crystals of quartz. Locally, the still open part of the vug may be lined with a fibrous layer of frondelite (Lindberg, 1949), which bends around the roscherite and quartz crystals and is in turn encrusted with an efflorescence of faheyite. Euhedral quartz crystals in the mineralized muscovite are indicative of a high concentration of roscherite and faheyite, and are often encrusted with faheyite. Finely crystalline roscherite intergrown with faheyite imparts a brown color to faheyite. A fibrous matted crust of faheyite, roscherite, and quartz crystals may interleave the thin edges of muscovite books with consequent bending, fraying, and exfoliation of the muscovite (Fig. 1).

---

* Publication authorized by the Director, U. S. Geological Survey.

In addition to its occurrence in a matrix of muscovite, roscherite also occurs sparsely, admixed with frondelite, in association with multicolored beryl, as brown coloring matter in the cleavage planes in beryl, as a granular crust on beryl, or disseminated in frondelite near the beryl-frondelite contact. In association with beryl, roscherite rarely occurs as a separate phase, but is usually admixed, as a minor constituent of a fine-grained aggregate, with other iron manganese phosphates or with manganoan variscite.

MORPHOLOGICAL AND *X*-RAY CRYSTALLOGRAPHY

Roscherite is monoclinic prismatic. The observed extinctions on single crystal *x*-ray patterns show that the space group is either $C2/c-(C_{2h}^6)$ or $Cc-(C_s^4)$. The habit of the crystals indicates that the symmetry elements include a 2-fold axis and a mirror plane; the preferred space group for roscherite is therefore $C2/c-(C_{2h}^6)$.

The orientation of the unit cell selected for crystals of roscherite from the Sapucaia pegmatite mine yields different axial ratios and β angle than those given by Slavík (1914) for roscherite crystals from Greifenstein, Saxony. The new orientation for roscherite follows the convention for monoclinic crystals, $c<a$, with β as nearly orthogonal as possible, and $>90°$ (Table 1). Owing to the scarcity of crystal forms, the crystallographic elements have been calculated from the axial ratios and β angle derived from the *x*-ray study (Table 2).

Crystals of roscherite from the Sapucaia pegmatite mine are characterized by faces of the forms $\{111\}$ and $\{010\}$ well developed in one zone, and faces of the forms $\{100\}$ at an angle to this zone (Fig. 2). On a few crystals faces of the forms $\{102\}$, $\{201\}$, $\{\bar{1}01\}$, $\{\bar{2}01\}$, $\{\bar{3}01\}$, and $\{\bar{1}11\}$ are present as small faces of poor quality (Fig. 3). The crystals are tabular parallel to (100). The crystals differ from those from Greifenstein, Saxony, in that the prism zone is well developed in the latter.

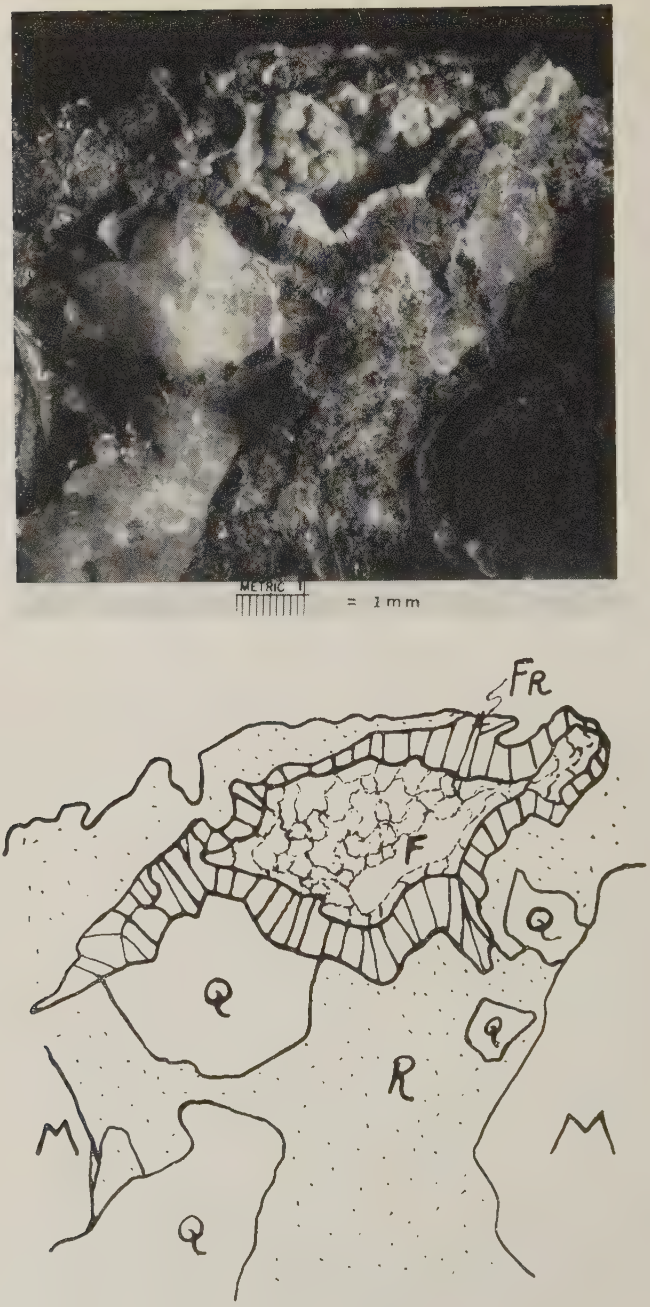

FIG. 1. Photograph showing euhedral quartz crystals (Q) in a matrix of granular roscherite (R) and muscovite (M) in a vug lined with a layer of fibrous frondelite (Fr) and an efflorescence of radiating fibers of faheyite (F).

TABLE 1. *X*-RAY DIFFRACTION DATA
Unit Cell Data

Space group $C2/c-(C_{2h}^6)$

Roscherite Sapucaia pegmatite mine[1]	Roscherite Greifenstein, Saxony[2] U.S.N.M. R6219	Roscherite Nevel Quarry, Newry, Maine[3] Harvard 92220
$a=15.95\pm .06$ A	$a=15.88\pm .04$ Å	$a=15.89\pm .04$ Å
$b=11.95\pm .04$ Å	$b=11.90\pm .03$ Å	$b=11.90\pm .03$ Å
$c=6.62\pm .04$ Å	$c=6.66\pm .03$ Å	$c=6.59\pm .03$ Å
$\beta=94°50'\pm 15'$	$\beta=94°42'\pm 15'$	$\beta=94°50'$ (assumed)
volume = 1257 A³	volume = 1254 A³	volume = 1242A³
Sp. gr. = 2.934 ± 0.006 (meas.)	Sp. gr. data from lit. = 2.916[4]	Sp. gr. = 2.936 ± 0.006 (meas.)
Sp. gr. = $2.93\pm$ (calc.)	Sp. gr. = 2.90 (calc.)	Sp. gr. = 2.94 (calc.)

X-ray Powder Diffraction Data
Fe/Mn = 1.9373 Å

I	$d_{meas.}$ (A)	*I*	$d_{meas.}$ (Å)	*I*	$d_{meas.}$	*hkl*	$d_{calc.}$ (Å)
9	9.58	9	9.51	9	9.51	110	9.51
1½	7.95	½	7.97	½	7.90	200	7.92
10	5.96	10	5.95	10	5.95	020	5.95
1	5.61	½	5.59	½	5.63	$11\bar{1}$	5.54
4	4.84	4	4.84	3	4.82	310	4.82
1½	4.42	1½	4.44	1½	4.40	021	4.41
½	3.97	½	3.97	½	3.95	400	3.96
½	3.76		3.77	½	3.76	221	3.76
						311	3.75
1½	3.37	1	3.36	½	3.37	$13\bar{1}$	3.35
						002	3.30
1	3.30	1	3.27	1	3.31	420	3.30
						131	3.29
7	3.18	8	3.17	8	3.17	330	3.17
½	3.15					$11\bar{2}$	3.15
						202	3.13
2B	3.08	2B	3.08	2B	3.06	510	3.06
						112	3.06
2B	2.975	2B	2.979	2B	2.973	040	2.975
				½	2.945	$20\bar{2}$	2.945
½	2.909	½	2.909			$33\bar{1}$	2.914
				½	2.867	511	2.865
						421	2.865
1B	2.839	½	2.831	½	2.825	$31\bar{2}$	2.819
5	2.796	6	2.788	6	2.780	240	2.785
½	2.715	½	2.706			041	2.710
4	2.652	4	2.644	4	2.637	$40\bar{2}$	2.640
						600	2.638
½	2.547	½	2.550			241	2.537
1½	2.428	1½	2.423	1½	2.410	402	2.430
						620	2.414
½	2.386			½	2.376	422	2.414
1	2.365	1	2.356	1	2.350	$53\bar{1}$	2.367
½	2.280	½	2.273			$44\bar{1}$	2.274
2	2.235	1	2.227	1	2.220	332	2.226
						$15\bar{1}$	2.225
						710	2.222
1½	2.176	1	2.181	1	2.196	350	2.170
1	2.060	1	2.062	1	2.061	711	2.054
2	2.040			1	2.033	532	2.042
						351	2.039
2	1.992			1	1.993	060	1.983
		½B	1.981	½	1.981	800	1.979
						602	1.977
1½	1.934			1½	1.922		
1½	1.780	½	1.771	½	1.773		
½	1.756	½	1.746				
½	1.704	½	1.695	½	1.687		
3	1.656	2	1.653	3	1.646		
½	1.619	½	1.608	½	1.608		
½	1.533	½	1.578	½	1.582		
				½	1.573		
½	1.442	½	1.499	½	1.497		
½	1.411	½	1.443				

Debye-Sherrer camera, diameter 114.59 mm.
B = Broad
Lower angle cut-off 11 A.

[1] Cell dimensions from Weissenberg photographs calibrated for film shrinkage by comparison with an indexed powder photograph; iron radiation, manganese filter, λ = 1.9373 Å.

[2] Cell dimensions from Weissenberg photographs calibrated for film shrinkage by means of a superimposed powder photograph of silver (method of Christ, 1956); copper radiation, nickel filter, λ = 1.5418 Å.

Cell dimensions from indexed powder diffractometer pattern; scale 2 inches = 1° of 2θ; copper radiation, nickel filter, λ = 1.5418 Å.

[4] Data of Slavík (1914).

TABLE 2. MORPHOLOGICAL DATA FOR ROSCHERITE FROM THE SAPUCAIA PEGMATITE MINE

A. Measured data (5 crystals)

Forms:	ϕ_2		ρ_2		Frequency
	Average	Range	Average	Range	
010	—	—	0°00′	—	5
100	0°00′	- -	90 54	89°35′–91°40′	8
102	74 30	—	88 38	—	1
201	43 30	42°30′–44°30′	90 25	90 04 –90 46	2
$\bar{1}01$	109 30	—	90 00	—	1
$\bar{2}01$	128 04	—	90 05	—	1
$\bar{3}01$	138 43	—	90 36	—	1
111	63 50	63 50 –64 30	63 44	63 19 –64 15	9
$\bar{1}11$	108 28	—	60 23	—	1

B. Angle table and elements calculated from x-ray data[1]

Crystal system: Monoclinic: primatic—$2/m$.

$a:b:c=1.335:1:0.5540$ $\beta=94°50'$ $p_0:q_0:r_0=0.4150:0.5520:1$

$r_2:p_2:q_2=1.812:0.7519:1$ $\mu=85°10'$ $p_0'0.4165$, $q_0'0.5540$, $x_0'0.0846$

Forms:	ϕ	ρ	ϕ_2	$\rho_2=B$	C	A
001	90°00′	4°50′	85°10′	90°00′	—	85°10′
010	0 00	90 00	—	0 00	90°00′	90 00
100	90 00	90 00	0 00	90 00	85 10	0 00
110	36 56	90 00	0 00	36 56	87 06	53 04
102	90 00	16 19	73 41	90 00	11 29	73 41
101	90 00	26 36	63 24	90 00	21 46	63 24
201	90 00	42 31	47 29	90 00	37 41	47 29
$\bar{1}01$	−90 00	18 21	108 21	90 00	23 11	108 21
$\bar{2}01$	−90 00	36 47	126 47	90 00	41 37	126 47
$\bar{3}01$	−90 00	49 20	139 20	90 00	54 10	139 20
111	42 07	36 45	63 25	63 39	33 38	66 20
$\bar{1}11$	−30 55	32 50	108 21	62 17	35 32	106 11
$\bar{3}11$	−64 33	52 11	139 20	70 09	56 36	135 30
$\bar{3}31$	−35 00	63 46	139 20	42 42	66 36	120 58

[1] Includes forms noted on crystals from Greifenstein, Saxony (U.S.N.M. R 6219).

In order to relate the crystallographic directions of the new orientation to the axial directions selected by Slavík in 1914, crystals of roscherite from the type locality (U. S. National Museum No. R6219) have been measured and the forms noted have been related to the new axes selected by x-ray methods (Table 3). The crystals of roscherite from Greifenstein, as observed by Lindberg, are characterized by being 6- or

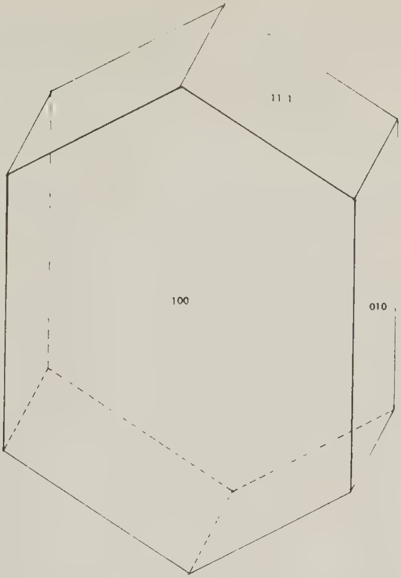

FIG. 2. Typical crystal of roscherite from the Sapucaia pegmatite mine.

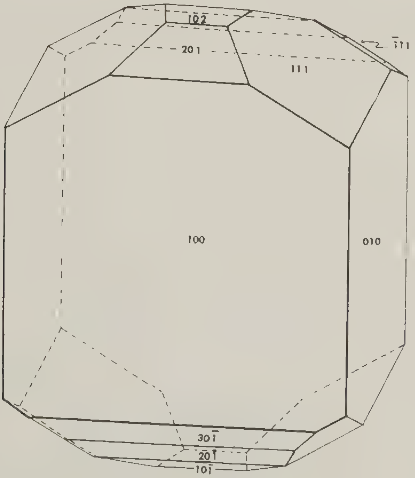

FIG. 3. Crystal of roscherite from the Sapucaia pegmatite mine showing development of the dome faces.

TABLE 3. MORPHOLOGICAL DATA FOR ROSCHERITE FROM GREIFENSTEIN, SAXONY

A. Interfacial angles from literature (5 crystals)[1]

Form	Average	Range	Frequency
a(100):*c*(001)	80°10′	80°00′ to 80° 20′	2
:*b*(010)	90°27′	87°58′ to 91°24′	9
:*d*(10$\bar{1}$)	52°02′	51°43′ to 52°21′	2
:*m*(110)	42°48′	42°14′ to 43°27′	3
c(001):*b*(010)	90°07′		1

[1] Data of Slavík, 1914

B. New angle measurements on faces related to axes selected for the unit cell[2]

Form	ϕ		ρ		Frequency	Quality
	Average	Range	Average	Range		
010	0°00′		90°30′	89°40′ to 90°52′	16	G
100	90°55′	89°15′ to 91°40′	90°15′	89°46′ to 90°44′	18	G
110	36°16′	34°38′ to 37°40′	90°37′	89°40′ to 91°23′	38	G
201	90°30′	90°15′ to 90°45′	45°30′	44°00′ to 47°00′	2	P
$\bar{1}01$	−93°00′	−92°30′ to 95°00′	19°33′	19°33′ to 20°45′	3	P
$\bar{2}01$	−91°05′	—	37°05′	—	1	P
$\bar{3}01$	−90°14′	—	48°20′	—	1	P
111	36°45′	—	37°45′	—	1	P
$\bar{1}11$	−31°10′	−31°00′ to −31°20′	33°31′	33°12′ to 33°50′	2	G
$\bar{3}11$	−65°25′	−65°00′ to −66°15′	51°28′	49°10′ to 52°45′	4	F
		ϕ_2		ρ_2		
001	85°00′	84°00′ to 86°00′	90°38′	—	1	P
$\bar{3}31$	138°20′	—	40°14′	—	1	F

[2] Data of Lindberg, roscherite U.S.N.M. no. R6219. The forms {001} and {$\bar{3}31$} were not measured with the crystal oriented [001] but were measurable with the crystal oriented [010].

C. Equivalent Forms

Slavík	Lindberg
1. The *c*-axes parallel with prism zone, cross section 6 or 8 sided; prisms {100}, {010}, and {110}	1. Same
2. Interfacial angle (100):(110) = 42°48′ Frequency: 3× on 5 crystals	2. Interfacial angle (meas) (100):(110) = 53°44′ Frequency: 38× on 12 crystals Note: interfacial angle ($\bar{1}$00):($\bar{3}$01) = 40°40′ (calc) = 41°17′ (meas) No equivalent intercepts of *b*-axis and the *ac* plane
3. $\beta = 99°50′$ measurements from basal reflections imperfect	3. $\beta = 94°42′$ from Weissenberg photograph
4. ρ of ($\bar{1}$01) = 37°58′	4. ρ of ($\bar{2}$01) = 37°05′ (meas.) ϕ of (110) = 36°16′ (meas.)
5. a:c = 1.1	5. $\frac{a}{2} = 1.2$

8 sided in cross section, prismatic parallel to [001], and having the prism zone bounded by {100}, {010}, and {110}.* The shape of the cross section varies with the relative importance of {100}, {010}, and {110}; {100} is usually larger than {110} and {010}, but any of the forms may dominate on individual crystals. Most of the crystals noted by Lindberg are segments of the prism zone, of varying length. Only a few crystals have terminating faces (Fig. 4).

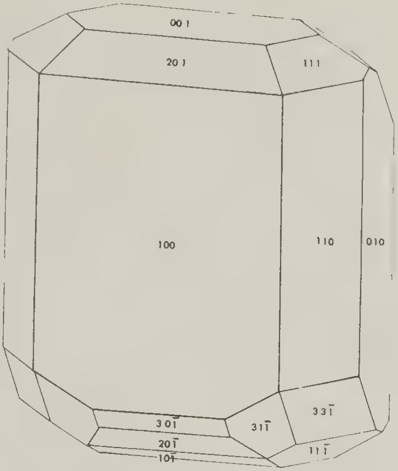

Fig. 4. Crystal of roscherite from Greifenstein, Saxony, showing full development of the terminating faces; typical crystals are usually segments of the prism zone.

The new measurements give different angular relationships and axial ratios than those previously recorded. The interfacial angle (100):(001) given by Slavík as 80°10′ ($\beta = 99°50'$) is considered by Slavík to be an approximate angle measured on crystals with imperfect reflections from the basal pinacoid; in the new measurements the (001) face gives a weak reflection ($\phi_2 = 84°$ to 86° equivalent to $\beta = 96°$ to 94°), but the optical signal is still not of accurately measurable quality. However, the β angle derived from the 0-level Weissenberg pattern of roscherite from Greifenstein is 94°42′ ± 15′. The ($\bar{1}$01) face of Slavík with a measured ρ of 37°58′ becomes the ($\bar{2}$01) face of Lindberg with a measured ρ of 37°05′; the new *a*-axis is double the old *a*-axis in length.

There are no equivalent intercepts of the *b*-axis and the *ac* plane in the two sets of data from which a transformation matrix may be calculated. The calculated ρ_2 value for the {110} form, data of Slavík, suggests an interchange of the *a* and *c* axial directions between the two authors. This

* The same crystal habit for roscherite is described by Slavík (1914) but the interfacial angle (010):(110) of the two authors is different

interchange is not consistent with the interpretation that the {101} form of Slavík is equivalent to the {201} form of Lindberg: i.e., both authors observe the presence of a dome face making a ρ angle near 37° with the axis of the prism zone, but no form in any zone, making a ρ_2 angle near 47° with the *b*-axis was observed by Lindberg during this study.

The {110} form observed by Lindberg is characteristic of the prism zone of all the Greifenstein crystals, although no face in any zone making a ρ_2 angle near 37° with the *b*-axis has been recorded by Slavík. Apparently the fact that the (110) face observed by Lindberg has approximately the same interfacial angle with the (100) face as does the $(\bar{1}01)$ of Slavík has made difficult the correct assignment of faces to zones, the crystallographic elements of Slavík having been calculated from interfacial angles of a given face with {100} and from an assumed zone relationship. In the new crystallographic measurements, pyramid faces, observed for the first time on crystals from Greifenstein, establish an interdependency of axes and zones.

The *x*-ray diffraction data for roscherite are given in Table 1. The unit cell dimensions and β angle for roscherite from the Sapucaia pegmatite mine and from Greifenstein, Saxony, were determined from the Weissenberg patterns of single crystals of roscherite. The unit cell dimensions of roscherite from the Nevel Quarry, Newry, Maine, were determined from an indexed *x*-ray powder diffractometer pattern, using copper radiation and nickel filter, and a scale of two inches to one degree 2θ, assuming the β angle derived for roscherite from the Sapucaia pegmatite mine.

The *x*-ray powder *d*-spacings listed in Table 1 have been obtained using a Debye-Sherrer camera with diameter 114.59 mm., with iron radiation and manganese filter. The resolution in the back reflection range is poor, but film shrinkage is apparently negligible.

PHYSICAL PROPERTIES

Crystals of roscherite from the Sapucaia pegmatite mine are dark brown to reddish-brown in color; those from Greifenstein, Saxony, are olive-green. Roscherite from the Nevel Quarry, Newry, Maine, occurs as light brown radiating fibrous masses. The specific gravities as measured by means of an Adams-Johnston pycnometer of fused silica on the samples used in the analyses are 2.934 ± 0.006 for roscherite from the Sapucaia pegmatite mine and 2.936 ± 0.006 for roscherite from the Nevel Quarry, Newry, Maine; the calculated specific gravities are 2.93 and 2.94, respectively.

The optical properties of crystals of roscherite from the Sapucaia pegmatite mine are: $\alpha = 1.636$, $\beta = 1.641$, $\gamma = 1.651$, $X = b$; biaxial +, dispersion $r>v$ strong; absorption yellow. Roscherite which occurs as a fine-grained replacement of frondelite, admixed with beryl, has higher indices of refraction, with $\gamma=1.67$ to 1.68.

CHEMICAL COMPOSITION OF ROSCHERITE

Roscherite is a hydrous calcium iron manganese beryllium phosphate with unit cell contents:

$$(Ca,Mn,Fe)_{12}Be_{12}(PO_4)_{12}(OH)_{12}\cdot 8\ H_2O.$$

Calcium, manganese, and iron substitute for each other in varying proportions similar to their mutual substitution in the mineral graftonite (Lindberg, 1950). Roscherite from the type locality at Greifenstein, Saxony, contains $Ca_{4.5}Mn_{4.5}Fe_{3.1}$ atoms per unit cell (Table 4). The present analyses extend the known range of substitution to $Ca_{4.0}Mn_{2.7}Fe_{5.3}$ for roscherite from the Nevel Quarry, Newry, Maine, and to $Ca_{3.0}Mn_{3.2}Fe_{5.8}$ for roscherite from the Sapucaia pegmatite mine. A new mineral name is not here proposed for the iron-rich component since the name roscherite as applied to the type material describes a three component system not predominantly rich in any one end member and in the new analyses the iron cations number barely half the combined calcium, manganese, and iron cations.

The beryllium content of roscherite has not been previously recognized. Spectrographic analyses (Table 5) of roscherite from the type locality (U. S. National Museum R6219) from Newry, Maine, and from the Sapucaia pegmatite mine indicate that beryllium is present in roscherite in quantities approximating the aluminum content previously recorded for roscherite. Standard methods for analyzing the Al_2O_3 content of minerals not known to contain beryllium proceed with the precipitation of the Al_2O_3 in the R_2O_3, followed by deduction from the R_2O_3 of the proper proportions of iron and manganese and calculation of the remaining R_2O_3 as Al_2O_3. Any BeO present in the R_2O_3 would hence be erroneously recorded as Al_2O_3. It may be assumed that this procedure has been followed in the original analysis of roscherite. In Table 4, the analysis of type roscherite by Preis (Slavík, 1914) is recalculated with BeO substituted for Al_2O_3. This substitution is consistent with the spectrographic data of Table 5 and with the new chemical analyses of roscherite (Table 4). The very small quantity of aluminum found in the spectrographic analyses of roscherite from Newry, Maine, and from the Sapucaia pegmatite mine is thought to be associated with the insoluble residues found in the chemical analyses,* as no Al_2O_3 was found collected with

---

* Albite occurs admixed with roscherite from the Nevel Quarry, Newry, Maine, and muscovite occurs admixed with roscherite from the Sapucaia pegmatite mine.

Table 4. Chemical Composition of Roscherite

Roscherite from Greifenstein, Ehrenfriedersdorf, Saxony

	Theoretical[1]	Analysis recalculated[2] to 100% without insoluble	Analysis[3] recalculated with BeO substituted for Al_2O_3	Ratios	Metals ions[4] +H per unit cell
CaO	11.39	11.48	11.48	.2047	4.6
MnO	14.41	14.47	14.47	.2040	4.6
FeO	10.16	10.13	10.13	.1410	3.2
Fe_2O_3					
BeO	13.69		13.74	.5494	12.3
Al_2O_3		13.74			
P_2O_5	38.85	38.01	38.01	.2678	12.0
H_2O	11.50	12.17	12.17	.6755	30.2
Insol.					
Total	100.00	100.00	100.00		
Sp. gr.		2.92[2]			

Roscherite from Nevel Quarry, Newry, Maine (Harvard 92220)

	Theoretical[5]	Analysis[6]	Analysis recalculated to 100% without insoluble	Ratios	Metal Ions +H[4] per unit cell
CaO	10.19	9.95	10.11	.1803	4.0
MnO	8.70	8.52	8.66	.1221	2.7
FeO	17.30	16.22	16.49	.2295	5.05 } 5.3
Fe_2O_3		0.89	0.90	.0056	.25
BeO	13.64	12.80	13.01	.5202	11.4
Al_2O_3					
P_2O_5	38.71	38.10	38.74	.2729	12.0
H_2O	11.46	11.89	12.09	.6711	29.5
Insol.		1.25			
Total	100.00	99.62	100.00		
Sp. gr.		2.936±0.006			

(*Continued on opposite page*)

[1] Theoretical calculated from $Ca_{4.45}Mn_{4.45}Fe_{3.1}Be_{12}(PO_4)_{12}(OH)_{12}\cdot 8H_2O$.

[2] Preis analysis in Slavík (1914).

[3] Spectrographic analysis shows that Be, not Al, is a major constituent of roscherite.

[4] Metal ions+H calculated on the basis of $12PO_4$ per unit cell.

[5] Theoretical calculated from $Ca_{4.0}Mn_{2.7}Fe_{5.3}Be_{12}(PO_4)_{12}(OH)_{12}\cdot 8H_2O$.

TABLE 4 (*continued*)

Roscherite from Sapucaia pegmatite mine, Minas Gerais, Brazil

	Theoretical[7]	Analysis[6]	Analysis recalculated to 100% without insoluble	Ratios	Metal Ions[1] +H per unit cell
CaO	7.59	7.60	7.68	.1369	3.1
MnO	10.24	10.04	10.14	.1430	3.2
FeO	18.80	6.26	6.32	.0880	2.0
Fe_2O_3		13.36	13.49	.0845	3.8
BeO	13.54	12.58	12.71	.0582	11.4
Al_2O_3					
P_2O_5	38.45	37.60	37.98	.2675	12.0
H_2O	11.38	11.56	11.68	.6483	29.1
Insol.		0.80			
Total	100.00	99.80	100.00		
Sp. gr.		2.934			

[6] M. L. Lindberg, analyst.

[7] Theoretical calculated from $Ca_{3.0}Mn_{3}\cdot 2Fe_{5.8}Be_{12}(PO_4)_{12}(OH)_{12}\cdot 8H_2O$.

the BeO precipitates from the acid soluble portions of either sample.*

In each of the analyses presented in Table 4 the theoretical analyses assume the ratios of Ca:Mn:Fe reported for the chemical analyses from the same locality. The metal ions and H are calculated on the basis of setting the PO_4 content exactly equal to 12. The measured number of H atoms per unit cell in the three analyses is 30.2, 29.5, and 29.0. The theoretical number of H atoms per unit cell is assumed to be 28. Twelve hydroxyls are required to balance the valencies, if all the iron is divalent. The space group requirement that the number of equivalent positions be divisible by 4 suggests a water content of 8 or 12 molecules per unit cell, corresponding to a total of 28 or 36 H per unit cell. The measured number of H per unit cell, and the molecular weight calculated from the x-ray data and specific gravity, are in closer agreement with 28 H per unit cell than with 36 H per unit cell. Similarly, the theoretical quantity of beryllium present is assumed to be 12 cations per unit cell, since the number of equivalent positions per unit cell must be divisible by 4.

---

* The optimum pH for the precipitation of $Be(OH)_2$ is slightly higher than that for the precipitation of $Al(OH)_3$ which then may result in incomplete precipitation of $Al(OH)_3$ together with $Be(OH)_2$. The aluminum correction on the ignited BeO precipitate was determined by the fluorometric method of Weissler and White (1946) which method would have detected 0.01% Al_2O_3.

TABLE 5. SEMIQUANTITATIVE SPECTROGRAPHIC EXAMINATION OF ROSCHERITE*

	1	3	4	4
Si	0.3%	0.3%	0.03%	0.01%
Al	0.3	0.3	0.3	0.1
Fe	M	M	10.0	10.0
Mg	0.1	0.1	0.3	0.3
Ca	1.0	3.0	3.0	3.0
Na	0.0	0.03	0.1	0.1
P	M	M	M	M
Mn	3.0	3.0	3.0	3.0
Ba	0.01	0.03	0.0003	0.01
Be	3.0	3.0	3.0	3.0
F	nd	nd	nd	nd
Sr	0.0	0.0	0.01	0.003
Zn	0.3	0.0	0.0	0.1
Zr	0.0	0.0	0.0	0.003
Cu	0.0	0.0003	0.0	0.0

1. Roscherite from the Sapucaia pegmatite mine, Minas Gerais, Brazil; analysis on a 2 mg. sample of purified crystals, sample 9 R, TWS-3016.
2. Roscherite from Greifenstein, Saxony (U. S. National Museum R6219); analysis on a 2.5 mg. sample, TWS-3082.
3. Roscherite from the Nevel Quarry, Newry, Maine (Harvard No. 92220); analysis on a 10 mg. sample, TWS-3149.
4. Roscherite from the Nevel Quarry, Newry, Maine, specimen courtesy of Mary Mrose; analysis on a 5 mg. sample, TWS-3149.

* Analyst, Katherine V. Hazel, U. S. Geological Survey. Figures are reported to the nearest number in the series 10, 3, 1, 0.3, etc., in per cent; M, major, greater than 10%. For comparison with chemical analyses, figures must be converted to oxides; for example, Be reported as 3.0% corresponds to a Be content varying between 2 and 7.5% or a BeO content varying between 6 and 21%. nd=not detected.

At the Sapucaia pegmatite mine the iron contained in the roscherite is in part oxidized, with concomitant adjustment of the hydroxyl-water ratio in order to balance the valencies. Roscherite probably derives its iron and manganese content from frondelite, which, in part, it replaces, and varies in composition in association with that mineral.* The analysis (and optical properties) are considered representative of the occurrence of roscherite as crystals and as granular crusts in a zone intermediate to a green fibrous layer of frondelite and to an efflorescent coating of faheyite in vugs in muscovite. Indices of refraction of roscherite which replaces

* Green frondelite in association with roscherite in muscovite contains 6.70% FeO, 5.54% MnO, and 41.93% Fe_2O_3; brown frondelite (type) contains 7.74% MnO, 1.75% Mn_2O_3, and 48.85% Fe_2O_3.

brown frondelite associated with multi-colored beryl are higher and indicate a range in iron content or in state of oxidation of the iron.

Roscherite, which contains only divalent metals, is easily soluble in dilute HCl, HNO_3 and H_2SO_4. With increasing oxidation of the iron the solubility in HCl remains the same, but in HNO_3 and in H_2SO_4 the solubility decreases.

Mineral Relationships

The crystal chemistry of beryllium phosphate minerals is not well understood. Many minerals now known to be beryllium minerals have been first described as aluminum minerals, due to the similarity in behavior of beryllium and aluminum ions in solution, and their co-precipitation of hydroxyl ions in nearly neutral solutions.

The beryllium content of roscherite is noted for the first time. Two new beryllium phosphate minerals, faheyite (Lindberg and Murata, 1953) and moraesite (Lindberg, Pecora, and Barbosa, 1953) have been first described from the Sapucaia pegmatite mine. One of these, moraesite, occurs as fine fibers in association with roscherite, at Greifenstein, Saxony (U. S. National Museum R6219). Childrenite, an aluminum bearing phosphate, occurs in association with roscherite at both localities and crystals of variscite grow in the same vugs as crystals of roscherite and fibers of faheyite at the Sapucaia pegmatite mine. It appears significant that aluminum and beryllium ions are effectively separated in nature into individual hydrous phosphate mineral species which co-exist in the same vug, when under laboratory conditions aluminum and beryllium ions coprecipitate. The amphoteric character of both aluminum and beryllium ions and the effective complete precipitation of beryllium from solutions slightly more basic than solutions from which aluminum quantitatively separates suggests that a changing pH in nearly neutral solutions may be a factor in the formation of these minerals.

Roscherite differs chemically from faheyite in that faheyite contains no calcium, less beryllium, more water, and no divalent iron.

Acknowledgments

The author is indebted to colleagues in the U. S. Geological Survey, particularly to William T. Pecora for providing the specimens containing the roscherite, to Katherine V. Hazel for the spectrographic analyses, and to Daphne Ross and Betsy Levin for *x*-ray powder photographs. The roscherite from the type locality at Greifenstein, Saxony was obtained through the courtesy of Dr. George Switzer of the U. S. National Museum; roscherite from the Nevel Quarry, Newry, Maine through the courtesy of Prof. Clifford Frondel of Harvard University.

BIBLIOGRAPHY

CHRIST, C. L. (1956), Precision determination of lattice constants of single crystals using the conventional Weissenberg camera: *Am. Mineral.*, **41,** 569–580.

LINDBERG, MARIE LOUISE (1949), Frondelite and the frondelite-rockbridgeite series: *Am. Mineral.*, **34,** 541–549.

LINDBERG, MARIE LOUISE (1950), Arrojadite, hühnerkobelite, and graftonite: *Am. Mineral.*, **35,** 59–76.

LINDBERG, MARIE LOUISE, AND MURATA, K. J. (1953), Faheyite, a new phosphate mineral from the Sapucaia pegmatite mine, Minas Gerais, Brazil: *Am. Mineral.*, **38,** 263–270.

LINDBERG, MARIE LOUISE, PECORA, W. T., AND BARBOSA, A. L. DE M. (1953), Moraesite, a new hydrous beryllium phosphate from Minas Gerais, Brazil: *Am. Mineral.*, **38,** 1126–1133.

SLAVÍK, F. (1914), Neue Phosphate vom Greifenstein bei Ehrenfriedersdorf: *Ak. Ceská, Bull.—Bull. intern. ac. sc. Bohême,* **19,** No. 4, 108–123.

WEISSLER, ALFRED, AND WHITE, C. E. (1946), Fluorometric determination of aluminum in steels, bronzes, and minerals: *Ind. and Eng. Chemistry*, Anal. Ed., **18,** 530–534.

Manuscript received January 24, 1958

THE AMERICAN MINERALOGIST, VOL. 43, SEPTEMBER–OCTOBER, 1958

THE EFFECTS AND GEOLOGIC SIGNIFICANCE OF POTASSIUM "FIXATION" BY EXPANDABLE CLAY MINERALS DERIVED FROM MUSCOVITE, BIOTITE, CHLORITE, AND VOLCANIC MATERIAL*

Charles E. Weaver, *Shell Development Company, Houston, Texas.*

Abstract

When muscovite→vermiculite and muscovite→montmorillonite are subject to mild treatment with KOH they will contract to 10 Å, indicating that they have inherited much of the high interlayer charge of the muscovite. A review of the data on potassium "fixation" indicates that the relation between the amount of "fixed" potassium and the number of contracted 10-Å layers is as yet not clear. Samples of montmorillonite were subjected to various treatments with KOH and it is shown that there is a direct relation between the per cent of contracted 10-Å layers and the per cent of tetrahedral charge.

Potassium treatments with vermiculite indicates that there are highly charged biotite and muscovite→vermiculites which readily contract to 10.0 to 10.2 Å and low-charged nonmica→vermiculites which resist contraction. An attempt is made to organize the easily measured parameters of expanded 2:1 clays and to show how these parameters relate one to the other and ultimately to the source material.

A sample of muscovite→montmorillonite exposed to sea water readily contracted to a 10-Å lattice, indicating the unstable character of such montmorillonites. An examination of clays from marine sediments indicates that muscovite and biotite→vermiculite and montmorillonite are relatively rare and that most of the expanded clays are derived from low-charged nonmicaceous minerals such as volcanic material, chlorite, and hornblende. The sequence illite→montmorillonite→illite is considered to indicate rejuvenation and not diagenesis. Further, it is speculated that mixed-layer illite→montmorillonites have an equilibrium ratio which is determined by the interlayer charge and the composition of the water in the environment of deposition.

A limited study of Recent sediments indicates that most of the expanded clays in the Gulf of Mexico are volcanic→montmorillonites and that those from the Atlantic Coast may be muscovite→montmorillonites.

Introduction

Agronomists, and to a lesser extent mineralogists, have accumulated a great amount of data on potassium "fixation" by soils and clay minerals. Relatively little effort has been made by geologists and petrographers to evaluate the geologic significance of this phenomenon. The experiments conducted during this investigation were designed to supplement the data in the literature and an attempt was made to obtain some preliminary ideas on the geological significance of the phenomenon of potassium "fixation" by expanded clay minerals.

A number of investigators have reported the alteration of trioctahedral biotite to vermiculite. The vermiculite has a 14.0- to 14.5-Å spacing; it will not expand when treated with ethylene glycol but will collapse to near 10 Å when treated with K or when heated. (Walker, 1949, 1950; Walker and Milne, 1950; Barshad, 1948, 1954; Van der Marel, 1954.)

---

* Publication No. 154, Shell Development Company, Exploration and Production Research Division, Houston, Texas.

Walker (1950) and MacEwan (1954) reported an example of biotite altering to montmorillonite. The montmorillonite was differentiated from vermiculite on the basis that it expanded to 17.7 Å when treated with glycerol and the vermiculite did not.

Recently, Brown (1953), Hathaway (1954), and Rich and Obershain (1955) reported the presence of a dioctahedral vermiculite-like mineral believed to have been formed by the alteration of muscovite. This vermiculite has a 14.0- to 14.7-Å (001) spacing, will not expand when treated with glycerol, but will collapse to near 10 Å when treated with potassium. Aluminum and iron can occur in the interlayer positions where they retard collapse by potassium treatment and by heat treatment.

For a long time it has been noted that many soils "fix" potassium. More recently, numerous instances have been reported where expanded 14 Å clay minerals in soils will collapse to near 10 Å when saturated with potassium and dried at room temperature (Jackson and Hellman, 1941; Rolfe and Jeffries, 1953; Kunze and Jeffries, 1953; Van der Marel, 1954). These clays do not expand appreciably with glycol and are considered by the writers of the latter two papers to be a vermiculite-like mineral derived from the weathering of muscovite and illite.

MUSCOVITE→MONTMORILLONITE AND MUSCOVITE→VERMICULITE

The Ordovician Womble shale and the Cambrian Collier schist in the Ouachita Mountains of southeastern Oklahoma are composed largely of well-crystallized illite (fine-grained 2 *M* muscovite) and a small amount of chlorite which, when weathered, alter to an expanded 2:1 clay and kaolinite. The expanded clay mineral has a 14.0- to 15.0-Å (001) spacing in its natural state. When treated with ethylene glycol, the Womble clay (BEC 70 meq per 100 gm.) expands to about 17 Å, whereas the Collier clay (BEC 50 meq per 100 gm.) shows no expansion (Fig. 1, Table 1). However, when these clays are allowed to stand in a 1 *N* KOH solution for 15 hours and dried at room temperature, both collapse to 10 Å. Before KOH treatment the Womble sample had 1.6% K_2O and after treatment 3.8%. Neither of the K-saturated samples will expand when treated with ethylene glycol. The K-saturated Womble sample, dried at room temperature and placed in a 1 *N* $CaCl_2$ solution for 15 hours, re-expands to 15.0 Å, and then when glycolated absorbs two layers of glycol and expands to 16.6 Å. When the K-saturated Womble sample was dried at 110° C. for one week and then placed in a 1 *N* $CaCl_2$ solution the expansion was less than for the sample dried at room temperature.

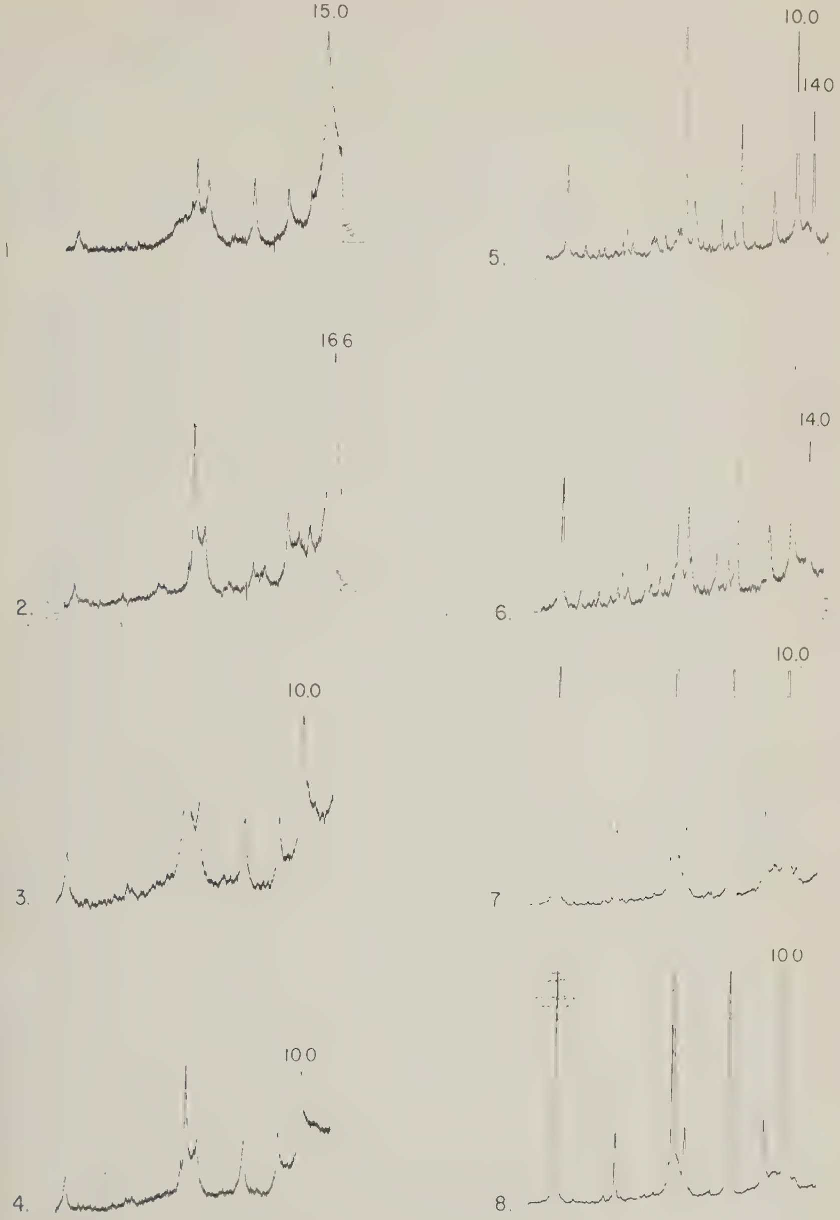

Fig. 1. (1) to (4)—Womble shale: (1) natural state; (2) with ethylene glycol; (3) with KOH; (4) with KOH and ethylene glycol. (5) to (8)—Collier schist; (5) natural state; (6) with ethylene glycol; (7) with KOH; (8) with KOH and ethylene glycol.

Table 1. X-Ray Data on Muscovite→Montmorillonite and Muscovite→Vermiculite

	Untreated	Ethylene Glycol	KOH	KOH E. G.	KOH $CaCl_2$	600° C.
Womble Shale	15 A	16.6 A	10 A	10 A	15 A	10 A
Collier Schist	14 A	14 A	10 A	10 A	14 A	—

Further, when the Ca-saturated Womble sample is heated to 600° C. for 15 hours, it will collapse to only 10.0 Å and not the 9.3-Å spacing characteristic of a Ca montmorillonite. An x-ray pattern of a sample of wet, K-saturated Womble clay indicated that it was completely collapsed to 10 Å. X-ray diffraction patterns of both K-saturated samples show a (060) value of 1.495 Å, indicating that the clay is dioctahedral. The series of reflections between 4.4 and 2.6 Å indicate that the clay has the 2 M muscovite structure (Table 2).

These expanded micas appear to have a strong preference for potassium. When placed in a solution containing one part KCl to ten parts $MgCl_2$ the Womble clay adsorbed the potassium and contracted to 10 Å. When given a choice, montmorillonite (volcanic) adsorbs magnesium more readily than potassium (Grim, 1953). This suggests that the preferential adsorption of potassium by the Womble clay may be a function of charge and/or structural order.

The preceding data indicate that these expanded clays were derived from muscovite. The Womble clay has some of the properties of montmorillonite, in that glycolation expands it to near 17 Å. However, it differs from the "typical" montmorillonite because it collapses to 10 Å

Table 2. X-Ray Spacings and Intensities; Womble (K-Saturated)

d Å	I	Indices	d Å	I	Indices	d Å	I	Indices
10.0	SM	002	2.86	W	115	1.83	W	$04\bar{6}$
5.0	M	004	2.78	W	$11\bar{6}$	1.67	W	$13\overline{10}$
4.48	S	110	2.67	WW	026	1.64	WM	312
3.90	W	112, $11\bar{3}$	2.56	S	$20\bar{2}$	1.62	W	313
3.72	W	023	2.46	W	$13\bar{3}$	1.49	WM	060
3.32	S	006	2.38	MW	133	1.34	WM	335
3.22	W	114	2.13	W	043	1.29	W	400
2.98	WM	025	1.98	SM	0010	1.24	W	0016

W—Weak.
M—Medium.
S—Strong.

when saturated with K and dried at room temperature. The ease with which the Womble clay collapses to 10 Å when saturated with K suggests that the interlayer charge is relatively large and that the predominant lattice charge is probably tetrahedral and was inherited from the original muscovite. The ability to contract is less in the finer grain sizes, suggesting that when weathering is sufficiently severe, the high lattice charge can be destroyed. The fact that the Ca-saturated Womble clay will collapse only to 10 Å when heated to 600° C. suggests that a sufficient number of the large K^+ ions remain between the layers to prevent complete collapse but apparently are not enough to prevent expansion. The differential thermal curve of the Womble clay shows the second endothermal reaction occurring at 550° C. The temperature of this reaction is characteristic of illite and approximately 100° lower than for volcanic montmorillonite.

The Collier muscovite→vermiculite is similar to those previously described by Brown (1953), Hathaway (1954), and Rich and Obershain (1955).

A question immediately arises as to how much of this muscovite→montmorillonite and biotite→montmorillonite is present in sediments and soils and has been overlooked or considered as typical montmorillonite (volcanic→montmorillonite). It seems likely that it would be fairly common in soils. In the latter part of this paper some preliminary data will be given concerning its presence in sediments.

The discovery of this material indicates how strongly clay minerals can inherit much of the character of their source material. Whereas the character of muscovite→montmorillonite is largely due to the structure and charge which the muscovite→montmorillonite inherits from the original muscovite, the "typical" montmorillonite is aggraded largely from a glass or gel and inherits no established structure or charge, but only chemical characteristics, and is a separate entity. To be able to differentiate between these various types of montmorillonite can be of considerable geological and agricultural significance.

POTASSIUM "FIXATION"

In the past twenty years many papers have described potassium "fixation" by montmorillonite (Volk, 1934; Truog and Jones, 1938; Page and Baver, 1940; Mortland and Geiseking, 1951; Wear and White, 1951; Dyal and Hendricks, 1952; Barshad, 1954). Reitemeier (1951) has defined "fixed" potassium as "applied potassium which is not immediately replaceable by the usual cation exchange reagents as NH_4 acetate." Barshad (1951) has suggested that "the term 'fixed' cations be applied to those present in a mineral with a contracted-type layered lattice resisting replacement by cations that are unable to expand the lattice, notwithstanding the application of the most efficient method of replacement." Accordingly, "the 'NH_4^+-fixation' capacity of a soil or a mineral would be defined as the absorbed NH_4^+ not replaceable by K^+, and 'K^+-fixation' capacity as the absorbed K^+ not replaceable by NH_4^+."

Barshad (1948, 1954) has shown that the amount of "fixation" of K^+ and NH_4^+ is a function of the type of cation used as a leaching agent. Thus " . . . cations present in a contracted crystal lattice (K^+ and NH_4^+) may be replaced by those which bring about an expansion of the crystal lattice (Na^+, Mg^{2+}, Ca^{2+}, Ba^{2+}) but not by those which cannot do so (K^+, NH_4^+)." The larger the size of the clay flake, the more difficult it becomes for the contracting-type cations to migrate into the interior of the flake and, as a result, "fixation" tends to increase as flake size increases (Barshad, 1954). Though no "fixation" measurements were made, the *x*-ray data indicated that Ca^{2+} was much more effective than NH_4^+ in replacing K^+ from the Womble muscovite→montmorillonite.

Barshad (1954) interprets his data to indicate that "fixation" is a function of the amount of total interlayer charge. He has shown that an expanded lattice with an interlayer charge of 150 or more meq per 100 gm. of material heated to 1000° C. will contract to 10.4 Å when saturated with K^+, whereas lattices with a charge of 110 or less meq per 100 gm. have an expansion equivalent to one molecular layer of water (12.4 Å). It appears that for lattices with charges greater than 150 meq per 100 gm., the amount of K^+ "fixed" increases from 51 per cent of the total exchange capacity for a sample with 159 meq per 100 gm. to 99.3 per cent for a sample with a charge of 215 meq per 100 gm. The maximum interlayer charge of the more common layer minerals would presumably be muscovite, which Barshad (1954) reports as having a charge of 262 meq per 100 gm. The muscovite→vermiculite and muscovite→montmorillonite, like Barshad's biotite→vermiculite, also appear to retain much of the high interlayer charge of the original muscovite as shown by their ready collapse to near 10 Å when saturated with K^+.

Truog and Jones (1938) indicated that K^+ could be "fixed" to the extent of 40 per cent of the cation exchange capacity by alternately wetting and drying montmorillonite at 80° C. Mortland and Gieseking (1951) indicated nearly 100 per cent "fixation" by drying the clays from a solution of K_2SiO_3 at 100° C.; however, it was necessary to dry Wyoming bentonite at 400° C. to obtain a contraction to 10 Å. Wear and White (1951) used a milder treatment which consisted of saturating the clay with K^+, washing, drying at 105° C., and wetting and washing with NH_4 acetate. Maximum "fixation" occurred with the Wyoming bentonite where "fixed" K^+ reduced the BEC by 22 to 28 per cent. Using even milder treatment, Barshad (1954) was able to "fix" less than 4 per cent NH_4^+ and less than 8 per cent K^+ in montmorillonite.

Wear and White (1951) reported a slightly greater than 25-per cent reduction in the (001) *x*-ray diffraction maximum of glycolated K^+ "fixed" Wyoming bentonite and believe that this implied that 25 to 30 per cent of the layers were contracted to 10 Å. If 25 per cent of the layers had collapsed to 10 Å they should be detectable in one of two ways: (*a*) by a discrete reflection at 10 Å, in which case it could be assumed that fairly sizeable packets of layers had collapsed to 10 Å and the resulting clay was essentially a discrete mixture of 10-Å and 17.7-Å layers, or (*b*) by a shifting of the 17.7-Å (001) reflection towards 10 Å, indicating a random interstratification of 10- and 17.7-Å layers. The *x*-ray patterns presented do not show either of these effects. Further, Jackson and Hellman (1941) state "It has been found in this laboratory that 0.7 to 0.9 per cent K_2O may be fixed in nonexchangeable form in montmorillonite from bentonite and soil clays without affecting the (001) *x*-ray diffraction line . . . ." As can be seen, the relation between the amount of "fixed" potassium and the number of contracted 10-Å layers is as yet not clear.

Montmorillonite and Nontronite

Both montmorillonites and nontronites have a BEC ranging from approximately 90 to 115 meq per 100 gm. air-dried material (or approximately 110 to 150 meq per 100 gm. of ignited material); however, analysis of the chemical data (Ross and Hendricks, 1945; and Osthaus, 1954, 1955) indicates that montmorillonites generally have from two-thirds to all the total lattice charge originating in the octahedral layer, whereas in the Garfield nontronite approximately 95 per cent of the charge originates in the tetrahedral layer. Three montmorillonites which have similar total interlayer charges but have widely varying ratios of tetrahedral and octahedral substitution were subjected to various potassium treatments (Table 3). In all cases the (00*l*) reflection of the K-treated samples and the glycolated K samples were irrational, indicating that a mixed-layer clay was formed. When the K-treated samples were washed with NH_4Ac a regular (00*l*) series with a fundamental periodicity of 12.4 Å was obtained,

The (00*l*) values for the K-treated samples obviously represent mixed-layered 10- and 12-Å layers; however, in many instances it is difficult to determine the exact ratio of the two types of layers. In several instances it appears that the layers are mixed in two different ratios. Regardless of the exact ratio of the mixed layers, the (001) values of the K-treated samples and the glycolated K samples indicate a shift towards a smaller spacing, therefore an increase in the number of 10-Å layers as the relative amount of tetrahedral charge increases. This is shown by both the room temperature and 90° to 100° C. samples. Of the room temperature sam-

Table 3. Effects of KOH on Various Montmorillonites

Samples	Charge meq[1]	Origin of Charge[2]	KOH Solution Room Temperature[3]	KOH Solution 90–100° C.[4]
Polkville	118	100% Octahedral	1:1 Mixed-layer 10/12.4 plus packets 12.4 (001) = 12.3 (001) = 15.5 e.g.	(001 = 12.1 (001) = 14.0–16.0 e.g.
Wyoming	94	45% Tetrahedral	1:4 Mixed-layer 10/12.4 (001) = 12.1 (001) = 13.5 e.g.	1:1 Mixed-layer 10/12.4 (001) = 11.6 (001) = 15.2 e.g.
Nontronite	115	95% Tetrahedral	1:4 and 3:2 Mixed-Layer 10/12.4 (001) = 12.0 and 11.2 (001) = 13.2 and 11.43 e.g.	2:3 and 7:3 Mixed-layers 10/12.4 plus packets 10.0 (001) = 11.5 and 10.0 (001) = 16, 12 and 10.0 e.g.

[1] Per 100 gm. air-dried material.

[2] Based on analyses by Wear and White (1951) and Osthaus (1954).

[3] Allowed to stand in 1 *N* KOH solution 15 hours, washed with distilled water, dried at room temperature.

[4] 90–100° C., 2 hours in 1 *N* KOH solution, washed with distilled water, dried at room temperature.

ples, only the K-Polkville sample will absorb two layers of glycol; the K-Wyoming and K-nontronite samples, which have considerable tetrahedral charge, will absorb only one layer of glycol.

The room temperature K-Wyoming samples were subjected to a confining pressure of 40,000 psi for two weeks but no further contraction was obtained. When the untreated Wyoming montmorillonite was boiled for 16 hours in a 1 *N* KOH solution, the (001) spacing shifted to 11 Å, indicating that 60 per cent of the layers were contracted to 10 Å. Boiling the nontronite for 16 hours caused a shift to 10 Å, indicating approximately 100-per cent contraction. Caillére and Hénin (1949) were able to contract a montmorillonite to 10 Å by boiling it in a 1 *N* KOH solution for 32 hours. It is certain that boiling these clays for 2 and 16 hours has caused considerable modification of the basic 2:1 lattice; however, the relative difference between the samples is retained. Barshad (1954) believes that it is the magnitude of the interlayer charge rather than the origin which determines "fixation." This may be true for expanded minerals which have an interlayer charge greater than 150 meq per 100 gm. of ignited material; however, as the above data indicate, for expanded 2:1 minerals with an interlayer charge less than 150 meq per 100 gm. of ignited material, the origin of the charge is quite significant in regard to the minerals' ability to "fix" potassium or to contract to 10 Å. These data also suggest why the montmorillonite in marine sediments is seldom pure, but usually contains from 10 to 90 per cent of intergrown 10-Å layers. It seems likely that if nontronite were exposed to sea water for any length of time, it would form a mixed-layer clay. The fact that these K montmorillonites form mixed-layer clays indicates that the distribution of charge among the layers is inhomogeneous and that some layers contain considerably more charge than others.

VERMICULITE

Barshad (1954) has shown that vermiculites with a relatively low interlayer charge of around 160 meq per 100 gm. of ignited material on a percentage basis "fix" only about half as much K^+ as those with a charge of 200. Vermiculites with a charge similar to montmorillonite, 106 meq per 100 gm. of ignited material, behave like montmorillonite when saturated with K^+ and contracts to only 12.4 Å.

Barshad's (1954) data indicate that all of his vermiculites with a relatively low interlayer charge (less than 160 meq per 100 gm of ignited material) contained some chlorite, and all of his vermiculites with a relatively high charge (greater than 190 meq per 100 gm of ignited material) were pure or contained biotite. The possibility that the vermiculites containing chlorite were formed from chlorite and that those containing biotite were formed from biotite immediately suggests that there may be some relation between the total charge and the origin of vermiculites.

Biotites in general have an interlayer charge of between 200 and 250 meq per 100 gm. of ignited material. The interlayer charge on a 2:1 chlorite lattice cannot be so readily calculated, since it is difficult to determine the relative amounts of Al_3^+ substituting in the tetrahedral and the two octahedral layers or to unequivocally account for the oxidation state of any iron.

Mica structural formulas are normally cited as 3 Si:Al in tetrahedral coordinations with a net deficiency of 1 charge per four. Chlorite analyses range from about 2.5 Si:1.5 Al to about 3 Si:1 Al, but internal compensation is assumed to reduce the net deficiency to 1 charge or less. No criterion other than hardness seems to be available generally to support the assumption. Gruner's (1934) average vermiculite analysis as cast by Hendricks and Jefferson (1938) for their vermiculite structure indicates 2.75 Si:1.25 Al, comparable with a chlorite mean, but it has since been established that vermiculite has a high capacity to exchange Mg.

A rationalization of the magnitude of vermiculite-layer charges was arrived at by W. F. Bradley as follows.

The mean of Gruner's (1934) analyses, cited by Hendricks and Jefferson (1938) in connection with their vermiculite structure was

$$(OH)_3(Mg_{2.75}Fe^{3+}_{0.25})(Al_{1.25}Si_{2.75})O_9\cdot 3.5\ H_2O.$$

Subsequent observations by Barshad (1948) indicate that of the order of 100 to 200 meq of Mg are exchangeable. If, instead of casting Gruner's average on the basis of seven cations, it be cast on the basis of $7+\frac{1}{2}$ the exchange-capacity cations for a 12 oxygen mica unit, a formula would emerge like

$$Mg_{0.33}(OH)_{2.0}(Mg_{2.55}Fe^{3+}_{0.26}Al_{0.19})(Al_{1.12}Si_{2.88})O_{10}4\ H_2O.$$

It is seen that allowance for exchangeability of Mg reduces the apparent tetrahedral contribution to the net layer charge deficiency and increases the apparent internal compensation by octahedral contribution.

Bradley has provided the following analysis of Grudemo's Sample C.

GRUDEMO SAMPLE C*

		Cations per 100 gm. air dry		Oxygen atoms per 100 gm. air dry	
SiO_2	33.92	5.66	tet=8.00	11.32	
		2.34			
Al_2O_3	16.20	.84	oct=6.01	4.77	
Fe_2O_3	7.12	.89		1.34	
FeO	1.50	.21		0.21	
MgO	19.12	4.07		4.80	
		.73	ex		
exch. capacity meq/100 gm. air dry		1.46			
H_2O (total)	21.12	23.50		11.75	
		3.11	Hydrogen in OH		
				34.19	total
		20.39	water	−.45	correction for Fe^{3+}
				−1.55	correction for (OH) by ignition
				32.19	
				22	oxygen in ignited model
				10.19	

* Grudemo, Å. (1954), An *X*-ray Examination of the Structure of Vermiculites. *Swedish Cement and Concrete Research Institute, Proceedings*, No. 22.

This says that this vermiculite is expressed by the formula:

$$\begin{array}{ll} \text{ex } Mg_{0.73} & \\ (OH)_{3.11}(Si_{5.66}Al_{2.34})((Al_{.84}Fe^{3+}_{.89}Fe^{2+}_{.21}Mg_{4.07} & O_{20.89}\cdot 10.2H_2O. \end{array}$$

Had it not been oxidized it would have been:

$$\begin{array}{ll} \text{ex Mg}_{0.73} \text{———} | & \\ (OH)_4(Si_{5.66}Al_{2.34})(Al_{.84}Fe_{1.10}Mg_{4.07}) | & O_{20}\cdot 10.2H_2O. \end{array}$$

Layer charge is 1.50 as compared to 2.0 for micas and 1.00 for montmorillonites. Broken down the same way the Gruner average used by Hendricks makes:

$$\begin{array}{ll} \text{ex Mg}_{0.86} \text{———} | & \\ OH_{3.84}(Si_{5.84}Al_{2.16})(Al_{.50}Fe^{3+}_{.52}Mg_{4.98}) | & O_{20.52}\cdot 8.9H_2O. \end{array}$$

Layer charge is 1.66, indicating an average exchange capacity around 166 meq/100 gm.

Quality of agreements illustrated

Exch cap'y	By charge	By Mg.
Grudemo	150	146
Gruner	166	172

It therefore seems fair to assume that an upper limit near one charge [per $O_{10}(OH)_2$ unit] exists for vermiculite, and that this limit is most nearly approached by muscovite→vermiculite, closely approached by biotite→vermiculite, and possibly only half reached by chlorite→vermiculite. Vermiculite derived from minerals such as hornblende, serpentine, and talc may have a charge as low as chlorite→vermiculite, possibly ranging as low as a charge of 0.3–0.5 or the charge of a typical volcanic →montmorillonites.

Nine vermiculite samples were studied; two contained considerable amounts of biotite and were believed to have formed from biotite; one sample was obtained by leaching biotite with $MgCl_2$; the other six samples contain such minerals as chlorite, talc, antigorite, and hornblende, and in most cases were formed by alteration of these minerals. It is thought that these last six vermiculites should have a lower interlayer charge than the muscovite→vermiculites and biotite→vermiculites.

Table 4 contains the results obtained when these samples were allowed to stand in a 1 *N* KOH solution for 15 hours, washed with distilled water, and dried at room temperature, and then placed in 90°-100° C. 1 *N* KOH solution for 6 hours, washed with distilled water and dried at room temperature. These results indicate that, when treated with potassium, the biotite→vermiculites readily contract to the 10.2 to 10.3-Å spacing characteristic of biotite. The nonbiotite→vermiculites contract to only 11 to 12.7 Å, indicating the retention of one molecular

TABLE 4. EFFECTS OF KOH ON VARIOUS TRIOCTAHEDRAL VERMICULITES

Sample	Composition	KOH Solution Room Temperature[1]	KOH Solution 90-100° C.[2]	Size
Biotite	Vermiculite (Formed by leaching Biotite with $MgCl_2$)	V=10.2		$<2\mu$
Broderick Mt., Bolton, Mass.	Biotite S Vermiculite W	No effect	V=10.2	100 Mesh
Libby, Montana	Biotite M M.L. Biotite-vermiculite M	V=10.2-11	V=10.4	100 Mesh
Granitized hornblendite, Austin, Tex.	M.L. Biotite-vermiculite M Vermiculite M[3] Hornblende	M.L.=10.2-11 V=12.6	M.L.=10.3 V=11.4	$<2\mu$
Leninite, Lenni. Pa.	Chlorite S Vermiculite W	V=12.4 regular, 00*l*	V=12	100 mesh
Jefferisite, W. Chester, Pa.	Antigorite S Vermiculite W	V=12.4	V=11.5 (M.L. 10.3/14, 7:3)	$<2\mu$
Halite, Pa.	M.L. Chlorite-Vermiculite		No effect	100 Mesh
Roan Mt., North Carolina	Vermiculite S Talc, serpentine, Chlorite	V=12.5 and 14.0	V—11-14.5 (some M.L. Chlorite-Vermiculite present)	$<2\mu$
Corrensite, Franklin Mts., Texas	Regular M.L. Chlorite-Vermiculite[3]		V=12.7	$<2\mu$
Cornwall, England	Vermiculite (fibrous; derived from serpentine)[3]	V=13.0-14.4	V=13.0	100 Mesh

[1] Allowed to stand in 1 *N* KOH solution 15 hours, washed with distilled water, dried at room temperature.

[2] 90-100° C., 6 hours in 1 *N* KOH solution, washed with distilled water, dried at room temperature.

[3] Samples which expand to 17 Å when treated with ethylene glycol.

layer of water between the vermiculite layers. Where good samples were available, as in leninite, it could be seen that the (00*l*) series was regular. A mixed-layer 10.3/14 Å, 7:3 clay was obtained in the case of Jefferisite. In many of these samples a portion of the vermiculite remained expanded to 14 Å after K treatment. However, when some of these samples were boiled in 1 *N* NH_4F for five minutes to remove interlayer Fe and Al, they would contract to 12 Å when subsequently treated with K.

The granitized hornblende contained a mixed-layer biotite-vermiculite and vermiculite. When treated with K, the mixed-layer vermiculite contracted to 10.3 and the unmixed vermiculite to only 11.4 Å. Further, the former would absorb only one layer of glycol but the latter absorbed two layers. This indicates that within one sample two types of vermiculite were formed. In this same sample the relatively large vermiculite flakes would absorb only one layer of glycol, whereas the vermiculite in the less-than-two-micron fraction absorbed two layers of glycol.

Vermiculites apparently inherit much of their charge from the original source mineral, as do the montmorillonites, and on the basis of contractability they can be divided into at least two inheritance groups: Those which contract to 10 to 10.3 Å when treated with K (biotite→vermiculites and muscovite→vermiculites) and those which contract to 11 to 12.7 Å when treated with K (nonmica→vermiculites).

Summary and Speculations

The above data need more substantiation, but a number of relations are apparent and some interesting speculations can be made. It is apparent that expanded 2:1 clay minerals of either the vermiculite- or montmorillonite-type can form by the alteration of muscovite, biotite, chlorite, serpentine, talc, and material which does not contain a layer-type lattice (volcanic material, hornblende, feldspar). These expanded minerals appear to have inherited enough of the character of their source material that by proper treatments it should be possible to make a reasonable assumption regarding the source.

Expanded clays (both vermiculite and montmorillonite) derived from muscovite (with a probable interlayer charge greater than 260 meq per 100 gm. of ignited material) will contract to near 10.0 Å when subjected to relatively mild treatment (placed in 1 *N* KOH suspension for 15 hours and dried at room temperature). This same treatment does not usually contract expanded clays derived from biotite, but by warming or boiling the K^+ solution for from 15 minutes to 6 hours these minerals can be made to contract to approximately 10.2 Å. When subjected to these treatments the expanded clays derived from nonmicaceous minerals will in general remain all or partially expanded and afford (001) spacings of 11 to 12.4 Å.

The mild potassium treatment used to contract all the layers of muscovite-derived clays will when used on expanded minerals derived from nonmicaceous minerals apparently contract approximately 40 per cent of the layers to near 10.0 Å if the interlayer charge is primarily tetrahedral in origin. Those clays in which a large portion of the charge originates in the octahedral layer have only 10 to 20 per cent of their layers contracted by this treatment. In order to attain any significant percentage of contracted layers by using potassium with this latter group of clays, it is necessary to apply relatively drastic techniques such as drying at temperatures of 300° to 400° C., alternately wetting and drying at 80° to 110° C., and boiling 20 to 30 hours. With these more drastic techniques it is more than likely that the basic 2:1 lattice is being modified and that it is not the potassium alone which is causing the contraction.

Table 5 summarizes the types of treatment necessary to contract expanded lattices of various interlayer charge. Considerably more data will be required to make a rigid classification of this type, but the present data suggest that a grouping of this sort exists in nature and further that this natural grouping is determined by the original source material.

TABLE 5. POTASSIUM TREATMENT NECESSARY TO CONTRACT EXPANDING LATTICES OF VARIOUS INTERLAYER CHARGE

Source Material	Interlayer Treatment Charge, meq*		(001) Spacing
Muscovite, other micas	260	Soak 15 hr. 1 *N* KOH Sol. Dry at room temperature	10.0 A
Biotite	260–150	Boil 15 min.–6 hr. 1 *N* KOH Sol. Dry at room temperature	10.2–10.4 A
Nonmicaceous Material	<150	Dry at 110°–400° C. from 1 *N* KOH Sol.; wet and dry from 1 *N* KOH Sol.; boil 16 hrs. in 1 *N* KOH Sol.	10.0–12.4 A

* Per 100 gm. of ignited material.

Figure 2 indicates how the contractibility of expanded minerals can provide a clue to the source material from which the expanded minerals are derived. The first division is based on the number of layers which will contract to 10.0 to 10.4 Å when the clay is placed in a 90° to 100° C. 1 *N* KOH solution for 2 to 6 hours, washed and dried at room temperature. More elaborate potassium contraction techniques as discussed above can also be used to provide additional information. Then after it is determined whether the mineral is dioctahedral or trioctahedral a reasonable prediction of the source material can be made. The assignment of source materials, as shown in Fig. 2, is not rigid since there will be some overlap; however, it is believed that the assignment is modal in character and will apply in most instances.

The generally accepted definition of vermiculite (absorb one layer of glycol) and montmorillonite (absorb two layers of glycol) is not a genetic one as both types of expanded lattice can be formed from any of the common source materials. Further, Bradley's (1945) investigations and the present study have shown the occurrence of expanded minerals with vermiculite crystallization which will absorb two layers of glycol. Another definition is based on the origin of the interlayer charge: mostly tetrahedral—vermiculite, mostly octahedral—montmorillonite. On the basis of this definition most saponites, nontronites, and beidellites, all of which absorb two layers of glycol, would be classed as vermiculites. It is obvious that these two definitions are incompatible.

Barshad (1954) has suggested that the difference between these two types of layers is largely one of total interlayer charge; however, this will not be known for certain until the interlayer charge on muscovite→montmorillonite and biotite→montmorillonite is determined. The sharpness of the (00*l*) reflections and the fairly standard sequence of (00*l*) intensities suggest that relatively large grain size and a specific type of crystal orientation are also attributes of the highly charged vermiculite type of layers. There is apparently a complete spectrum of expanded minerals, as clays can be found that contain nearly all possible combinations of these criteria. For example, an expanded clay derived from a chlorite may give the *x*-ray pattern of a typical vermiculite, indicating large grain size and good vermiculite crystallization, but because of low interlayer charge may absorb two layers of glycol and not contract to 10 Å when it is potassium-saturated. Similarly, an expanded clay derived from muscovite may have a high interlayer charge but be fine-grained and have a montmorillonite crystallization.*

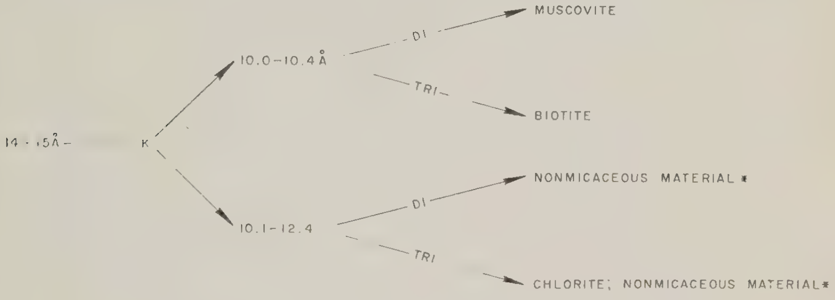

* GENERALLY VOLCANIC AND MAFIC ROCKS AND MINERALS

FIG. 2. Method of obtaining information pertaining to the origin of expanded minerals.

The type of expanded mineral formed is probably a combined function of the type of source material and the type and degree of weathering, with the latter probably being the more important. The present division (absorb one or two layers of glycol) between these two types of expanded minerals is more frequently a reflection of weathering differences than of source differences. The present data suggest that the degree of contractibility affected by potassium is of more genetic significance than the degree of glycol expandability. For example, muscovite alters to expanded clays, some of which will absorb one layer of glycol and others which will absorb two layers; however, both types of expanded clays readily contract to 10 Å when treated with potassium.

---

* It is quite possible that a fundamental difference between these two types of expanded minerals is the relative homogeneity of the silicate sheets. At one extreme are the fine-grained "montmorillonite" minerals which appear to have considerable differences in composition and charge between their silicate sheets; whereas the silicate sheets of the relatively coarse-grained "vermiculite" minerals are probably quite homogeneous.

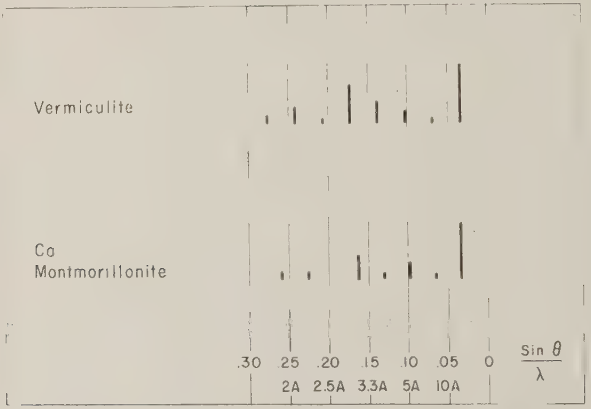

FIG. 3. Characteristic x-ray spacings and intensities of vermiculite and montmorillonite, after Bradley (1953).

It would seem best for the present to divide the vermiculites from the montmorillonites on the basis of the relative sharpness and intensities of their (00l) reflections (Bradley, 1953) (Fig. 3). This division would be based largely on type of crystallization. A further division could then be based on the degree of contractibility when potassium-saturated (Fig. 2). The contractibility would be a reflection of the interlayer charge and, to some extent, the type of source material. Whether the clay absorbed one or two layers of glycol could be the basis of an additional subdivision. Figure 4 is an attempt to organize these easily measured parameters of expanded 2:1 clays and show how these parameters relate one to the other and ultimately to the source material. A useful terminology based on this scheme might be: muscovite-derived vermiculite or muscovite→vermiculite, chlorite→montmorillonite, volcanic→montmorillonite, hornblende→vermiculite. This is only a preliminary scheme and experiments are being continued to determine whether more quantitative potassium and glycol techniques can be used to provide more specific information.

It might be worth while here to consider the agronomist definition of "fixation" as applied to potassium. Agronomists are primarily concerned with the cation and its ease of extractibility (fixation), whereas the mineralogist and geologist are more concerned with the effects of the cation on the clay lattice (contraction) and the implications regarding the lattice composition, which can be inferred from the contraction data. It is apparent from the available data that fixation does not necessarily imply contraction, and conversely contraction does not necessarily imply fixation. Contraction data may provide more useful geologic information than does fixation.

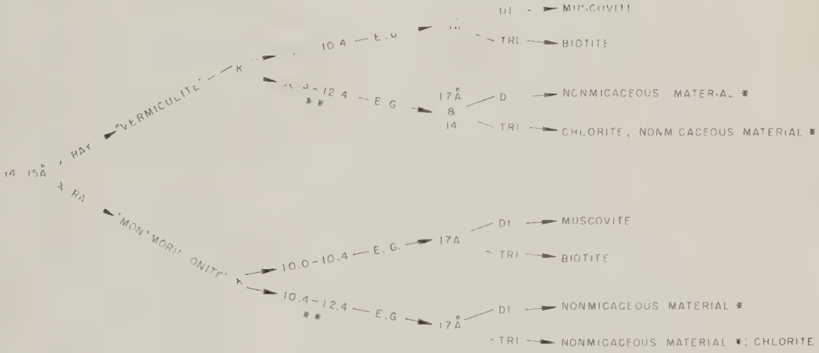

*GENERALLY VOLCANIC OR MAFIC ROCKS AND MINERALS
**10.0/12 4 MIXED-LAYER MINERAL MAY BE FORMED

FIG. 4. Organizational scheme to subdivide the expanding clay minerals into groups, and the relation of these groups to source materials.

The degree of contraction appears to afford some measure of the total charge and the amount of tetrahedral charge in a 2:1 layer lattice. In most cases the amount of contraction will be a function of the expanded mineral's origin; i.e., complete collapse will occur only in those expanded minerals which have a relatively high tetrahedral charge, which would be those derived from mica-type minerals. No collapse would indicate relatively low total charge or a high percentage of octahedral charge, and in most cases, an expanded mineral which formed from nonmicaceous material or chlorite. Expanded minerals, in which only part of the layers contract, would imply intermediate amounts of tetrahedral charge and a probable origin from nonmicaceous material or chlorite. This intermediate group may have inheritance implications which are not yet known. It is possible that the amount of contraction in minerals that do not completely contract is a function of the chemical composition of the source material.

Geological Significance

As the preceding section has indicated, if muscovite→montmorillonite will readily contract to 10 Å when mildly treated with KOH, possibly there is sufficient potassium in sea water to accomplish this contraction. One gram of muscovite→montmorillonite was placed in a gallon of sea water and shaken mildly for 10 days. As can be seen from the x-ray pattern (Fig. 5), a sizable amount of the expanded clay has contracted to 10 Å. The glycolated patterns indicate that the expanded clay formed three discrete phases: completely contracted packets, mixed-layer packets (7:3), and completely expanded packets.

At the end of 30 and 60 days, the first two phases increased in amount and the last phase decreased. When the 30-day sample was dried at 105° C., nearly all the clay contracted to 10 Å. When the muscovite →montmorillonite was evaporated to dryness (60° to 80° C.) three times from sea water, most of it contracted to 10 Å (Fig. 5).

These experiments indicate that expanded clays derived from muscovite and probably biotite are unstable and are not likely to be found in marine sediments. Over 100 marine samples containing expanded 2:1 clays and representing 40 formations were treated with potassium to determine the amount of contraction. In only one highly weathered sample was there any suggestion of appreciable 10-Å contraction. Most of these samples expanded to 12.0 to 12.4 Å after being saturated with potassium. In several of the samples, the x-ray reflection remained at 14 Å. This may be due to the presence of H^+ (and associated Al^{3+}) as the exchangeable cation, which as Barshad (1954) has shown tends to inhibit exchange.

It might be thought that many mixed-layer illite-montmorillonite minerals found in sediments are formed by the weathering of micas. However, samples of 35 mixed-layer illite-montmorillonite clay from 20 marine formations were potassium-treated and none contracted to 10 Å. It seems likely that mixed-layer illite-montmorillonites which were formed by the weathering of micas and deposited under marine conditions have already been contracted to 10 Å by adsorbing the potassium from the sea water.

Four expanded 2:1 clay samples from ancient continental shales were found that contracted to 10 Å when saturated with potassium.

These data suggest that most of the expanded 2:1 clays and intergrowths of expanded and nonexpanded 2:1 clays found in marine sediments were derived from nonmicaceous material and that the expanded clays which were derived from micas have largely reverted to mica. Thus, "stripped" micas or expanded clays derived from micas have only a transient existence, remaining expanded during weathering, transportation, and continental deposition, but reverting to near their original state when deposited, as most of them are, in a marine environment.

This type of transformation is merely a rejuvenation and is frequently cited as an example of the diagenesis of montmorillonite to illite. The actual case is more analogous to going from a Mg or Ca montmorillonite to a Na montmorillonite and back to a Mg or Ca montmorillonite.

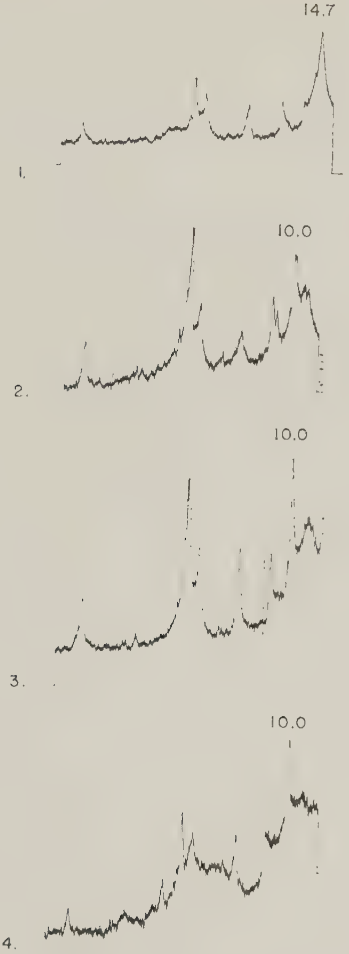

FIG. 5. Womble shale: (1) natural state; (2) in sea water 10 days; (3) in sea water 30 days; (4) evaporated to dryness from sea water 3 times.

$$\begin{array}{c} \text{Mg or Ca montmorillonite} \rightarrow \text{Na montmorillonite} \rightarrow \text{Mg or Ca montmorillonite} \\ \text{Degradation} \qquad\qquad \text{Aggradation} \\ \text{K illite} \rightarrow \text{Ca illite} \rightarrow \text{K illite} \end{array}$$

It has been noted also that although mixed-layer chlorite-vermiculite is quite common in unweathered marine sediments, mixed-layer biotite-vermiculite is rare. This further suggests that the highly charged vermiculite layers derived from biotite when exposed to sea water will contract to near 10 Å, whereas the relatively low-charged chlorite→vermiculite layers will not tend to contract. The low charge in the chlorite →vermiculite is suggested by the fact that the layers usually absorb two layers of glycol and do not contract to 10 Å when treated with KOH.

The montmorillonite in most marine sediments is not a pure montmorillonite but frequently contains 10 to 30 per cent of intergrown contracted 10 Å ("illite") layers and sometimes chlorite layers. If, in areas of relatively slow deposition, it is assumed that the variously charged 2:1 lattices attain some sort of equilibrium with the surrounding sea water, then most volcanic→montmorillonites apparently contain sufficient interlayer charge to afford 10 to 30 per cent of the layers to contract to 10 Å by absorbing potassium from sea water. Expanded clays with a higher interlayer charge, such as bravaisite and the Ordovician K-bentonites, will have 50 to 80 per cent of their layers contracted under similar conditions. The present data on mixed-layer illite-montmorillonite suggest a definite relation between interlayer charge and per cent of contracted 10-Å layers; however, the chemical and x-ray data are not sufficiently accurate to make a positive correlation, nor is it definite that the mixed-layer ratio represents actual equilibrium with sea water; i.e., the original montmorillonite was not in contact with sea water long enough to contract all the layers potentially contractible.

In summary, it might be speculated that for any given expanded mineral there is an equilibrium ratio of expanded to nonexpanded layers which is determined by the location and amount of interlayer charge and the composition of the water in the environment of deposition. Sea water might be considered the standard environment.

It is of interest to note that most of the partially contracted clays that have formed from an expanded lattice by the fixation of potassium have more K_2O than illite clays formed by moderate weathering and mechanical breakdown of muscovite. If all the K_2O in K-bentonite, bravaisite, and most glauconites is assigned to the contracted 10 Å layers, it is found that these layers generally contain 10 to 12 per cent K_2O as contrasted to the 5 to 7 per cent of K_2O normally found in detrital→illites. As both of these types of layers have a relatively high interlayer charge, it is probable that it is slow growth of the aggraded material that allows individual layers to reach an equilibrium condition and absorb the maximum possible amount of potassium. Thus, as might be expected, a high K_2O content between contracted layers might be a reflection of an aggradation and low K_2O of a degradation origin. Further speculation based on scattered data suggests that the K_2O content of illitic material, or the relative amount of aggraded illite, tends to increase with increasing geologic age.

RECENT MUDS

Seventeen mud samples from the Brazos River of central Texas and marine and brackish water samples from the western Gulf of Mexico were saturated with potassium to determine the extent of contractibility. All samples contained an appreciable amount of montmorillonite and/or mixed-layer illite-montmorillonite (1:9 to 3:7). The upstream Brazos River muds obtain most of their clay from soils developed on Pennsylvanian illite, chlorite, and kaolinite shales. A sizable portion of the expanded clay in these river samples contracted to 10 Å, which suggests that it was formed by the weathering of illite. Further downstream, the outcropping sediments are of Cretaceous and Tertiary age and contain an abundance of montmorillonite which is thought to have had a volcanic origin. The expanded clays from the mud in the lower sections of the river showed no detectable contraction to 10 Å when saturated with potassium. The clays all contracted from 14 to 15 Å to 12 to 13 Å. None of the clays from the western Gulf of Mexico showed any detectable 10-Å contraction. As these clays are generally derived from the Cretaceous and Tertiary, this is to be expected. Thus, it appears that "stripped" mica or illite→montmorillonite supply only a minor portion of the clays being deposited in the western Gulf of Mexico and that volcanic→montmorillonite is the major expanded mineral present. As illite is the predominant clay mineral in the sedimentary and metamorphic rocks along much of the Atlantic Coast, it might be expected that much of the expanded clay being supplied to the Atlantic Ocean would have been derived from muscovite and illite. Samples were not available for study, but Powers (1953) has reported that expanded clays from the Patuxent River in Maryland, when treated with potassium acetate, contract to 10 Å; further, he shows that the expanded material progressively disappears as the environment becomes more saline.

In considering the diagenesis of montmorillonite to illite in a marine environment, it would be wise to be more specific as to the source material from which the "montmorillonite" was formed. It seems unlikely that low-charged volcanic→montmorillonites would ever alter to 10-Å illite in a marine environment.

REFERENCES

BARSHAD, ISAAC (1948), Vermiculite and Its Relation to Biotite as Revealed by Base Exchange Reactions, X-ray Analysis, Differential Thermal Curves, and Water Content, *Am. Mineral.*, **33**, 655–678.

——— (1950), The Effect of the Interlayer Cations on the Expansion of the Mica Type of Crystal Lattice, *Am. Mineral.*, **35,** 225–238.

——— (1951), Cation Exchange in Soils: 1. Ammonium Fixation and Its Relation to Potassium Fixation and to Determination of Ammonium Exchange Capacity, *Soil Sci.*, **72,** 361–371.

——— (1954), Cation Exchange in Micaceous Minerals: II—Replaceability of Ammonia and Potassium from Vermiculite, Biotite, and Montmorillonite, *Soil Sci.*, **78,** 57–76.

Bradley, W. F. (1945), Diagnostic Criteria for Clay Minerals, *Am. Mineral.*, **30,** 704–713.

——— (1953), *X*-ray Diffraction Criteria for the Characterization of Chloritic Material in Sediments, *Proc. Second Nat. Conf. on Clays and Clay Minerals*, 324–335.

———, and Weaver, C. E. (1956), A Regularly Interstratified Chlorite-Vermiculite Clay Mineral, *Am. Mineral.* **41,** 497–504.

Brown, G. (1953), The Dioctahedral Analogue of Vermiculite, *Clay Min. Bull.*, **2,** 64–69.

———, and MacEwan, D. M. C. (1950), The Interpretation of *X*-ray Diagrams of Soil Clays, Part II, *Soil Sci.*, **1,** 239–253.

Caillére, S., and Hénin, S. (1949), Transformation of Minerals of the Montmorillonite Family into 10 Å Micas, *Mining Mag.*, **28,** 606–611.

Dyal, R. S., and Hendricks, S. B. (1952), Formation of Mixed Layer Minerals by Potassium Fixation in Montmorillonite, *Soil Sci. Amer. Proc.*, **16,** 45–48.

Gruner, J. W. (1934), The Structure of Vermiculites and Their Collapse by Dehydration, *Am. Mineral.*, **19,** 557–574.

Hathaway, J. C. (1954), Studies of Some Vermiculite-Type Clay Minerals, *Proc. Third Nat. Conf. on Clays and Clay Minerals*, 74–86.

Hendricks, S. B., and Jefferson, M. E. (1938), Crystal Structure of Vermiculites and Mixed Vermiculites-Chlorites, *Am. Mineral.*, **23,** 851–862.

Jackson, M. L., and Hellman, N. N. (1941), *X*-ray Diffraction Procedure for Positive Differentiation of Montmorillonite from Hydrous Mica, *Soil Sci. Soc. Amer. Proc.*, **6,** 133–145.

Kunze, G. W., and Jeffries, C. D. (1953), *X*-ray Characteristics of Clay Minerals as Related to Potassium Fixation, *Soil Sci. Soc. Amer. Proc.*, **17,** 242–244.

MacEwan, D. M. C. (1954), "Cardenite," A Trioctahedral Montmorillonite Derived from Biotite, *Clay Min. Bull.*, **2,** 120–125.

Mortland, M. M., and Geiseking, J. E. (1951), Influence of the Silicate Ion on Potassium Fixation, *Soil Sci.*, **71,** 381–385.

Osthaus, B. B. (1954), Chemical Determinations of Tetrahedral Ions in Nontronite and Montmorillonite, *Proc. Second Nat. Conf. on Clays and Clay Minerals (1953)*, 404–417.

——— (1955), Interpretation of Chemical Analyses of Montmorillonites, *Proc. First Nat. Conf. on Clays and Clay Tech.* (*(1952)*, 95–100.

Page, J. B., and Baver, L. D. (1940), Ionic Size in Relation to Fixation of Cations by Colloidal Clays, *Soil Sci. Soc. Amer. Proc. (1939)*, **4,** 150–155.

Powers, C. P. (1953), *The Adjustment of Land Derived Clays to the Marine Environment*, Ph.D. Thesis, University of North Carolina.

Reitemeier, R. F. (1951), *Advances in Agronomy*, Vol. III, Edited by A. G. Norman, Academic Press Inc., New York.

Rich, C. I., and Obershain, S. S. (1955), Chemical and Clay Mineral Properties of a Red-Yellow Podzolic Soil Derived from Muscovite Schist, *Soil Sci. Soc. Amer. Proc.*, **19,** 334–339.

Rolfe, B. N., and Jeffries, C. D. (1953), Mica Weathering in Three Soils in Central New York, U.S.A., *Clay Min. Bull.*, **2,** 85–93.

Ross, C. S., and Hendricks, S. B. (1945), *Minerals of the Montmorillonite Group*, U. S. Geol. Survey Prof. Paper 205-B, 23–79.

Truog, E., and Jones, R. J. (1938), Fate of Soluble Potash Applied to Soils, *J. Ind. and Eng. Chem.*, **80,** 822–885.

Van der Marel, H. W. (1954), Potassium Fixation in Dutch Soils: Mineralogical Analyses, *Soil Sci.*, **78,** 163–179.

Volk, N. J. (1934), The Fixation of Potash in Difficult Available Forms in Soils, *Soil Sci.*, **37,** 267–287.

Walker, G. F. (1949), The Decomposition of Biotite in the Soil, *Mineralogist*, **28,** 693 703.

——— (1950), Trioctahedral Minerals in the Soil-Clays of North-East Scotland, *Mineralogist*, **29,** 72–84.

———, and Milne, A. (1950), Hydration of Vermiculites Saturated with Various Cations, *Trans. 4th International Congr. Soil Sci.*, Amsterdam 2, 62–67.

Wear, J. I., and White, J. L. (1951), Potassium Fixation in Clay Minerals as Related to Crystal Structure, *Soil Sci.*, **71,** 1–14.

Manuscript received January 6, 1958

THE AMERICAN MINERALOGIST, VOL. 43, SEPTEMBER-OCTOBER, 1958

CALCIUM-BEARING MAGNESIUM-IRON OLIVINES

TH. G. SAHAMA AND KAI HYTÖNEN, *Institute of Geology, University of Helsinki, Finland.*

ABSTRACT

Chemical and optical data are presented for ten calcium-bearing magnesium-iron olivines, five of which are previously unpublished. The *d*-spacings of the plane (130) have been measured for these olivines. Indexed powder patterns and calculated unit cell dimensions of the iron-poor monticellite from Dewey Mine and of a synthetic kirschsteinite are tabulated.

Excluding calcio-olivine and the manganoan olivines, the variation of the chemical composition in the olivine group is diagrammatically presented in Fig. 1. Optical and x-ray identification of olivines belonging to the monticellite-kirschsteinite series, of sub-calcium olivines and of slightly calcian olivines of the forsterite-fayalite series is discussed.

INTRODUCTION

If pure calcio-olivine and the manganoan olivines are excluded, the compositions of olivines may be summarized as in Fig. 1. In natural rocks forsterite and fayalite are known to form solid solutions with each other in all proportions. No evidence has ever been produced that would indicate any immiscibility gap in the sub-solidus range. Despite the common occurrence of olivines of the forsterite-fayalite series in rocks, analyzed olivines of this series never show appreciable contents of calcium. The figures for CaO are usually insignificant and only exceptionally reach 2 percent. From the Island of Fogo, Cap Verde Islands, an olivine with ca. 5% CaO has been reported in 1855 (Doelter, 1914, p. 299), but this information needs verification. Accordingly, the composition of the olivines belonging to the forsterite-fayalite series may be schematically represented by the small open circles on the bottom of Fig. 1.

On the other hand, the olivines of the natural monticellite-iron monticellite series mostly show a very slight deficiency in calcium. The ratio of magnesium to ferrous iron varies within relatively narrow limits. This range of variation that is schematically indicated by the small open circles near the left top of Fig. 1, has been recently expanded through the discovery of a calcium-bearing olivine from Mt. Shaheru in the Nyiragongo area (Sahama and Hytönen, 1957). The composition of this olivine, No. 2 in Fig. 1, lies closer to the iron end member of the series for which the name kirschsteinite was proposed.

Of synthetic orthosilicates corresponding to the natural olivines of Fig. 1, the Mg_2SiO_4–Fe_2SiO_4 series represents one of the most classical examples of unlimited solid solubility. An unbroken solid solution series has also been found between Fe_2SiO_4 and $CaFeSiO_4$ by Bowen, Schairer and Posnjak (1933). The phase diagram of this series contains a minimum melting point and no eutectic. Finally, between $CaMgSiO_4$ and $CaFeSiO_4$

a continuous solid solution series was shown to exist by Schairer and Osborn (1950). In the iron-free Mg_2SiO_4–$CaMgSiO_4$ series, on the other hand, the conditions are different. As has been recently shown by Ricker and Osborn (1954), the solid solubility in this series is very limited. At 1100° C., exsolution was observed in all mixtures except the 10% Mg_2SiO_4 and 10% $CaMgSiO_4$ compositions. At lower temperatures the solid solubility is apparently still more limited.

On the basis of the experience obtained from the above synthetic studies combined with observations on natural olivines, the compositions of calcium-magnesium-iron olivines in proper olivine-bearing rocks may

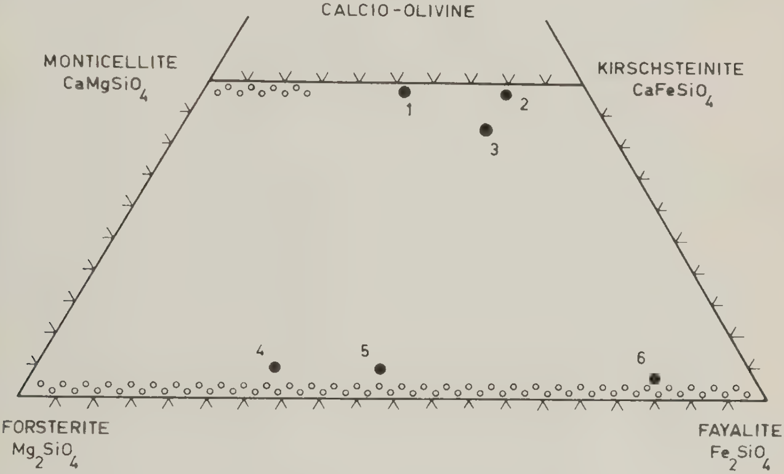

FIG. 1. The calcian-magnesian-ferroan olivines.

1. Ferroan monticellite. VM 394. Shaheru.
2. Magnesian kirschsteinite. S. 80. Shaheru.
3. Sub-calcium olivine. R.G. 22778. Nyiragongo.
4. Calcian hyalosiderite. S. 81. Shaheru.
5. Calcian hyalosiderite. Lunghezza.
6. Calcian ferrohortonolite. S. 90. Baruta.

be anticipated to cover the whole range from monticellite to kirschsteinite. In addition, in contrast to the magnesium end in the field Mg_2SiO_4–$CaMgSiO_4$–$CaFeSiO_4$–Fe_2SiO_4 of Fig. 1, nothing is known at present that would make impossible the existence of olivines intermediate between the monticellite-kirschsteinite and the forsterite-fayalite series close to their iron ends. In analogy to the augitic clinopyroxenes, the olivines of such intermediate compositions may be called sub-calcium olivines. The fact that these hypothetical sub-calcium olivines and, with the exception of olivine No. 2 in Fig. 1, the iron-rich members of the monticellite-kirschsteinite series have not been recognized in nature, might be caused by the great rarity of rock types in which those olivines may crystallize. Olivines of such extraordinary rocks have not been subjected to sufficiently detailed mineralogical study.

The authors of this paper were led to the above views on studying the mineralogy and petrology of the lavas of the Nyiragongo area in North Kivu, Belgian Congo. The rocks of this area are largely melilite-nephelinites with varying ratio of magnesium to iron. Such rocks seem to provide a chemical environment suitable for the formation of olivines of compositions indicated above. For that reason, some of the rock specimens available to the authors from that area were studied with respect to their olivines. The chemical, optical and physical data for these olivines and for samples from other sources are presented.

DESCRIPTION OF SAMPLES

Optical and physical data and calculated molecular compositions for the olivines used in this investigation are summarized in Table 1. The unpublished chemical analyses made of these olivines are collected in Table 2. The source of the specimens is listed below. All *d*-spacings of the plane (130) were measured by the authors according to the method that was used by Yoder and Sahama (1957) for the olivines of the forsterite-fayalite series.

Monticellite. Dewey Mine, San Bernardino Co., Calif. Batch of the original analyzed material chemically and optically investigated by Schaller (1935). Indexed powder pattern measured by the authors is given in Table 3.

Monticellite. Island of Skye, Broadford area, Scotland. Batch of the original analyzed material investigated by Tilley (1951).

Monticellite. Magnet Cove, Ark. Batch of the original analyzed material investigated by Neuvonen (1952).

Ferroan monticellite. Specimen VM. 394. Eastern wall of the Shaheru crater, Nyiragongo area, Belgian Congo. Previously not published. The rock represents a fine-grained compact melilite-nephelinite lava with very few small phenocrysts of melilite, partly altered in the margins, and a few small aggregates of nepheline. The mesostasis consists of beautifully euhedral nepheline prisms poikilitically enclosed in crystals of colorless clinopyroxene, ferroan monticellite and, more rarely, by pale biotite. Magnetite, perovskite, apatite and small amounts of götzenite. A few patches of sodalite ($a_0 = 8.93$ Å). Composition of nepheline 34.7 mol. % Ks. The powder pattern of the separated nepheline fraction indicates presence of kalsilite of composition 98.6 mol. % Ks.

Magnesian kirschsteinite. Specimen S. 80. Northeastern wall of the Shaheru crater, Nyiragongo area, Belgian Congo. Original material in-

Table 1. Optical and Physical Data and Calculated Molecular Compositions of Some Calcian Magnesium-Iron Olivines

	Monticellite	Monticellite	Monticellite	Ferroan monticellite	Magnesian kirschsteinite	Sub-calcium olivine	Synthetic kirschsteinite	Calcian hyalosiderite	Calcian hyalosiderite	Calcian ferro-hortonolite
	Dewey Mine, Calif.	Skye, Broadford area, Scotland	Magnet Cove, Ark.	Shaheru, Nyiragongo area	Shaheru, Nyiragongo area	Nyiragongo, Nyiragongo area	-	Shaheru, Nyiragongo area	Lunghezza, Rome	Baruta, Nyiragongo area
	—	—	—	VM. 394	S. 80	R.G. 22778	—	S. 81	—	S. 90
α	1.641	1.645	1.651	1.674	1.689	1.693	1.696	1.687	1.728	1.792
β	1.649	1.654	1.657	1.694	1.720	1.728	1.734	1.707	1.757	1.827
γ	1.655	1.660	1.664	1.706	1.728	1.735	1.743	1.724	1.772	1.844
$2V\alpha$	80° ±	80°	72°	65°	51°	61°	50° ± 2°	89°	n.d.	55°
Sp. gr.	n.d.	3.09	3.269	3.313	3.434	n.d.	n.d.	3.552	n.d.	4.019
d_{130}	2.9347	2.9392	2.9372	2.9415	2.9489	2.9379	2.9573	2.7927	2.8056	2.8306
Fe_2SiO_4	1.6	5.8	7.2	25.6	38.4	38.9	50	30.2	44.2	79.6
Mn_2SiO_4	—	—	1.3	1.3	2.1	1.9	—	1.2	1.7	3.8
Mg_2SiO_4	50.3	43.9	42.5	24.6	11.3	16.6	—	63.7	49.5	13.2
Ca_2SiO_4	48.1	50.3	49.0	48.5	48.2	42.6	50	4.9	4.6	3.4

TABLE 2. NEW CHEMICAL ANALYSES OF CALCIUM-BEARING MAGNESIUM-IRON OLIVINES

	Ferroan monticellite	Sub-calcium olivine	Calcian hyalosiderite	Calcian hyalosiderite	Calcian ferrohortonolite
	Shaheru, Nyiragongo area	Nyiragongo, Nyiragongo area	Shaheru, Nyiragongo area	Lunghezza, Rome	Baruta, Nyiragongo area
	VM. 394	R.G. 22778	S. 81	—	S. 90
SiO_2	33.57	31.93	36.64	35.12	31.58
TiO_2	0.05	0.28	0.25	0.16	0.28
Al_2O_3	1.95	0.71	0.19	0.44	0.66
Fe_2O_3	1.40	1.87	3.02	1.65	3.26
FeO	19.34	28.94	23.66	34.53	52.97
MnO	1.06	1.50	1.01	1.34	2.64
MgO	11.07	7.33	31.26	22.64	5.22
CaO	30.40	26.15	3.37	2.95	1.84
Na_2O	0.60	0.38	0.18	0.26	0.54
K_2O	0.39	0.32	0.22	0.25	0.53
H_2O+	0.13	0.46	0.23	0.56	0.38
H_2O-	0.05	0.03	0.06	0.10	0.10
Total	100.01	99.90	100.09	100.00	100.00

vestigated by Sahama and Hytönen (1957). Petrographic description of the rock has been given by Meyer and Sahama (1958).

Sub-calcium olivine. Specimen R. G. 22778. Top of Mt. Nyiragongo, Belgian Congo. Previously not published. Petrographic description of the rock has been given by Meyer and Sahama (1958). The rock is sprinkled with vesicles up to 2–3 mm. or sometimes even more in diameter. The vesicles are partly or wholly filled with well-developed crystals of green clinopyroxene, leucite, nepheline, reddish melilite, magnetite and drop-like nodules of pyrrhotite. In addition, these vesicles often contain yellowish or slightly greenish crystals of olivine that may reach the size of 1 mm. and sometimes show good crystal form of a shape indicated in Fig. 2. To separate the olivine for chemical analysis, the rock was crushed with a jaw crusher, not ground. The olivine crystals, thus liberated from the matrix, were collected with heavy liquids, then ground and subjected to a final heavy liquid separation. The deficiency in calcium in relation to the sum of iron, manganese and magnesium is considerably more pronounced than in the olivines of the monticellite-kirschsteinite series of which chemical composition is known. No sign of joint occurrence of two separate olivine phases, calcium-free and calcium-bearing, was detected in the analyzed material by powder pattern

TABLE 3. POWDER PATTERN OF MONTICELLITE FROM DEWEY MINE, SAN BERNARDINO CO., CALIF. FILTERED COBALT RADIATION WITH SILICON STANDARD
Indexing based on $a_0=4.827$ Å, $b_0=11.084$ Å, $c_0=6.376$ Å

hkl	*I*	$2\theta_{\text{obs.}}$	$d_{\text{obs.}}$	$Q_{\text{obs.}}$	$Q_{\text{calc.}}$
020	15	18.525	5.557	0.03238	0.03252
021	35	24.685	4.185	0.05709	0.05711
101	10	26.905	3.845	0.06764	0.06750
111	40	28.475	3.637	0.07559	0.07563
002	15	32.59	3.188	0.09839	0.09836
130	35	35.49	2.9347	0.11611	0.11608
131	100	39.205	2.6661	0.14068	0.14067
112	40	40.48	2.5855	0.14959	0.14940
041	30	41.18	2.5434	0.15458	0.15467
*140	25	43.735	2.4014	0.17340	0.17299
122					0.17379
210	7	44.65	2.3547	0.18035	0.17977
211	5	47.775	2.2088	0.20496	0.20436
*113	15	55.66	1.9159	0.27242	0.27235
222	30	58.96	1.8175	0.30272	0.30252
061	10	60.46	1.7766	0.31682	0.31727
241	7	61.455	1.7505	0.32634	0.32631
133	15	62.655	1.7203	0.33790	0.33739
152	5	63.34	1.7036	0.34456	0.34452
043	5	64.04	1.6870	0.35137	0.35139
* 062	15	67.99	1.5997	0.39077	0.39104

* Broad line.

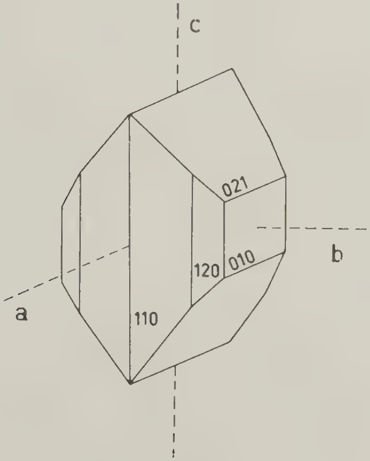

FIG. 2. The shape of the sub-calcium olivine crystals from Mt. Nyiragongo. Specimen R.G. 22778.

TABLE 4. POWDER PATTERN OF SYNTHETIC KIRSCHSTEINITE. FILTERED COBALT RADIATION WITH SILICON STANDARD

Indexing based on $a_0=4.886$Å, $b_0=11.146$ Å, $c_0=6.434$ Å

hkl	*I*	$2\theta_{\text{obs}}$	$d_{\text{obs.}}$	$C_{\text{obs.}}$	$Q_{\text{calc.}}$
020	50	18.445	5.581	0.03210	0.03216
021	35	24.48	4.219	0.05617	0.05631
101	7	26.59	3.895	0.06591	0.06603
111	60	28.20	3.672	0.07416	0.07407
130	100	35.21	2.9573	0.11434	0.11424
040	30	37.43	2.7877	0.12867	0.12864
131	90	38.885	2.6872	0.13848	0.13839
112	95	40.05	2.6121	0.14656	0.14652
041	20	40.91	2.5594	0.15265	0.15279
*140 122	35	43.36	2.4212	0.17058	0.17052 0.17064
132	10	48.545	2.1759	0.21121	0.21084
* 240	60	58.34	1.8351	0.29694	0.29616
062	35	67.51	1.6098	0.38588	0.38604

* Broad line.

or under the microscope. Accordingly, the mineral is to be regarded a sub-calcium olivine intermediate between the monticellite-kirschsteinite and the forsterite-fayalite series. The optical orientation is the same as for the magnesian kirschsteinite from Shaheru.

Synthetic kirschsteinite. Optical data from Schaller (1935) and *x*-ray data on material obtained from Professor C. E. Tilley. The indexed powder pattern measured by the authors is summarized in Table 4.

Calcian hyalosiderite. Specimen S. 81. Southern wall of the Shaheru crater, Nyiragongo area, Belgian Congo. Previously not published. A brief description of the rock has been given by Meyer and Sahama (1958).

Calcian hyalosiderite. Lunghezza near Rome, Italy. Previously not published. The olivine occurs as well-developed crystals up to ½ mm. in length together with nepheline, leucite, melilite and green clinopyroxene in cavities of a melilite-nepheline-leucitite lava.

Calcian ferrohortonolite. Specimen S. 90. Southern upper part of Baruta, Nyiragongo area, Belgian Congo. Previously not published. A brief description of the rock has been given by Meyer and Sahama (1958).

The analyzed materials for three of the olivines (Shaheru VM. 394; Lunghezza; Baruta S. 90) were slightly contaminated by clinopyroxene. The analyses of these olivines were made by dissolving the materials in hot diluted hydrochloric acid and filtering off the remaining clinopyroxene. The clinopyroxene residue was separately tested by partial analysis to be free from gelatinous silica. Accordingly, the results of the analyses that have been reduced to one hundred percent give the compositions of the olivines free from the clinopyroxene contamination.

MONTICELLITE-KIRSCHSTEINITE SERIES

Iron-rich olivines of the monticellite-kirschsteinite series have so far been found only in the melilite-nephelinite lavas of the Nyiragongo area. Accordingly, with the exception of the magnesian end of the series, optical and physical data for natural olivines of this series are too scarce for constructing determinative charts with the same accuracy as for the olivines of the forsterite-fayalite series. For that reason, no attempt will be made in this paper to prepare such charts. For purpose of identification of the olivines of the monticellite-kirschsteinite series, however, some qualitative statements may be made.

The following review, taken for forsterite and fayalite from Poldervaart (1950) and for monticellite and kirschsteinite from Schaller (1935), summarizes the refractive indices of these olivine end members:

	Forsterite	Fayalite	Monticellite	Kirschsteinite
α	1.636	1.823	1.639	1.696
β	1.651	1.863	1.646	1.734
γ	1.669	1.875	1.653	1.743

If these refractive indices are plotted against the molecular content of the iron component, it will be seen that an accurate determination of the refractive indices alone will serve for distinguishing between the monticellite-kirschsteinite and the forsterite-fayalite series only if the molecular content of the iron component exceeds ca. 40 per cent. If, in addition to the refractive indices, the optic axial angle and/or the specific gravity is known, the distinction between the two series becomes possible even in the magnesian end.

The distinction between the monticellite-kirschsteinite and the forsterite-fayalite series becomes, however, more convenient by powder patterns. The *d*-spacings for the plane (130) of the above natural olivine end members are summarized below. The values for forsterite and fayalite have been taken from Yoder and Sahama (1957) and those for monticellite and kirschsteinite were roughly extrapolated from the data of Table 1.

	$d_{(130)}$		$d_{(130)}$
Forsterite	2.7659 Å	Monticellite	2.934±0.001 Å
Fayalite	2.8328 Å	Kirschsteinite	2.956±0.003 Å

By measuring the value for $d_{(130)}$, the distinction between the two series is unequivocal and, in addition, gives an idea of the ratio of magnesium to iron. Such a determination of the composition of olivine by powder pattern is relatively accurate for the forsterite-fayalite series and, at present, only very rough for the monticellite-kirschsteinite series. No additional optical or other physical data are necessary.

The above statements for the identification of the olivines of the monticellite-kirschsteinite series are valid only if the atomic content of calcium closely equals that of the sum of magnesium and iron (plus the small amount of manganese that is usually present). For a sub-calcium olivine, like R.G. 22778 from Nyiragongo that shows a marked deficiency in calcium, both optical and *x*-ray method alone will yield erroneous values for the content of $CaFeSiO_4$. The molecular content of the kirschsteinite component will be found too high if deduced from the refractive indices and too low if estimated on the basis of the value for $d_{(130)}$. If the two methods give results considerably differing from each other, then it may be deduced that the olivine does not belong to the monticellite-kirschsteinite series proper but represents a sub-calcium variety. Such a discrepancy between the optical and *x*-ray data is actually the case for the sub-calcium olivine from Nyiragongo that is included in Table 1. As a general recommendation it may be stated that, if chemical analysis of an iron-rich olivine supposed to belong to the monticellite-kirschsteinite series will not be undertaken, the result of the *x*-ray determination should be tested by determining the refractive indices.

CALCIAN OLIVINES OF THE FORSTERITE-FAYALITE SERIES

Tables 1 and 2 contain three olivines (Shaheru S. 81; Lunghezza; Baruta S. 90) that represent slightly calcian members of the forsterite-fayalite series. These three olivines occur in melilite-bearing lavas very rich in calcium. If the values for $d_{(130)}$ for these calcian olivines are plotted in the *x*-ray determinative curve that has been published by Yoder and Sahama (1957), the fictive points will be found clearly above the curve. The amount of calcium contained in these olivines is sufficient to make the *x*-ray method inapplicable. This conclusion is illustrated by the following data:

$\frac{Mg}{Mg+Fe(+Mn)}$	Calcian hyalosiderite	Calcian hyalosiderite	Calcian ferrohortonolite
According to	Shaheru S. 81	Lunghezza	Baruta S. 90
Chemical analysis	67.0 mol. %	51.9 mol. %	13.7 mol. %
$d_{(130)}$*	60.0	37.5	3.3
Refractive indices†	73	50	17

* Calculated according to the equation given by Yoder and Sahama (1957).

† According to the chart published by Poldervaart (1950).

The molecular content of the forsterite component is found too low with the x-ray method and mostly too high by determining the refractive indices. If the optical and the x-ray method give results clearly differing from each other, then the olivine may be expected to contain more calcium than is generally the case with the olivines of the forsterite-fayalite series.

ACKNOWLEDGMENTS

The authors are greatly indebted to the following contributors of specimens: Dr. Waldemar T. Schaller, of the U. S. Geological Survey, Washington, D. C. (Dewey Mine); Professor C. E. Tilley, of the University of Cambridge, England (Skye, synthetic kirschsteinite); Dr. K. J. Neuvonen, of the Geological Survey of Finland, Helsinki (Magnet Cove); Mr. André Meyer, of the Geological Survey of Belgian Congo, Goma (Shaheru VM. 394); Dr. Lucien S. Cahen, of the Musée Royal du Congo Belge, Tervuren, Belgium (Nyiragongo R. G. 22778); Professors Ettore Onorato and Mario Fornaseri, of the University of Rome, Italy (Lunghezza). The chemical analyses of Table 2 have been made by Mr. Pentti Ojanperä, of the Geological Survey of Finland, for which deep gratitude is expressed. The expenses of the analyses were covered by funds obtained from the Government Scientific Council of Finland. The authors are grateful for this generosity.

REFERENCES

BOWEN, N. L., SCHAIRER, J. F. AND POSNJAK, E. (1933), The system, Ca_2SiO_4-Fe_2SiO_4: *Am. Jour. Sci.*, **25,** 273.

DOELTER, C. (1914), Handbuch der Mineralchemie, II Erste Hälfte, p. 299.

MEYER, A. AND SAHAMA, TH. G. (1958), Study of the volcano Nyiragongo. A progress report: Institut des Parcs Nationaux du Congo Belge, Mission d'études vulcanologiques, fascicule 2.

NEUVONEN, K. J. (1952), Heat of formation of monticellite and merwinite: *Am. Jour. Sci.*, Bowen volume, 373.

POLDERVAART, ARIE (1950), Correlation of physical properties and chemical composition in the plagioclase, olivine, and orthopyroxene series: *Am. Mineral.*, **35,** 1067.

RICKER, R. W. AND OSBORN, E. F. (1954), Additional phase equilibrium data for the system CaO-MgO-SiO_2: *Jour. Am. Ceram. Soc.*, **37,** 133.

SAHAMA, TH. G. AND HYTÖNEN, KAI (1957), Kirschsteinite, a natural analogue to synthetic iron monticellite, from the Belgian Congo: *Min. Mag.*, **31,** 698.

SCHAIRER, J. F. AND OSBORN, E. F. (1950), The system CaO-MgO-FeO-SiO_2: I. Preliminary data on the join $CaSiO_3$-MgO-FeO: *Jour. Am. Ceram. Soc.*, **33,** No. 5, 160.

SCHALLER, WALDEMAR T. (1935), Monticellite from San Bernardino County, California, and the monticellite series: *Am. Mineral.*, **20,** 815.

TILLEY, C. E. (1951), The zoned contact skarns of the Broadford area, Skye: a study of boron-fluorine metasomatism in dolomites: *Min. Mag.*, **29,** 621.

YODER, H. S., JR. AND SAHAMA, TH. G. (1957), Olivine X-ray determinative curve: *Am. Mineral.*, **42,** 475.

Manuscript received January 15, 1958

THE AMERICAN MINERALOGIST, VOL. 43, SEPTEMBER-OCTOBER, 1958

THE ALKALI FELDSPARS: IV. THE COOLING HISTORY OF HIGH-TEMPERATURE SODIUM-RICH FELDSPARS*

J. V. SMITH, *The Pennsylvania State University*

AND

W. S. MACKENZIE, *Manchester University, England.*

ABSTRACT

A redetermination of part of the alkali feldspar solvus has been made using single crystal x-ray methods to obtain the composition of the sodium-rich phase of a natural cryptoperthite subjected to various heat treatments. This solvus differs considerably from that previously determined by Bowen and Tuttle for synthetic feldspars. The discrepancy is believed to be caused by errors in the determination from powder patterns of the compositions of the separate phases of perthites and by metastability of the synthetic feldspars in the temperature range of the solvus.

Single crystal x-ray photographs of some natural sodium-rich high-temperature alkali feldspars revealed several different orientations for the twinned components and the perthitic units of unmixed crystals. Interpretation of the x-ray photographs in the light of the position of the monoclinic-triclinic inversion and the revised position of the solvus has given information on the cooling history of these specimens.

INTRODUCTION

Bowen and Tuttle (1950) made one of the most significant advances in the study of the feldspars when they determined experimentally the position of the solvus for synthetic alkali feldspars. Although evidence for exsolution in the alkali feldspar series had been available from a number of previous studies, the experimental proof of its existence and the determination of its position were of the greatest importance. The amount of calcium in most natural alkali feldspars, with the exception of some sodium-rich specimens, is sufficiently small for the effect of calcium in raising the temperature of the solvus to be neglected: in addition it was shown that the position of the solvus is virtually independent of pressure (O. F. Tuttle, personal communication). For these two reasons it appeared that this was a very valuable geologic thermometer and a number of investigators have attempted to use it as such. However, many perthitic feldspars (orthoclase and microcline perthites) cannot be homogenized except by heating at temperatures well above the crest of the experimentally determined solvus (660° C.) and the position of the solvus must, therefore, be affected by the Si, Al arrangement in the unmixed components. Since the synthetic feldspars used by Bowen and Tuttle (1950) to determine the position of the solvus are almost certainly metastable in the temperature range 500°-670° C., and natural feldspars belonging to the sanidine-anorthoclase series (Tuttle, 1952) are probably closer to the stable form of the feldspar at this temperature range, a more reliable measurement of the position of the stable solvus should be obtainable from natural high-temperature specimens.

---

* Contribution No. 57-49, College of Mineral Industries, The Pennsylvania State University.

This paper presents the results of a new determination of part of the alkali feldspar solvus obtained from a study of the change in composition of the sodium-rich phase of a natural crypto-perthite subjected to various heat treatments. In addition, information on the cooling history of a number of sodium-rich alkali feldspars has been obtained by interpretation of the crystallographic relations found in single-crystal *x*-ray patterns and in the light of the revised position of the solvus.

An optical and *x*-ray study of a series of natural alkali feldspars obtained mainly from volcanic rocks was given in paper III of this series (MacKenzie and Smith, 1956). These quickly cooled specimens were found to have retained their high-temperature structure and with two exceptions belong to the sanidine-anorthoclase series. Specimens in the composition range $Or_{60}(Ab+An)_{40}$ to $Or_{25}(Ab+An)_{75}$ were found to be unmixed but could be rendered homogeneous by heating at 700° C. for a few hours. When homogeneous, specimens more sodium-rich than $Or_{37}(Ab+An)_{63}$ are triclinic, whereas more potassium-rich specimens are monoclinic.

Because the high-temperature albite structure can accommodate both potassium and calcium, it is desirable at this stage to make a clear distinction between a high-temperature plagioclase, an anorthoclase and a sanidine. For this purpose the compositional properties of the monoclinic-triclinic inversion may be utilized. Those homogeneous triclinic high-temperature feldspars which invert reversibly to monoclinic symmetry before beginning to melt are called anorthoclases, those which begin to melt before acquiring monoclinic symmetry are plagioclases and those high-temperature feldspars which are monoclinic are called sanidines. The compositional fields of these three types are shown in Fig. 1 (modified slightly from MacKenzie, 1952). Upon heating, the boundary between the triclinic and monoclinic high-temperature sodium-rich feldspars changes and an attempt to delineate the change with temperature has been made in Fig. 1 on the basis of the limited data at present available. Thus all anorthoclases invert to sanidines at elevated temperatures but high-temperature plagioclases do not. In petrography no confusion in nomenclature should arise since observations are normally made at room temperature.

The alkali feldspar solvus

Bowen and Tuttle (1950) determined the position of the alkali feldspar solvus by crystallizing homogeneous glasses of composition $Or_{50}Ab_{50}$;

$Or_{45}Ab_{55}$ and $Or_{40}Ab_{60}$ at temperatures below 660° C. They obtained two feldspars, the compositions of which were estimated from the diffraction angles of the $\overline{2}01$ planes in *x*-ray powder diffraction patterns. They were also able to unmix a previously crystallized homogeneous feldspar of composition $Or_{45}Ab_{55}$ by holding it at 530° C. in the presence of water vapor under pressure. Bowen and Tuttle emphasized that these syn-

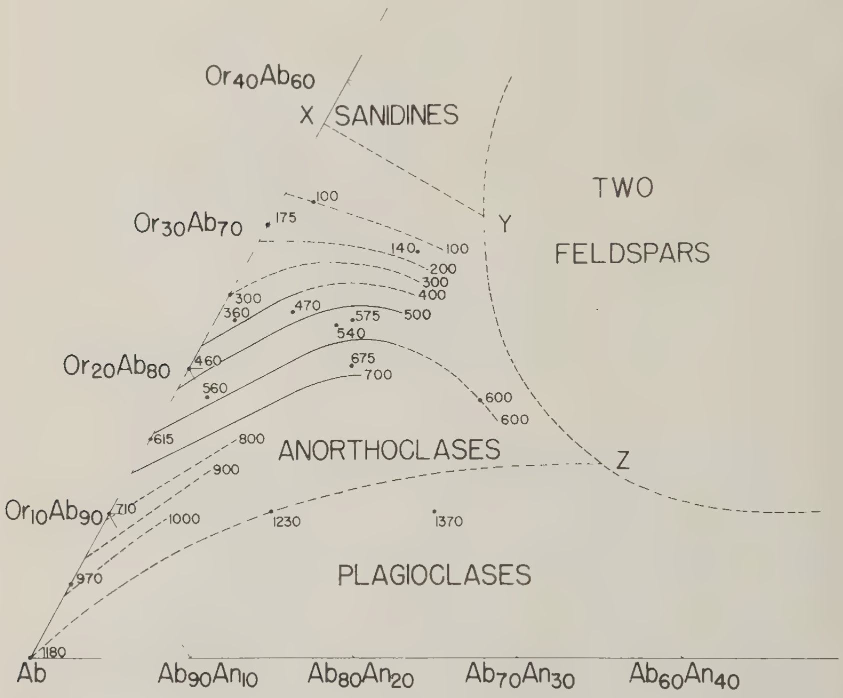

FIG. 1. Triangular diagram showing the composition fields of high-temperature ternary feldspars (modified from MacKenzie, 1952). The compositions of some natural and synthetic feldspars are plotted and the temperature of the monoclinic-triclinic inversion is given for each point plotted. Isotherms of the monoclinic-triclinic inversion temperatures are drawn, the data (MacKenzie, 1952; Laves, 1952, being very limited where the lines are dashed. The boundary between the fields of one feldspar and of two feldspars is arbitrarily drawn through $Or_{10}Ab_{50}An_{40}$, $Or_{20}Ab_{60}An_{20}$ and $Or_{40}Ab_{50}An_{10}$.

The one feldspar field has been divided into the fields of sanidine, anorthoclase, and high-temperature plagioclase by the line XY and the line from Ab to Z. Homogeneous high-temperature feldspars in the plagioclase field are triclinic at all temperatures. Triclinic feldspars in the field Ab Z X Y are called anorthoclases. All anorthoclases become monoclinic at a particular temperature that varies with the composition as shown by the isotherms. All monoclinic high-temperature feldspars are called sanidine. The extent of the sanidine field varies with temperature, gradually taking over the anorthoclase field as the temperature is raised.

thetic feldspars retain the characteristics of high-temperature feldspars. The same authors also determined the composition of the separate phases in a number of perthitic feldspars both in their natural state and after the various heat treatments, and they very kindly placed their results and the heated samples at our disposal.

Using single crystal *x*-ray methods we have made a new determination of the sodium-rich part of the alkali feldspar solvus and we believe that this represents more closely the equilibrium solvus than that previously determined. The material selected for this purpose was a sanidine-cryptoperthite from Korea ($Or_{47.4}Ab_{52.1}An_{0.5}$) described by Spencer (1937) and denoted as specimen P. This specimen was chosen because of its low calcium content and because of the relatively simple pattern given by single crystal *x*-ray diffraction. The effect of heat treatment of the sodium-rich phase was studied by measuring the reciprocal lattice angles α^* and γ^* of the pericline twinned sodium-rich phase from single crystal *x*-ray photographs using the method described in paper II of this series (Smith and MacKenzie, 1955) and from these angles determining the chemical composition of the sodium-rich phase using the data of Donnay and Donnay (1952). After each period of heat treatment an *x*-ray photograph was taken and the reciprocal lattice angles α^* and γ^* measured, the data are set down in Table 1. In Fig. 2 curves are drawn of the variation in α^* and γ^* with chemical composition for anorthoclases and high-temperature albite using the values determined by Donnay and Donnay (1952) for synthetic feldspars of composition $Or_{30}Ab_{70}$, $Or_{20}Ab_{80}$, $Or_{10}Ab_{90}$ and the value determined for high-temperature albite by Smith

TABLE 1. RECIPROCAL LATTICE ANGLES OF THE SODIUM-RICH PHASE OF SPECIMEN P. ($Or_{47.4}Ab_{52.1}An_{0.5}$)

Number of crystal	Heat treatment	α^*	γ^*	Or content (from Fig. 2)
1	unheated	87°56′	89°0′	25.5%
1	then 17 hrs. at 433° C.	87°43′	88°59′	24.0%
1	then 23 hrs. at 470° C.	87°51′	89°2′	25.5%
1	then 16 hrs. at 490° C.	88°9′	89°5′	27.5%
1	then 16 hrs. at 515° C.	88°17′	89°7′	28.5%
1	then 20 days at 525° C.	88°42′	89°14′	30.5%
2	105 days at 400° C.	87°20′	88°45′	20.5%
3	95 days at 500° C.	88°30′	89°19′	30.5%
4	8 days at 425° C.	88°1′	89°1′	26.0%
5	8 days at 450° C.	88°1′	88°57′	26.0%
6	8 days at 475° C.	88°14′	89°9′	28.0%
7	8 days at 560° C.	90°0′	90°0′	≧37.0%

(1956). Feldspars more potassic than $Or_{37}Ab_{63}$ are monoclinic and so have $\alpha^*=\gamma^*=90°$. The values of α^* determined for the sodium-rich phase of each of the heat-treated crystals are joined by a vertical line to the determined values of γ^* and the position of the vertical line adjusted so that the deviations of α^* and γ^* from the reference curves are equal. The ends of the lines all fall close to the two reference curves and if the error in the chemical composition depends only on the error in determining the reciprocal lattice angles the predicted composition should be accurate to $\pm 1\frac{1}{2}\%$ Or. There are, however, other errors to be considered and these will be discussed below.

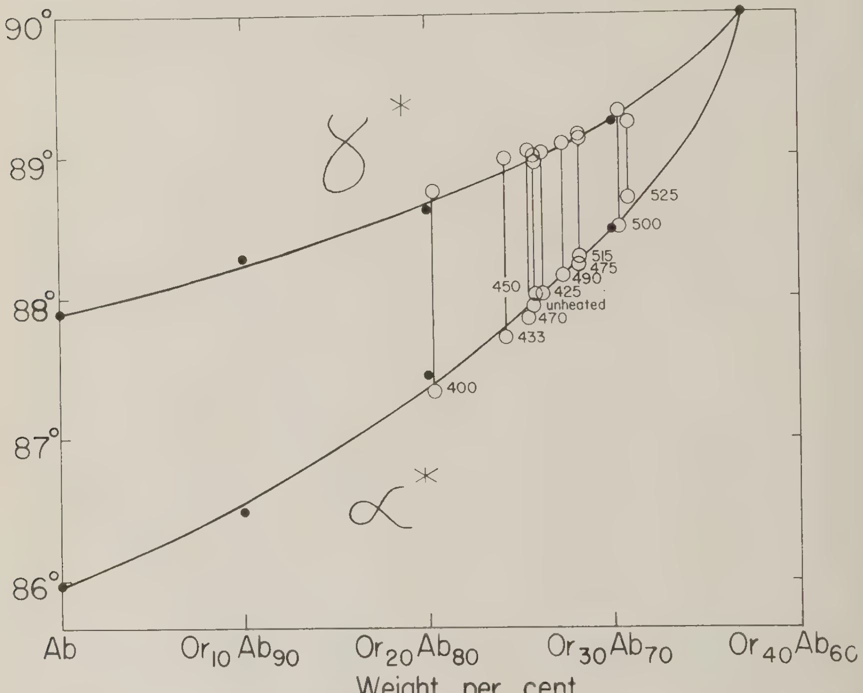

FIG. 2. Curves relating changes in the reciprocal lattice angles α^* and γ^* with chemical composition for the anorthoclases: data from Donnay and Donnay (1952) and Smith (1956) are plotted as solid circles. The values of α^* for the sodium-rich phase of heat treated samples of specimen P (Spencer, 1937) are joined by vertical lines to the values of γ^* and the lines adjusted so that α^* and γ^* show equal deviations from the reference curves. The temperature of heat treatment is given beside each point. The estimated compositions of the sodium-rich phase are given in Table 1.

Before heating, the sodium-rich phase of specimen P had lattice angles which indicated a composition $Or_{25.5}(Ab+An)_{74.5}$. Heating for several hours between 400° C. and 500° C. produced no appreciable change in the lattice angles, but longer periods led to significant changes. Heating for 105 days at 400° C. decreased α^* and γ^* whereas treatment at 500° C. for 95 days increased them, from which it may be deduced that specimen P is in a state that would be stable at some temperature between 400° C. and 500° C. Heating for 20 days at 525° C. produced little change over that achieved at 500° C., but on heating at 560° C. for 8 days the sodium-feldspar component became monoclinic giving a two-sanidine perthite. As the composition of the symmetry change is $Or_{37}(Ab+An)_{63}$ the solvus should pass through this composition at some temperature not higher than 560° C. The data are given in Table 1 and plotted in Fig. 3 in which a curve is drawn as close as possible to the points representing the longer periods of heating. This curve is believed to give a good representation to the sodium-rich boundary of the solvus in the range 400°–550° C.

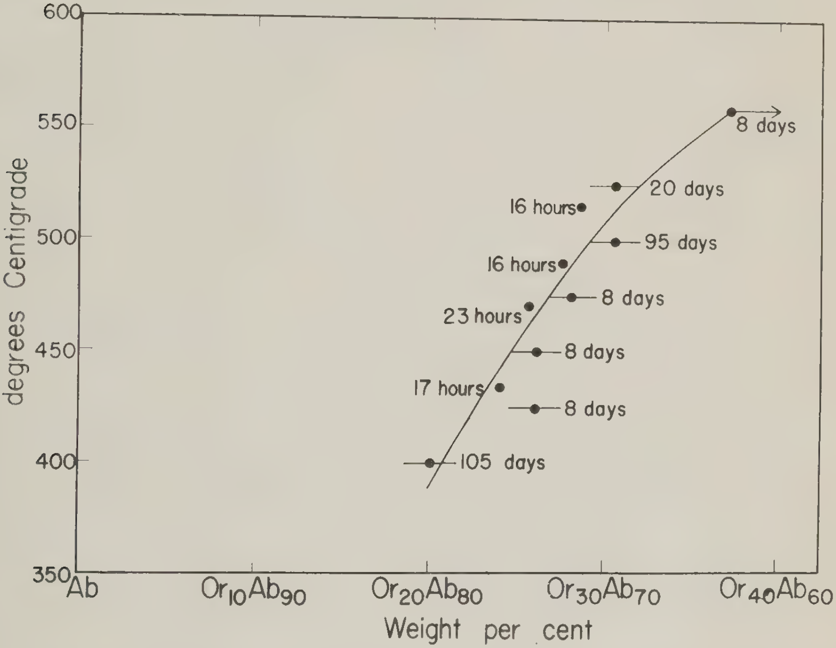

FIG. 3. Plot of the composition of the sodium-rich phase of heat treated samples of specimen P against temperature. The estimated error in the determination of chemical composition ($1\frac{1}{2}\%$ Or) is marked for the runs of longer duration. The curve of best fit is drawn through the points with a strong bias towards the runs of longer duration.

In Fig. 4 three solvi are shown. Curve A represents the solvus deter-

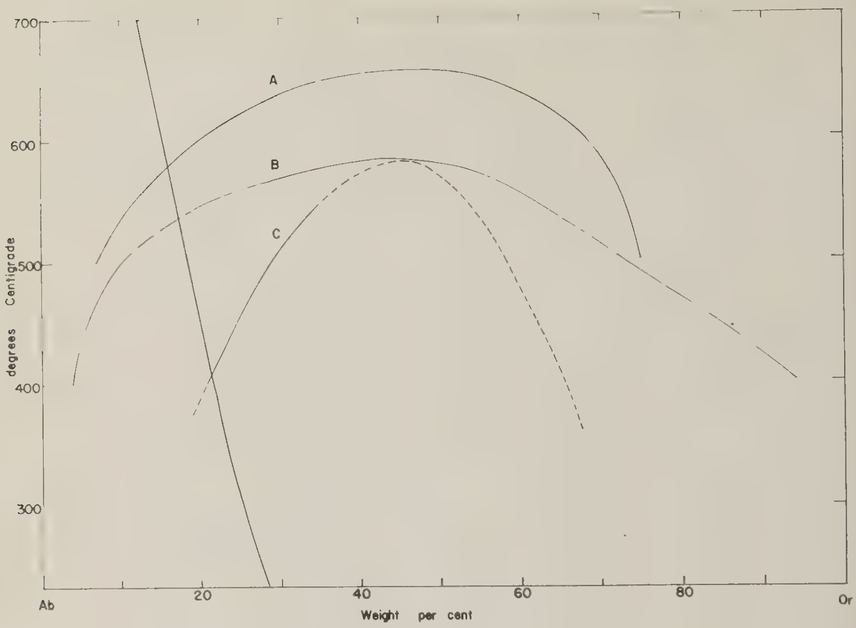

FIG. 4. Curves representing various determinations of the alkali feldspar solvus. Curve A is the solvus determined by Bowen and Tuttle (1950) from synthetic feldspars using the $\bar{2}01$ method. Curve B is the solvus determined by Tuttle and Bowen (unpublished data) from a natural sanidine-cryptoperthite using the $\bar{2}01$ method. The solid line part of curve C is that part of the solvus determined in the present study and reproduced from Fig. 3: the dashed part of curve C is inferred from the known boundaries between unmixed and homogeneous natural feldspars.

The curve showing the relation between chemical composition and temperature of the symmetry change in anorthoclases is reproduced from MacKenzie (1952).

mined for synthetic specimens by Bowen and Tuttle (1950) and curve B the solvus determined by Bowen and Tuttle for specimen P using the ($\bar{2}01$) method for the estimation of composition. The continuous part of curve C represents that part of the solvus determined in the present study and the broken line represents the position of the solvus inferred from the known boundaries between unmixed and homogeneous natural sanidine-perthites (MacKenzie and Smith, 1956). As the immiscibility gap for orthoclase and microcline perthites is even larger than in sanidine perthites, the stable solvus must continue to approach the Ab and Or sidelines as the temperature falls.

It is obvious that there are large discrepancies to be explained. The discrepancy between the two sets of results on specimen P can be explained if either or both of the methods give an incorrect estimate of the composition. It is now well known that the 201 method is inaccurate for perthitic materials because Laves (1952), Coombs (1954) and MacKenzie and Smith (1956) have noted that impossible results are commonly obtained for the compositions of the separate phases of orthoclase perthites. The error is believed to result from the lattice distortion caused by strain between the unmixed components. Despite this evidence for lattice distortion we believe that the lattice angles α^* and γ^* give a good estimate of the composition of the sodium-rich phase for the following two reasons. First, the values of α^* and γ^* for the soda-rich phases in orthoclase, sanidine and anorthoclase perthites have all been reasonable and not in conflict with the values obtained from homogeneous sodic feldspars (Donnay and Donnay, 1952, MacKenzie and Smith, 1955, 1956). Secondly, the heating experiments of specimen P showed that ionic movement was becoming sluggish at 400° C. and consequently the boundaries between homogeneous and unmixed volcanic specimens would be expected to be near the positions of the solvus at this temperature. The observed sodic boundary, $Or_{20}(Ab+An)_{80}$ (paper III), agrees well with the solvus determined from α^* and γ^* but disagrees strongly with the solvus determined from the $(\bar{2}01)$ spacing. Additional confirmation of the validity of the α^* and γ^* angles is given by agreement of the boundary composition with the compositions Or_{16} to Or_{25} determined from the α^* and γ^* angles of the exsolved sodic phases of sanidine perthites (paper III).

The position of the crest of the solvus would be unaffected by errors in α^*, γ^* and the $(\bar{2}01)$ spacing and the discrepancy between the crests for the specimen P and the synthetic feldspar probably must be ascribed to some structural difference, the most likely variation being in the Si, Al arrangement.

It seems certain that both factors have contributed to differences in the position of the solvi shown in Fig. 4, and we believe that the small part of the solvus determined by us is more applicable to natural feldspars and is probably closer to the equilibrium solvus than that determined by Bowen and Tuttle.

TWINNING IN TRICLINIC FELDSPARS

Laves (1950) made an important contribution to our knowledge of twinning in feldspars when he discovered that in the cross-hatched twin structure of microcline the twin axis *b* of the pericline twins was normal to the twin plane (010) of the albite twins. He noted that this arrangement would not be expected if twinning occurred while the microcline were triclinic for there is no simple crystallographic relationship, based on the triclinic unit cell, between the *b* axis and the (010) plane. However, the arrangement could be readily understood if twinning had occurred as the result of inversion from a monoclinic phase, for parts of the crystal could retain the diad axis and other parts the plane of symmetry. The validity of the argument was strengthened when Laves (1952) found a similar twin structure in some anorthoclases, for in this case it can be shown in the laboratory that anorthoclases acquire monoclinic symmetry on heating and revert to triclinic symmetry on cooling.

Laboratory studies have shown that, except possibly for pure albite, plagioclase feldspars do not acquire monoclinic symmetry on heating and must crystallize directly as triclinic crystals (MacKenzie, 1952). Thus we should not expect to find the twin axis of the pericline twins lying normal to the twin plane of the albite twins. Single crystal x-ray photographs of plagioclase crystals twinned on both laws generally show that there are three components which may be denoted A, B, and C: B is related to A by the albite law and to C by the pericline law. The b axis and the 010 plane of unit B are not perpendicular and the crystallographic relations of the twin structure are consistent with the triclinic symmetry. Sometimes more than three components occur, say A, B, C, D, E. . . . In this case alternate pairs AB, CD, EF, . . . are related by one twin law and BC, DE, . . . by the other. Laves (1952, p. 558) has noted that it is geometrically impossible for the fourth unit in sequence to be related to the first unit by a twin relation. [This repeated twinning may explain some of the discrepancies commonly noted in angular measurements of plagioclase twins, discrepancies which have led to the postulation of vicinal faces and compositional differences in the twin components among other things (see Barber, 1935, for example), for it is possible that angular comparison may unwittingly be made between units A and D of a sequence of albite and pericline twins.] For convenience, the two types of twin relationship will be designated 'M' and 'T'; for the remainder of the paper these will be understood to have a genetic significance indicating that twinning occurred either during inversion from a monoclinic crystal (M type) or directly in a triclinic crystal (T type).

The different origins of the twinning lead to characteristic optical differences. Although the twin lamellae sometimes intersect in plagioclases it is more common to find an area which is pericline twinned and an adjacent area which is albite twinned. In anorthoclases the two sets of twin lamellae can be seen in a suitable orientated section to intersect very frequently, giving an appearance that has variously been described by the adjectives cross-hatched, tartan or quadrille. One exception has been noted, an anorthoclase from Mt. Franklin which has the plagioclase type of twinning. X-ray study to be described later in this paper shows that it has the T-type twinning and presumably twinned while triclinic. Thus the presence of cross-hatching can be used to characterize an anorthoclase, but the presence of the first type of twinning does not necessarily indicate a plagioclase, though the inference is strong. Twinned microclines generally show the cross-hatched or quadrille twin structure but the lamellae are frequently spindle-shaped in contrast to the parallel sides of the anorthoclase lamellae. The difference is probably caused by the different character and velocity of the monoclinic-triclinic inversions: the sanidine-anorthoclase inversion is displacive and almost instantaneous whereas the sanidine-microcline inversion is caused by order-disorder of Si and Al atoms and is extremely sluggish.

From a study of the crystallographic relations between twin components and unmixed phases of anorthoclase perthites, it should be possible to deduce something about the crystallization history of the containing rock, and such attempts have been made in the next section for several specimens.

THE CRYSTALLIZATION HISTORY OF SOME HIGH-TEMPERATURE ALKALI FELDSPARS

A detailed study of the single crystal *x*-ray photographs of a few of the sanidine and anorthoclase-cryptoperthites described in paper III of this series (MacKenzie and Smith, 1956) has been made and a brief description of four of these specimens is given below. Each of the *x*-ray photographs was taken in the standard orientation used by the present authors, i.e. a 15° oscillation about the morphological *b*-axis of the crystal, the (001) plane being set in the center of the arc of oscillation.[1] By using this one orientation, interpretation of the photographs is simplified as they can be directly compared with one another.

In Fig. 4, in addition to the three solvi represented by curves A, B, and C, the curve showing the relation between composition and temperature of the change in symmetry in the anorthoclases is reproduced (MacKenzie, 1952). This diagram will be referred to in discussing the sequence of changes in the cooling of alkali feldspars.

a) Sanidine cryptoperthite from Cebolla Creek ($Or_{40.3}Ab_{57.6}An_{2.1}$).

This specimen consists of a monoclinic potassium phase and a four-component triclinic sodium phase twinned on the albite and pericline laws such that the relation is of the M type. The *x*-ray oscillation photograph is reproduced in Fig. 5 and a key to its interpretation is

---

[1] Because cryptoperthites consist of more than one phase and commonly have albite or pericline twinning of the triclinic phase, the simplest method of specifying the axis of oscillation is to refer to the morphological axis of the crystal. Generally when a monoclinic potassium phase is present its orientation is that of the morphology of the crystal.

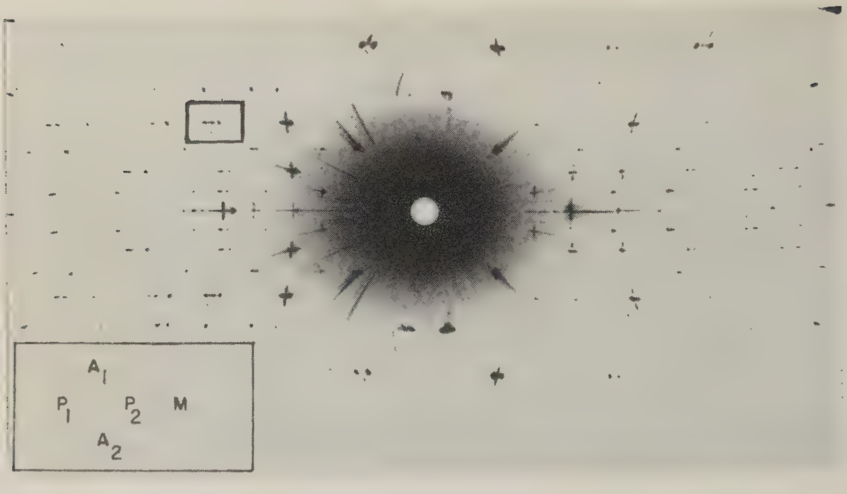

FIG. 5. Sanidine cryptoperthite from Cebolla, Creek, *b* axis oscillation photograph with the *x*-ray beam parallel to (001) in the center of a 15° oscillation. The inset diagram in the bottom left hand corner provides a key for the interpretation of the reflections enclosed in the small rectangle in the upper left. There are five components: A_1A_2 and P_1P_2 are albite and pericline twins of the soda-rich phase and M is the monoclinic potash phase. The components are related by the M type of association because reflections P_1 and P_2 lie on the same layer lines whereas reflections from A_1 and A_2 lie on bent layer lines symmetrically related to the P_1P_2 layer lines. The *b* twin axis, therefore, is perpendicular to the (010) twin plane. The M reflections lie on the same layer lines as the P_1P_2 reflections indicating unmixing from an original homogeneous monoclinic phase.

given as an inset. The twin elements of the sodium-rich phase are coincident with the symmetry elements of the potassium-rich phase and this relation indicates that the unmixing took place from a monoclinic crystal: it also indicates that the twinning of the sodium-rich phase took place on inversion from monoclinic to triclinic symmetry. Most sanidine cryptoperthites show only pericline twinning of the sodium-rich phase but those which show both albite and pericline twinning will be expected to have this special orientation.

If this specimen cooled under equilibrium conditions it would have begun to unmix at 560° C. (see Fig. 4) and the two monoclinic phases would have changed in composition along the solvus until at about 400° C. the sodium-rich phase of composition $Or_{21}(Ab+An)_{79}$ changed to triclinic symmetry and adopted the M type twinning. From measurements of α^* and γ^* (Table 2), the composition of the sodium-rich phase was estimated to be $Or_{21}(Ab+An)_{79}$, and it appears that unmixing has not proceeded below the inversion temperature: if unmixing had occurred below this temperature, additional reflections, as in the photographs of the next specimen, would have been expected.

Table 2. Reciprocal Lattice Angles of the Sodium-Rich Phase of Cryptoperthites

Specimen	Albite twinning		Pericline twinning	
	α^*	γ^*	α^*	γ^*
Cebolla Creek	87°30′	88°38′	87°28′	88°36′
Grande Caldeira				
1	not present		88°15′	89°2′
2	88°18′	89°9′	88°18′	89°9′
Mt. Franklin	87°40′	88°46′	87°32′	88°42′
Victoria	87°6′	88°30′	not present	

b) Anorthoclase cryptoperthite from Grande Caldeira, Azores ($Or_{31.7}Ab_{66.5}An_{1.8}$).

Some of the crystals show the M type of relation between the albite and pericline twins of the sodium phase together with a potassium phase which gives three sets of *x*-ray reflections (see Fig. 6). (Other crystals show only one twin law.) One set of reflections from the potassium phase has its *b* axis parallel to the *b* axis of the pericline twinned units of the

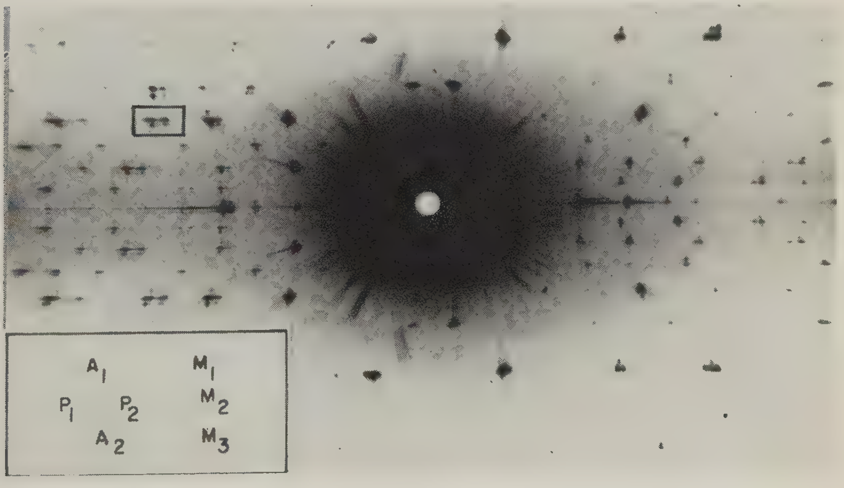

Fig. 6. Anorthoclase cryptoperthite from Grande Caldeira, *b* axis oscillation photograph with the *x*-ray beam parallel to (001) in the center of a 15° oscillation. The inset diagram at the bottom left provides a key for the interpretation of the reflections enclosed in the rectangle at the upper left. There are seven components: $A_1A_2P_1P_2$ are albite and pericline twins of an anorthoclase showing the M type of association; $M_1M_2M_3$ are three potassic components. The reflections from M_1 and M_3 lie in the same bent layer lines as the reflections from A_1 and A_2, and the reflections from P_1P_2 and M_2 also lie on the same layer lines. Hence M_1A_1, M_3A_2, $P_1P_2M_2$, respectively, have parallel *b* axes.

sodium phase, while the other two have their *b* axes parallel, one each, to the *b* axes of the albite twins of the sodium phase. This arrangement would be expected from a specimen which unmixed after inverting from monoclinic to triclinic symmetry: on inversion the M type twinning was produced and from each of the four twinned units a potassium-rich unit exsolved with its *b* axis constrained to be parallel to the *b* axis of the host; since the *b* axes of the pericline twinned units are identical there are three sets of reflections for the potassium-rich phase. However, it is possible that some unmixing occurred before the inversion temperature was attained: in this case, unmixing would have continued after the inversion had occurred in the sodic component.

Reciprocal cell angle measurements (Table 2) indicate that the composition of the sodium-rich phase is $Or_{29}(Ab+An)_{71}$ so that the unmixing has not proceeded very far. If no unmixing had occurred before inversion, the specimen would have become monoclinic at 100° C. (MacKenzie, 1952): if unmixing had occurred before inversion the sodic component could have inverted at a temperature not higher than 200° C. Under equilibrium conditions unmixing would have begun at 525° C. It may be concluded that the lava in which these crystals occur was extruded and quenched at some temperature above 525° C. and that most, if not all, of the unmixing now observed took place at a very low temperature near 100° C., probably over an extended period of time.

c) Anorthoclase cryptoperthite from Mt. Franklin ($Or_{24.9}Ab_{67.5}An_{7.6}$).

This specimen was described as a homogeneous anorthoclase in paper III of this series but some crystals have now been found to be unmixed. This difference in crystals from the same sample indicates that cooling of the feldspar in the temperature range in which unmixing took place has been too rapid for the attainment of equilibrium. The photograph in Fig. 7 shows the *x*-ray diffraction pattern obtained from an unmixed crystal of this sample, and a key to the interpretation of the photograph is given as an inset. The sodium-rich phase shows three sets of reflections (A, B, and C) and the potassium-rich phase two sets of reflections (D and E). A and B are albite twinned and B and C are pericline twinned so that this is an example of T type twinning in an anorthoclase indicating that twinning was acquired from a triclinic untwinned crystal.

From the *x*-ray photograph it can be seen that the sets B, C and E have parallel *b* axes and also that A and D have parallel *b* axes (reflections D cannot be seen clearly except on the original film). Thus the unmixing must have occurred after the twinning was adopted and it is known that the twinning did not form on inversion to triclinic symmetry (assuming that the crystal was originally monoclinic). An approximate value of

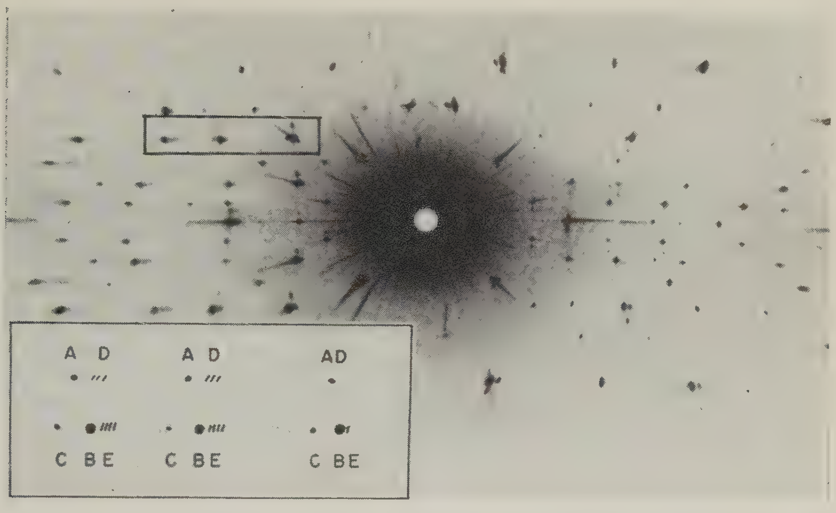

Fig. 7—Anorthoclase cryptoperthite from Mt. Franklin, *b* axis oscillation photograph with the *x*-ray beam parallel to (001) in the center of a 15° oscillation. The inset diagram provides a key to the reflections occurring in the small rectangle. The soda-rich phase gives three sets of reflections, ABC: reflections from B and C lie on the same layer lines so B and C are pericline twinned; reflections from A and B lie on the same row lines so A and B are albite twinned. This is the T type of association and is readily recognized from the groups of three reflections lying at the corners of a numeral 7. The D and E reflections have their *b* axes parallel to A and BC respectively. The extent of unmixing has been slight, for the reflections from D and E are weak and diffuse, so weak in fact that they are only barely visible on the reproduction of the *x*-ray photograph.

500° C. for the temperature of the monoclinic triclinic inversion for this specimen may be obtained from Fig. 1, and since the twinning did not occur as a result of this inversion, the bulk of the unmixing occurred at a much lower temperature. A feldspar of composition $Or_{25}Ab_{75}$ would begin to unmix at about 450° C. (see Fig. 4) and this specimen with 7.6% An should, under equilibrium cooling, begin to unmix at a considerably higher temperature. It is not surprising to find some homogeneous crystals as well as unmixed crystals in the same sample since the unmixing has occurred metastably at low temperature.

d) Anorthoclase-cryptoperthite from Victoria, Australia ($Or_{23.3}Ab_{75.5}$-$An_{1.2}$).

This specimen was described in some detail in paper III but the evidence from the *x*-ray photograph and from the other data available were somewhat conflicting. In the light of the new determination of the solvus these difficulties can be resolved. The *x*-ray photograph of this crystal is reproduced in Fig. 8 and the feldspar can be seen to consist

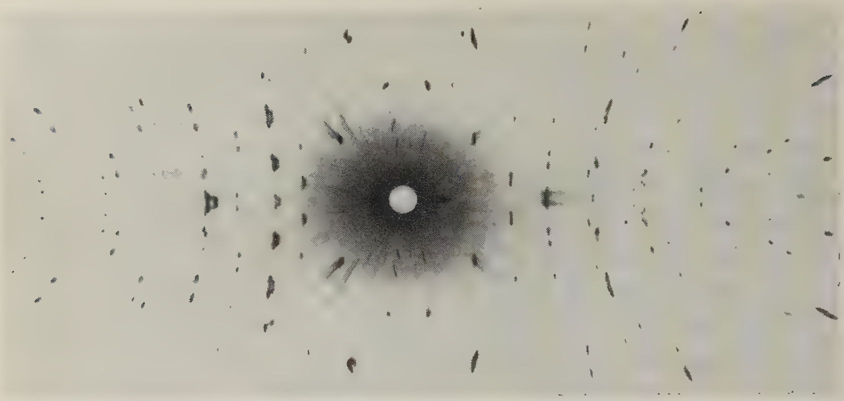

FIG. 8. Anorthoclase cryptoperthite from Victoria, *b* axis oscillation photograph with the *x*-ray beam parallel to (001) in the center of a 15° oscillation. There are four components, two soda-rich and two potash-rich. The reflections occur in groups of four lying at the corners of a trapezium, the trapezium being outlined by diffuse streaks linking the corners. Both pairs of components are in the positions required for albite twinning, the apparent deviation from monoclinic geometry of the potassic phase being smaller than that for the sodic phase.

of two phases. The sodium-rich phase is albite twinned and the potassium-rich phase consists of two units, the *b* axes of which lie between the positions required for monoclinic symmetry and for parallelism with the *b* axes of the albite twinned sodium phase. Since only albite twinning of the sodium phase is present it cannot be stated whether the twinning was formed from a triclinic or monoclinic crystal. The bulk chemical composition of this specimen corresponds very closely to that of the intersection of the solvus and the monoclinic-triclinic inversion curve, and it is likely that the process of unmixing began just after the specimen had turned into an anorthoclase. From each of the albite twin lamellae unmixing occurred and the potassium-rich component 'adopted' the *b* axis of the dominant sodium-rich component. The strain between the unmixed phases has resulted in triclinic symmetry of the potassium-rich phase as is shown by the difference in intensity of the (hkl) and ($h\bar{k}l$) reflections. The streaks connecting the corresponding reflections of the sodium and potassium phases are in harmony with the above interpretation.

This is the same material as that investigated by Tuttle (1952) who found that the crystals of this specimen were optically monoclinic in their natural state but after heating until homogeneous and then cooling they were distinctly triclinic. The optically monoclinic symmetry in this material may be due either to the sub-microscopic albite twinning or to the cryptoperthitic unmixing or to a combination of both of these factors. It is possible that the optical symmetry of this specimen in the unmixed state may be related to its bulk composition but until other anorthoclases of similar composition are investigated such a suggestion must be considered very tentative.

Conclusions

From the observations reported here it is clear that the cooling of natural anorthoclases may be a non-equilibrium process and for this reason caution must be used in attempting to interpret the cooling history of a rock from the alkali feldspars alone.

The use of a mineral as a geologic thermometer depends on a measurable variation of some property which is temperature dependent. As has already been noted, the compositions of the unmixed phases of alkali feldspars would appear to provide an ideal thermometer since the position of the solvus is virtually independent of pressure. However, the relation between the rate of cooling and the rate at which unmixing can occur at equilibrium will determine whether the temperature is that of crystallization of the feldspar or that of final consolidation of the rock or even merely the temperature at which no further unmixing in the solid state can occur because of the slowing down of ionic movement at lower temperatures. It is believed that unmixing of an alkali feldspar of intermediate composition is sufficiently rapid to approach equilibrium in a cooling magma provided sufficient fluxes are available for fluid to exist at temperatures in the range 600° C.–500° C. However, in the case of a sodium-rich or potassium-rich feldspar encountering the solvus below 450° C. 500° C. the rate of attainment of equilibrium may not be sufficiently great to permit an interpretation of the exact meaning of the temperature which is determined. Studies of the rates of unmixing of nephelines in the system $NaAlSiO_4$ -$KAlSiO_4$ (Tuttle and Smith, 1958) have shown the strong influence of the bulk composition of the homogeneous crystal, the rate of unmixing at any particular temperature being much more sluggish for compositions near the boundaries of the solvus.

The intersection of the solvus by the monoclinic-triclinic inversion curve does increase the possible usefulness of the solvus as a temperature indicator. Thus our conclusion that the Grande Caldeira feldspar was unmixing metastably in a temperature range near 100° C. could only be reached because of the existence of the monoclinic-triclinic inversion and our knowledge of the relation between temperature and composition for this inversion. Likewise the conclusion that the Mt. Franklin feldspar did not unmix under equilibrium conditions on encountering the solvus was based on the crystallographic evidence of the relation between the temperature of formation of the twinning and the unmixing process.

The optical and x-ray data at present available indicate that there are an infinite number of stable forms of both sodium and potassium feldspar between the highest and lowest temperature forms. The most useful phase diagram, therefore, is one showing stable equilibrium relations, since there will be an infinite number of possible metastable equilibrium diagrams. That part of the alkali feldspar solvus which we have redetermined is believed to represent stable equilibrium relations more nearly than the previously determined solvus. It cannot be assumed that changes in the feldspars of volcanic rocks have taken place under stable equilibrium conditions but, provided this factor is recognized, useful information is nevertheless obtainable. In plutonic rocks it is possible that the changes in the alkali feldspars have often occurred under conditions approaching those of stable equilibrium and in subsequent papers we shall deal in some detail with the alkali feldspars in certain granites.

ACKNOWLEDGMENTS

The writers wish to express their indebtedness to Dr. O. F. Tuttle and the late Dr. N. L. Bowen for providing feldspar samples and the data they obtained from them. We are grateful to Dr. J. Zussman for his kindness in taking a number of x-ray photographs of alkali feldspars.

REFERENCES

BARBER, C. T. (1936), The Tertiary igneous rocks of the Pakokku district and the Salingyi township of the lower Chindwin district, Burma, with special reference to the determination of the feldspars by the Fedoroff method: *Mem. Geol. Surv. India*, **48,** 121–296.

BOWEN, N. L., AND TUTTLE, O. F. (1950), The system $NaAlSi_3O_8$—$KAlSi_3O_8$—H_2O: *Jour. Geol.*, **58,** 489–511.

COOMBS, D. S. (1954), Ferriferous orthoclase from Madagascar: *Mineral. Mag.*, **30,** 409–427.

DONNAY, G., AND DONNAY, J. D. H. (1952), The symmetry change in the high-temperature alkali-feldspar series: *Am. Jour. Sci.*, **Bowen Volume,** 115–132.

LAVES, F. (1950), The lattice and twinning of microcline and other potash feldspars: *Jour. Geol.*, **58,** 548–571.

——— (1952), Phase relations of the alkali feldspars: *Jour. Geol.*, **60,** 436–450, 549–574.

MACKENZIE, W. S. (1952), The effect of temperature on the symmetry of high-temperature soda-rich feldspars: *Am. Jour. Sci.*, **Bowen Volume,** 319–342.

——— AND SMITH, J. V. (1955), The alkali feldspars: I. Orthoclase-microperthites: *Am. Mineral.*, **40,** 707–732.

——— AND ———, (1956), The alkali feldspars: III. An optical and x-ray study of high-temperature feldspars: *Am. Mineral.*, **41,** 405–427.

Smith, J. V. (1956), The powder patterns and lattice parameters of plagioclase feldspars. I. The soda-rich plagioclases: *Mineral. Mag.*, **31**, 47–68.

——— and Mackenzie, W. S. (1955), The alkali feldspars: II. A simple *x*-ray technique for the study of alkali feldspars: *Am. Mineral.*, **40**, 733–747.

Spencer, E. (1937), The potash-soda feldspars. I. Thermal stability: *Mineral. Mag.*, **24**, 453–494.

Tuttle, O. F. (1952), Optical studies of alkali feldspars: *Am. Jour. Sci.*, **Bowen Volume**, 553–567.

——— and Smith, J. V. (1958), The nepheline-kalsilite system. II. The phase relations, in press.

Manuscript received January 21, 1958

THE AMERICAN MINERALOGIST, VOL. 43, SEPTEMBER-OCTOBER, 1958

SIGNIFICANCE OF AMPHIBOLE PARAGENESIS IN THE BIDWELL BAR REGION, CALIFORNIA

Robert R. Compton, *Stanford University, Stanford, California.*

Abstract

In the northwest Sierra Nevada, regionally extensive low-grade metabasaltic rocks containing abundant actinolite [$(Na,K)_{0.35}Ca_{1.9}(Mg,Fe'')_{4.4}Al_{0.4}(OH)_{1.6}Si_{7.7}Al_{0.3}O_{22}$] are converted to hornblendic rocks in the contact aureole of a small batholith. Hornblende in the outer part of the aureole is associated with oligoclase, epidote, and minor chlorite, and has the composition $(Na,K)_{0.35}Ca_{1.7}(Mg,Fe'')_{4}(Fe''',Al)_{1.1}(OH)_{1.9}Si_{6.7}Al_{1.3}O_{22}$, while hornblende in the inner part of the aureole is associated with andesine (and locally clinopyroxene), and has the composition $(Na,K)_{0.4}Ca_{2}(Mg,Fe'')_{3.8}(Al,Fe''')_{1.1}(OH)_{1.7}Si_{6.7}Al_{1.3}O_{22}$. The abrupt conversion of actinolite to aluminous hornblende in the outer part of the aureole contrasts with gradational conversions in some regionally metamorphosed schists, and this contrast is probably caused largely by differences in the dehydration and reaction rates of the two environments. Ferrohastingsite [$(Na,K)_{0.8}Ca_{2}(Fe'',Mg)_{3.8}(Fe''',Al)_{1}(OH,Cl)_{2.1}Si_{6}Al_{2}O_{22}$] formed in the inner part of the aureole from rocks (metatuffs) low in Si and high in Fe. Igneous hornblende that crystallized with biotite in the border zone of the batholith has the composition $(Na,K)_{0.5}Ca_{1.9}(Mg,Fe'')_{4.4}(Fe''',Al)_{0.8}(OH)_{0.8}Si_{7.1}Al_{0.9}O_{22}$.

Introduction

Amphiboles are essential constituents of almost all of the abundant metavolcanic rocks of the northern Sierra Nevada, and also occur widely in granitic rocks that have been emplaced into this terrane. In general, the metamorphic amphiboles are products of two plutonic episodes, the first being low temperature dynamothermal metamorphism on a regional scale, and the second contact metamorphism by the granitic intrusions. Much of the igneous amphibole formed directly from the more mafic granitic magmas, but some is doubtless the result of contamination of acidic magmas by amphibole-rich metamorphic rocks. Because reactions involving amphiboles are very important in the evolution of the Sierran rocks, and because little is known about the exact nature of these minerals, pure amphibole samples were separated from five rocks that form a reasonably well known genetic series. The purposes of this paper are to present the chemical compositions and physical properties of these minerals and to consider the reactions involved in their formation, especially the conversion of actinolite to aluminous hornblende.

Petrologic Basis of the Study

The general geologic setting of the Bidwell Bar region has been described elsewhere (Compton, 1955), and only the most necessary relations will be presented here. The region is an excellent one in which to explore the general amphibole evolution outlined above because almost all the metamorphic rocks have similar (basaltic) compositions, the relations between these rocks and a small granitic batholith are well exposed, and the contact metamorphic aureole around the batholith is distinct. Moreover, the aureole shows progressive variations of texture and mineralogy that indicate variation in metamorphic intensity, and it was mapped in two zones on the basis of textural criteria. The outer contact of the aureole was drawn where greenschists and greenstones give way (in a few hundred feet) to fine-grained tough hornfelses, and the contact between the outer hornfels zone and the inner zone of the aureole was drawn where metamorphic amphibole is clearly visible to the unaided eye. The contact between the batholith and the metamorphic rocks is generally sharp, but veins and nodes of tonalite occur widely in the inner zone of the aureole, some being intrusive and some metasomatic.

Although the aureole zones were not mapped on the basis of thin sections, the cartographic units can be correlated with gross petrographic variations. The dominant mineral assemblage outside the aureole is actinolite-albite-epidote-chlorite; in the outer zone of the aureole it is hornblende-oligoclase-epidote (locally with chlorite); and in the inner zone of the aureole it is hornblende-andesine (locally with clinopyroxene). The metasomatic veins in the inner zone generally consist of andesine or labradorite, hornblende, and quartz, while the intrusive veins consist of andesine or oligoclase, quartz, hornblende, and biotite.

The five analyzed amphiboles were chosen so as to give a picture of amphibole variation correlative with the critical changes in this paragenesis. One is from the low grade regional terrane, one from the outer zone of the aureole, two from the inner zone of the aureole, and one from an intrusive outlier of the batholith. The specimen from the regional terrane is a mafic greenstone that lies 6,000 feet outside the aureole. It is especially important to this study because a large part of the analyzed actinolite clearly pseudomorphs igneous clinopyroxene, while the same actinolite is abruptly overgrown here and there by thin rims of green metamorphic hornblende identical to that of the contact aureole. Thus two-stage amphibole reactions are well displayed, and the sharpness of the overgrowths of aluminous hornblende is important in the interpretation of the actinolite-hornblende reaction. The specimen is of further interest because it shows that partial contact metamorphism extended far beyond the mapped aureole.

The second amphibole is from a hornfels that lies near the middle of the outer zone of the aureole. The rock contains less epidote than most metabasaltic rocks of the outer zone; however, it was selected because the presence of chlorite suggested its amphibole might be intermediate between actinolite and the aluminous hornblendes of the inner zone, a suggestion that was not borne out by the chemical analysis.

The first of the two amphiboles from the inner zone was separated from an amphibolite that lies only 200 feet from the batholith, and is veined by tonalite that is probably metasomatic. The separation utilized only the amphibolite, although the hornblendes of amphibolite and veins are physically identical. Like several other amphibolites from the immediate contact zone, this rock contains small amounts of clinopyroxene, and it may well represent the most advanced stage of contact metamorphism.

The second amphibole from the inner zone is from a ferrohastingsite schist that is interbedded with andesine-hornblende amphibolites and biotite-quartz-hornblende-oligoclase schists about 2,500 feet from the batholith. It is of interest in this study because similar ferrohastingsites occur in several parts of the inner zone, and this mineral is the only unusual amphibole of the entire complex.

Finally, the hornblende separated from the mafic outlier of the batholith occurs only a few feet from a sharp intrusive contact with typical amphibolite of the inner zone. The abundance of hornblende at such contacts with amphibolites, and the heterogeneity of the border tonalites suggest that the hornblende of the tonalite might well have formed by contamination of a more acidic magma by amphibolite (Compton, 1955, p. 33–37). The purpose of the analysis was to determine the compositional differences between hornblende of the wall rock and hornblende of the new biotite-rich igneous assemblage.

AMPHIBOLES

Separation

The fractionations of the different constituents from the greenstone and the hornfels were complicated by the intricately interdigitated shapes of many of the minerals, yielding a large number of composite grains in all but the finest materials. This was overcome by using very well-sorted fractions of 0.01 to 0.03 mm. size, obtained by repeated decanting of −250 mesh material for settling periods of between 3 and 5 minutes. These well sorted samples responded well to centrifuging in heavy liquids, the principal separatory procedure used. The impurities were counted in all samples submitted for analysis, and in each case amounted to less than 0.5 per cent of the sample.

Compositions

The chemical analyses are listed in Table 1. Analyses 2 and 3 are each the average of two analyses which differed only slightly from the amounts listed. The H_2O^+ determinations were made by the Penfield method, using an oxy-coal gas blast flame.

The numbers of atoms in the formulae of the amphiboles (Table 2)

TABLE 1. COMPOSITIONS AND PHYSICAL PROPERTIES OF FIVE AMPHIBOLES FROM THE BIDWELL BAR REGION, CALIFORNIA

	1	2	3	4	5
SiO_2	53.41	45.33	45.87	38.04	47.80
Al_2O_3	4.56	10.12	11.17	11.09	6.94
TiO_2	0.37	0.54	0.57	0.87	0.80
Fe_2O_3	0.83	5.51	4.82	7.38	4.98
FeO	9.70	14.61	9.72	21.30	9.65
MnO	0.25	0.59	0.25	0.36	0.38
MgO	15.09	10.00	11.69	4.00	14.58
CaO	12.52	10.53	12.62	11.99	12.19
BaO	0.10	0.02	0.03	0.10	0.06
Na_2O	0.88	1.04	1.14	1.40	1.44
K_2O	0.63	0.36	0.29	1.69	0.63
H_2O^+	1.63	1.89	1.73	1.85	0.77
H_2O^-	0.05	0.15	0.32	0.19	0.05
F	0.01	0.01	0.01	0.02	0.06
Cl	n.d.	n.d.	n.d.	0.66	n.d.
P_2O_5	0.04	0.01	0.01	0.11	0.07
Total	100.07	100.71	100.24	101.05	100.40
Less O for F and Cl	0.01	0.01	0.01	0.16	0.03
Total (corrected)	100.06	100.70	100.23	100.89	100.37
Specific gravity	3.07–3.12	3.25–3.29	3.22–3.24	3.39–3.40	3.20–3.21
α	1.626	1.654	1.660	1.692	1.651
γ	1.645	1.674	1.680	1.714	1.670
$\gamma-\alpha$	0.019	0.020	0.020	0.022	0.019
$2V_\alpha$	77–80°	65–69°	64–66°	30–31°	64–67°
$Z \wedge c$	15–18°	16–18°	20–21°	15–17 °	16–18°
Orientation	Y=b	Y=b	Y=b	Y=b	Y=b
X	Colorless	Straw	Straw	Grayish yellow	Straw
Y	Very pale yellow-green	Olive	Olive	Deep olive	Olive
Z	Very pale green	Blue-green	Slightly bluish green	Deep greenish blue	Slightly bluish green

1. Actinolite from mafic greenstone (BB-1-16). Bidwell Bar (7½′) quadrangle; lat. 39°36′12″ N., long. 121°27′39″ W.* Analyst, R. Klemen.
2. Hornblende from hornfelsed metadiabase (BB-4-171c). Bidwell Bar (7½′) quadrangle; lat. 39°33′03″ N., long. 121°25′50″ W. Analyst, R. Klemen.
3. Hornblende from clinopyroxene-bearing amphibolite (F-1-120b). Forbestown quadrangle; lat. 39°35′45″ N., long. 121°19′43″ W. Analyst, R. Klemen.
4. Ferrohastingsite from ferrohastingsite schist (CM-1-11). Clipper Mills quadrangle; lat. 39°35′38″ N., long. 121°14′26″ W. Analyst, R. Klemen (except that Cl determination was made by writer).
5. Hornblende from mafic tonalite (RRC-9). Bidwell Bar (7½′) quadrangle; lat. 39°32′54″ N., long. 121°25′06″ W. Analyst, R. Klemen.

* Note: to plot specimen localities on geologic map of area (Compton, 1955, plate 1), change all latitudes of map from 37° to 39°.

Table 2. Numbers of Atoms in Formulae of Amphiboles from the Bidwell Bar Region, California

		1		2		3		4		5	
(Z)	Si	7.66	8.00	6.72	8.00	6.68	8.00	6.04	8.00	7.06	8.00
	Al	0.34		1.28		1.32		1.96		0.94	
(Y)	Al	0.43	0.56	0.48	1.11	0.61	1.20	0.10	1.07	0.25	0.89
	Ti	0.04		0.06		0.07		0.09		0.09	
	Fe'''	0.09		0.57		0.52		0.88		0.55	
(X)	Mg	3.25	4.44	2.23	4.10	2.57	3.78	0.95	3.83	3.21	4.44
	Fe''	1.16		1.80		1.18		2.83		1.18	
	Mn	0.03		0.07		0.03		0.05		0.05	
(W)	Ca	1.92	2.28	1.69	2.04	1.97	2.33	2.02	2.78	1.92	2.45
	Ba	0.01		0.00		0.00		0.01		0.00	
	Na	0.24		0.28		0.31		0.42		0.41	
	K	0.11		0.07		0.05		0.33		0.12	
	OH	1.56	1.56	1.89	1.89	1.69	1.70	1.96	2.14	0.76	0.79
	Cl	n.d.		n.d.		n.d.		0.17		n.d.	
	F	0.00		0.00		0.01		0.01		0.03	

were calculated on the basis of 24 (O,OH,F,Cl) (Warren, 1930, p. 504–516), and they are close to the values determined structurally by Warren, except that number 5 is distinctly low in the OH group and high in the total of the X and Y groups. The total positive charges of number 5 also are too high, and can be balanced only by assuming that the "vacant" OH positions are occupied by O ions; however, the rather low Fe_2O_3 does not support this possibility. If, on the other hand, it is assumed that the H_2O^+ determination is low, the composition can be recalculated so as to agree reasonably well with the ideal structural ratio of atoms. Since this possibility cannot be certain, however, the values in Table 2 are those calculated from the original analysis.

The impurities were calculated out of the analyses before the atomic compositions of the amphiboles were computed, but these corrections are so small that the only value improved by more than 0.01 of an atom is the Fe''' of amphibole 2, which is decreased by 0.03 of an atom to correct for included magnetite.

Physical properties

The principal physical properties of the analyzed amphiboles are given in Table 1. The range of specific gravity listed is that of the two heavy liquids in which the final mineral sample was separated from heavier and lighter materials. The amphiboles in rock specimens 3, 4, and 5 were so homogeneous that by far most of the monomineralic amphibole grains were included in the final sample. The amphiboles of specimens 1 and 2, on the other hand, were so heterogeneous that much monomineralic material had to be separated from the analyzed samples in order to free the samples from composite grains. Judging from the composition of these impure fractions, amphibole 1 is somewhat more dense and presumably a little richer in iron than the average actinolite of the rock, and amphibole 2 is distinctly more dense, more deeply colored, and probably contains more iron and aluminum than the average amphibole of the rock.

The indices of refraction were determined by the immersion method, using a sodium light source; all liquids were measured at once with a refractometer. The very fine-grained material submitted for analysis was used, and because the material was somewhat variable (note the specific gravity ranges) an error as large as 0.002 is possible for samples 3, 4, and 5, and an error as large as 0.003 for samples 1 and 2. The values for 2V and $Z \wedge c$ were determined in sodium light on the universal stage. The ranges listed include all values that recurred frequently in measurements of a number of grains, and this variation is likely to be caused at least in part by the compositional variations within each sample.

PETROGRAPHY

The general petrography of the Bidwell Bar rocks has been described (Compton, 1955), and only the petrography of the rocks from which amphiboles were separated will be presented here. These rocks are in many respects representative of the other rocks with which they are associated; the greenstone, however, is considerably more mafic than the typical metabasaltic rocks of the regional terrane.

Mafic greenstone

Amphibole 1 is from a non-schistose, actinolite-rich greenstone that originally contained abundant large phenocrysts of augite and calcic plagioclase, but now consists entirely of metamorphic minerals. The following approximate mode, in weight per cent, was computed from a count of 1,000 points:

albite	8.0	chlorite	4.0
epidote	26.0	leucoxene	5.0
actinolite	53.0	calcite	2.0
hornblende	2.0		

An approximate chemical composition calculated from this mode is given in Table 3.

Actinolite occurs both as pseudomorphs after augite and as acicular

TABLE 3. CALCULATED CHEMICAL COMPOSITIONS OF AMPHIBOLE-BEARING ROCKS FROM THE BIDWELL BAR REGION, CALIFORNIA

	1 Mafic greenstone	2 Hornfelsic metadiabase	3 Amphibolite	4 Ferrohastingsite schist	5 Tonalite
SiO_2	46.3	49.3	49.2	37.9	59.5
Al_2O_3	12.6	14.3	16.5	10.9	18.0
TiO_2	2.0	1.1	1.7	1.6	0.5
Fe_2O_3	3.4	6.0	3.0	7.2	1.8
FeO	7.1	9.0	6.2	20.6	3.8
MnO	0.2	0.3	0.1	0.4	0.1
MgO	8.9	6.7	7.1	3.8	4.1
CaO	14.0	8.6	11.6	12.3	5.9
Na_2O	1.5	2.9	3.1	1.3	4.4
K_2O	0.4	0.5	0.4	1.6	1.4
H_2O	2.7	1.3	1.1	1.8	0.5
Cl	—	—	—	0.6	—
CO_2	0.9	—	—	—	—

prisms intergrown with albite, chlorite, and epidote. Here and there the faintly colored actinolite is abruptly overgrown by small patches of a more deeply colored hornblende that is blue-green in Z, with $\gamma=1.674$, $2V=62°–68°$, and $Z\wedge c=17°–18°$. These data indicate that it is identical with the hornblende of the contact aureole (see number 2, Table 1).

The original plagioclase grains are largely pseudomorphed by clusters of epidote and calcite. Most of the epidote is iron-rich, but some grains are zoned to iron-poor rims, and euhedral clinozoisite crystals occur in clusters associated with chlorite. The chlorite is optically positive, has a birefringence of 0.002, and a refractive index of approximately 1.580.

Hornfelsic metadiabase

Amphibole 2 is from a fine-grained hornfelsed metadiabase that has the following mode, in per cent by weight:

quartz	1.5	titaniferous ore	5.0
oligoclase (An_{22})	28.5	chlorite	0.4
hornblende	62.5	apatite	0.1
epidote	2.0		

The point count runs used to compute this mode were unusually consistent, and therefore the calculated chemical composition in Table 3 should be quite reliable.

Most of the hornblende is in small rather deeply colored prisms that interfinger with feldspar in a randomly oriented hornfelsic fabric. Some larger (0.5 mm.) grains have lighter colored cores that grade abruptly out to the deeper hornblende of the prisms. The cores probably represent large actinolites from the original metadiabase that were not completely reacted to aluminous hornblende; it is also possible, though less likely, that they are iron-poor aluminous hornblende. It is the more deeply colored hornblende that was analyzed.

Chlorite occurs here and there with the aluminous hornblende, but its genetic relation to the amphibole could not be determined. Epidote is iron-poor and is commonly included in oligoclase. Rather large skeletal ore grains are scattered evenly through the rock.

Clinopyroxene-bearing amphibolite

Amphibole 3 is from a typical amphibolite of the inner zone, characteristically veined and spotted by mafic tonalite. Judging from the consistency of point counts, the following mode (measured on amphibolite only) should be quite reliable:

andesine (An_{38})	36.0	magnetite	0.1
hornblende	60.0	apatite	0.3
clinopyroxene	0.3	zircon	tr.
sphene	3.3	alkali feldspar and zeolite	tr.

The texture is granoblastic but the hornblende shows a moderate degree of crystallographic orientation, *c* and {100} tending to lie in a plane. The hornblende is evenly colored and free of inclusions. Clinopyroxene was detected only in crushed samples of the rock; however, judging from its textural relations in other sectioned rocks, it is granular, as coarse-grained as the hornblende, and shows no obvious reaction relation to the hornblende. The properties of the clinopyroxene (determined in part on the universal stage) are: $\gamma=1.719$, $\alpha=1.689$, $Z\wedge c=48°$, $2V=60°$. Andesine is zoned from An_{45} out to about An_{35}.

Ferrohastingsite schist

Amphibole 4 is from a heavy, very dark green lineate schist that consists of ferrohastingsite along with only 2 per cent of sphene, 0.5 per cent of oligoclase or quartz, and 0.5 per cent of epidote. The unusual rock composition listed in Table 3 should be very reliable. In thin section the amphibole is seen to be evenly colored, medium-grained, and moderately prismatic; {100} tends to parallel the schistosity and the prism axes define the rock's strong lineation. The sphene is very fine-grained and is scattered evenly throughout the amphibole as though it had separated from it.

Biotite-hornblende tonalite

Amphibole 5 is from one of the most mafic rocks of the batholith; however, its properties are essentially the same as those of hornblendes from other batholith rocks. The calculated chemical analysis of the tonalite must be considered as approximate only because many point counts showed the rock to be heterogeneous, especially with respect to the ratio of biotite to hornblende and of quartz to plagioclase. The approximate mode is:

quartz	14.0	magnetite	1.0
plagioclase (An_{34})	58.0	epidote	0.2
hornblende	14.5	apatite	0.1
biotite	12.0	zircon	tr.

Plagioclase is subhedral to euhedral and is zoned in an oscillatory manner from cores of about An_{46} to rims of about An_{22} (as determined by the Rittmann method on the universal stage). Quartz is in fine-grained aggregates between the plagioclase grains, while clots of mafic grains tend to wrap around plagioclase. Hornblende prisms are subhedral and about 1 2 mm. long, and biotite forms ragged anhedra that are twice that size. Hornblende is not rimmed by biotite, though it is locally replaced by it. Coarse-grained pistachite occurs here and there with chloritized biotite. The minor chlorite and fine-grained alteration products of plagioclase are included in the mode as the minerals they replaced.

PARAGENESIS

The sequence of metamorphic assemblages in basaltic rocks of the Bidwell Bar area is outlined in Fig. 1. The arrows indicate only the principal sources of materials for each mineral of a new assemblage; actually, almost all of the minerals in adjacent columns are linked in some degree.

The derivation of greenschist minerals from basaltic rocks is based purely on textural evidence because igneous relics are very scarce. These

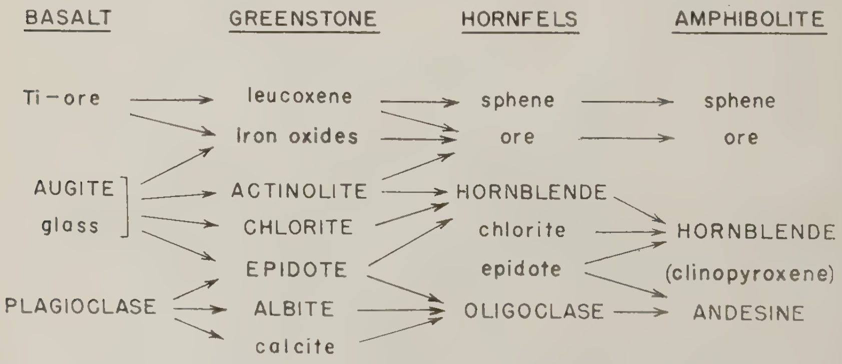

FIG. 1. Sequence of mineral assemblages in metabasaltic rocks of the Bidwell Bar region. The principal minerals are in capital letters.

reactions were definitely earlier than the contact metamorphism, and all of the rocks of the aureole were once similar to the rocks now found in the regional terrane. The conditions of greenschist metamorphism are not critical here, and have already been described (Compton, 1955, p. 17–18).

The progressive contact metamorphic assemblages are essentially isochemical, except that water was lost at each stage. The changes of leucoxene and hydrated iron oxides to ore and sphene, and the conversion of actinolite to hornblende apparently took place abruptly in the outer zone of the aureole. The amphibole reactions involved both the addition of Al to actinolite and the combination of chlorite and epidote to yield more hornblende, with magnetite and water as additional products. The principal partial reactions are:

1) chlorite+epidote+Si→hornblende+Al+Fe‴+water
2) actinolite+Al→hornblende+Si+(Mg, Fe″)
3) Fe‴+Fe″→magnetite

The overall reaction formed by combining these partial reactions is:

actinolite+chlorite+epidote→hornblende+magnetite+water+Mg

For partial reaction 2, the analyses indicate that Mg rather than Fe″ is the dominant product, and it is therefore necessary to consider plagioclase as a reactant with the excess Mg, forming more (though minor) hornblende. In the inner zone of the aureole, aluminous hornblende was increased only slightly by the further reactions of epidote and minor chlorite. In the case of the plagioclase reactions, however, albite reacted with epidote to produce oligoclase in the outer part of the aureole and then continued to react in a progressive way so that plagioclase compositions tend to be more and more calcic as the batholith is approached. The appearance of clinopyroxene near the batholith contact probably involves the destruction of some hornblende; however, there is insufficient data on the compositions and distribution of these pyroxenes to determine whether they were formed by local high temperatures, by the dehydrating effects of the adjacent magma, or simply by local concentrations of Ca and Mg.

The paragenesis of the ferrohastingsite schist involves rocks with unusual compositions. Ferrohastingsite occurs at several localities in the inner zone of the aureole, in one place with abundant andesine and accessory magnetite and sphene, in another place with abundant labradorite, clinopyroxene, and titaniferous ore. In an important exposure on the Cascade road 1,300 feet northeast of the Feather Falls village Forest Service station, ferrohastingsite schist is associated with metacherts, suggesting that the schists were once iron-rich basic tuffs, perhaps palagonite tuffs enriched in iron hydroxides. That they were not impure limy beds that have undergone iron metasomatism is indicated by the fact that they are not associated with tactites that occur in the same part of the aureole. In any case, the hastingsitic amphibole formed because of the high Fe/Mg ratio of the rocks and their low silica content; it cannot be correlated with a higher grade of metamorphism.

The hornblende of the tonalite is notably less aluminous than the hornblendes of the aureole, and this fact, coupled with its large grain size and euhedral (110) faces, indicate that it crystallized from a magma, rather than being xenocrystic after amphibolite. The low alumina content is doubtless a result of partition of materials with aluminous biotite that was growing at the same time.

Significance of the Actinolite-Hornblende Reaction

Conversion of actinolite and other greenschist minerals to aluminous hornblende is petrologically significant at Bidwell Bar because the two minerals are abruptly superimposed, the rocks involved are extensive, and the reaction produced a textural change that affords a basis for mapping the extent of a new metamorphic environment. How does this abrupt change correlate with what might be expected from the progressive metamorphism of actinolites to hornblendes? Comparison of analyses of many actinolites, hornblendes, and hastingsites (from rocks of various compositions) indicates that these minerals form a continuous solid solution series, with the number of Al atoms in Z positions ranging from 0 to somewhat more than 2 (see esp. Hallimond, 1943, p. 80–87). In metamorphic rocks containing appreciable alumina, the number of Al atoms in Z positions of hornblendes is greater in higher grade rocks than in lower grade rocks, and it seems most reasonable to expect a continuous increment of Al atoms in Z positions of actinolites and hornblendes during the progressive metamorphism of basaltic rocks (Foslie, 1945, p. 98; Turner, 1948, p. 90, 98; Turner and Verhoogen, 1951, p. 465). The inconsistency between these views and the Bidwell Bar paragenesis requires a review of the mineral data that substantiate ideal gradation from actinolite to hornblende in metabasalts. When this is done, it will be possible to consider why the Bidwell Bar metamorphism produced a different paragenesis.

Compositions of all chemically analyzed actinolites and hornblendes from greenschists, greenstones, and epidote amphibolites are presented in Table 4, in order of increasing amount of Al in Z positions. Number 4 was calculated from an unpublished chemical analysis generously furnished by Prof. C. O. Hutton, and the complete analysis and optical measurements, all made by Hutton, are given in Table 5. All of the rocks concerned have compositions reasonably close to that of basalt, although

TABLE 4. NUMBERS OF PRINCIPAL ATOMS IN FORMULAE OF AMPHIBOLES FROM GREENSCHISTS, GREENSTONES, AND EPIDOTE AMPHIBOLITES

		1	2	3	4	5	6	7	8	9	10	11	12
(Z)	Si	7.73	7.74	7.66	7.64	7.61	7.54	7.47	7.16	7.06	6.72	6.58	6.48
	Al	0.24	0.26	0.34	0.36	0.39	0.46	0.53	0.84	0.94	1.28	1.42	1.52
(Y)	Al	0.00	0.19	0.43	0.27	0.02	0.21	0.13	0.56	0.55	0.48	0.16	0.41
	Ti	0.02	0.03	0.04	0.04	0.05	0.08	0.04	0.14	0.08	0.06	0.05	0.07
	Fe'''	0.00	0.12	0.09	0.25	0.28	0.42	0.52	0.33	0.32	0.57	0.64	0.59
(X)	Mg	3.78	3.25	3.25	3.48	2.85	2.47	3.12	1.58	1.98	2.23	2.80	2.28
	Fe''	1.14	1.39	1.16	0.97	1.87	1.82	1.28	2.22	2.14	1.80	1.17	1.56
	Mn	0.02	0.00	0.03	0.02	0.03	0.04	0.00	0.03	0.03	0.07	0.03	0.05
(W)	Ca	1.93	1.90	1.92	1.68	1.73	1.60	1.57	1.68	1.63	1.69	1.99	1.92
	Na	0.39	0.15	0.24	0.27	0.27	0.44	0.41	0.39	0.19	0.28	0.18	0.35
	K	0.00	0.02	0.11	0.02	0.09	0.02	0.00	0.15	0.26	0.07	0.08	0.10
	OH	2.14	1.94	1.56	2.00	2.02	1.92	2.06	2.06	2.02	1.89	2.60	2.14

1. "Hornblende from fibrous hornblende-clinozoisite-albite schist, Limebury point, Salcombe Estuary' South Devon." (Tilley, 1938, p. 505).
2. "Hornblende from hornblende-epidote-albite schist below Signal Station, Prawle Point, Start District, South Devon." (Tilley, 1938, p. 504).
3. Actinolite from mafic greenstone. (Tables 1 and 2, analysis 1).
4. Actinolite from albite-epidote-chlorite-actinolite schist of Chl. 3 subzone; 32 chains E.N.E. of Jessie Peak, Mid-Wakatipu Survey District, Western Otago, New Zealand. Analyst, C. O. Hutton.
5. "Hornblende out of chlorite-epidote-albite-amphibolite (26); 0.4 mile south-east of Loch Gair Hotel, Argyll." (Wiseman, 1934, p. 368).
6. "Actinolite from albite-stilpnomelane-actinolite-schist, No. 2646, 56 chains east of Billy Goat Creek-Arrow River junction, western Otago." (Hutton, 1940, p. 13–14).
7. "Amphibole from albite-epidote-actinolite-calcite-schist, No. 2718, from the summit of Coronet Peak, Wakatipu region." (Hutton, 1938, p. 209; 1940, p. 13).
8. "Hornblende out of garnet-biotite-epidote-albite-amphibolite (68/4), 0.2 mile N. 51° E. from northern end of Loch-na-Craige, near Achahoish, South Knapdale." (Wiseman, 1934, p. 382).
9. "Hornblende out of biotite-epidote-albite-amphibolite (65/4)." Same locality as 8. (Wiseman, 1934, p. 383).
10. Hornblende from hornfelsic metadiabase. (Tables 1 and 2, analysis 2).
11. Hornblende from hornblende schist (with quartz, oligoclase, epidote, and biotite); northwest of Lake Pappilanselka, Orivesi. (Seitsaari, 1953, p. 89, table 5).
12. Hornblende from stratified hornblende schist (with quartz, oligoclase, epidote and biotite); northeast of Lake Vaavujarvi, Orivesi, Finland. (Seitsaari, 1953, p. 89, table 4).

some were originally clastic rocks. Numbers 1 and 2 are from the greenschists of the Start region of Devonshire, England; numbers 4, 6, and 7 are from the widespread greenschists of the Otago region, New Zealand; numbers 5, 8, and 9 are from the progressively metamorphosed epidiorites (metadiabases) of the Central and Southwest Highlands of Scotland; numbers 11 and 12 are from epidote-oligoclase amphibolites (originally basic sediments) of the Tampere schist belt, Finland; and numbers 3 and 10 are from greenstone and epidote-oligoclase-hornblende hornfels of the Bidwell Bar area. It is notable that the actinolites from the lower grade parts of the various areas are closely comparable (numbers 1, 2, 3, 4, and 5). None, however, are pure "end member" actinolite; apparently

TABLE 5. COMPOSITION AND PHYSICAL PROPERTIES OF ACTINOLITE FROM OTAGO, NEW ZEALAND

SiO_2	54.07	$\alpha=1.629$
Al_2O_3	3.81	$\beta=1.643$
TiO_2	0.40	$\gamma=1.650$
Fe_2O_3	2.45	$\gamma-x=0.021$
Cr_2O_3	0.08	$Z\wedge c=19°$
NiO	0.03	$2V_\alpha=73°\pm 2°$
MgO	16.45	X = colorless
FeO	8.25	Y = pale green
MnO	0.24	Z = pale green with bluish tinge
CaO	11.13	$Z\geqq Y>X$
Na_2O	1.03	$G_{20°}=3.17$
K_2O	0.17	
H_2O^+	2.13	
H_2O^-	0.11	
Total	100.35	

Analysis and physical measurements by C. O. Hutton. See Table 4 for locality description.

even at lowest metamorphic grade a quarter or third of an atom of the 8 Z atoms is Al, a fact that must be kept in mind when comparing actinolites of metabasaltic rocks with those of less aluminous metamorphic rocks. The actinolites of the Otago region are of particular interest because they show a variation within the greenschist realm itself. The validity of progressive metamorphism in these rocks is undeniable, being based on regional mapping of zones of progressive mineral and textural changes, keyed by several thousand thin sections (Hutton and Turner, 1936). The chlorite zone was divided into four subzones on the basis of degree of reconstitution of the original graywacke beds. In Chl. 3 subzone, from which amphibole number 4 was collected, the rocks are fine-grained schists with a few relics of sedimentary grains, while in Chl. 4 subzone, the source of amphiboles 6 and 7, the rocks are exceptionally coarse-grained and even show segregation banding. In keeping with this progressive change, actinolites 6 and 7 have more Al in Z positions than does actinolite 4, and they are also more aluminous than any analyzed actinolites from greenschists. Still another amphibole from Chl. 4 subzone, not listed in Table 4 because it is from too mafic a rock, has 0.71 atom of Al in the 8 Z positions (Hutton, 1940, p. 15; 1956, p. 231–232). The approach of these amphiboles to aluminous hornblende may be explained by Turner's view (1948, p. 39) that "In Chlorite 4 the temperature appears to have been somewhat higher than in the other subzones, and was certainly maintained for a much longer period." Certainly, the compositional range of these amphiboles supports the concept of gradual conversion of actinolite to hornblende during progressive metamorphism.

The amphiboles studied by Wiseman (5, 8, and 9 of Table 4) supply an additional step in the progressive increase of Al in Z positions during increasing grade of metamorphism. Proof of progressive metamorphism lies in the zonal pattern of mineral changes, based in this case on the classical mineral zones mapped in metashales of the Southern Highlands (Barrow, 1912, p. 274-279; Tilley, 1925). The compositional change from the greenschist actinolite (number 5) to the two hornblendes from epidote amphibolites of the garnet zone (numbers 8 and 9) is distinct; however, the garnet zone amphiboles are not much more aluminous than Hutton's Chl. 4 subzone amphiboles, and they are less aluminous than the hornblendes of typical epidote-free amphibolites of comparable areas. Therefore, these garnet zone hornblendes fit exactly into a serial change from greenschist through epidote amphibolite to amphibolite facies conditions, further supporting the view that reactions of actinolite to hornblende are continuous, not discontinuous.

Just as surely as in the Southern Highlands, the epidote amphibolites at Bidwell Bar represent an intermediate step in the conversion of greenschists to epidote-free amphibolites. Furthermore, the texture of the hornfels from which amphibole 10 (Table 4) was separated indicates it was a massive metadiabase, directly comparable with Wiseman's epidiorites; nor was it any more aluminous than the rocks from which Wiseman separated his two hornblendes. The one obvious difference between the Bidwell Bar rocks and those of either the Southern Highlands or the Otago region is that contact metamorphism produced the rocks at Bidwell Bar while regional metamorphism produced the other two assemblages. What are the physical differences between these particular cases of contact and regional metamorphism that account reasonably for the differences in mineral parageneses? Probably, there are three principal factors that produced the differences, and perhaps the most important of these was the difference between rate of escape of water and rate of increase of temperature during inception and progress of the amphibole reactions described above. The theoretical basis for this factor has been presented in some detail by Thompson (1955) and in part by Yoder (1955, p. 513-516). On this basis, I interpret the gradational amphibole changes in the Otago and Highlands schists as occurring in broad terranes which were heated so slowly that water never accumulated rapidly enough to inhibit the progress of the reaction at each temperature increment. Deformation and continuous recrystallization may have been important factors in moving water continuously out of the terrane. In the Bidwell Bar aureole, rapid increase in temperature relative to rate of escape of water created a high water pressure almost at the outset of metamorphism, and the amphibole reaction was inhibited in the low temperature range. By the time that escape of fluids was sufficient to allow appreciable reaction, temperatures were so high as to produce an aluminous hornblende. It is possible that a complicating abnormality may have been produced by fluids forced through the outer part of the aureole by rapid dehydration nearer the batholith.

Another factor that probably contributed to the contrast in mineral parageneses is the difference between rates of reaction at any one temperature and rates of heating. In the regional terranes, temperatures rose slowly enough so that even sluggish (low temperature) reactions were usually at or near equilibrium. The coarse-grained Otago schists of Chlorite subzone 4 seem to emphasize this factor strongly. In contrast to this true progressive metamorphism, the contact rocks were heated so rapidly that low temperature reaction of actinolite was volumetrically ineffective in the relatively short period of time between inception of heating and rapid reaction at intermediate to high temperature. Finally, the third factor is based on the degree of comminution and mixing of constituents before and during recrystallization. Dynamic metamorphism of the rocks of the Southern Highlands and Otago produced a fine-grained mixture of mineral units that could react readily as temperatures increased. Because of the lack of granulation in the outer zone of the Bidwell Bar aureole, only the finest grained constituents of the greenschists could react easily in the lower temperature range, a situation substantiated by minor hornblende overgrowths and relict actinolite cores in the larger Bidwell Bar amphiboles.

There is insufficient data to determine which of these factors was dominant in controlling the amphibole parageneses of the two environments; however, epidote amphibolites from other areas indicate the Bidwell Bar conditions were not unique. The epidote amphibolites of the Tampere schist belt of Finland are comparable in several ways to the Bidwell Bar epidote amphibolites, although there is apparently no chance of tracing the progression of changes from greenschists to amphibolites in the Tampere terrane. The hornblendes of these rocks are aluminous (11 and 12 of Table 4) and in several cases they are heterogeneous, like those in the outer part of the Bidwell Bar aureole (Seitsaari, 1953, p. 87–88). With regard to their origin, Seitsaari (1953, p. 96) "suggests that the crystallization of the blue-green hornblende in the Tampere schists is generally related to a late increase of temperature, and that the penetrative movements have been weak, if not terminated, during its formation." A close approach to contact metamorphic conditions is supported by these facts: 1) the hornblende occurs as porphyroblastic prisms that cut across the schistosity, 2) the hornblende occurs only in the finer grained rocks, and 3) the analyzed hornblendes were collected less than a mile from granitic intrusions of batholithic size.

A case of contact metamorphic amphiboles showing abrupt reaction relations is reported from the Misaka series of Japan by Sugi (1931). No analyses of these amphiboles are available, but Sugi studied textural and refractive index changes carefully enough so that there is little doubt but that he detected the same amphibole relations as those at Bidwell Bar. The Misaka rocks are basic to intermediate lavas and greenschists that have been progressively metamorphosed to epidote amphibolites and amphibolites near a quartz diorite intrusion. In the transition between greenschists and amphibolites, actinolite and hornblende occur together with epidote, sodic plagioclase, and chlorite. It is notable that the new blue-green hornblende of this transition forms sharp rims on actinolite, or else clear-cut prisms that lie on or near large actinolite grains (Sugi, 1931, p. 115–116). In mafic schists, hornblende typically has formed first in areas containing chlorite, indicating the importance of this mineral in the formation of aluminous hornblende. Perhaps the greatest value of Sugi's work on these rocks was to demonstrate that abrupt reaction of actinolite to hornblende may be detected without laborious separations and analyses.

Considering the general situation presented above, the actinolite-hornblende reaction must be considered carefully in assigning rocks of basaltic composition to one of the metamorphic facies. Wiseman's epidote amphibolites fit exactly the albite-epidote amphibolite facies of many authors (see esp. Turner, 1948, p. 88–89), but the compositions of Hutton's actinolites from the Chl. 4 subzone indicate that some metabasalts from the biotite zone might well contain hornblende rather than actinolite. According to the picture presented above, the temperature realm of albite-epidote amphibolite facies in the Bidwell Bar region is represented by metastable greenschists and greenstones that lie outside the aureole; in the aureole itself, conditions of the transitional facies have been essentially overstepped, and the aureole is entirely in amphibolite facies. The abrupt appearance of cordierite and andalusite in the outermost parts of some pelitic aureoles may be explained by the same sort of overstepping of transitional assemblages. Before the hornblende analyses of the Bidwell Bar amphiboles were available, I interpreted the oligoclase-epidote-hornblende hornfelses as representing a stress-free variant of the albite-epidote amphibolite facies (Compton, 1955, p. 42). On the basis of the hornblende reaction, however, I would reject this view, much as Thompson questioned the "stress" and "antistress" control of aluminum silicates in regional and contact terranes (Thompson, 1955, p. 98).

The eventual disappearance of epidote from epidote amphibolites provides a useful physical basis for defining the upper limit of the epidote amphibolite facies as used by Foslie (1945), Seitsaari (1953, p. 95), Barth (1952, p. 338), and others. This limit is, of course, well beyond the upper limit of the albite-epidote amphibolite facies. The analyses presented above show clearly that hornblendes occurring with epidote and oligoclase are almost as aluminous as those of epidote-free amphibolites, indicating that the actinolite-hornblende reaction takes place over a lower temperature range than the epidote-plagioclase reaction.

CONCLUSIONS

Through more data are wanting, it is likely that the series actinolite-hornblende-hastingsite is controlled by temperature, and that a continuous reaction series might be produced by ideally progressive metamorphism of basaltic rocks. Discontinuities in the series appear to be valuable in pointing up physical conditions of metamorphism, especially those affecting reaction rates. It is suggested that serial analyses of any temperature-variant solid solution series will be of unique value in interpreting metamorphism of a given suite of rocks, even where the absolute temperature-pressure dimensions of the series are not known.

ACKNOWLEDGMENTS

I am grateful to Prof. C. O. Hutton for his generous help and suggestions regarding the separatory and analytical procedures, for his contribution of an unpublished analysis of an Otago actinolite, and for his reading the manuscript. A Supplementary Research Grant from Stanford University covered the cost of the analyses.

REFERENCES

BARTH, TOM. F. W. (1952), Theoretical petrology: N. Y., John Wiley and Sons, Inc., 387 p.

BARROW, G. (1912), On the geology of lower Dee-side and the southern Highland border: *Geol. Assoc., Proc.*, **23**, 274–290.

COMPTON, R. R. (1955), Trondhjemite batholith near Bidwell Bar, California: *Geol. Soc. Amer., Bull.*, **66**, 9–44.

FOSLIE, STEINAR (1945), Hastingsites, and amphiboles from the epidote-amphibolite facies: *Norsk geol. Tidsskr.*, **25**, 74–98.

HALLIMOND, A. F. (1943), On the graphical representation of the calciferous amphiboles: *Am. Mineral.*, **28**, 65–89.

HUTTON, C. O. (1938), A chemical and optical study of a low-grade metamorphic actinolitic amphibole from Coronet Peak, western Otago, New Zealand: *Min. Mag.*, **25**, 207–211.

——— (1940), Metamorphism in the Lake Wakatipu region, western Otago, New Zealand: *New Zealand Dept. Sci. and Industr. Res., Geol. Mem.*, **5**, 1–84.

——— (1956), The composition of an actinolite: *Acta Cryst.*, **9**, 231–232.

——— and Turner, F. J. (1936), Metamorphic zones in north-west Otago: *Roy. Soc. New Zealand, Trans.*, **65,** 405–406.

Seitsaari, Juhani (1953), A blue-green hornblende and its genesis from the Tampere schist belt, Finland: *Comm. géol. Finlande, Bull.*, **26,** 83–98.

Sugi, Ken-ichi (1931), On the metamorphic facies of the Misaka series in the vicinity of Nakagawa, Prov. Sagami: *Jap. Jour. Geol. and Geogr.*, **9,** 87–142.

Thompson, J. B., Jr. (1955), The thermodynamic basis for the mineral facies concept: *Am. Jour. Sci.*, **253,** 65–103.

Tilley, C. E. (1925), A preliminary survey of metamorphic zones in the southern Highlands of Scotland: *Quart. Jour. Geol. Soc. London*, **81,** 100–112.

——— (1938), The status of hornblende in low grade metamorphic zones of green schists: *Geol. Mag.*, **75,** 497–511.

Turner, F. J. (1948), Mineralogical and structural evolution of the metamorphic rocks: *Geol. Soc. Amer., Mem.* **30,** 1–342.

——— and Verhoogen, J. (1951), Igneous and metamorphic petrology: N. Y., McGraw-Hill Book Co., 602 p.

Warren, B. E. (1930), The crystal structure and chemical composition of the monoclinic amphiboles: *Zeit. Krist.*, **72,** 493–517.

Wiseman, J. D. H. (1934), The central and south-west Highlands epidiorites: a study in progressive metamorphism: *Quart. Jour. Geol. Soc. London*, **90,** 354–417.

Yoder, H. S., Jr. (1955), Role of water in metamorphism: *Geol. Soc. Amer.*, Spec. Paper **62,** 505–524.

Manuscript received February 3, 1958

THE AMERICAN MINERALOGIST, VOL. 43, SEPTEMBER-OCTOBER, 1958

SOME OBSERVATIONS ON THE CRYSTALLIZATION OF AMORPHOUS SILICA

R. M. Carr and W. S. Fyfe, *University of Otago, Dunedin, New Zealand.*

Abstract

Experiments have been carried out to determine the effect of pressure and temperature on the rate of formation of quartz from silicic acid. The rate is much more sensitive to pressure than temperature and this is discussed in terms of possible mechanisms. Cristobalite and silica K appear as intermediate phases before quartz is formed in appreciable quantity. In this system increasing pressure favours the attainment of equilibrium more than increasing temperature.

Introduction

In most experimental studies designed to determine phase relations in a mineral system the starting materials chosen are those which allow reaction to proceed in a reasonable time. The constituents are often used in some amorphous reactive condition, a glass or gel, which also assists in the final *x*-ray analysis to determine the phases present. It is always desirable that the phases which are grown at a given pressure and temperature, be those having the lowest possible free energies of formation and thus represent the thermodynamically stable assemblage. But by using the most reactive starting materials the difficulty of obtaining stable products may be at a maximum. From such unstable reactants many metastable assemblages, more stable than the reactants, may easily be formed.

It has been recognized for a long time that during hydrothermal crystallization of amorphous silica, metastable phases commonly are formed and persist for considerable periods. As an understanding of such phenomena appears fundamental in the interpretation of experimental results a more detailed study of the crystallization of amorphous silica was undertaken.

Experimental Procedure

The general procedure followed was to allow samples of amorphous silica to react with water at a fixed pressure and temperature for various times and then to rapidly cool the reaction vessels. The products were then examined with an *x*-ray diffractometer. The silica used in this study was powdered A. R. silicic acid (100 mesh) manufactured by Mallinckrodt Chemical Co. This material was not completely amorphous but an *x*-ray pattern showed a broad diffuse hump (see Fig. 1) with a centre close to the position of the strongest line of cristobalite. Hydrothermal experiments were carried out in test-tube bombs with the sample in a silver capsule with ends pinched off to avoid contamination. The tubes were not sealed. Temperature control was to ±3° C.

EXPERIMENTAL RESULTS

In Table I, data from a series of experiments are summarized.

DISCUSSION

The reproducibility of the times of conversions is not high but in general anomalies were less than 20%. Temperature has a rather small effect on the rate, but pressure has a very marked effect and an error in pressure could cause a significant variation, particularly at low pressures. Only three experiments were conducted at 15,000 p.s.i. where the times were inconveniently long and the results, while being of the order of time expected are anomalies with respect to temperature. This anomaly could be explained by pressure uncertainty.

From an inspection of the results in Table I a number of conclusions which have important bearing on the mechanism are apparent. These are:

1. Quartz does not appear in significant quantities until two other phases have formed.
2. Cristobalite is the first phase to form although in some series where run times are short a really sharp cristobalite pattern may not develop.
3. When cristobalite is well developed, silica K is normally present.
4. Silica-K appears to change rapidly to quartz once it is well formed.
5. In all runs the assemblages recorded are quartz, quartz and silica-K, silica-K and cristobalite, cristobalite. In one run only a very small amount of quartz was observed along with major silica-K and minor cristobalite.
6. Tridymite was not formed in any experiments in sufficient quantity to appear in an *x*-ray pattern.
7. Pressure has a much greater influence than temperature on the reaction rate in the temperature range studied.
8. In this system a pressure increase of 1000 bars favours the attainment of equilibrium more than a temperature increase of 100° C. This may not have been anticipated from the great mass of chemical data on temperature effects on reaction kinetics.

We may now consider what details of mechanism may be deduced from these observations. It is certain that the path followed in these reactions is:

$$\text{almost amorphous silica} \rightarrow \text{cristobalite} \rightarrow \text{silica-K} \rightarrow \text{quartz.}$$

The change silica-K to quartz appears to occur more rapidly than stages leading to silica-K. A set of typical *x*-ray patterns illustrating these changes is shown in Fig. 1. It should be noted that in some longer runs at lower pressures cristobalite develops more strongly before silica-K appears. In Fig. 2 data are plotted to illustrate the effect of pressure on

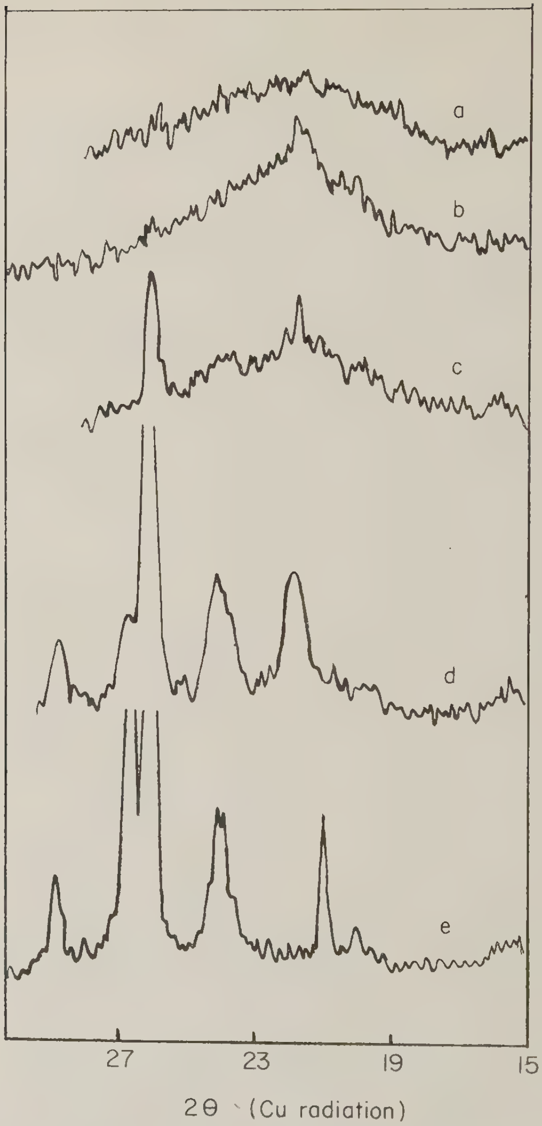

FIG. 1. A set of diffractometer patterns illustrating changes in structure with time, taken from runs at 45,000 p.s.i. and 430° C.

(a) Largely amorphous SiO_2.
(b) Cristobalite developing.
(c) Silica-K developing with cristobalite.
(d) Silica-K the major phase with cristobalite and a small amount of quartz.
(e) Silica-K the major phase with strong quartz. Cristobalite has disappeared.

TABLE 1. PHASES FORMED BY HYDROTHERMAL CRYSTALLIZATION OF SILICIC ACID AT VARIOUS PRESSURES, TEMPERATURES AND TIMES

Pressure (p.s.i.)	T° C.	t (hours)	Products
Set 1			
59,000	428	6	poor C
	440	7	K+Q
	448	8	Q
	440	9	Q
Set 2			
59,000	340	8	poor C
	330	9	Poor C
	340	10	Q
	325	12	Q
Set 3			
45,000	435	7	poor C
	442	8	poor C
	440	9	poor C
	425	9	K+C (minor Q)
	433	10	K+C
	440	12	Q+K
	440	12	K+Q
	426	13	Q
	436	14	Q
	430	14	Q
Set 4			
45,000	330	14	poor C
	330	15	K+Q
	330	16	Q
	337	18	Q
Set 5			
30,000	430	24	C
	430	48	Q+K
	438	72	Q+K
	440	96	Q
	430	120	Q
Set 6			
30,000	325	48	poor C
	334	72	K+poor C
	335	96	Q+K
	330	120	Q
Set 7			
15,000	438	576	C
	426	840	K+C
	335	840	Q

(*Note:* C=cristobalite, K=silica-K or keatite, Q=quartz. A mixture K+Q signifies that silica-K is the major phase).

the time necessary for the 100% conversion to quartz. A qualitative picture of the process is illustrated diagrammatically in Fig. 3.

The process of the formation of a new phase may be considered to involve the following steps listed on page 912.

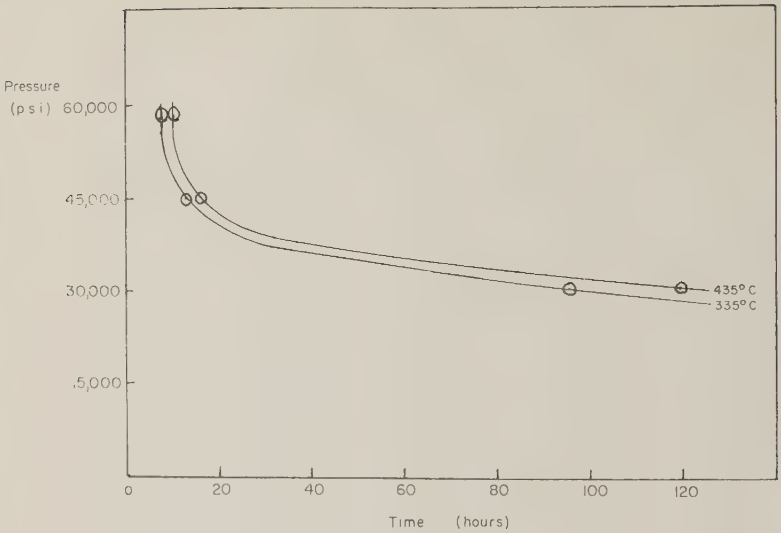

FIG. 2. The variation with pressure of the time for 100% conversion to quartz.

(a) the starting materials pass into solution,
(b) nuclei of the new phase form,
(c) nuclei of the new phase grow by transfer of material from the decaying phase.

Any of these three steps can be rate controlling.

Some selection of these possibilities can be made and with this in view some measurements were made of the rate of solution of quartz and its

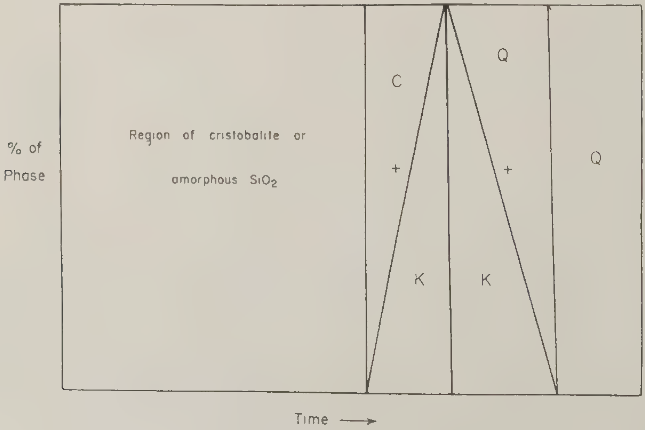

FIG. 3. Diagrammatic representation of phase assemblages during typical runs.

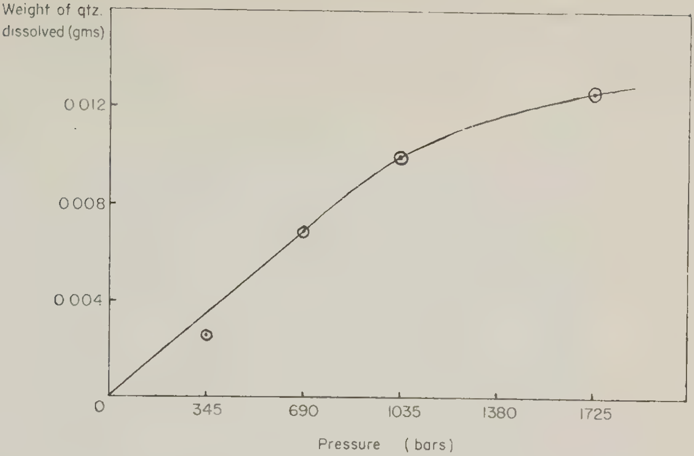

FIG. 4. Effect of pressure on the rate of solution of quartz at 400° C.

variation with temperature and pressure. While quartz was used in these experiments, it is not unreasonable to assume that the rate of solution of the other phases of silica will show similar variation. In these experiments a single quartz crystal was suspended in a pressure vessel for a given time at constant pressure and temperature. The amount of silica which had passed into solution was determined by weight loss. It is obvious that the rate is proportional to surface area but this factor can be made negligible by using the same crystal in all experiments forming a set, and as the amount lost in each is very small a fairly constant surface area can be assumed. In Fig. 4 some results are shown for the amount dissolved in one hour at 400° C. and varying pressures. It will be noticed that the amount dissolved in unit time increases fairly steadily with pressure but tends to fall off as higher pressures are reached. In Fig. 5 data are given to illustrate the effect of temperature at constant pressure for a time of one hour. The temperature effect is quite large and tends to increase with temperature. Inspection of these results indicates no correlation with the rates of transformation with respect to both pressure and temperature. For example from the temperature effect we would anticipate a four-fold increase in the rate for 100° C. if the rate of solution was controlling. The data indicates a very much smaller effect. It is thus reasonable to assume that the rate of solution does not control the overall rate.

A study of the rate of solution at constant pressure and temperature indicated that the solution obeys an equation of the type

$$\frac{dw}{dt} = K(W_s - w)$$

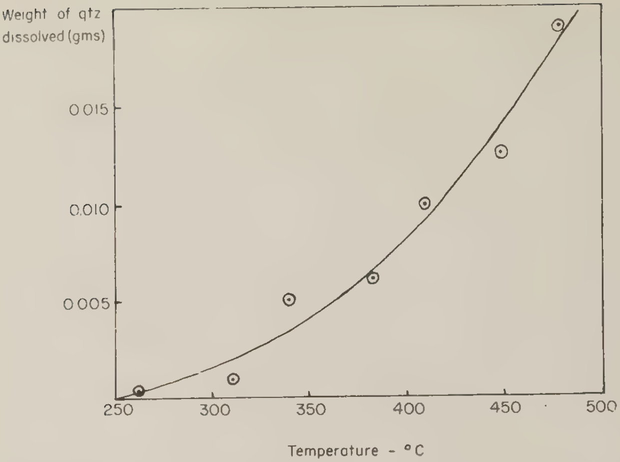

FIG. 5. Effect of temperature on the rate of solution of quartz at 15,000 p.s.i.

This is typical of many solution processes. (1) (w = weight dissolved, W_s is the weight at saturation. K is the rate constant including constant terms for the volume of the system and surface area). On integration this becomes

$$Kt = \ln\left(\frac{W_s}{W_s - w}\right)$$

and

$$\ln\left(\frac{W_s}{W_s - w}\right)$$

should be a linear function of time. A plot for a typical set of results is shown in Fig. 6. We have found, however, that the data is not of sufficient accuracy to allow calculation of other kinetic functions.

A few experiments were attempted to obtain information on the rate of growth of a quartz crystal in a solution saturated with amorphous silica. Results were erratic and present data indicate little more than that pressure increases the rate of growth. It is probably possible to eliminate rate of solution as the major factor on the following grounds. A phase should grow most rapidly in an environment where the supersaturation is largest. Thus if quartz nuclei were forming at the start of crystallization, then they should grow rapidly in the presence of amorphous silica, perhaps more so than the other possible phases. Experiments indicate that quartz does grow very rapidly from silica-K, in a small fraction of the total time, even though the supersaturation with respect to quartz must be less than in an environment with amorphous silica or cristobalite.

If rates of growth and solution are not the controlling processes then

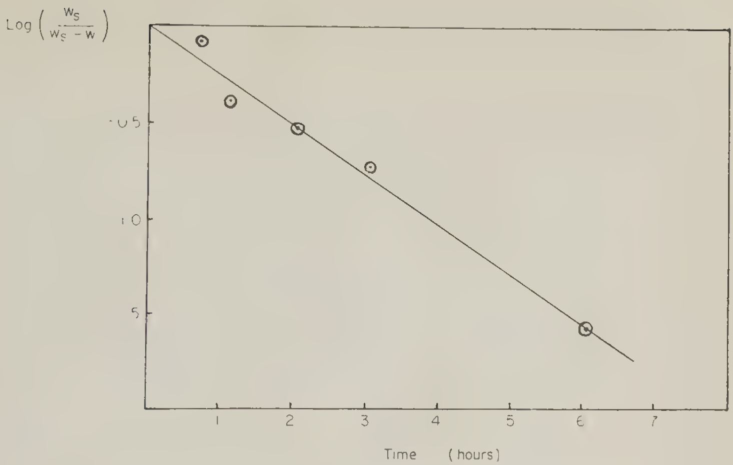

FIG. 6. Test of rate equation for solution of quartz, at 400° C. and 15,000 p.s.i.

we must examine the possibility that nucleation is rate controlling. The main problem in this respect is to explain the order of appearance of the phases. Normally it would be anticipated that a phase would form nuclei in a medium where the supersaturation factor is large. This is not in accord with these observations. However, in this system the amount of supersaturation cannot be very large and the results suggest that nucleation is induced on solid phases already present. Thus the starting material shows some order suggesting a relationship to cristobalite and cristobalite is the first phase of form. The general physical properties of silica-K such as density and refractive index (2) suggest that it is intermediate between cristobalite and quartz and in this case it may form nuclei on cristobalite with greater ease than quartz. Similarly, quartz might form nuclei readily on silica-K.

On this model of induced nucleation it might be expected that early formed cristobalite would produce silica-K and that this in turn would produce quartz and all would appear together. This is not typical of what is observed. An explanation can be made along the following lines. Nucleation is an unfavourable reaction and can be considered to start from a suitably oriented group of atoms condensed on a surface. It is obvious that the greater the area of suitable surface available the greater is the chance of this process occurring. In this way the number of nuclei of silica-K forming becomes large only when a large, rapidly growing surface of cristobalite is present and similarly the rate of nucleation of quartz becomes large only when a large surface of silica-K is present. This relationship to surface also explains why an added seed crystal has little effect as it presents relatively little new surface. It is also commonly observed in the experiments that pseudomorphs initially form such as balls of cristobalite covered with a high index skin of silica-K (cf. the remarks of Keat (2) on the difficulties of refractive index determinations).

If the above arguments are reasonable then nucleation induced on other phases is the overall rate controlling process, coupled to some extent with growth. It remains to explain why this is so sensitive to pressure and less sensitive to temperature in the range examined. It is well known that alkalis catalyse the reaction and this may perhaps provide a clue. We have observed complete conversion to quartz, from the same starting materials, in a few hours in the presence of dilute KOH at 250° C. If hydroxyl ions catalyse the reaction it is possible that nucleation is controlled by the number of some species of silicate anion. The behaviour reported is not opposed to such a proposition. In the absence of alkali the silicate ion concentration will be controlled by the dissociation constants of silicic acid and dissociation constants vary steadily with pressure. Franck (3) has carried out extensive calculations on the variation of the ionic product of water in the supercritical region and one would expect other weak acids to show similarities. Pressure has a large effect on the dissociation, increasing at low pressures. The effect of temperature varies greatly depending on the region. For example, at 1000 bars and 350° C., log K_w is -10.97, while at 450° C. and 1000 bars the value is -10.90. At both these temperatures a change to 2000 bars increases the strength by a much larger factor. At other temperatures, both higher and lower, temperature may have a larger effect. With silica, as well as the acid strength increasing, the concentration in solution increases with pressure. An analysis of the kinetics suggests, however, that for the pressure effect to be explained qualitatively on the basis of a silicate ion concentration this ion would have to be doubly charged. Before any final statement can be made a wider temperature range should be studied.

It should be emphasized that the pattern followed in this series of experiments is not always observed. In a great number of experiments when glasses and mixes of compositions corresponding to Na_2O, Al_2O_3, 6–$10SiO_2$ were crystallized mixtures of quartz and cristobalite were formed but never silica-K. Tridymite did not appear even at temperatures above 800° C. A few experiments with a much less dense sample of silica gel indicated that the rate was much slower. In all these runs the same pressure sensitivity was observed.

References

1. E. A. Moelwyn-Hughes, "The Kinetics of Reactions in Solutions," Oxford, (1947).
2. P. P. Keat, "A New Crystalline Silica," *Science*, **120**, 328, (1954).
3. E. U. Franck, "Ionendissoziation von HCl, KOH und H_2O in überkritischem Wasser," *Zeit. Phys. Chemie*, **8**, 192, (1956).

Manuscript received February 4, 1958

THE AMERICAN MINERALOGIST, VOL. 43, SEPTEMBER-OCTOBER, 1958

THE CHARACTERIZATION OF SERPENTINE MINERALS

E. J. W. WHITTAKER, *Ferodo Ltd., Chapel-en-le-Frith, Stockport, England* AND J. ZUSSMAN, *The University, Manchester, England.*

ABSTRACT

Two papers published in recent issues of The American Mineralogist (Nagy & Faust, 1956; Kalousek & Muttart, 1957) have dealt with serpentine minerals under the titles "Serpentines: natural mixtures of chrysotile and antigorite" and "Studies on the chrysotile and antigorite components of serpentine" respectively. Certain statements in these papers are at variance with results presented in our paper (Whittaker & Zussman, 1956) and we therefore offer the following comments. Whereas the above two papers classify all serpentine minerals into two categories only, we believe that it is necessary to take account of at least one other serpentine variety whose character is as distinctive as that of chrysotile or antigorite.

Nagy & Faust (p. 825) state that "the existence of distinct serpentine minerals other than chrysotile and antigorite (or their polymorphs), is not confirmed on the basis of chemical, morphological, optical, differential thermal analysis, and x-ray data," and their main conclusion (p. 833), which is also embodied in the title of the paper, is that "these experimental studies show that minerals classified as serpentines are either chrysotile or antigorite or mixtures of these two minerals." The evidence which they present (with the exception of that based on differential thermal analysis) is, however, of such a nature that it would not be expected to reveal the existence of other distinct serpentine minerals even if they were present, as the following considerations will show, and it cannot therefore lead to so positive a conclusion.

(i) Chemical data. The statistics quoted for $Al_2O_3+Fe_2O_3$ contents of chrysotile and antigorite have such large standard deviations that they do not permit a significant assignment of most specimens of serpentine to one species or the other on this basis. It is indeed notable that the undoubted antigorites F-1 and F-14 of Table 2 have Al_2O_3 contents substantially lower than the mean given for chrysotile. Furthermore the fact that the $Al_2O_3+Fe_2O_3$ content of most serpentines lies within the (overlapping) ranges for chrysotiles and antigorites by no means precludes the existence of yet other distinct serpentine species.

(ii) Morphological data. It is stated that "electron micrographs of serpentines (natural mixtures) show fibrous (tubular) or irregular or flaky particles or both." No reason is suggested for believing that distinct serpentine minerals other than chrysotile and antigorite would not have one or other of these morphologies. In fact they would be expected to do so, and the morphological data would therefore be incapable of revealing them.

(iii) Optical data. In view of the wide variations in refractive indices of acknowledged samples of chrysotile and antigorite, the possibility that other species may occur with refractive indices within the scatter of the values for those species cannot be neglected, so that the evidence from these data also is inconclusive.

(iv) Differential thermal analysis data. This might be expected to reveal other serpentine species if they exist, and it is fair to say that it does not confirm their existence. A similar conclusion has been reached on similar evidence by Kourinsky & Satava (1954). It is however not sufficient evidence to establish that such species do not exist in the face of x-ray evidence, and in fact the D.T.A. curve for lizardite illustrated by Midgley (1951) is very similar to that of chrysotile although the two minerals are readily distinguishable by morphology and diffraction.

(v) X-ray diffraction data. No x-ray diffraction data are presented by Nagy & Faust apart from the use of the intensity of a single x-ray reflection to assess the degree of structural collapse of various specimens as a result of a certain acid treatment. In this connection they show:
  (a) As judged by the effect on the intensity of a certain x-ray reflection, chrysotile is decomposed and antigorite is not decomposed by this treatment.
  (b) Mixtures of chrysotile and antigorite are partly decomposed by this treatment to an extent which depends on the chrysotile content.
  (c) All serpentine minerals are also either decomposed, not decomposed, or partially decomposed when submitted to the same treatment. The only conclusion which can be drawn from these data is that the serpentine minerals do not all consist of pure chrysotile or pure antigorite. Given (a) and (b) there is no conceivable behaviour under the prescribed acid treatment which could confirm the existence of other serpentine species.

Thus the only part of the statement by Nagy & Faust on p. 825 of their paper which is justifiable is that the existence of distinct serpentine minerals other than chrysotile and antigorite (or their polymorphs) is not confirmed by differential thermal analysis. But this does not disprove the existence of such minerals. Lizardite (Whittaker & Zussman, 1956) justifies consideration as a distinct serpentine mineral just as much as do chrysotile and antigorite. Admittedly all three minerals may be regarded as polymorphs (at least to a first approximation), but if it is desired to distinguish any different types of serpentine mineral it is necessary to distinguish all three types. Lizardite differs from the other two in its diffraction effects, and, while it resembles chrysotile in some respects (optics and D.T.A.), it resembles antigorite in others (morphology and behaviour with acid). We have treated green massive serpentine (which had been identified as lizardite by x-ray diffraction) with one normal HCl at 95° C. for one hour as prescribed by Nagy & Faust, and have found that its powder diffraction pattern is only slightly weakened. (Treatment with somewhat stronger acid destroys the lizardite structure while still not affecting that of antigorite). It is therefore probable that much of what was recorded by Nagy & Faust as antigorite was in fact lizardite, a very common constituent of massive serpentine. Their quantitative analyses of serpentines in terms of chrysotile and antigorite must therefore be subject to revision in the light of new data. It is of course not denied that the acid treatment test can give a useful quantitative analysis of specimens which are known on other grounds to contain only chrysotile and antigorite.

A further minor criticism of Nagy & Faust's paper relates to their Fig. 3 showing photographs of a glass rod and a glass tube. While we believe that tubular chrysotile fibres do exist, the evidence that fosters this belief does not include that suggested by these photographs. The illustration of glass rod and glass tubing seen in ordinary light is not an appropriate analogy to the electron micrograph since the phenomenon it demonstrates is mainly one of refraction rather than absorption.

The possibility that the use of the term antigorite to include lizardite may lead to erroneous conclusions is illustrated in the paper by Kalousek & Muttart who appear to equate antigorite with the matrix rock in which chrysotile veins occur. In particular the comparison of the observed density of the matrix (Table 6 of their paper) with the calculated density of antigorite is misleading since the latter is based on incorrect data. It has been pointed out (Zussman, 1954) that the figure 5.42 Å often assumed for the cell parameter of antigorite has no structural or experimental foundation and was obtained merely by dividing the measured value of c_0 (Aruja, 1944) by eight. It has also been shown that the true cell of antigorite does not contain the ideal atomic proportions. The measured density of antigorite is approximately 2.6, not 2.5 gms./cc., i.e. it is greater than that of chrysotile not less. The correspondence of the measured density of the matrix material with that calculated for antigorite is thus both fortuitous and unfortunate. In fact the vein-bearing matrix material of most of the specimens which we have examined by *x*-ray diffraction has been found to consist of lizardite or some other flat layer variant, or chrysotile or mixtures of these.

Another criticism of the paper by Kalousek & Muttart is that the implications of their *x*-ray data have not been adequately considered. Sufficient information is now available for most serpentine powder patterns to be assigned to specific varieties, and, moreover, to have their lines indexed. It is therefore possible to tell with certainty whether impurity lines are present. The authors do in fact recognise that "the serpentine specimens from Globe, Arizona, and from Eden Mills, Vermont, contained a second phase, possibly chlorite and magnesite, respectively," (though the Globe matrix also contains 21% CaO), and that "the Montville fibre also probably contained an unidentified impurity." They assumed that the other specimens were homogeneous phases, and "extraneous ions were assumed to be lattice constituents." No comment was made on the fact that impurity lines are present in the powder patterns of other specimens referred to in their Table 4, so that conclusions about details of their ion distributions are weakened. The presence of impurities may also affect the interpretations of the density measurements and the details of the thermal effects which are discussed. The pattern from the matrix from Globe, Arizona contains too few serpentine lines to permit its identification with any particular serpentine mineral; however, the positions of serpentine powder lines in the patterns from all other matrices in their Table 5, when compared with published data for antigorite show clearly that none of them is in fact antigorite. Thus Kalousek & Muttart's results are relevant to the distinctions between fibre and matrix but have not the relevance to antigorite which is implied in the title of the paper and elsewhere. None of the specimens dealt with was identified as a true antigorite, but among them Yu-Yen stone is now known to be predominantly antigorite by its electron diffraction patterns (Zussman, Brindley & Comer, 1957), and powder x-ray diffraction pattern (unpublished).

One of us (E.J.W.W.) wishes to thank the Directors of Derodo Ltd. for permission to publish this paper.

REFERENCES

ARUJA, E. (1944), An x-ray study of the crystal-structure of antigorite. *Mineral. Mag.*, **27,** 65–74.

KALOUSEK, G. L., AND MUTTART, L. E. (1957), Studies on the chrysotile and antigorite components of serpentine. *Am. Mineral.*, **42,** 1–22.

KOURINSKY, J., AND SATAVA, V. (1954), A contribution to the question of the determination of minerals of serpentine group. *Sbornik Narodniko Musea v. Praze*, **10,** No. 4.

MIDGLEY, H. G. (1951), A serpentine from Kennack Cove, Lizard, Cornwall. *Mineral. Mag.*, **29,** 526–530.

NAGY, B., AND FAUST, G. T. (1956), Serpentines: Natural mixtures of chrysotile and antigorite. *Am. Mineral.*, **41,** 817–838.

WHITTAKER, E. J. W., AND ZUSSMAN, J. (1956), The characterisation of serpentine minerals by x-ray diffraction. *Mineral. Mag.*, **31,** 107–126.

ZUSSMAN, J., BRINDLEY, G. W., AND COMER, J. J. (1957), Electron diffraction studies of serpentine minerals. *Am. Mineral.*, **42,** 113–153.

Manuscript received February 4, 1958

THE AMERICAN MINERALOGIST, VOL. 43, SEPTEMBER-OCTOBER, 1958

STRUCTURAL AND CHEMICAL VARIATION IN CHROMIUM CHLORITE

DAVIS M. LAPHAM,* *Columbia University, New York, New York.*

ABSTRACT

A detailed analysis of *x*-ray powder diffraction graphs of chromium chlorite yields evidence for chromium substitution between 0 per cent and 8 per cent Cr_2O_3 in both the octahedral and tetrahedral sites of the talc and brucite layers. "Comorphism" is suggested for this substitution of one element in two different structural positions.

X-ray powder diffraction measurements based on *x*-ray spectrographic analyses provide accurate determinations of total chromium content. Certain *x*-ray "*d*" spacings and intensity values correlate with Cr_2O_3 content, while others indicate the extent of octahedral or tetrahedral chromium substitution.

Indices of refraction increase almost linearly with chromium content, the octahedral and tetrahedral substitution curves having slightly different slopes which converge at approximately 2 per cent Cr_2O_3. A similar convergence is noted for *x*-ray powder and differential thermal data.

Below 2 per cent, there is no correlation of properties and chromium content, because the net effects are overcome by Fe substitutions for Mg. Thermal data indicates that the chromium chlorite structure may have either greater or lesser stability than the Fe-Mg chlorites. Thermal stability is inversely proportional to chromium content.

Chromium chlorites with more than 2 per cent Cr_2O_3 may be classified as kotschubeite (dominantly tetrahedral chromium) and kammererite (dominantly octahedral chromium). When the Cr_2O_3 content is less, a terminology analogous to the corundophilite-prochlorite-clinochlore-penninite grouping for the Fe Mg chlorites may be used. The term "chromium chlorite" is a useful field term applicable to pink or rose-violet chlorite.

PART I. SYNOPSIS

INTRODUCTION

The research on which this paper is based, covering a period of three years, is devoted to the differentiation of members of the chromium chlorite group. Samples were collected from chromite localities in Pennsylvania. Specimens from the National Museum, Washington, D. C. were kindly loaned by Dr. George Switzer and the late Dr. W. F. Foshag. Additional samples were available from the research collection at Columbia University.

Optical, *x*-ray and thermal data have been combined with chemical analyses, *x*-ray spectrographic studies, and information on the general chlorite structure to develop a simple classification based both on the Si/Al ratio and the position of chromium substitution.

I extend my sincere appreciation to Professor Paul F. Kerr of Columbia University, under whose direction this project has been carried out. Very fine specimens of chromium chlorite from Erzincan Province, Turkey were kindly sent to Professor Kerr by Mr. Raoul Bergman of the Mutual Chemical Company of America. Additional specimens from this province were supplied by Mr. James Hillebrand, Ouray, Colorado through Mr. Otto Kopp, Columbia University. The writer is also grateful to Dr. Hugo Steinfink, Shell Research Laboratory for permission to use his single crystal *x*-ray data, and to Mr. William A. Bassett for stimulating discussions on many phases of this work.

---

* Present address: Bureau of Topographic and Geological Survey, Harrisburg, Pennsylvania.

Chlorite Chemistry

As chromium is introduced into the general chlorite structure, corresponding variations occur in the relative amounts of other cations. Chemical analyses and *x*-ray spectrographic determinations have been used to determine chemical composition. Chemical analyses by W. H. Herdsman, analytical chemist, Glasgow, Scotland and other analyses from the literature have been coordinated with *x*-ray, optical, and differential thermal data. Published analyses have not, as a rule, been utilized in constructing standardization curves. Shannon's analysis (1920) of a chromium chlorite from Deer Creek, Wyoming was used as an end point for the chromium *x*-ray spectrographic curve. Gonyer's chromic oxide analysis (Ross, 1929) for #27 has also been used.

Table I includes six chemical analyses by W. H. Herdsman and Shannon's Deer Creek analysis, listed in order of increasing chromium content, from left to right. Silica is nearly constant throughout the range of chromium substitution from 0.10 per cent to 7.88 per cent Cr_2O_3. However, Al_2O_3 varies considerably, exhibiting a sharp decrease between 1.14 per cent and 6.47 per cent Cr_2O_3. The lack of a consistent relation between Al_2O_3 per cent and Cr_2O_3 per cent at a constant SiO_2 per cent suggests that chromium substitution is only indirectly related to aluminum content. CaO and MgO increase with increasing chromium content in a regular manner, representing an attempt at charge equalization, especially at high Cr_2O_3 percentages. High K_2O and Na_2O in the Zermatt chlorite tend to maintain charge neutrality. All analyzed material was carefully selected under a binocular microscope to eliminate impurities. *X*-ray patterns served as an additional check.

Theoretical specific gravities calculated from chemical analyses and unit cell dimensions are compared with specific gravities determined with a Berman balance in Table II. Specimen #27 from Webster, North Carolina was too fine-grained for accurate specific gravity measurements. Discrepancies greater than 0.01 may be attributed to chromite, mica, and or vermiculite impurities, especially in #3 which is closely associated

TABLE I. CHEMICAL ANALYSES OF CHROMIUM CHLORITES

Sample	#4 Zermatt Valais, Switz.	#3 Chester Cy., Pa.	#9 Ogushi, Hizen, Japan	#2 West Chester, Pa.	#10 Siskiyou Cy., Calif.	#24 Erzincan, Turkey	#11* Deer Creek, Wyo.
Oxide							
SiO_2	32.92	33.60	36.43	31.18	32.08	32.22	32.12
Al_2O_3	14.57	10.14	12.24	17.68	13.98	8.66	9.50
Fe_2O_3	2.31	8.42	0.94	1.88	0.42	0.46	—
Cr_2O_3	0.10	0.12	0.54	1.14	3.40	6.47	7.88
TiO_2	Trace	0.12	Trace	Trace	Trace	—	—
FeO	3.44	2.39	6.87	1.72	1.36	1.38	1.98
MgO	32.68	29.32	30.94	32.58	34.66	35.06	35.36
MnO	0.06	0.23	0.11	0.01	0.02	Trace	—
CaO	0.05	0.05	0.33	0.10	0.72	1.04	1.24
NiO	0.05	0.08	0.09	0.09	0.09	Nil	—
$H_2O-105°$	0.09	1.26	0.13	0.48	0.32	0.58	—
$H_2O+105°$	13.13	13.78	11.42	12.93	12.93	13.82	10.25
K_2O	0.15	Trace	Nil	Trace	Trace	—	—
Na_2O	0.52	0.53	Trace	0.14	Trace	—	—
Total	100.10	100.04	100.04	99.93	99.98	99.69	98.33

Analyses by W. H. Herdsman.
* Analyses by E. V. Shannon (1920)
— Oxide not analyzed.
#9 U. S. National Museum #87144.
#10 U. S. National Museum #104723.
#11 U. S. National Museum #93908.

with vermiculite. Specific gravity tends to increase with increasing chromium content.

The schematic chemical composition of magnesian chlorite is as follows:

$$\text{Brucite layer: } (Mg, Al)_3(OH)_6$$
$$\text{Talc layer: } Mg_3(Si, Al)_4O_{10}(OH)_2$$

Chemical formulas based on the chemical analyses, given in Table III, were carried out on the basis of 18 oxygen atoms per unit cell, ten of which are bonded to metallic cations, and the remainder present as (OH). In accordance with the theoretical formula, the tetrahedral layer was filled first with Si, Al, Ti, and Cr to a total of four cations per unit cell. The remainder were placed in the octahedral position, with the exception of Ca, K, and Na, whose position is probably within the Si-O hexagonal

TABLE II. COMPARISON OF THEORETICAL AND OBSERVED SPECIFIC GRAVITY DETERMINATIONS

Sample	Theoretical Sp. Gr.	Observed Sp. Gr.
# 4	2.662	2.653
# 3	2.708	2.631
# 9	2.733	2.738
# 2	2.678	2.648
#10	2.619	2.622
#27*	2.637	—
#24	2.639	2.645
#11	2.747	2.718

* Analysis by Gonyer (Ross, 1929).

TABLE III. CALCULATED FORMULAS OF CHROMIUM CHLORITES FROM TABLE I

# 4 Zermatt, Valais, Switzerland
$Na_{.13}K_{.02}Ca_{.005}(Mg_{4.53}Al_{.66}Fe^{2}_{.27}Fe^{3}_{.14}Cr_{.007}Mn_{.005}Ni_{.004})(Si_{3.06}Al_{.94})O_{10}(OH)_{8.11}$
$(Na,K,Ca,)_{.16}(Mg,Al,Fe^{2},Fe^{3},Cr,Mn,Ni)_{5.62}(Si,Al)_{4}O_{10}(OH)_{8.11}$

# 3 Chester Co., Pennsylvania
$Na_{.13}Ca_{.005}(Mg_{4.07}Fe^{3}_{.59}Al_{.25}Fe^{2}_{.19}Mn_{.02}Cr_{.009}Ni_{.006})(Si_{3.13}Al_{.86}Ti_{.01})O_{10}(OJ)_{8.73}$
$(Na,Ca)_{.14}(Mg,Fe^{3},Al,Fe^{2},Mn,Cr,Ni)_{5.13}(Si,Al,Ti)_{4}O_{10}(OH)_{8.73}$

# 9 Ogushi, Hizen, Japan
$Ca_{.04}(Mg_{4.57}Al_{1.04}Fe^{2}_{.57}Fe^{3}_{.07}Cr_{.04}Mn_{.01}Ni_{.01})(Si_{3.61}Al_{.39})O_{10}(OH)_{7.53}$
$Ca_{.04}(Mg,Al,Fe^{2},Fe^{3},Cr,Mn,Ni)_{6.31}(Si,Al)_{4}O_{10}(OH)_{7.53}$

# 2 Chester, Pennsylvania
$Na_{.03}Ca_{.01}(Mg_{4.5}Al_{.82}Fe^{2}_{.15}Fe^{3}_{.13}Cr_{.08}Ni_{.007})(Si_{2.89}Al_{1.11})O_{10}(OH)_{8.28}$
$(Na,Ca)_{.04}(Mg,Al,Fe^{2},Fe^{3},Cr,Ni)_{5.66}(Si,Al)_{4}O_{10}(OH)_{8.28}$

#10 Siskiyou Co., California
$Ca_{.07}(Mg_{4.64}Al_{.62}Fe^{2}_{.1}Fe^{3}_{.03}Ni_{.006}Mn_{.001})(Si_{2.9}Al_{.86}Cr_{.24})O_{10}(OH)_{7.97}$
$Ca_{.07}(Mg,Al,Fe^{2},Fe^{3},Ni,Mn)_{5.4}(Si,Al,Cr)_{4}O_{10}(OH)_{7.97}$

#27 Webster, North Carolina (anal. by Gonyer)
$Ca_{.015}(Mg_{5.03}Al_{.36}Cr_{.27}Fe^{2}_{.23}Fe^{3}_{.11}Ni_{.02})(Si_{2.91}Al_{1.09})O_{10}(OH)_{7.99}$
$Ca_{.015}(Mg,Al,Cr,Fe^{2},Fe^{3},Ni)_{6.02}(Si,Al)_{4}O_{10}(OH)_{7.99}$

#24 Erzincan Prov., Turkey
$Ca_{.1}(Mg_{4.75}Cr_{.46}Fe^{2}_{.1}Fe^{3}_{.02})(Si_{2.93}Al_{.93})O_{10}(OH)_{8.74}$
$Ca_{.1}(Mg,Cr,Fe^{2},Fe^{3})_{5.33}(Si,Al)_{3.86}O_{10}(OH)_{8.74}$

#11 Deer Creek, Wyoming (anal. by Shannon)
$Ca_{.14}(Mg_{5.46}Al_{1.16}Fe^{2}_{.17})(Si_{3.34}Cr_{.65})O_{10}(OH)_{7.08}$
$Ca_{.14}(Mg,Al,Fe^{2})_{6.79}(Si,Cr)_{3.99}O_{10}(OH)_{7.08}$

TABLE IV. X-RAY SPECTROGRAPHIC CHROMIUM CONTENT DERIVED FROM CHEMICAL ANALYSES AND K_α PEAK INTENSITY

	Cr Peak Intensity	% Cr_2O_3 Chem. Anal.	% Cr_2O_3 X-ray Spectrographic
No. 4. Zermatt, Valais, Switz.	1.3	0.10	0.10
No. 3. Chester, Pa.	1.9	0.12	0.12
No. 9. Ogushi, Hizen, Japan	7.1	0.54	0.50
No. 2. West Chester, Pa.	16.6	1.14	1.16
No. 17. U.S.S.R.	29.0		2.22
No. 23. Texas, Pa.	37.1		2.94
No. 27. Webster, N. C.	38.8	3.54	3.08
No. 25. Wood's Mine, Pa.	39.7		3.16
No. 10. Siskiyou Co., Calif.	41.9	3.40	3.40
No. 21. Bilimbaievsk, Urals	67.3		5.94
No. 24. Erzincan, Turkey	72.4	6.47	6.47
No. 11. Deer Creek, Wyo.	83.0	7.88	7.79

No. 27. Anal. by Gonyer (Ross, 1929).
No. 11. Anal. by Shannon (1920).
No. 9. U. S. National Museum No. 87144.
No. 17. U. S. National Museum No. 103312.
No. 27. U. S. National Museum No. 97548.
No. 23. U. S. National Museum No. R4534.
No. 10. U. S. National Museum No. 104723.
No. 21. U. S. National Museum No. 16261.
No. 11. U. S. National Museum No. 93908.
Nos. 4, 3, 2, 25, and 24 Columbia University Research Collection.

networks. For reasons presented later, all the chromium in #10 and #11 is placed in tetrahedral coordination. In general, it may be seen that chromium chlorites conform to the theoretical chlorite structure, differences being of a minor order. Specimen #24 contains insufficient cations to fill the tetrahedral layer if all of the chromium is octahedral, as is believed to be the case.

X-ray spectrographic values for chromium were taken from an average of a minimum of 7 runs per sample. The same sample and sample holder were used for each determination. An attempt was made to pack each sample to the same degree to eliminate errors in the amount of sample irradiated per unit surface area. The average of the highest consistent set of three values was used, and is reproducible within the limits of error for instrument reproducibility. Table IV gives the chromium peak intensities for all the chlorites considered in this paper, and the corresponding Cr_2O_3 per cent from both chemical analyses and x-ray spectrographic data.

PART II. MINERALOGY

X-RAY POWDER ANALYSIS

Introduction

The general chlorite structure is shown in Fig. 1. The details to follow, concerning chromium substitution in chlorite, are based on modifications of this model.

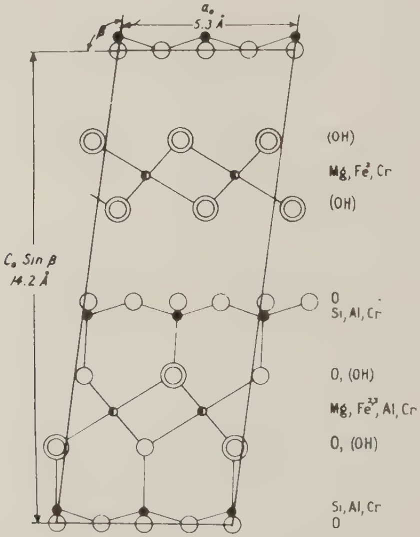

FIG. 1. General chlorite structure. Unit cell in the *a-c* plane (modified after Brindley, 1951, Fig. VI, 4).

Tables and graphs giving *x*-ray data are based on three runs per sample. Sample holders were back-filled to eliminate errors due to sample packing. Curves were obtained at intervals over a two year period to determine the maximum error in reproducibility. An average of three runs was found to yield consistent results, regardless of the time span between runs. A silicon standard was used at each running period to correct for 2θ errors in alignment. All intensity measurements are relative to the strongest line. Since the majority of peaks, with the exception of (020), are sharp, reliable intensities were obtained by subtracting background from peak height. The regularity of the intensity changes, and the ability to utilize *d* value variations to ±0.1 Å, as illustrated in the graphs, indicate adequate accuracy.

Only chlorites containing more than 1.0 per cent Cr_2O_3 are considered, because lesser amounts have a negligible effect on chlorite structures. Intensity values for (001) reflections below 1 per cent are anomalous

(Fig. 2). The line in Fig. 2 was approximated by sight, because the (001) intensity is affected by ions other than chromium, resulting in a wide scatter of points.

Table V lists *d* values and intensities for chromium chlorites containing more than 1 per cent Cr_2O_3. Chromium content increases to the right. The samples follow the order given in Table IV.

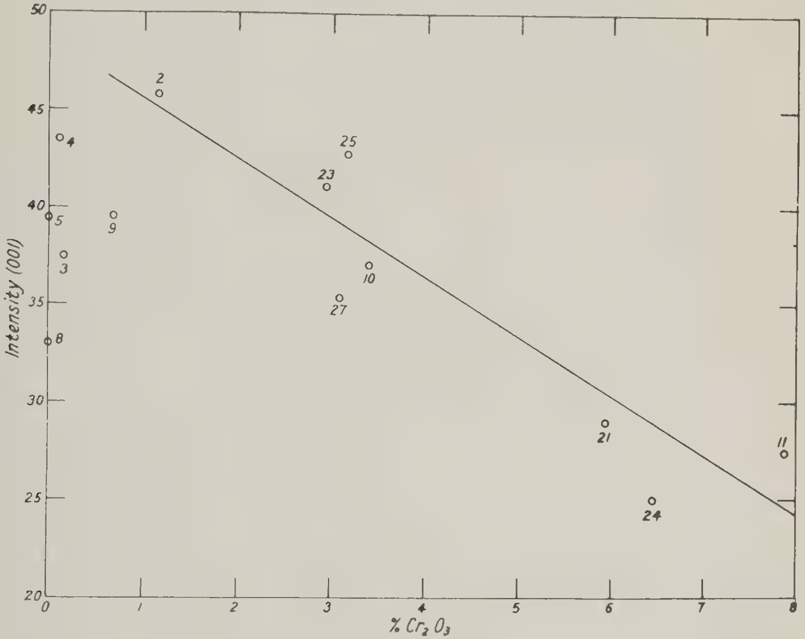

FIG. 2. Variation in chromic oxide content with (001) intensity.

d Spacing—Composition Graphs

Figure 3 represents the effect of chromium substitution on a basal spacing reflection, the (007). Lattice expansion accompanies increasing chromium content. The values suggest an upper and lower curve, the same chlorite samples being located along similar curves for other basal spacings. Chlorites 10, 21, and 11 exhibit lesser expansion with increasing chromium, while chlorites 23, 27, 25, and 24 exhibit greater expansion. Chromium is responsible for this expansion, since it is the only element which varies directly and consistently with *d* values. Although aluminum generally decreases as chromium increases, the relation is irregular. Calcium also increases slightly with chromium (Table I), but

TABLE V. INTERPLANAR SPACINGS AND INTENSITIES

#2		#17		#23		#27		#25		#10		#21		#24		#11		(hkl)
d(A)	Int.	d(A)	Int.	d(A)	Int.	d(A)	Int.	d(A)	Int.	d(A)	Int.	d(A)	Int.	d(A)	Int.	d(A)	Int.	
14.10	45.7			14.10 7.72	41.1 1.9	14.13	35.3	14.17 7.88	42.8 1.9	14.15	37.0	14.13	29.0	14.15 7.90	25.0 1.4	14.15	27.4	001
7.083	96.7			7.09	97.0	7.11	100.0	7.12	95.7	7.11	95.2	7.11	96.2	7.14	100.0	7.12	97.6	002
4.727 4.585	87.8 6.0	6.99	99.8	4.746 4.592	97.5 3.6	4.749 4.604	97.7 3.4	4.762 4.595	98.8 2.6	4.741 4.581	92.6 7.0	4.757 4.589	97.3 5.8	4.774 4.595	92.4 2.6	4.756 4.600	99.5 3.8	003 020
3.921 3.549	1.3 97.3	4.525	2.6	3.951 3.564	1.8 86.7	3.943 3.567	1.4 97.7	3.951 3.573	1.9 89.9	3.931 3.561	2.0 93.5	3.951 3.570	2.1 86.3	3.964 3.589	1.2 90.7	3.572	89.6	004
2.841	25.0	3.507	93.5	2.851	24.8	2.852	28.4	2.858	25.3	2.847	24.9	2.855	22.8	2.868	22.4	2.857	22.9	005
2.580 2.539	5.6 9.3	2.602	3.1	2.578 2.538	2.7 6.2	2.577 2.539	2.8 3.8	2.583 2.539	3.2 5.3	2.583 2.538	5.7 9.3	2.585 2.541	3.5 7.1	2.585	1.4	2.581 2.539	3.0 5.4	131, 20$\bar{2}$ 13$\bar{2}$, 201
2.435 2.376	7.7 4.9	2.475	8.0	2.439 2.379	4.9 3.4	2.442 2.380	3.7 2.6	2.442 2.382	5.0 3.2	2.440 2.377	7.2 4.1	2.443 2.380	5.5 4.0	2.442 2.387	1.2 5.8	2.441 2.381	4.0 3.7	132, 20$\bar{3}$ 006, 13$\bar{3}$
2.257	3.3	2.338	8.2	2.261	2.6	2.261	2.2	2.262	2.1	2.322 2.260	2.0 3.3	2.261	3.1			2.328 2.260	1.4 2.8	20$\bar{4}$, 133
2.029 2.001	7.4 10.4	2.112	2.1	2.039 2.006	5.6 7.7	2.040 2.006	6.8 5.2	2.043 2.009	6.3 6.6	2.033 2.003	7.1 7.9	2.040 2.008	6.9 8.2	2.048 2.015	6.7 2.8	2.044 2.008	7.1 6.9	007 204, 13$\bar{5}$
1.880 1.821 1.785	3.8 3.1 1.6	1.924	6.4	1.886 1.829 1.782	2.5 2.7 0.8	1.888 1.830 1.805	1.9 1.9 0.8	1.888 1.830 1.782	2.7 2.5 0.8	1.883 1.825 1.803	3.2 2.9 1.5	1.889 1.832 1.789	2.1 3.0 1.1	1.893 1.793	0.7 0.9	1.889 1.832 1.790	2.6 2.4 1.1	20$\bar{6}$, 135 13$\bar{6}$ 215
1.722 1.660	1.2 2.0	1.754	3.8	1.733 1.721 1.667	1.2 1.1 1.4	1.730 1.714 1.667	0.9 0.9 1.4	1.738 1.724 1.666	0.8 0.8 1.6	1.711 1.666	1.3 1.8	1.725 1.668	1.0 1.6	1.724 1.674	1.3 3.6	1.728 1.671	0.9 1.5	300 20$\bar{7}$ 136 206, 13$\bar{7}$
1.564 1.535	7.4 5.7	1.600	2.4	1.571 1.537	6.4 3.0	1.572 1.538	5.0 2.1	1.572 1.536	5.8 3.5	1.569 1.537	6.0 6.1	1.571 1.538	6.7 4.7	1.567 1.538	1.8 2.0	1.573 1.536	5.6 3.4	20$\bar{8}$, 137 060
1.500	2.3	1.529	3.2	1.502	1.2	1.504	1.0	1.504	1.3	1.501	2.3	1.503	1.7	1.503	0.9	1.503	1.4	331, 062
1.419	3.1	1.462	3.3	1.428	3.2	1.427	3.0	1.430	2.8	1.425	2.8	1.428	3.2	1.435	3.4	1.432	3.4	00.10
1.393	7.2	1.402	2.3	1.401	5.8	1.401	5.1	1.400	5.1	1.396	5.7	1.402	6.3	1.408	0.4	1.402	5.5	13$\bar{9}$, 208

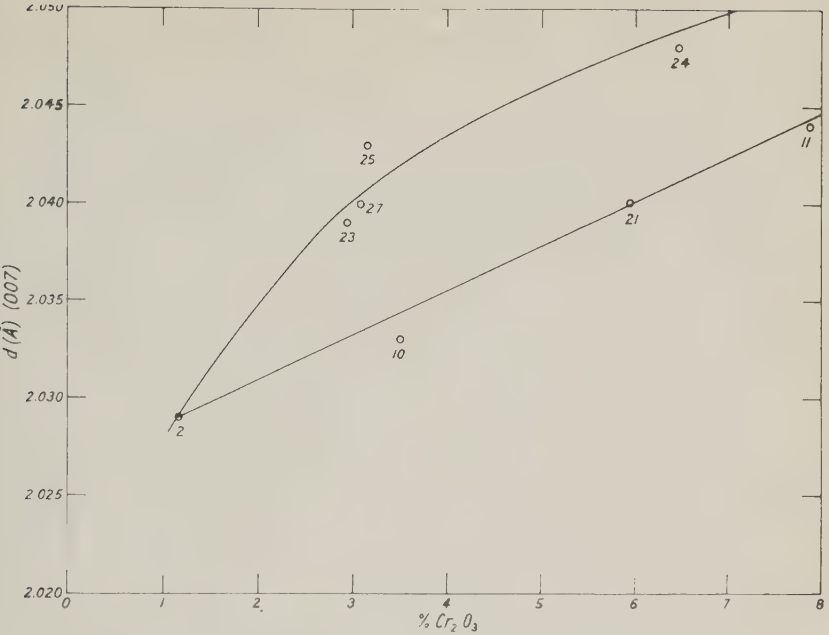

FIG. 3. Variation in chromic oxide content with (007) spacing. The upper curve represents octahedral Cr and the lower curve tetrahedral Cr.

it is present in insufficient amounts to cause the observed shifts. Similarly, iron and the Si/Al ratio show no correspondence.

Variations in the diffraction pattern of a chlorite may be attributed to structural and/or chemical variations. Polytypic (stacking) variations such as rotations in the a–b plane result in symmetry changes and hence affect the intensity of reflection. However, they cannot be directly responsible for expansions of basal spacings as long as the mineral is trioctahedral; i.e., as long as all possible atomic positions are filled. Thus the rotation or shift of succeeding layers does not affect the position of reflection, although it does affect the reflecting power from atomic planes.

The other way in which the expansion of atomic planes may result, if the unit cell structure and degree of crystallinity remain the same, is by varying the position of substitution of one or more cations, in this case, chromium. A comparison of the d values in Table V shows that the fundamental structure remains unchanged. Variations in degree of crystallinity affect peak intensities and peak shapes, but not their position.

Two different sites are available, tetrahedral and octahedral, corresponding to silicon and magnesium positions respectively (Fig. 1).

The substitution of aluminum for silicon contracts the lattice (Brindley, 1951, Fig. VI-7), or conversely, a high Si/Al ratio will expand it. The substitution of aluminum results in an excess negative charge on the tetrahedral layer. This resulting charge imbalance on the tetrahedral layer may be compensated by substitution of ferric iron in the octahedral layer, tending to draw the brucite and talc layers closer together. Here, however, the irregularity of the change in the Si/Al ratio (Tables I and III) indicates that the consistently regular *d* value changes cannot be due to silicon-aluminum substitutions.

Cr^3 has the same ionic vàlence as Al^3, but its ionic size is slightly larger. As a result of this increase in size, the substitution of chromium for aluminum in the tetrahedral position would be expected to expand the lattice. In the case of aluminum substitution for silicon, the lattice contracts, because of a local charge imbalance, but the substitution of the somewhat larger Cr^3 ion will expand the lattice only slightly beyond that caused by substitution of an equivalent amount of aluminum, because there is no change in charge. The lower curve in Fig. 3 illustrates such a small linear increase.

The substitution of a trivalent ion, such as chromium, for a divalent ion, such as magnesium, in the octahedral layer creates a greater than normal positive cation charge on this layer. This may be compensated by increasing the amount of $(OH)^-$, or by substituting more aluminum for silicon in the tetrahedral layer. Since the Si/Al ratio generally increases with increasing chromium content, this cannot be a factor in restoring charge balance. A large part of the imbalance is probably made up by the substitution of (OH) . For example, #24 contains the greatest amount of $(OH)^-$ (Table I). It is significant that this sample exhibits the greatest expansion for the highest Cr_2O_3 percentages. The high Si/Al ratio in the tetrahedral layer, in conjunction with increased chromium in the octahedral layer, results in increased positive cation charge for these cation positions. In such a situation, these two layers tend to expand, because the charge binding the two layers is weak. Because of the nearly equal ionic radii of chromium and magnesium, chromium can be expected to fit easily into this octahedral position. Since there is little change in the sizes of the substituting ions, expansion can be attributed to local charge imbalances which are compensated over a large number of unit cells by substitutions which tend to maintain electrical neutrality. As a result of this chromium substitution, a larger lattice expansion would be expected for octahedral chromium than for tetrahedral chromium. The upper curve in Fig. 3 would then represent octahedral chromium chlorite. Plots for (004), (005), (006), $(13\bar{5})(204)$, (062)(331), c_0, and $(13\bar{7})(206)$ against composition have been found to yield graphs which contain the same separation of points as Fig. 3.

Intensity—Composition Graphs

Since two positions of chromium substitution have been suggested, the effects of this substitution will be considered first, postponing a discussion of polytypism.

If there is a difference in substitution position between octahedral and tetrahedral layers, this difference should be observable from (002) intensities, because the degree of phase addition or subtraction for this reflection is a function of the difference in scattering power between octahedral and tetrahedral sites. Figure 4 illustrates such a separation. The lower curve represents tetrahedral chromium and the upper curve octahedral chromium. Phase relations for normal chlorites indicate that scattering from the octahedral layer is normally greater than that from the tetrahedral layer (See Brindley, 1951, Fig. VI-4). Thus as chromium is substituted in this layer, the larger scattering power of chromium with respect to magnesium increases the intensity of reflection as shown. As chromium substitutes in the tetrahedral layer, the normal situation with greater scattering from the octahedral layer is opposed, so that reflected intensities from these two layers tend to cancel out, and the intensity of reflection decreases. The intensity increase toward #11 is the

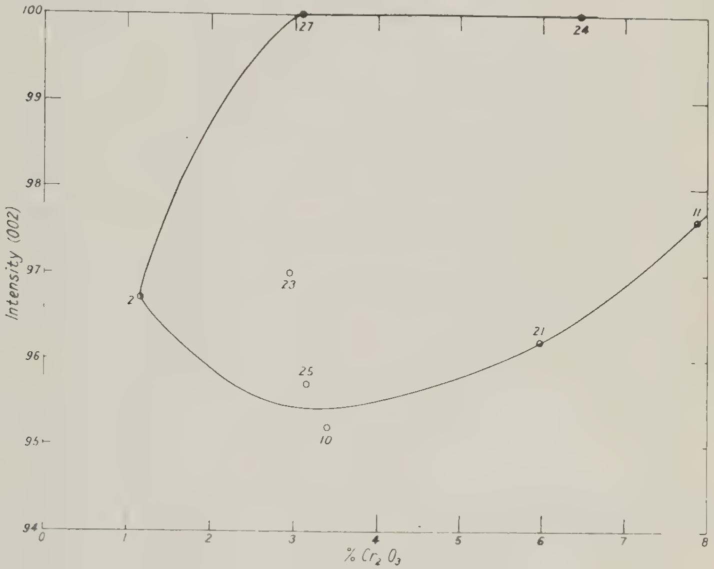

FIG. 4. Variation in chromic oxide content with (002) intensity. The upper curve represents octahedral Cr and the lower curve tetrahedral Cr. No. 23 is anomalous, possibly because of the replacement of octahedral Mg by Ni.

result of an unusually large number of octahedral cations, and is not a direct result of tetrahedral chromium substitution.

Sample #23 falls between the two curves in Fig. 4. It may represent chromium substitution in both the tetrahedral and octahedral positions. However, it seems more likely that this particular value is either in error, or anomalous. In all *d* spacing-composition plots this sample lies on the octahedral chromium curve. Similarly, other intensity-composition plots (Fig. 5) show that it belongs among the octahedral variety. Insufficient material prevented a complete chemical analysis, so that structure factor calculations were not possible. *X*-ray spectrographic data do show that #23 contains considerably more nickel than any of the other samples. Figure 7 shows that its index of refraction is unusually low. These anomalies may be an expression of the high nickel content.

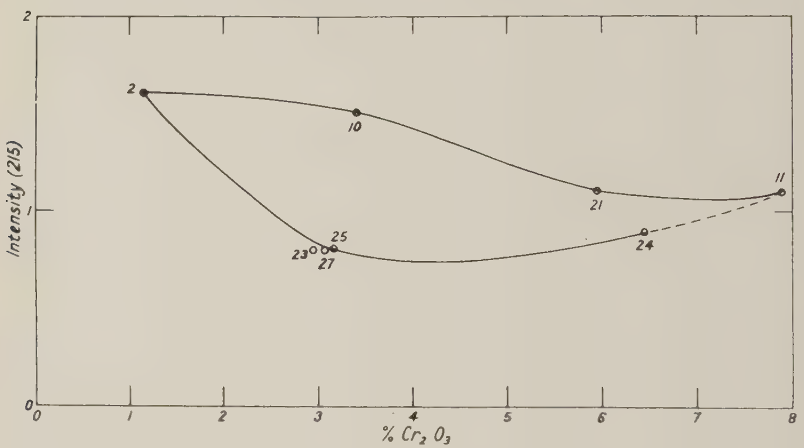

FIG. 5. Variation in chromic oxide content with (215) intensity. The upper curve represents tetrahedral Cr and the lower curve octahedral Cr.

For the (215) reflection (Fig. 5), both tetrahedral and octahedral substitution will decrease intensity, but the contribution due to tetrahedral chromium will have the least effect, because substitution in octahedral sites is the larger contributor to reflection (see Brindley, 1951, Fig. VI-5). Similar plots for (020) and (060) intensity against Cr_2O_3 per cent result and can be explained in a similar manner.

More important than these qualitative considerations are structure factor (F) calculations from observed intensities, which can be compared with F values determined from the samples with a known chemical composition. Table VI gives such a comparison for samples #2, #10, #11, and

#24 for the (001), (002), (003), (004), and (020) reflections. Calculations are based on an "M" type structure which has an a_3 displacement. Coordinates given by Brindley (1951, p. 186) were adjusted to an origin at the octahedral cation position of the talc layer for ease in calculation. The methods of calculation are outlined in Appendix A and B.

For these five reflections, there was only one combination of chromium and iron positions which would satisfy the F order obtained from observed intensities. This data verifies the previous qualitative observations that curves containing #2 and #24 represent octahedral chromium, and curves containing #10 and #11 represent tetrahedral chromium. In addition, the best fit of theoretical and observed values is obtained when octahedral chromium is placed in the brucite layer, and when the total iron content is divided between the talc and brucite layers. In three instances out of four, the majority of the iron is talc-octahedral. It is interesting to note that plus three chromium, substituting in the octahedral brucite position, is as far removed from the tetrahedral silicon position as the structure permits. Since there is less aluminum than is normally present in Fe-Mg chlorites, the tetrahedral position has a relatively higher positive charge. Chromium would be expected to substitute

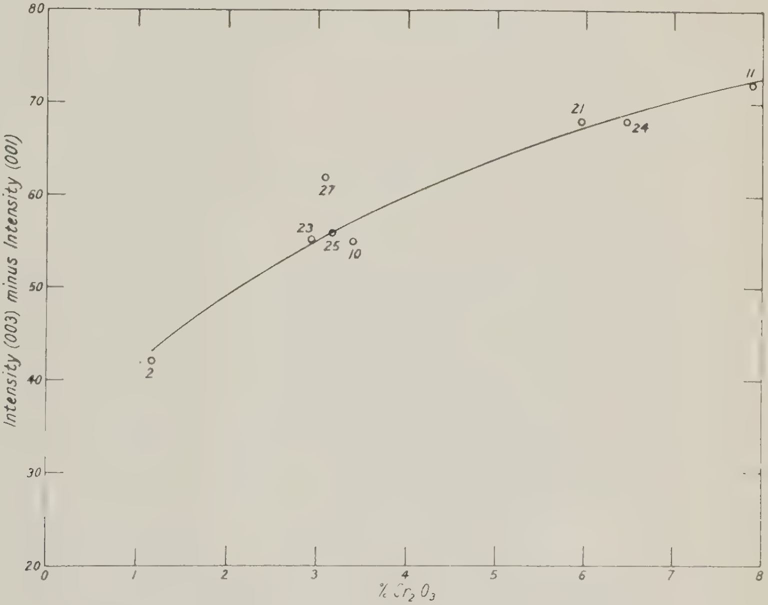

FIG. 6. Variation in chromic oxide content with (003) intensity minus (001) intensity.

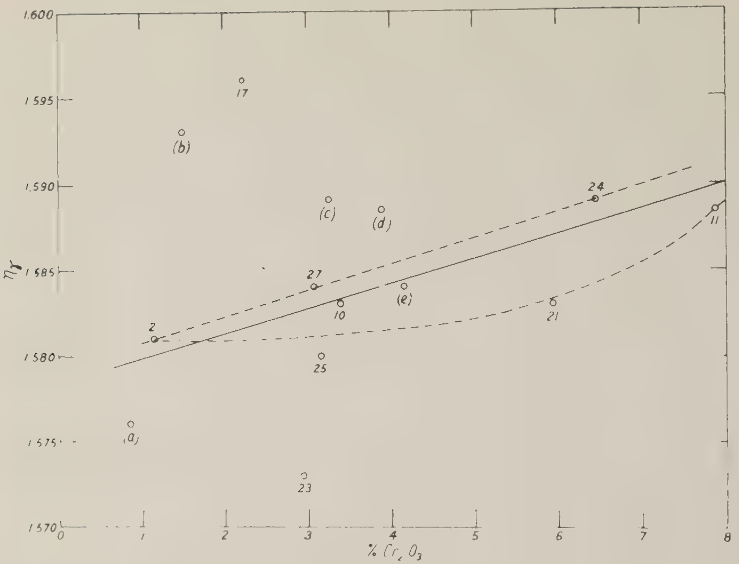

FIG. 7. Variation in chromic oxide content with gamma index of refraction. Lettered points represent published values, and numbered points represent chlorites studied in this report.

No. 23 is anomalous probably because of the presence of Ni. The upper dashed curve represents octahedral Cr, and the lower curve tetrahedral Cr.

as far away as possible. Slight adjustments were made for the large $(OH)^-$ content of #24, and for the $(OH)^-$ deficiency of #11 (see Table III).

Considering that certain assumptions have been made concerning the structure, the agreement is good. Theoretical F values are very close to those given by Brown (1955) for Fe-Mg chlorite. Garrido (1949) lists comparisons for a chromium chlorite containing $b_0/3$ and $2b_0/3$ shifts with similar discrepancies between theoretical and observed values.

From a consideration of planes whose intensities are unaffected by positional chromium substitution, the amount of Cr_2O_3 may be determined for any chromium chlorite. One of the most accurate of these is the plot of (003) intensity minus (001) intensity against Cr_2O_3 per cent (Fig. 6). The negative F of (003) and the positive F of (001) cancel out positional differences, yielding a straight-line curve.

Stacking variations and lattice displacements (polytypism and polymorphism, respectively) have been mentioned as another mechanism affecting the intensity of reflection. An a_1 shift shift perpendicular to b would not affect intensities to a large extent, nor would it be a continuous function of chromium content. A similar reasoning holds for a_2 and a_3 shifts. Furthermore, although #24 contains successive 120° rotations, #10 is a normal chlorite without structural displacements (personal communication, Hugo Steinfink), thus indicating that such variation is not the primary cause of observed intensities. However, a consideration of polytypic forms might well yield a closer agreement between theoretical and observed F values.

X-RAY SINGLE CRYSTAL ANALYSIS

Laue Photographs

Laue photographs were taken of samples #17, 21, 10, 24 and 11. Because of a lack of good crystals, the photographs are generally streaked with diffuse or multiple spots. The photographs of #10, #21, and #24 are reproduced in Plate I. Their maximum symmetry is monoclinic. Differences in structure and composition result in differences in intensities for planes with the same index, and in different relative placement of spots and streaks. Sharp spots as in #24 represent well crystallized material. Extreme thickness of the crystal may result in diffuse spots (Schiebold, 1944), and is probably a contributing factor in these photographs. Double or triple spots may be produced in several ways. Lonsdale (1945) notes that double spots result if white radiation contains a strong characteristic component. However, this collimating system has given sharp spots (Plate I, #24), and hence doublets would seem to have a crystallographic origin. Schiebold (1944) reports a similar phenomenon caused by inhohomogeneous crystal distortion. Cleavage flakes with such distortions are expected in chlorite crystals. Multiple spots may also be produced by differential absorption or by a mosaic crystal surface (Lonsdale, 1945). The triple spots of #24 might be the result of successive 120° rotations of the 14 Å unit cell, requiring three such rotations to form a repeatable unit cell. If these rotations were not exactly coincident, then reflections from each of the three positions would appear. Maguin (Plate VIII, 1928) shows a Laue photograph of biotite which has a similar tertiary symmetry and which he ascribes to orientations of +120° and −120°. He states that chlorites also show this feature. Rotations of this type have been described by Brindley, Oughton, and Robinson (1950). Streaks are probably the result of diffuse reflections where $k \neq 3n$, and hence are most prominent in the *b* direction.

Unexplained hatchet-shaped spots are typical of #10. Good reflections are almost non-existent. #24 exhibits pseudotrigonal symmetry which is expressed surficially by "trigonal prisms" around the *c* axis. Since a solid solution of one kind of atom in the lattice position of another may yield diffuse spots (Lonsdale, 1945), the greater diffuseness in

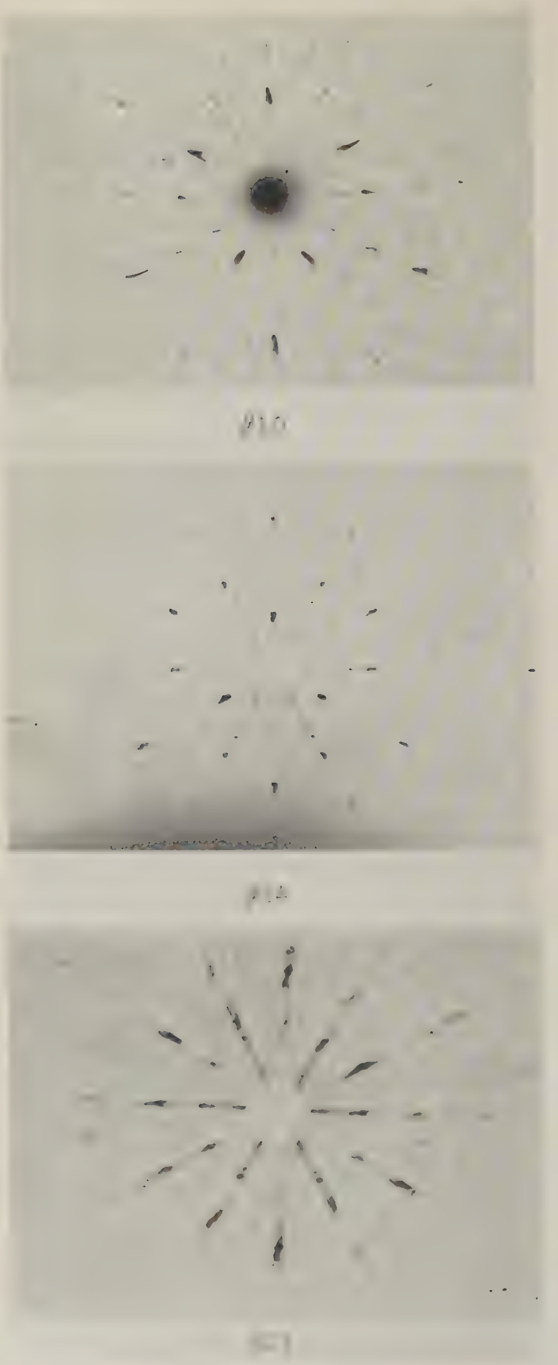

Plate I. Laue Photographs.

TABLE VI. COMPARISON OF OBSERVED AND THEORETICAL STRUCTURE FACTOR CALCULATIONS

Sample	Intensity	F-observed	F-theoretical	Cr*	Fe*
(001)					
24	25.0	4.0	50	Brucite	$\frac{2}{3}$ Talc
11	27.4	4.3	52	Talc-Tet.	$\frac{2}{3}$ Brucite
10	37.0	5.1	56	Talc-Tet.	$\frac{2}{3}$ Talc
2	45.7	5.5	59	Brucite	$\frac{2}{3}$ Talc
(002)					
10	95.2	15.7	79	Tet.	—
2	96.7	15.8	89	Oct.	—
11	97.6	15.9	91	Tet.	—
24	100.0	16.1	94	Oct.	—
(003)					
2	87.8	22.9	− 86	Brucite	$\frac{2}{3}$ Talc
24	92.4	23.5	− 90	Brucite	$\frac{2}{3}$ Talc
10	92.6	23.6	− 91	Talc-Tet.	$\frac{2}{3}$ Talc
11	99.5	24.3	−102	Talc-Tet.	$\frac{2}{3}$ Brucite
(004)					
11	89.6	31.2	147	Tet.	—
24	90.7	31.2	147	Oct.	—
10	93.5	32.0	153	Tet.	—
2	97.3	32.4	159	Oct.	—
(020)					
24	2.6	4.1	91	Oct.	—
11	3.8	4.9	92	Tet.	—
2	6.0	6.4	96	Oct.	—
10	7.0	7.0	99	Tet.	—

* Brucite: brucite layer.
Talc: talc layer.
Tet.: tetrahedral position.
Oct.: octahedral position.

samples #10 and #21 may be the result of chromium substitution for aluminum in the tetrahedral position, which is not so well suited to ions as large as chromium.

In general, the Laue method is not sufficient for detailed differentiation among chromium chlorites, but it does illustrate that structural variations may be present.

Rotation and Precession Data

Samples #10 and #24 were given to Dr. Richards A. Rowland, Shell Development Company, who kindly offered to have single crystal photographs taken as an aid in determining structure. Data presented here are from one rotation and several precession photographs taken by Dr. Hugo Steinfink.

Characteristic streaking, such as that found on Laue photographs, indicates that $k \neq 3n$. Complete streaking would indicate a complete randomness of 1/3 *b* shifts. However, there are some spots present along $k \neq 3n$ layers in addition to the streaking, which indicates that the 1/3 *b* shifts have a preferred sequence of displacements. These spots occur at integral values of *l* and can be seen to subdivide the *c* spacing into three equal divisions, indicating a tripling of the normal 14 Å unit cell spacing. Thus the true height of a unit cell in the *c* direction is actually 3×14.3 Å or about 43 Å.

Although the true intensities of the spots along $k = 2$ are masked by streaking, they appear to be the same on both $(0kl)$ and $(0\bar{k}l)$, suggesting that the sample is monoclinic. A similar crystal, Brindley's "D" (Brindley, Oughton, and Robinson, 1950), is interpreted as triclinic on the basis of differing intensities for positive and negative indices.

If the unit cell is then taken as 43 Å, there will be an extinction of $(00l)$ spots for which $l \neq 3n$, as the precession photographs show, implying that the *c* axis of a pseudo unit cell 9×14 Å acts like a 3_1 screw axis. A similar type of pseudo unit cell for the 14 Å variety (normal) of 3×14 Å (orthohexagonal cell) may be constructed. Such a structure means that the stacking of one complete chlorite layer occurs so that each succeeding layer is rotated 120° and then placed on top of the previous layer.

Single crystal photographs of #10 from Siskiyou County contain sharp spots for $k \neq 3n$, indicating a normal well ordered structure. Thus, in one case, the substitution of tetrahedral chromium resulted in a stable 14 Å unit cell, while the octahedral substitution of chromium (#24) resulted in a layer rotation. In the latter instance, a repeatable 14 Å unit cell was not a stable configuration. Additional data from differential thermal analyses supports the hypothesis that polymorphism, unit cell stability, and positional substitution may be inter-related.

Optical Properties

General Characteristics

Table VII summarizes the optical properties of the nine chlorites discussed. Changes in refractive indices and optic sign will be considered separately. Column 3 shows that there is no consistent change in birefringence with chromium content, although Winchell (1936) has suggested that it might decrease with increasing chromium. The following are additional published values supporting this conclusion:

Sample	% Cr_2O_3	Birefringence	Reference
Newcastle, Calif.	1.5	.012	Shannon (1920)
Patevi, Togo	1.84	.004	Orcel (1927)
Patevi, Togo	4.18	.005	Orcel (1927)
Mt. Albert, Quebec	3.3	less than .010	Osborne and Archambault (1948)
Sweden	13.46	.004	DuRietz (1935)

The accuracy of DuRietz' data is questionable, since the optic sign and indices of refraction do not correspond to the stated chromium content, according to the relation in Fig. 7. The birefringence in Table VII is the difference between the alpha and gamma indices of refraction.

Column 5 suggests that there is no direct correspondence between 2V and chromium content. As in the Fe-Mg chlorites, this angle is generally 10° or less, although Miller (1953) reports a kammererite from Webster, North Carolina containing 3.9 per cent Cr_2O_3 and a 2V of 20°.

In general, chromium chlorites range from colorless or light green to pale pink and violet-pink as chromium increases (column 6). Axial colors are occasionally present.

Pleochroism and absorption tend to increase with increasing chromium (column 7).

Interference colors (column 8) show that chlorites low in chromium have normal first order gray birefringence, while those containing 3 per cent or more Cr_2O_3 exhibit anomalous blue or yellow. Anomalous first order red is characteristic of #24.

Habit (column 9) is commonly irregular to pseudo-hexagonal, viewed on basal plates. Basal sections of #24 are pseudo-trigonal.

Several of the chlorites exhibit additional features of note. Sample #24 has been divided into two types, I and II, on the basis of differing indices of refraction. Type I is not noticeably pleochroic and has lower indices than type II. Type II may represent a higher chromium content. Crystals of #24 taper to a point in the *c* direction and basal sections make internal angles of 120°. Sample #21 has been divided into two types on the basis of differing optic signs. When optically negative, the indices are slightly higher than when optically positive. The optically positive material predominates.

Optic Sign as a Function of Polarizability

The change in optic sign from positive at low Cr_2O_3 percentages to negative at high percentages is dependent on the degree to which the electric vectors of light waves passing through the mineral are additive. This addition is dependent upon the geometry of ionic groups within the mineral structure. Three types of geometrical shapes can be considered: spherical, rod-shaped, and flat or planar. Layer lattices, to which

TABLE VII. CHROMIUM CHLORITE OPTICAL PROPERTIES

No.	Indices of Refraction ±.002			Birefringence ±.002	Optic Sign	2V	Color	Absorption and Pleochroism	Interference Colors	Habit	%Cr_2O_3
	α	β	γ								
2	1.577	1.578	1.581	.004	Biaxial (+)	5–25	colorless to pale green	pale green parallel to N-S nicols	gray	irregular	1.14
17	1.590	1.590	1.596	.006	Biaxial (+)	0–18	colorless to pale pink	absent	gray	pseudo-hexagonal	2.2
23	1.568	1.569	1.573	.005	Uniaxial to Biaxial (+)	0 to 10	colorless	absent	rarely blue	irregular	2.9
27	1.580	1.580	1.584	.004	Uniaxial to Biaxial (+)	0 to 10	X, Y-colorless, pink, blue Z—colorless or yellow	blue to yellow	yellow to rarely blue	pseudo-hexagonal	3.08
25	1.573	1.574	1.578	.005	Uniaxial to Biaxial (+)	0 to 10	colorless to pale pink and bluish	absent	blue and yellow	rarely pseudo-hexagonal	3.2
10	1.579	1.580	1.583	.004	Uniaxial to Biaxial (+)	0 to 30	colorless	absent	blue and yellow	rarely pseudo-hexagonal	3.4
21 I	1.580	1.581	1.583	.003	Biaxial (+)	0 to 15	colorless to pale pink	absent	blue and yellow	pseudo-hexagonal	5.9
II	1.580	1.583	1.584	.004	Uniaxial to Biaxial (−)	0 to 8	as above	absent	as above	as above	
24 I	1.582	1.586	1.586	.004	Biaxial (−)	0 to 10	I- pale pink	absent	blue and red	pseudo-trigonal	6.47
II	1.584	1.588	1.589	.005	Biaxial (−)		II-X—light pink YZ—violet pink	yellow to pink			
11	1.583	1.588	1.589	.006	Biaxial (−)	8	violet pink	X—pale red YZ—dark red	blue to yellow	pseudo-hexagonal	7.88

the chlorites belong, are planar. Their symmetrical ionic arrangement because of the framework structure of the SiO_4 tetrahedra and MgO octahedra, result in a low birefringence, so that their interference colors are almost nil, approaching isotropism.

As a result, substitution in either or both tetrahedral and octahedral positions changes polarizabilities and may also change the optic sign. Light passing through a crystal encounters this directional character of the ionic groups and is consequently polarized. Light vibrating along strongly planar groups will show a strong negative birefringence, with high indices for vibration directions parallel to the planes of the plates, and a low index for light vibrating normal to this direction (Hartshorne and Stuart, 1950). If the ionic groups are still parallel but more rod-shaped, or if they are planar but no longer parallel to each other, then a strong positive birefringence will result (Evans, 1952, p. 272).

Normally chlorites will be slightly positive. However, as chromium is substituted for Si-Al in the tetrahedral layer, and for magnesium in the octahedral layers, these groups increase in planar character and parallelism, and thereby increase their optically negative character. The point at which chlorite changes from optically positive to negative is the point at which the indicatrix is no longer triaxial, changing from an optically positive ellipsoid to one that is negative. Chlorite #21 represents a close approximation to this situation. To the left of the change in optic sign in Fig. 7, positive birefringence tends to increase, while to the right, toward the higher indices and chromium content, negative birefringence tends to increase (Table VII).

The inter-relationship between *x*-ray analysis and optical studies may be seen to be a function of polarizability, which in turn is dependent upon variations in charge distribution accompanying the substitution of chromium. The greatest effect on optical properties results from octahedral chromium substitution, because substitution of the widely differing chromium ions for magnesium has a greater effect on the planar character of the ionic groups, while the more nearly similar chromium and aluminum produce less significant changes. *X*-ray data also suggested that octahedral chromium produced more marked effects on lattice spacings and intensities.

Effects of Chromium on Indices of Refraction

Figure 7 is a plot of Cr_2O_3 per cent against the gamma index of refraction. Alpha and beta show similar relations. The solid line curve is considered to be relatively accurate between 3 and 8 per cent, but the wide scatter of points at lower percentages renders this part of the curve inaccurate. The refractive indices of points 2, 17, 23, 25, 10, 27, 21, 24, and 11 were determined using liquids calibrated with sodium light at approximately 0.005 intervals. With the exception of 17 and 23, these points yield a curve with relatively narrow range. Lettered points representing analyses and determinations by other authors indicate that the results of different workers may vary considerably.

Point *a* is a green chromium chlorite from Togo (Orcel, 1927). Point *b* represents Shannon's analysis of a chromium chlorite from Newcastle, California (1920). Since Cr_2O_3 per cent is often too high because of small inclusions of chromite, this determination is probably either anomalous, similar to 17 and 23, or represents an error in index determination. Point (*c*) is from a Quebec sample, analyzed by Osborne and Archambault (1948). Point (*d*) is only an approximate gamma index, since Miller (1953) only listed beta (1.5855) and a positive optic sign. Point (*e*) represents another specimen from Togo (Orcel, 1927). An additional chromium chlorite not shown on the graph has been reported by DuRietz (1935) with the following properties:

$n = 1.590$
optically (+)
13.46% Cr_2O_3

Since no other chromium chlorites with more than 5.9 per cent Cr_2O_3 have been found with a positive optic angle, it would seem that either the sign determination or the chromium analysis is in error.

Point 17, representing the 7 Å chlorite, is not directly comparable to the other 14 Å structures. Similarly, points 23 and 25 appear to be anomalous. The presence of other ions such as Fe, Ni, or Ca is suggested as a source of this discrepancy, since *x*-ray spectrographic analyses show that 23 has a NiO content of approximately 0.4 per cent, and 25 of about 0.1 per cent. All other chromium chlorites contained less than 0.1 per cent NiO. Since the index of refraction increases with polarization, substitution of the smaller Ni^2 ion for the larger Fe^2 would tend to lower the index, the nickel ion being less polarizable.

Effects of Chromium Substitution on Polarizability

The solid line curve in Fig. 7 represents changes in refractive indices with increasing chromium substitution. However, in the light of the *x*-ray evidence presented previously, a better approximation to composition may be obtained by utilizing the effects of polarizabilities on optical properties. In unsymmetrical structures such as the chlorites, polarization of a given ion is determined both by the electric vector of the light wave and by the field which results from polarization of its neighboring ions and ionic groups (Evans, 1952, p. 271). Since "the interaction of electromagnetic waves and matter arises from the polarization of the electronic structure of the individual atoms by the electric vector of the light waves" (Evans, 1952, p. 270), the index of refraction of a mineral is a function of this interaction, and directly related to polarizability. Refractive indices increase with increasing polarizability, which itself increases with the looseness of the ionic bonding. As a result, substitution of a larger ion with equivalent or smaller valence charge tends to increase the refractive indices. Conversely, the substitution of a smaller ion with equivalent or greater charge tends to decrease refractive indices.

Although there is no charge difference between chromium and aluminum, the ionic radius of chromium is larger than that of aluminum (or silicon). Substitution therefore results in looser bonding, greater polarizability, and hence higher refractive indices. However, since chromium is about 0.12 units larger than aluminum, and since the "overwhelming contribution to the refractivity of any ionic compound is . . . due to the anion" (Evans, 1952, p. 25), this substitution will not increase the refractive indices to a large extent.

The lower dashed curve in Fig. 7 corresponds to this case, in which the indices are increased slightly by chromium substitution into the tetrahedral position. It should be noted that the same chlorites fall on this curve as on the *d* spacing-composition-intensity plots in the previous section, with the exception of the anomalous #23 and #25.

On this theoretical basis, it might be expected that substitution of chromium for magnesium, which has a larger ionic radius and a smaller valence charge than chromium, would decrease the polarizability and hence also decrease the refractive indices. A glance at Fig. 7 immediately reveals that this is not the case. However, if it is remembered that the controlling factor in polarizability and variation in indices of refraction is the quantity and distribution of anions, then the increase in indices may be explained. No 24 has more $(OH)^-$ than any of the other chlorites (Table I). Also contributing to this high index is the low Si/Al ratio, which can be compared with a higher ratio for #11. No. 24 also contains more anion radicals per cation than any of the other chromium chlorites studied. Thus the uper curve in Fig. 7 represents octahedral substitution of chromium, and is controlled by anion variation.

Winchell (1936) and Hey (1954) have both remarked that chromium substitution might increase refractive indices analogous to the increase caused by iron substitution for magnesium. Although there is a small general increase in index, the increase is not due directly to substitution of chromium for magnesium, as in the case of Fe^2 for Mg^2, but is primarily due to the amount of anions (or the cation-anion ratio) accompanying octahedral chromium substitution. In addition, not all of the chromium chlorites can be explained in this manner alone, since tetrahedrally substituted chromium also exists and increases the indices at a different rate. As a result, no single simple relationship appears to exist between indices of refraction and the chromium content in chlorites.

Differential Thermal Analysis

Technique and Description

Powdered samples finer than 120 mesh were heated at 12° C. per minute to record the differential exothermic and endothermic reactions between an alundum standard and the sample. Kaolinite was used as a temperature calibration standard, and a minimum of two runs per sample was averaged. The samples were part of uncontaminated material previously examined by other methods. Representative curves appear in Fig. 8.

One exothermic and two endothermic peaks are consistently present, and an additional exothermic peak at about 350° appears in most of the

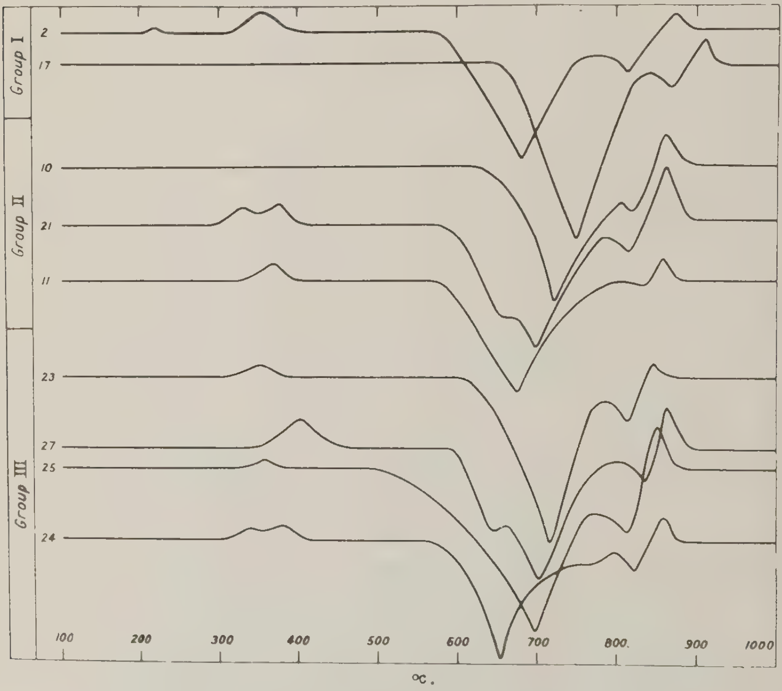

Fig. 8. Differential thermal curves.

Group I: Low chromium chlorite (No. 2) and 7A chromium chlorite (No. 17).
Group II: Tetrahedral Cr.
Group III: Octahedral Cr.

samples (Fig. 8). These peaks have been illustrated or mentioned in the literature and will only be summarized here (Ali and Brindley, 1948; Brindley and Ali, 1950; Bradley and Grim, 1951; Nelson and Roy, 1953).

The broad exothermic peak at 350° does not seem to have been noted. A differential thermal curve of penninite given by Ali and Brindley (1948) exhibits a similar peak, but it is not explained. The low temperature of the reaction and the rather broad character of the peak suggest a weak oxidation. No correspondence could be found with chemical composition. No significant changes in *x*-ray reflections have been noted at this temperature (Brindley and Ali, 1950; Weiss and Rowland, 1956-A and 1956-B).

The first endothermic peak may vary from 550° to 750° C., depending on grain size and chemical composition. Sabatier (1950) reports that single chlorite flakes increase the temperature of this peak to as much as 820° from 620° for the same material finely ground. Increasing substitution of iron for magnesium in the octahedral sites generally decreases this decomposition temperature from a maximum of about 700° to well below 600° C. Brindley and Ali (1950) have correlated this endothermic reaction with the loss of two-thirds of the (OH) in the brucite layer. A one-dimensional electron density Fourier analysis shows a migration of magnesium toward the Si-Al tetrahedra to the position formerly held by the hydroxyls in the brucite layer (Brindley and Ali, 1950).

The second endothermic peak, at about 810° C., represents the completion of dehydration of the chlorite structure, with the loss of two hydroxyls from the brucite layer, and two from the talc layer.

The exothermic peak at about 825° C. accompanies the formation of olivine from chlorite and represents the final destruction of the chlorite lattice. Silicon and magnesium ions must shift slightly to form the olivine structure. If there is more aluminum than an Si/Al ratio of 4 to 1, then difficulties arise and the transition is retarded (Brindley and Ali, 1950). Increasing aluminum tends to raise the temperature of both this exothermic reaction and the previous endothermic reaction. These conclusions are based largely on *x*-ray data. Differential thermal curves did not show a correspondence between the ease of olivine formation and aluminum content.

General Thermal Characteristics

Three groups of curves in Fig. 8 represent (I) a low chromium chlorite (#2) and the anomalous 7 Å sample (#17); (II) tetrahedral chromium chlorite (#10, #21, and #11); and (III) octahedral chromium chlorite (#23, #27, #25, and #24). The members of each group are arranged in order of increasing Cr_2O_3 content. Only the endothermic peak between 640° and 750° C. shows a consistent change together with composition. No systematic variation in the 810° endothermic or 840° exothermic peaks appears with respect to aluminum content. However, the high temperatures of these two peaks for #17 indicates difficulty in the olivine transition, and may be a function of the Si/Al ratio, as proposed by Brindley and Ali (1950).

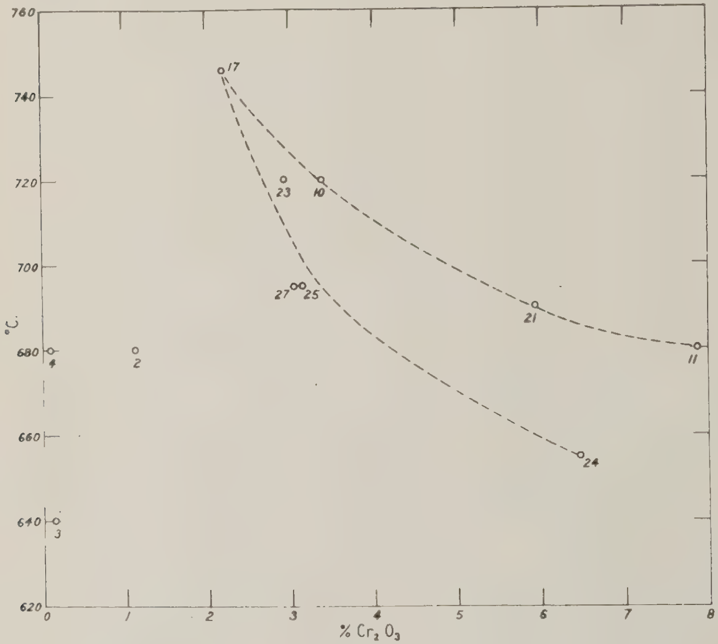

FIG. 9. Variation in chromic oxide content with temperature of decomposition of the brucite layer. The upper curve represents tetrahedral Cr and the lower curve octahedral Cr.

The correlation between chromium content and temperature is illustrated in Fig. 9. Two features appear: (1) above 2 per cent, the Cr_2O_3 content increases as the temperature of decomposition of the brucite layer decreases—this is approximately the same limit above which correspondence with x-ray reflections becomes significant; (2) correlation with chromium follows two different curves which contain the same samples as on the previous x-ray and optical curves, differentiating between tetrahedral and octahedral chromium. In this instance, tetrahedral chromium is represented by the upper curve and octahedral by the lower.

Effects of the Position of Chromium Substitution

From Fig. 9 it appears that the substitution of chromium in the tetrahedral position increases the thermal stability of the brucite layer over the thermal stability for octahedral substitution at the same Cr_2O_3 percentages. It seems likely that tetrahedral substitution, once accomplished, yields a more stable chlorite. Hence although substitution is governed largely by ionic size which usually results in octahedral chromium, the stability of a lattice once formed will depend largely on charge distribution, as long as the substituting ions do not differ greatly in size. Tetrahedral substitution probably represents the replacement of aluminum (and secondarily, silicon) by chromium in Si-O tetrahedra, and hence results in no change in local charge distribution for this position beyond the normal (Fe-Mg) chlorite balance. In the specimens studied, chromium in the aluminum position does not exceed one ion per unit cell. Such a substitution may be indicative of high temperatures, allowing chromium to substitute in the less favorable tetrahedral site. On the other hand, the replacement of Mg^2 by Cr^3, while more common because of their similar ionic sizes, results in a local charge imbalance in the octahedral sites, decreasing the thermal stability of the lattice. Thus octahedral substitution may be indicative of lower temperatures of crystallization because of the greater ease of chromium substitution. It is interesting to note that the two curves converge toward the 7 Å specimen (#17), suggesting that it has been converted to a 14 Å structure, as Nelson and Roy (1953) have reported.

Referring to chromium substitution in chlorite, Roy and Tuttle (1956) state, "the decomposition temperatures are lowered 50 to 100° C. when compared to the pure Al members." From this data, it may be seen that such a lowering of temperature does not necessarily occur. The maximum decomposition temperature for the normal chlorite structure is slightly less than 700° C., while the maximum for chromium chlorite is about 745° C., or nearly 50° C. higher. Only at Cr_2O_3 percentages greater than 4 per cent does the decomposition temperature decrease below that of the pure Al member. As iron is substituted for magnesium, regardless of the amount of aluminum present, the temperature is decreased so that conceivably there could be no difference at all between the chromium and pure aluminum chlorites.

Ionic charge, size, and position of substitution do not completely explain the data, because Fig. 9 represents the decomposition of the brucite layer, which does not contain a tetrahedral position. Yet the substitution of chromium in the tetrahedral position also decreases the thermal stability of the brucite layer. As would be expected, tetrahedral chromium has less effect, since substitution directly into that layer affects that layer more, and as a result, the octahedral curve is at a lower temperature and has a steeper slope. This can be explained on the basis of local charge imbalances, resulting in decreased bond strength as chromium substitution increases.

The chemical formulas for samples #2, #10, #27, #24, and #11 have been given in Table III. Considering these to be relatively accurate, the following total charge imbalance exists, according to the above sample order, which is arranged according to increasing chromium content: −0.98; −1.49; −0.33; −2.89; and +2.25. Qualitatively it may be seen that increasing charge imbalance is roughly parallel to both increasing chromium content and decreasing temperature of decomposition (or decreasing lattice stability). Orcel, Caillere, and Henin (1950) have discussed charge imbalances and noted that they affect the decomposition temperature of the brucite layer. They make an analogy between excess charge on the brucite layer and the role played by potassium in micas. However, they state that the quantity of trivalent elements necessary to compensate for the deficit of charges on the mica (talc) layer (or the excess on the brucite) is insufficient, resulting in a chlorite whose structure approaches that of the expanding chlorites. These local charge imbalances are compensated by substitution of Na, K, or Ca into hexagonal network cavities of the chlorite structure. An excess positive charge might tend to be balanced by an increase in $(OH)^-$. It is significant that calcium content increases with chromium content, tending to balance local charge deficiencies.

The explanation for decreasing decomposition temperature with increasing chromium can be given more accurately than the above approach. If one takes the theoretical number of octahedral cations per unit cell, which is six, and finds the amount by which this differs from the actual case, this difference is then a measure of the degree of charge imbalance in the octahedral position, and should thus be directly comparable to the decomposition temperature of the brucite layer. In the following list, the compensation of charge imbalance by $(OH)^-$ is included:

#2 . . . 0.62 relative degree of charge imbalance
10 . . . 0.57 relative degree of charge imbalance
27 . . . 0.03 relative degree of charge imbalance
24 . . . 1.41 relative degree of charge imbalance
11 . . . 1.71 relative degree of charge imbalance

This list is also in order of increasing chromium content. In order of decreasing stability, according to octahedral cation charge imbalance, this would be:

#27—#10—#2—#24—#11.

The observed order from differential thermal data is:

#10—#27 -#2 #11—#24.

Numbers 10 and 11 appear to be out of order, if this theoretical picture were to correspond to observed thermal stabilities. However, when one considers that these two samples are the only ones in the above list in which the chromium occupies a tetrahedral site, and that a charge imbalance in the tetrahedral position would have less effect on the more distant brucite layer, then the theoretical picture fits the observed data. Thus, although the actual amount of charge imbalance is not accurate because of limitations such as the chemical analyses, the relative degree of imbalance is accurate and does explain the order of instabilities as observed from the breakdown temperatures of the brucite layer.

Conclusion

If this theoretical picture is correct, and it seems to explain the data as well as support the conclusions from *x*-ray analyses, then a small total charge imbalance exists on a unit cell which is not compensated by cation or hydroxyl substitution. It seems that substitution of these ions is in such a position as to be nearest the greatest charge imbalance. Since charge imbalances are effective only over short distances, the instability of the lattice is minimized. However, there is a further mechanism which may help to alleviate lattice stress caused by charge imbalances. If rotations or glides of successive unit cells occurred so that positions of charge excesses were placed over charge deficiencies, or nearer to them, greater stability would result. Octahedral chromium should create the most significant imbalances, because a trivalent ion is being substituted for a divalent one. The octahedral chromium chlorite from Erzincan (#24) has just such a rotation of successive layers. On the other hand, as would be expected in a substitution of chromium for aluminum, the tetrahedral California chromium chlorite (#10) has a normal structure without rotations. Thus the structures of two samples of chromium chlorite can be explained as a function of charge imbalance. That this imbalance might be a cause of polytypism and polymorphism in layer lattices should be investigated.

Substitution of chromium in the chlorite lattice results in minor structural variation, since unit cell symmetry is changed by the positioning of the chromium ion. Aluminum is another element which also substitutes in two different coordination sites. Both polymorphism and polytypism are used for structural variations. Polymorphism results in "structures characterized by different lattices" while polytypism is "any possible structural modification which alters the (*c*) axis dimension of the smallest unit cells referable to . . . lattice types by some multiple of a single layer . . . without altering the structure in the plane perpendicular thereto" (Strock and Brophy, 1955). Polytypism may be thought of as variations in the stacking sequence along the *c* direction, while polymorphism refers to a major symmetry change.

Neither polymorphism nor polytypism accurately describes the chromium chlorite situation. Since diadochy is the substitution of one element for another in the same structure, "positional diadochy" could be used to describe octahedral and tetrahedral chromium substitution. However, to avoid confusion, with existing nomenclature, perhaps the term "comorphism" is preferable, to be defined as follows:

> the substitution of one element in two different coordination positions in the same mineral lattice, resulting in a minor structural variation without necessarily changing the unit cell composition.

PART III. CLASSIFICATION

Review

The nomenclature of chromium chlorite contains many revised species descriptions. Old terms have been replaced and superseded as new data has become available and as the basis for mineral classification has shifted toward an emphasis on internal structures. A brief summary of the most common names is discussed as a step toward a new classification.

The term "chrome chlorite" has frequently been used to refer to rose-violet chlorite in order to avoid confusion with the green Fe Mg chlorites. The term has also been used for green chlorites containing a maximum of 2 per cent Cr_2O_3. However, this color composition boundary is indistinct. Shannon (1920) reports a pale lavender kammererite from Newcastle, California, averaging 1.53 per cent Cr_2O_3. Pearse (1864) noted a green chromium chlorite from Lancaster County, Pennsylvania containing 1.967 per cent Cr_2O_3. Orcel (1927) used 2 per cent as the color composition boundary, while Hey (1954) suggests the term "chrome chlorite" for samples with less than 4 per cent Cr_2O_3. Hey's preference for this percentage lies in an analogy with a 4 per cent Fe_2O_3 boundary often used to separate orthochlorites (largely $MgO+FeO$) from leptochlorites (containing more than 4 per cent Fe_2O_3).

Kammererite is the most widely used and oldest term for rose-violet chromium chlorite. Dana (Garrett, 1853) first placed it in the pyrosclerite group, now believed to be a member of the vermiculite family. Later he described it as a Cr-variety of penninite (Dana, 1892, 6th ed.) and used rhodochrome for optically negative kammererite and rhodophyllite for the optically positive variety. Vernadsky (1901), Orcel (1927), and Hey (1954) use kammererite for a chromiferous variety of penninite. Since penninite has a higher Si/Al ratio than the other Fe–Mg chlorites, the definition of kammererite is based on this ratio, rather than on any direct relation to chromium.

In 1852, Dr. F. A. Genth proposed the name rhodophyllite for violet chromium chlorite from Texas, Pennsylvania containing between 4 per cent and 7 per cent Cr_2O_3. Somewhat earlier, the name rhodochrome had been applied to violet chromium chlorite (Smith and Brush, 1853) but without a chemical analysis. When the analysis (from Lake Iktul, Urals) was published, it was found to fall within the Cr_2O_3 range of the Texas rhodophyllite. Smith and Brush then proposed that since the two were identical, rhodochrome had precedence. However, the terms appear to have become somewhat confused, since Dana (1892) differentiated the two on the basis of optic sign and placed both under the kammererite subdivision of penninite.

In 1861, Kokscharow is credited with having proposed the name kotschubeite for an optically positive variety of chrome clinochlore (Melville and Lindgren, 1889).* On the basis of this definition, the distinction between kammererite and kotschubeite is one of aluminum content, analogous to the distinction between penninite and clinochlore respectively. According to the analysis by von Leuchtenberg (Melville and Lindgren, 1889), kotschubeite from Lake Iktul contained 4.09 per cent Cr_2O_3. Thus this locality produced two chromium chlorites, rhodochrome and kotschubeite, containing similar amounts of chromium, but apparently differing in Si/Al ratio. Based on this ratio, Melville and Lindgren used kotschubeite for a California sample containing 11.39 per cent Cr_2O_3. Orcel (1927) concurred that kotschubeite was an optically positive variety of clinochlore. Fisher (1929) stated that kotschubeite had a lower birefringence than kammererite. Hey (1954) used only the terms "chrome-clinochlore" where the Cr_2O_3 content was less than 4 per cent, and "kotschubeite" for chrome clinochlore containing more than 4 per cent.

In summary, it seems that there are by original definition two distinct varieties, kammererite and kotschubeite, based on their Si/Al ratio. Rhodochrome and rhodophyllite are indistinguishable from them. Both optically negative and positive chromium chlorites exist; published Cr_2O_3 percentages range up to 13.5 per cent; and, the Si/Al ratio of penninite to clinochlore represents a minimal variation. Color is not a reliable criterion for classification.

PROPOSED NOMENCLATURE

The value of any mineralogic classification lies both in its simplicity and the ease with which it may be applied in the field and laboratory. Both the Fe–Mg and Cr– chlorite literature is studded with names, many of them overlapping and most of them subdivided on an arbitrary basis. In 1950, Orcel, Caillere, and Henin proposed a classification based primarily on the number of tetrahedral silicon ions, and secondarily on iron content, the boundaries being arbitrary for the most part. Their main divisions are as follows:

---

* The reference which is given as Bull. Acad. St. Petersburg, 1861, p. 369, appears to be incorrect.

	Tetrahedral Si
Amesite	2.0–2.2
Prochlorite	2.3–2.8
Clinochlore	2.9–3.5
Pennine	3.5 or greater

Nelson and Roy (1953) largely followed this main division, but reduced the prochlorite field and added corundophilite between amesite and prochlorite. Max Hey (1954) also divided the chlorites according to amount of tetrahedral silicon, using corundophilite, sheridanite, clinochlore, and penninite for the relatively iron-free members, but including many other names for more iron-rich members.

The distinction between one mineral and another should be based both on crystal structure and chemical composition. When a substitution series exists in one group, as it does in the chlorites, arbitrary amounts of cation substitution have little meaning in the construction of a classification. If there are no structural variations, names applied to subdivisions should be kept to a minimum. Such a subdivision has been useful in the Fe–Mg and Si–Al series of chlorite substitutions.

Chromium chlorites present a different problem. The correspondence between chromium content and structure, evidenced by x-ray, optical, and differential thermal analyses, begins between 1 per cent and 2 per cent Cr_2O_3, indicating that below this amount chromium substitution has little structural effect. Hence, it is proposed that chlorites containing less than 2 per cent Cr_2O_3 retain the Fe–Mg chlorite nomenclature, adding "Cr" as a prefix (Group I, Table VIII). At greater than 2 per cent a significant and recognizable correspondence exists with the chlorite structure. In addition, there is a distinct separation into octahedral and tetrahedral types of chromium substitution. Here then, is a structural variation which will allow a nomenclature based on a measurable difference—one which is perhaps less arbitrary than previous usages. The two most commonly used names for chromium chlorite are kammererite and kotschubeite. Their previous distinction, based on optic sign or Si/Al ratio, has not been consistent nor does it have a fundamental structural basis. Since the type locality for kotschubeite is Lake Iktul, Urals, it seems appropriate that the tetrahedral Bilimbaievsk sample

TABLE VIII. CLASSIFICATION OF 14Å CHLORITES

<table>
<tr><th colspan="5">I—Mg—Fe—Cr Chlorite</th></tr>
<tr><th rowspan="2">Tetrahedral Si</th><th rowspan="2">Mg Chlorite</th><th colspan="2">Fe Chlorite</th><th rowspan="2">Cr Chlorite—less than 2% Cr_2O_3</th></tr>
<tr><th>Ortho-chlorite $>4\%$ FeO</th><th>Lepto-chlorite $>4\%$ Fe_2O_3</th></tr>
<tr><td>2.0–2.5</td><td>Corundophilite</td><td colspan="2">Fe corundophilite</td><td>Cr corundophilite</td></tr>
<tr><td>2.5–2.8</td><td>Prochlorite</td><td colspan="2">Fe prochlorite</td><td>Cr prochlorite</td></tr>
<tr><td>2.8–3.1</td><td>Clinochlore</td><td colspan="2">Fe clinochlore</td><td>Cr clinochlore</td></tr>
<tr><td>3.1 or greater</td><td>Penninite</td><td colspan="2">Fe penninite</td><td>Cr penninite</td></tr>
<tr><th colspan="5">II—Chromium Chlorite—more than 2% Cr_2O_3</th></tr>
<tr><th colspan="2">Tetrahedral Cr</th><th colspan="3">Octahedral Cr</th></tr>
<tr><td colspan="2">Kotschubeite</td><td colspan="3">Kammererite</td></tr>
</table>

(#21), which is named kotschubeite, be taken to represent the tetrahedral group. Octahedral chromium chlorites, which appear to be more common, have generally been referred to as kammererites. This name is suggested to represent the octahedral group (Group II, Table VIII). "Chromium chlorite" is suggested as a general and field term for pink to rose-violet chlorite.

On the basis of this nomenclature, the 14 Å samples studied would have the following species names:

#2	West Chester, Pa.	Cr-clinochlore
23	Texas, Pa.	kammererite
27	Webster, N. C.	kammererite
25	Woods Mine, Pa.	kammererite
10	Siskiyou County, Calif.	kotschubeite
21	Bilimbaievsk, Urals	kotschubeite
24	Erzincan, Turkey	kammererite
11	Deer Creek, Wyo.	kotschubeite

Chlorites containing both octahedral and tetrahedral chromium may be classified according to the position which contains the majority of chromium. Nomenclature for the 7 Å chlorites has yet to be agreed upon, and hence #17 has not been included in this classification.

SUMMARY

Chromium substitutes into both the octahedral and tetrahedral positions of chlorite. Above 2 per cent chromic oxide content, the former are termed kammererite, and the latter kotschubeite. This structural variation is referred to as positional diadochy, or comorphism. It is suggested that such positional substitution is related to local unit cell charge imbalances, which in turn may have a causal effect on polytypic variations.

Appendix

A. Calculation of F values from observed intensities:

$$F^2 = \frac{I}{(j)\dfrac{1+\cos^2 2\theta}{2}\cdot\dfrac{1}{2\sin^2\theta\cos\theta}\cdot A(\theta)}$$

where

F = structure factor
I = observed intensity
j = multiplicity factor
2θ = Bragg reflection angle
$A(\theta)$ = absorption factor evaluated from NaCl standard as $1/u$
where

$$u = p\Sigma\frac{\text{At. wgt.}}{\text{Tot. wgt.}}\cdot\frac{u}{p}$$

where

p = chlorite density
$\dfrac{u}{p}$ = mass absorption coefficient for each element

B. Calculation of theoretical F values

$$F = 8\cos^2 2\pi\frac{h+k}{4}\cos^2\pi(hx+lz)\cos 2\pi ky$$

expanded using

$$\cos(a+b) = \cos(a)\cos(b) - \sin(a)\sin(b)$$

and

$$\cos^2\theta = \tfrac{1}{2}(1+\cos 2\theta)$$

$$F = 4\left[1+\cos\left(2\pi\frac{h}{2}\right)\cos\left(2\pi\frac{k}{2}\right)-\sin\left(2\pi\frac{h}{2}\right)\sin\left(2\pi\frac{k}{2}\right)\right]$$
$$\cdot\left[\cos(2\pi hx)\cos(2\pi lz)-\sin(2\pi hx)\sin(2\pi lz)\right]\cdot\cos(2\pi ky)$$

References

Ali, Sultana Z. and Brindley, G. W. (1948), X-ray study of thermal transformations in the chlorite mineral, penninite, *Leeds Phil. and Lit. Proc.*, **V**, part II, sci. sect., 109–115.

Bradley, W. F. and Grim, R. E. (1951), High temperature and thermal effects of clay . . . , *Am. Mineral.*, **36**, 182–201.

Brindley, G. W. and Ali, Sultana Z. (1950), X-ray study of thermal transformations in some magnesian chlorite minerals, *Acta Cryst.*, **3**, 25–30.

———, Oughton, Beryl M., and Robinson, Keith (1950), Polymorphism of the chlorites, Part I, ordered structures, *Acta Cryst.*, **3,** 408–416.

——— (edit.) (1951), *X-ray Identification and Crystal Structures of Clay Minerals*, pub. Taylor and Francis Ltd., London, pp. 173–198, 186.

Brown, George (1955), The effect of isomorphous substitution on the intensities of (001) reflections of mica and chlorite type structures, *Min. Mag.*, **30,** 657–665.

Dana, E. S. (1892), *System of Mineralogy*, 6th ed., New York, pp. 653–654.

DuRietz, Torsten (1935), Peridotites, serpentines and soapstones of Northern Sweden, *Geol. For. Forh. Stockholm*, **57,** 133–260.

Evans, R. C. (1952), *An Introduction to Crystal Chemistry*, pub. University Press, Cambridge, pp. 24–25, 270–274.

Fisher, Lloyd W. (1929), Origin of chromite deposits, *Ec. Geol.*, **24,** 691–721.

Garrett, Thomas H. (1853), On minerals accompanying chromic iron, *Am. Jour. Sci.* 2nd Ser., **15,** 332–334.

Garrido, Jules (1949), Structure cristalline d'une chlorite chromifere, *Bull. Soc. Franc. Min. et Crist.*, **72,** 549–570.

Genth, F. A. (1852), On rhodophyllite, a new mineral, *Proc. Nat'l. Acad. Sci. Phila.*, **6,** 121–124.

Hartshorne, N. H., and Stuart, A. (1950), *Crystals and the Polarizing Microscope*, 2nd ed., publ. Edward Arnold & Co., London, pp. 130–155.

Hey, Max H. (1954), A new review of the chlorites, *Min. Mag.*, **30,** 277–292.

Lonsdale, K. (1945), The shape of reflections on X-ray single crystal photographs, *Min. Mag.*, **27,** 112–125.

Mauguin, Ch. (1928), Etude des micas au noyen des rayons X, *Soc. Franc. Min. Bull.*, **51,** 321.

Melville, W. H. and Lindgren, W. (1889), Contributions to the mineralogy of the Pacific Coast, *U. S. Geol. Surv. Bull.*, **61,** 11–40.

Miller, Rosewall (1953), The Webster-Addie ultramafic ring, Jackson Cy., Nor. Car. and secondary alteration of its chromite, *Am. Mineral.*, **38,** 1134–1147.

Nelson, Bruce W. and Roy, Rustum (1953), New data on the composition and identification of chlorites, *2nd National Conference on Clays and Clay Minerals*, Nat'l. Acad. Sci. Pub. #**327,** 335–348.

Orcel, M. J. (1927), Recherches sur la composition chimique des chlorites, *Bull. Soc. Franc. Min.*, **50,** 75–456.

———, Caillere, S., and Henin, S. (1950), Nouvel essai de classification des chlorites, *Min. Mag.*, **29,** 329–340.

Osborne, F. F. and Archambault, M. (1948), Chromiferous chlorite from Mount Albert, Quebec, *Roy. Soc. Canada Trans.* Ser. 3, **42,** 61–67.

Pearse, J. B. (1864), On some minerals of the chlorite group, *Am. Jour. Sci.* 2nd Ser., **37,** 221–225.

Ross, Clarence S. (1929), Is chromite always a magmatic segregation product?, Part II, *Ec. Geol.*, **24,** 641–645.

Roy, Rustum and Tuttle, O. F. (1956), Investigations under hydrothermal conditions, *Physics and Chemistry of the Earth*, **1,** 166–167.

Sabatier, G. (1950), Sur l'influence de la dimension des cristaux de chlorites sur leurs courbes d'analyse thermique differentielle, *Soc. Franc. Min. Crist. Bull.*, **73,** 43–48.

Schiebold, E. (1932), *Methoden der Kristallstrukturbestimmung mit Rontgenstrahlen*, Akad. Verlag. M.B.H. Leipzig, pub. J. W. Edwards, 1944, pp. 137, 144.

Shannon, E. V. (1920), Analyses and optical properties of amesite and corundophilite from Chester, Mass. and of chromium-bearing chlorites from Calif. and Wyo., *U. S. Nat'l. Museum Proc.*, **58,** 371–379.

Smith, J. Lawrence and Brush, George J. (1853), A reexamination of American minerals, *Am. Jour. Sci.* 2nd Ser., **16,** 47–48.

Strock, L. W. and Brophy, V. A. (1955), Synthetic ZnS polytype crystals, *Am. Mineral.*, **40,** 94–106.

Vernadsky, W. J. (1901), Zur theorie der silicate, *Zeit. Krist.*, **34,** 37–66.

Weiss, E. J. and Rowland, R. A. (1956-A), Oscillating heating *X*-ray diffractometer studies of clay mineral dehydroxylation, *Am. Mineral.*, **41,** 117–126.

——— (1956-B), Effect of heat on vermiculite and mixed layer vermiculite-chlorite, *Am. Mineral.*, **41,** 899–914.

Winchell, A. N. (1936), A third study of chlorite, *Am. Mineral.*, **21,** 642–651.

Manuscript received February 13, 1958

THE AMERICAN MINERALOGIST, VOL. 43, SEPTEMBER-OCTOBER, 1958

A STUDY OF THE DIRECTIONAL HARDNESS IN SILICON*

A. A. GIARDINI, *U. S. Army Signal Engineering Laboratories, Fort Monmouth, New Jersey.*

ABSTRACT

The directional hardness of single crystal silicon has been investigated both by a method of peripheral grinding on oriented thin circular specimens and by Knoop micro-indentations. Grinding hardness has been evaluated in the principal zones [100], [110] and [111]. Knoop Hardness Numbers are given for planes (100), (110) and (111) with indentations extended over 90° azimuths. Experimental results are compared with published data on diamond, which has the same crystal structure.

INTRODUCTION

Several workers (1, 2, 3, 4, 5, 6, 7) have made both qualitative and quantitative studies on the directional variation of grinding hardness in diamond. A review of the literature, however, has failed to yield any record of previous work on the anisotropy of hardness in silicon. Because of the structural similarity and bonding dissimilarity between diamond and silicon, a comparison of the relative hardness vectors of the two materials is desirable. The results of a hardness investigation on planes in the [100], [110] and [111] zones in silicon are presented herein.

Both grinding and indentation hardness have been evaluated. The former has been carried out by a method of peripheral (zonal) grinding on oriented thin disks of single crystal silicon, whereas the latter was performed with a Knoop microindenter with impressions made on the flat surfaces of the circular specimens.

Considering the difficulties encountered in quantitative hardness studies, the results obtained by the peripheral grinding technique have been found to be pleasingly systematic and reproducible. Microindentation data also can be reasonably correlated with structural symmetry, but on a statistical basis.

The advantages and disadvantages of the peripheral grinding technique compared to the usual procedure of grinding on fixed planes are as follows.

Advantages

(a) All planes in a given zone may be simultaneously evaluated relative to each other, with an automatic time integration of results.
(b) Selected zones can be easily examined and compared.
(c) Mounting, orientation and measuring procedures are greatly simplified.
(d) Experimental conditions can be easily varied and easily reproduced.
(e) The symmetrical nature of grinding hardness can be evaluated directly.

---

* Contribution No. 224 of the Dept. of Mineralogy, Univ. of Michigan.

Disadvantages

(a) Relatively large crystal specimens are needed.
(b) Accurate, oriented disks are required.
(c) The possibility of evaluating various grinding azimuths on given planes is restricted.

The silicon used in this study was obtained from the U. S. Army Signal Engineering Laboratories, Fort Monmouth, New Jersey, and is of transistor-grade purity. Specimens were cut from two boules, both of which were elongated (pulled) parallel to [111]. Although some spinel-type twinning was present in both boules, specimens were cut from areas free of recognizable twinning. The latter was determined both by visual inspection of ground surfaces and by *x*-ray diffraction

Specimen Preparation

As previously mentioned, crystallographically oriented thin disks of single crystal silicon have been used for this study. Specimen orientation was carried out by the Laue method of *x*-ray diffraction. The apparatus and technique have been described earlier (8). Orientational error of specimens was maintained within ±30 minutes of arc.

Oriented, flat and parallel wafers were cut from boules with a precision diamond saw. A small diamond core drill was designed and constructed in order to cut true circular disks of constant diameter from the wafers. An accurate drill press was used to operate the core drill. The diametrical variation among disks amounted to less than ±0.5%.

A total of six disks were cut for quantitative investigations, two each of the following orientations: the normal to the circular face of the disk, (a) parallel to the [100] zone axis, (b) parallel to the [110] zone axis, (c) parallel to the [111] zone axis. In order to eliminate small cleavage irregularities which developed along the edges of the disks during core drilling, all were simultaneously cemented on a lapping block with a thin film of Canada balsam and carefully ground until free of noticeable imperfections. The same procedure was repeated for the opposite side of the disks. A machinist's micrometer was used to maintain parallelism, and therefore, correct orientation. The thickness of all disks was 0.165 cm. ±0.001. The diameters were 1.05 cm. ±0.005.

The same specimens have been used for both the peripheral grinding and microindentation studies.

Experimental Apparatus for Peripheral Grinding

The experimental technique used for this part of the study consists of peripheral grinding on oriented silicon disks using a flexible, bonded

SiC abrasive cloth. The disks were coaxially mounted on the end face of a machined brass spindle by means of a special centering jig. Dopping wax was used as the cementing agent. The spindle, with disk, was then mounted in a Jacobs chuck which in turn was mounted on a 10″ machinist's lathe. Centering of the disk in the lathe was accomplished by use of shims and a dial indicator. During the grinding operation the disks were rotated at 68 rpm.

A $\frac{1}{2}$ inch wide strip of 240 grit SiC abrasive cloth moving in the direction opposite to the peripheral motion of the disk was used as the grinding medium. A flat spring, equipped with a pair of parallel rollers and mounted on the lathe tool holder, served as a flexible backing for the abrasive and as a constant pressure regulator. The diameter of each roller was 0.25 cm. giving a disk to roller diametrical ratio of approximately 4 to 1. Although a higher ratio (smaller roller diameter) would be desirable, the dimensions constitute a practical compromise between an acceptable minimum contact area between the disk and abrading medium, and a smooth movement of the abrasive cloth over the rollers. The abrasive feed was controlled by a 1,725 rpm motor geared to 2.9 rpm. The latter provided an average rate of feed of 35 cm. per minute for a 15 minute grinding period.

Prior to grinding operations, the abrasive strip and rollers were aligned parallel to the axis of the disk and spindle, and centered directly below the center of the disk. A compensating force was placed on the spring to counterbalance the pull of the abrasive cloth moving over the rollers. An additional force of 200 grams was then applied to the system. The operational contact surface between the disk and the abrasive strip was empirically determined to be $0.01\ \text{cm.}^2 \pm 10\%$.

The above values for experimental variables such as disk surface speed, abrasive feed, abrasive grit size and grinding force, were fixed on the basis of available equipment, disk dimensions, positive contact between disk and abrasive, loading of the abrasive cloth, and the relative hardness of the material under investigation.

In order to interpret properly and record hardness data, the orientation of the principal crystallographic directions and direction of rotation were directly scribed on the exposed flat surface of the disks. The disks were photographed in situ before grinding and at regular intervals during grinding operations. Maximum and minimum diametrical measurements and their respective orientations were determined during these intervals by use of a micrometer which could be read to ±0.0005 inch. The accuracy of this orientational procedure was found to be approximately ±3°. Figure 1 provides a view of the grinding apparatus.

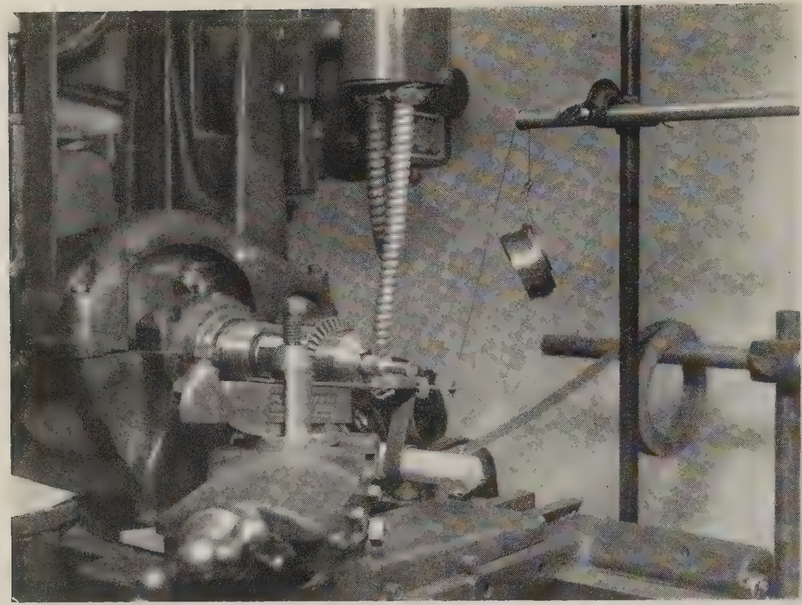

FIG. 1. A view of the experimental peripheral grinding hardness apparatus.

EXPERIMENTAL DATA FROM PERIPHERAL GRINDING

The experimental data obtained from peripheral grinding are given in graphical form in the following three ways:

(1) Radial reduction curves are presented for the three crystallographic zones investigated, namely, [100], [110] and [111]. The orientations, grinding azimuths and relative hardness (in terms of reduction in disk radii*) are included in the presentation. Data are given for a grinding period of 15 minutes and a total time of 30 minutes. No corrections have been made between the two grinding periods for the initial distortion of the circular periphery due to the directional hardness, and for the progressive reduction of peripheral surface area with decreasing diameter of the disk. The surface area reduction was determined by measuring the circumference on enlarged photographs of the disks and found to be approximately 6% for the first 15 minute grinding interval and 8% for the second 15 minute period. The 2% difference represents the resultant effect of the initial out-of-round shape which the disk assumes early in the first grinding period and the progressive reduction

---

* Since all experimental variables are held approximately constant in this work, disk radii are proportional to the hardness constant, K, defined by Denning (5) in his studies of the hardness vectors in diamond.

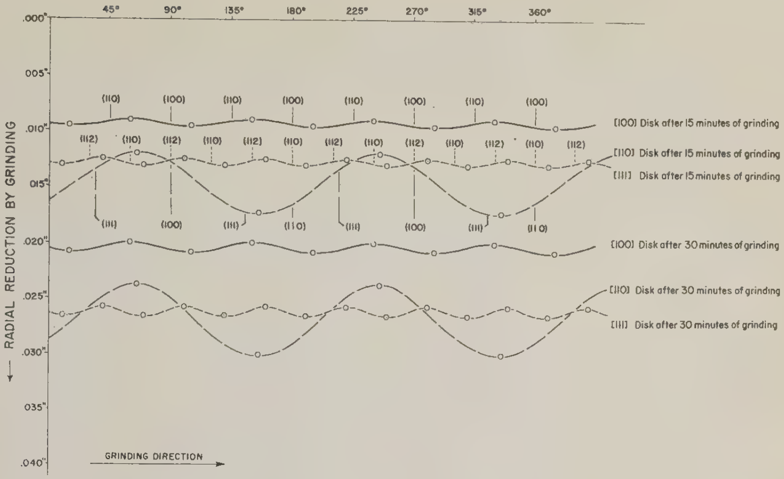

FIG. 2. Radial reduction curves for the [100], [110] and [111] zones in silicon. The indices represent forms rather than specific faces.

of the peripheral speed. Data presented in each curve are the averages obtained from two separate specimens of the same orientation. All specimens have been exposed to the same experimental conditions. The grinding curves are given in Fig. 2.

(2) Data are presented in terms of the per cent weight loss resulting from peripheral grinding for a 30 minute period for each of the three zones investigated. Data from each of the two disks for each of the three zonal orientations are individually represented. Averaged values are also indicated. It can be seen that the variance of the individual measurements is no greater than ±5% from the respective averaged values. These data are given in Fig. 3.

(3) Principal relative grinding hardness vectors are given in Fig. 4 in stereographic form. Vector magnitudes are plotted in linear units. The point of origin for each vector corresponds to its reference plane. Because of symmetry considerations (*m3m*), data are presented only in one stereogram quadrant. A vector presentation of Knoop Hardness Numbers, to be discussed later, also is included in Fig. 4. Due to the nature of the microindentation, all Knoop vectors are given as bidirectional, parallel to the long diagonal of the indenter. Again, because of symmetry, data are presented for only one quadrant.

Experimental conditions for all data described above are as follows: (a) average surface speed of the disks during the first 15 minutes of grinding was approximately 220 cm./minute, (b) the average surface speed of the disks during the second 15 minutes of grinding was approximately 210 cm./minute, (c) the rate of feed of the 240 grit SiC abrasive cloth averaged 35 cm./minute, (d) the grinding pressure during all grinding cycles was 20 kg./cm.^{2}±10%.

SOURCES OF ERROR IN PERIPHERAL GRINDING

Sources of error in grinding hardness research are numerous, difficult to control, and difficult to correct. No theoretical corrections have been derived in this present study; however, most of the recognized sources of error have been minimized by careful and repeated measurements. A listing of several sources of error and their approximate limits is given in Table 1.

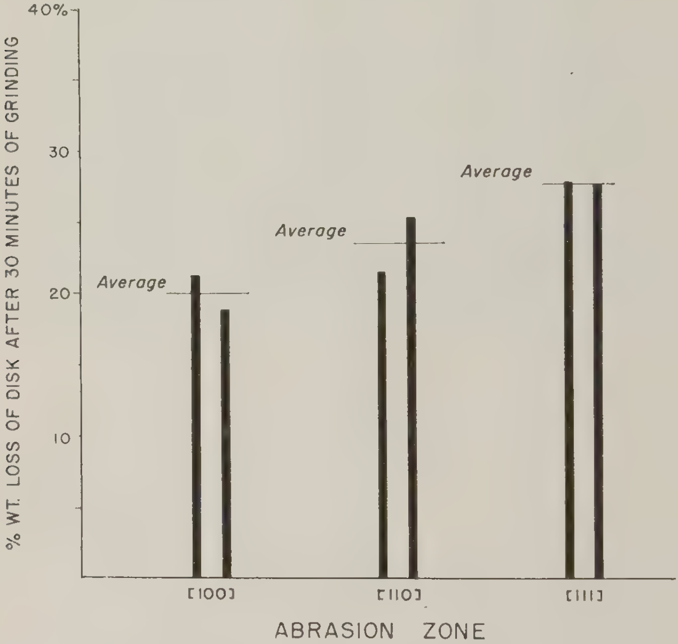

FIG. 3. The weight lost by each of the [100], [110] and [111] zonal disks of silicon during a 30 minute grinding period.

The total accountable variance amounts to ±15.4%. This value represents the sum of the limits. An indication of the actual degree of error in the reported experimental data can be obtained, however, from the general agreement of data both from the individual disks of zonal pairs and by comparison of weight loss and radial reduction measurements.

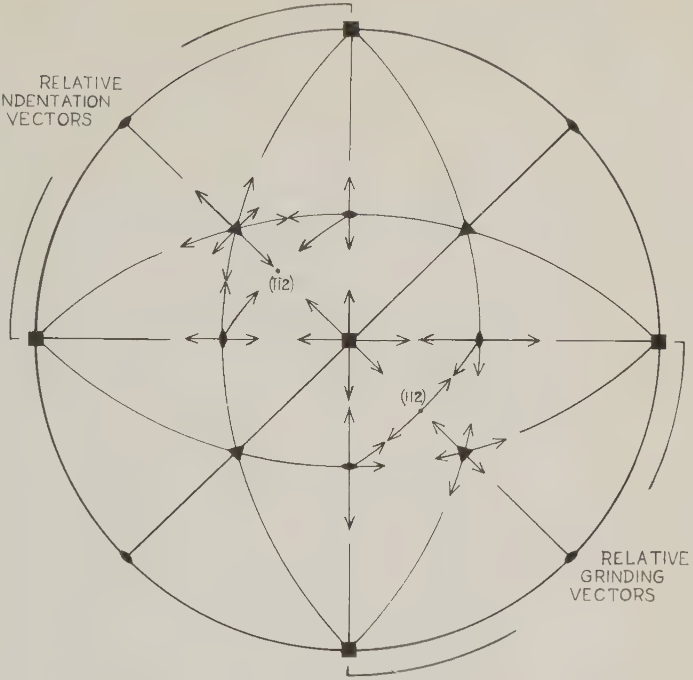

FIG. 4. A composite stereographic presentation of both peripheral grinding and microindentation relative hardness vectors. Magnitudes are plotted in linear units based on a common relative scale derived from maximum and minimum values. See Tables 2, 3, 4 and 6 for relative numerical values. KHN vectors are pictured as bidirectional parallel to the long diagonal of the indentation.

TABLE 1. SOME SOURCES OF ERROR ENCOUNTERED IN GRINDING EXPERIMENTS AND OBSERVED LIMITING VALUES

Sources	Limits
Surface speed of the silicon disks	± 1.0%
Rate of feed of the abrasive cloth	± 0.05%
Grinding contact area	±10.0%
Micrometer measurements	± 0.15%
Disk orientational error	± 0.5%
Orientational error in hardness vectors	± 3.33%
Weight loss measurements	± 0.2%
Time of the grinding periods	± 0.15%
Non-uniformity of the grinding force	±?

Variations show an approximate maximum of ±5%. The latter undoubtedly could be reduced through refinements in apparatus and procedure.

MICROINDENTATION EXPERIMENTAL APPARATUS

A Bergsman micro-hardness tester, model number 4-418, equipped with a certified Knoop point, was used for the indentation part of this study. The Bergsman instrument was mounted on a Vickers projection microscope. The latter was set on rubber pads to minimize the effect of building vibrations.

The indenter load (100 grams) and optical system (Spencer 1.25 N. A. oil immersion objective and a Bausch and Lomb filar eyepiece) were chosen to produce the "ideal" 500-600 filar unit length of indentation image. The filar graduations of the eyepiece were calibrated with a Bausch and Lomb stage micrometer. The loading time for indentations was approximately 10 seconds.

The flat surfaces of the cylindrical peripheral grinding specimens were used for the indentation study. The latter were given an optical quality polish with 0–2 micron diamond paste. The specimens were then mounted in lucite cylinders. Indentation azimuths were positioned by rotation of the graduated microscope stage. Light figure reflections from the roughened edges of the disks were used to orient the indentation azimuths with respect to principal crystallographic directions.

MICROINDENTATION EXPERIMENTAL DATA

A total of 100 indentations were made on each of the planes (100), (110) and (111). Groups of ten indentations were made on azimuths spaced at 10° intervals. A larger azimuth range is unnecessary because of the high symmetry.

Almost all indentations were accompanied by fracturing, and in some cases by octahedral micro-cleavage on the (111) plane, and fine cracking across the narrow tips of the indentations. The fracturing generally occurred on either or both sides of the indentation long diagonal in approximately half circular or elliptical shape. The "radii" of these fractures in some cases were as much as the full length of the indentation. In general, however, the shape of most indentations with respect to the long diagonal were of perfect apparent symmetry. Data are reported only for those of the latter quality.

No special correlation was apparent between the occurrence and severity of fracturing (and cracking), and crystallographic orientation. Although undoubtedly related to the mechanics of producing the indentation, these structural disruptions also probably reflect the distribution of micro-defects in the silicon.

The experimental data, in terms of Knoop Hardness Numbers for a 100 gram load, are presented in Tables 2, 3 and 4. Each of the values given represents the arithmetic average of ten consecutive indentations along a given azimuth. As previously mentioned, a composite stereographic presentation of peripheral grinding and microindentation data is given in Fig. 4.

TABLE 2. KNOOP HARDNESS NUMBERS (0.1 Kg LOAD) FOR THE (001) PLANE OF SILICON

(SEE FIG. 4)

Azimuth*	Average KHN_{100}	Av. Variance of 10 Indentations	Limiting Variance
0°	960	±1.0%	±1.1%
Towards $(\bar{1}01)$†	950	0.4	0.7
20°	960	0.3	0.7
30°	960	0.5	1.0
40°	965	0.3	0.7
50°	970	0.5	1.0
Towards $(\bar{1}\bar{1}1)$†	—	—	—
60°	980	0.5	1.0
70°	960	0.4	0.9
80°	970	0.5	0.9
90°	965	0.4	0.7
Towards (011)†	—	—	—
	Overall average = 964 ± 0.5%		

* The limit of absolute collective orientational error for all azimuths on a given plane is estimated at ±5°; the relative error is ±0.25°.

† The long diagonal of the indentations are toward the respective planes indicated. See Fig. 4.

SOURCES OF ERROR IN MICRO-HARDNESS TESTING

Several of the factors influencing micro-hardness testing have been analyzed and discussed by Bergsman (9). In this study, care was exercised wherever possible to minimize sources of error and to empirically evaluate limits. The latter are given in Table 5.

No attempt has been made to evaluate the effects of specimen surface preparation and the observed fracturing, cleavage and cracking on KHN values.

DISCUSSION OF RESULTS

The hardness of silicon on the Mohs scale is 7. The results of this study have shown a significant directional variation of grinding hardness con-

TABLE 3. KNOOP HARDNESS NUMBERS (0.1 Kg LOAD) FOR THE $(\bar{1}01)$ PLANE OF SILICON
(SEE FIG. 4)

Azimuth*	Average KHN_{100}	Av. Variance of 10 Indentations	Limiting Variance
Towards (001)*	940	±0.6%	±1.4%
10°	955	0.5	1.0
20°	945	0.6	1.7
30°	960	0.5	1.0
40°	965	0.7	1.5
50°	980	0.8	1.5
Towards $(\bar{1}\bar{1}2)$*	—	—	—
60°	970	0.7	1.5
70°	980	1.0	1.7
80°	965	1.1	1.7
Towards $(\bar{1}\bar{1}1)$*	980	0.5	1.0
	Overall average = 964 ± 0.7%		

* See Table 2.

sistent with the *m3m* symmetry of silicon, and a reasonable statistical correlation of KHN values with atomic arrangement.

The greatest variation of grinding hardness was found to exist in the [110] zone. The maximum variance of microindentation hardness was observed on the (110) and on the (111) planes. For both grinding and indentation, the higher relative hardness values were obtained when

TABLE 4. KNOOP HARDNESS NUMBERS (0.1 Kg LOAD) FOR THE $(\bar{1}\bar{1}1)$ PLANE OF SILICON
(SEE FIG. 4)

Azimuth*	Average KHN_{100}	Av. Variance of 10 Indentations	Limiting Variance
Toward (001)*	970	±0.5%	±1.2%
10°	940	0.7	1.4
20°	940	0.5	0.9
30°	945	0.5	0.8
40°	960	0.3	0.5
50°	940	0.6	1.4
Toward $(\bar{1}01)$*	970	0.6	1.2
70°	945	0.6	1.2
80°	935	0.4	1.0
Toward $[\bar{1}10]$*	935	0.7	1.4
	Overall average = 948 ± 0.5%		

* See Table 2.

Table 5. Some Sources of Error Encountered in Microindentation Experiments and Observed Limiting Values

Sources	Limits
Calibration of the filar eyepiece	±1.6% limiting variance, ±1.1% av. of 12 meas.
Loading time of indentation	±5%
Inter-azimuth orientation	±1%
Crystallographic-azimuth orientation	±5.5%

resultant forces were directed into planes of greater atomic density. Similarly, the lower values were observed against planes of lesser density.

A summary of the relative directional hardness in silicon for the principal planes and azimuths is given in Table 6. Although at first glance a general inconsistency may appear to exist between similar grinding and indentation vectors, consideration of the resultant force directions with respect to crystal structure and bonding vectors at once reveals a correlation which, in view of experimental differences and difficulties, is surprisingly good.

The relative grinding hardness of the principal planes and similar azimuths in diamond, as reported by Slawson and Kohn (3), and Denning (5, 6, 7) is given in Table 7. Also indicated are the Knoop Hardness Numbers reported by Peters and Knoop (10), and Wolff *et al.* (11).

A comparison of the relative grinding hardness values for diamond with those currently observed in silicon shows a decided difference between certain of the principal vectors. Whereas (001) toward (111), and (101) in the direction toward (001), are the two hardest grinding directions in diamond; (101) in the direction toward (001), and (001) in the direction toward (101) are the two hardest in silicon. No difference in the two vectors could be resolved in diamond and essentially no difference was observed for the two hardest in silicon.

Further observed differences between the two materials are apparent in the principal azimuths on the (111) plane, and the softest grinding vector. Whereas little difference appears to exist between (111) toward (101), and (111) toward (001) in diamond; (111) toward (001) is a moderately hard vector in silicon, and (111) toward (101) is the softest vector. Grinding on plane (101) toward (111) is the softest vector in diamond.

The above differences in relative grinding hardness between diamond and silicon are compatible with the differences in morphology (surface energy), and microcleavage (as determined by light figure studies) which have been observed by Wolff (12, 13).

TABLE 6. THE RELATIVE GRINDING AND INDENTATION HARDNESS ON THE PRINCIPAL PLANES OF SILICON IN THE SPECIFIED AZIMUTHS
(SEE FIG. 4)

Grinding on Plane	In the Direction Toward	Descriptive Relative Hardness	Comparative Numerical Hardness[*]
(a) (101)	(001)	Hardest	2.0
(b) (001)	(101)	Slightly less hard than (a)	1.95
(c) (112)	(101)	Third hardest	1.55
(d) (101)	(112)	Fourth hardest[†]	1.50
(e) (001)	(111)	Same as (d) within experimental error[†]	1.50
(f) (111)	(001)	Same as (d) within experimental error[†]	1.50
(g) (101)	(111)	Fifth hardest	1.2
(h) (111)	(101)	Softest	1.05

Indentation on Plane	Long Diagonal ± Toward[‡]	Average KHN_{100}
(i) $(\bar{1}01)$	$(\bar{1}\bar{1}1)$	980
(j) (001)	$(\bar{1}\bar{1}1)$	980
(k) $(\bar{1}01)$	$(\bar{1}\bar{1}2)$	980
(l) $(\bar{1}\bar{1}1)$	(001)	970
(m) (001)	$(\bar{1}01)$ and $(0\bar{1}1)$	approx. 955
(n) $(\bar{1}\bar{1}1)$	$[\bar{1}10]$	935
(o) (001)		overall av. 964
(p) $(\bar{1}01)$		overall av. 964
(q) $(\bar{1}\bar{1}1)$		overall av. 948

[*] Radial reduction for the softest direction (unity) divided by the radial reduction for the specified direction.

[†] No significant difference could be observed between vectors (d), (e) and (f) above; however, the hardness from (e) decreases in the direction of peripheral grinding whereas the hardness increases from (f).

[‡] The orientation of indentation azimuths are correct to ±5°.

There are insufficient data available on diamond for a comparison of Knoop Hardness Values.

Another point worthy of notice from this study is the ability of the peripheral grinding technique to provide a direct and clear evaluation of the symmetrical nature of grinding hardness. This effect is nicely illustrated by Fig. 2. As expected for materials of class *m3m*, two-, three- and four-fold symmetries are displayed by the respective principal zones. The symmetry of the maximum and minimum hardness vectors with respect to crystallographic directions as a function of peripheral grinding direction also has been confirmed during the course of this investigation. Since this type of zonal hardness test can be made quite easily and

TABLE 7. THE RELATIVE HARDNESS OF THE PRINCIPAL PLANES OF DIAMOND IN THE SPECIFIED AZIMUTHS

Grinding on Plane	In the Direction Toward	Descriptive Relative Hardness
(a) (101)	(001)	Hardest*
(b) (001)	(111)	Hardest*
(c) (001)	(101)	Soft
(d) (111)	(001)	Hardest in (111) (Slawson & Kohn)
(e) (101)	(111)	Softest
(f) (111)	(101)	Hardest in (111) (Denning)
Indentation on Plane	**Long Diagonal Parallel to**	**Average KHN**
(111)	?	av. KHN_{1Kg} 8200–8500 (Knoop and Peters)
(111)	?	KHN_{100g} 8820±1380 (Wolff *et al.*)

* Of equal hardness within experimental error.

quickly, it should prove of value with respect to the basic question of the centro-symmetrical nature of grinding hardness.

ACKNOWLEDGMENTS

I would like to gratefully acknowledge the assistance of M. Conrad in carrying out the experimental work and Prof. R. M. Denning for many helpful discussions and suggestions on the problems of grinding hardness.

This work was carried out with financial assistance from the Chemical Physics Branch of the U. S. Army Signal Engineering Laboratories, Fort Monmouth, N. J., and the Office of Naval Research.

REFERENCES

1. BERGHEIMER, H., *Neues Jahrb. Min., Geol. and Pal.*, **74,** 318–332 (1938).
2. KRAUS, E. H. AND C. B. SLAWSON, *Am. Mineral.*, **24,** 661–678 (1939).
3. SLAWSON, C. B. AND J. A. KOHN, *Ind. Dia. Rev.*, **10,** 168–172 (1950).
4. WILKS, E. M., *Phil. Mag.*, Ser. 7, **43,** 1140 (1952).
5. DENNING, R. M., *Am. Mineral.*, **38,** 108–117 (1953).
6. ———, *Am. Mineral.*, **40,** 186–191 (1955).
7. ———, *Am. Mineral.*, **42,** 362–366 (1957).
8. GIARDINI, A. A., *Am. Mineral.*, **43,** 370–375 (1958).
9. BERGSMAN, E. B., *A.S.T.M. Bull.*, No. **176** (Sept. 1951).
10. PETERS, C. G. AND F. KNOOP, Metals and Alloys (Sept. 1940).
11. WOLFF, G., L. TOMAN, N. FIELD AND J. CLARK, *Proc. of Int'n. Symposium on Semiconductors and Phospors*, Garmisch, Germany (1956).
12. WOLFF, G., *Am. Mineral.*, **41,** 60–66 (1956).
13. ———, *Acta Cryst.*, **10,** 848 (1957).

Manuscript received February 17, 1958

THE AMERICAN MINERALOGIST, VOL. 43, SEPTEMBER–OCTOBER, 1958

THE STRUCTURE OF LEACHED GILLESPITE, A SHEET SILICATE

A. Pabst, *University of California, Berkeley, California.*

Abstract

Gillespite, a tetragonal sheet silicate, $BaFeSi_4O_{10}$, can be leached by hydrochloric acid leaving flakes of hydrated silica. By means of x-ray precession patterns it is shown that these flakes retain the chief features of the sheet structure. Gradual destruction of this structure which attends dehydration by heating and final recrystallization to an unoriented aggregate of crystobalite has been followed by x-ray diffraction observations.

Introduction

A number of natural silicates yield a residue of hydrated silica when acted on by acid (Murata, 1943). Some zeolites and phyllosilicates may be completely stripped of cations leaving a remnant of hydrated silica that retains the crystal shape and often has optical properties similar to those of the parent material. Rinne (1911) concluded the hydrated silica residue constituted a "well ordered remnant of the biotite structure" and suggested the name baueritization for the natural leaching of biotite. Soon thereafter (Rinne, 1913) he described experiments on the leaching of heulandite, brewsterite and stilbite. A few years later (Rinne, 1924, p. 152) he reported that "*X*-ray diagrams are no longer obtainable for the residual silica of the zeolites and mica."

The observations on leached zeolites were extended by Wyart (1933). He examined leached single crystals of heulandite by the rotating crystal x-ray method and obtained only diffraction rings characteristic of amorphous silica. Mehmel (1937) made an extensive study of the leaching of biotite by acids. In those cases in which he studied the product by x-ray diffraction by the powder method only amorphous silica was indicated. Bailey (1941) described "skeletonized apophyllite" whose retention of some optical and physical properties of the original mineral suggested "a selective leaching process in which calcium, fluorine and potassium have been removed without destroying the silica framework of the crystals." "A preliminary x-ray examination, using the powder method, failed to give any definite lines."

Gillespite, $BaFeSi_4O_{10}$, can be leached so that only "glistening silica scales" with a composition $8SiO_2 \cdot 5H_2O$ remain (Schaller, 1929). At the time that the tetragonal sheet structure of gillespite was established (Pabst, 1943) the leaching experiments were repeated and earlier results confirmed. "Attempts to observe x-ray diffraction in the leached material by powder and rotation methods led to negative results, but a long exposure Laue pattern made with the aid of an intensifying screen, with beam normal to the base of a well leached flake still shows a very faint tetragonal design" (Pabst, 1943, p. 388 and Fig. 5).

Improved techniques now available permit the study of x-ray diffraction effects that formerly escaped notice or remained uninterpretable. A study of leached gillespite by means of precession patterns has shown the extent to which the original structure is retained in the leached product.[1]

MATERIAL

The new observations were carried out entirely on gillespite from California (Rogers, 1932). It occurs as small anhedral crystals with sanbornite, quartz, celsian, witherite and minor accessories in several compact lenses a few feet wide and some yards in extent in quartzite a few miles from the western contact of the Sierra Nevada batholith and the large barite-witherite deposits near El Portal. The locality is at an elevation of about 4,300 feet near the top of the eastern slope of Ned Gulch and a quarter of a mile north of the summit of Trumbull Peak in the NE $\frac{1}{4}$, Sec. 9, R. 19 E.; T. 3 S., El Portal Quadrangle, Mariposa County, California.

A pure concentrate of this gillespite was prepared by Dr. R. M. Douglass by repeated passing through the Frantz Isodynamic Separator and centrifuging in heavy liquids. The concentrate consisted of clean cleavage fragments, half a millimeter or less in maximum dimensions and 0.1 mm. or so in thickness, well suited for leaching experiments and x-ray study. An analysis of this purified material was made by Dr. R. Klemen of Vienna and is shown in Table 1. Spectrographic examination by Dr. T. G. Kennard showed also traces of Na, Mg, Sr, Cr, Mn and V.

The cell content calculated from the new analysis and the cell dimensions and measured density in Table 2 agrees well with the ideal cell content. The count of oxygen atoms shown in column 3 of Table 1 is not adjusted; it happens to come out just at the ideal value. It seems probable that there may be some substitution of Al for Si and a little shortage of Fe compensated for by other ions. The material prepared for analysis yielded an x-ray powder pattern free of extraneous lines. Still it may be that the impurities shown by the analysis, or some of them, are due to minute bits of contaminants that escaped detection.

NEW OBSERVATIONS

Leaching of the gillespite was carried out in 5N hydrochloric acid at room temperature. It is rapid enough to permit its recognition under

---

[1] A preliminary report on this work was presented at the Pasadena meeting of the American Crystallographic Association in June, 1955.

TABLE 1. ANALYSIS AND CELL CONTENT OF GILLESPITE FROM MARIPOSA COUNTY, CALIFORNIA

	I	II	III		IV
SiO_2	49.98%	51.62	Si	15.44	16
TiO_2	0.29		Ti	0.07	
Al_2O_3	1.51		Al	0.55	
Fe_2O_3	0.22		Fe‴	0.05	
FeO	14.61	15.43	Fe″	3.78	4
CaO	0.60		Ca	0.20	
BaO	32.38	32.95	Ba	3.92	4
H_2O^-	0.22				
H_2O^+	0.17		H	0.37	
	99.98				
			O	40.00	40

I. Analysis by Dr. R. Klemen.
II. Ideal composition corresponding to $BaFeSi_4O_{10}$.
III. Cell content calculated from analysis in column I and data in Table 2.
IV. Ideal cell content.

the microscope by progressive bleaching and slight exfoliation of the deep red flakes treated individually on spot plates. *X*-ray examination of numerous flakes showed that the leaching is complete after half an hour or more and that continued acid treatment up to several months produces no further change.

Figures 1 and 2 show *hk*0 precession patterns of gillespite and of leached gillespite. It is clear that the flakes remain tetragonal and the dimensions in the *xy*0 plane are not greatly changed. The pattern of the leached material is very diffuse and the intensity relations entirely al-

TABLE 2. PROPERTIES OF GILLESPITE AND LEACHED GILLESPITE

	Gillespite	Leached Gillespite
a_0	7.51 Å	7.64
c_0	16.08	15.10
Cell Content	$4(BaFeSi_4O_{10})$	$4(H_4Si_4O_{10})+2H_2O$
Density$_{\text{obs.}}$	3.40	2.05
Density$_{\text{calc.}}$	3.41	2.15
Space Group	*P4/ncc*	*
N_0	1.621	1.449 to 1.465
N_e	1.619	1.441 to 1.455
Color O	pale pink	colorless
E	deep rose red	colorless

* See text.

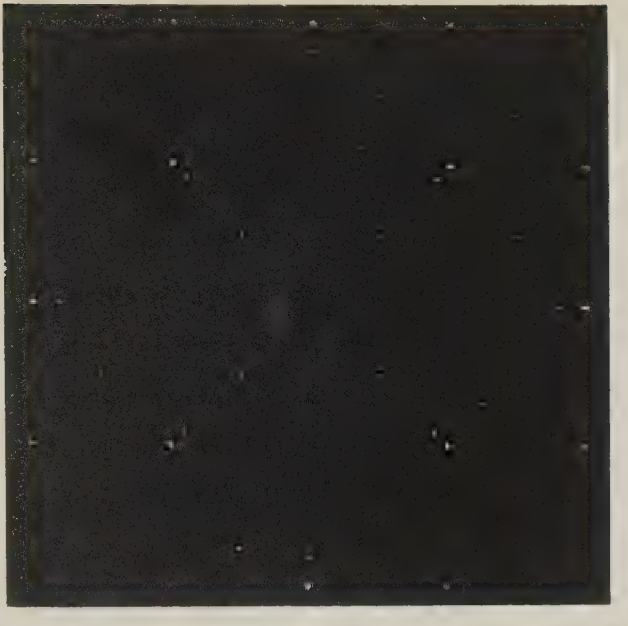

FIG. 1. Gillespite: *hk*0 precession pattern. Unfiltered Cu radiation. Exposure 4 hours.

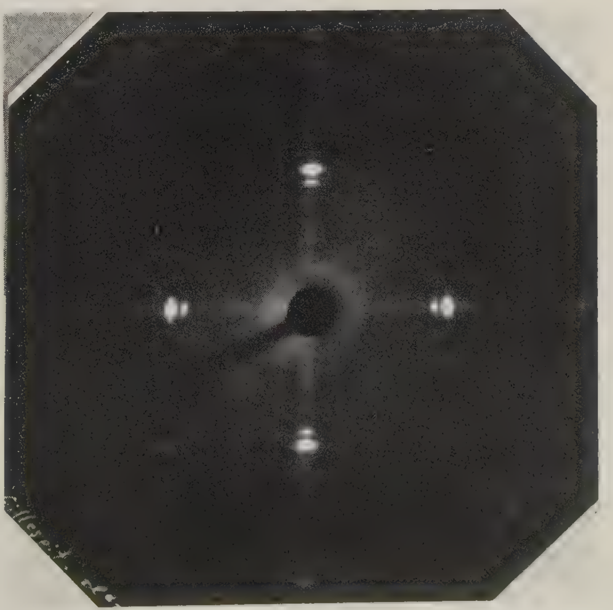

FIG. 2. Gillespite: leached for 45 minutes with 5N HCl: *hk*0 precession pattern. Unfiltered Cu radiation. Exposure 12 hours.

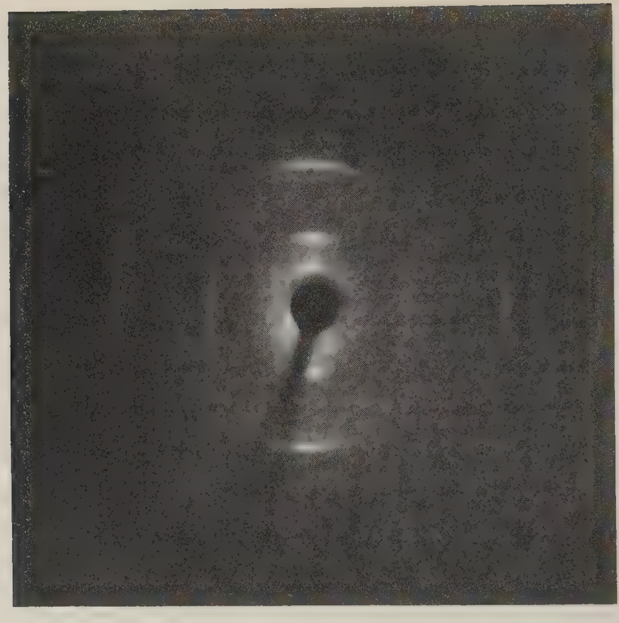

FIG. 3. Leached gillespite. Same flake as used for Fig. 2. *hhl* precession pattern. Unfiltered Cu radiation. Exposure 12 hours.

tered. The strongest spots seen on Fig. 2 are 200 "reflections." Weak 100 and 210 spots are also present. These are absent in the pattern for gillespite, being "prohibited" by the space group criteria. The cell dimensions of gillespite and leached gillespite are shown in Table 2 together with a few other data. There is a slight expansion of the Si_4O_{10} sheets which parallel (001). The basal spacing is reduced. The c_0 value given for leached gillespite is one that would correspond to a 2-sheet structure. The diffuse reflections seen on such patterns as Fig. 3 require no more than a 7.55 Å c axis.

In gillespite the two sheets within one cell height are fixed with respect to each other by the n glide parallel to (001). The loss of this relation shown by the $hk0$ pattern as well as the appearance of $h0l$ and hhl patterns suggests that there is little, if any, order in the stacking of the sheets in leached gillespite. It is, thus, impossible to assign a space group to it in the usual manner.[2] The arcuate appearance of the spots in Fig. 3 is due largely to the macroscopic bending of the sheets that attends the leaching and exfoliation. That this exfoliation leaves few closed voids is shown by the fact that the observed density of fully leached flakes was found by suspension in a bromoform-alcohol mixture to be only a few per cent below the calculated value based on cell dimensions determined from such patterns as shown in Figs. 2 and 3 and a cell content corresponding to the composition reported by Schaller.

---

[2] No way has been found of adapting the new concept of "space groupoids" (Dornberger-Schiff, 1957, p. 273) to this case.

In a powder pattern of ground, leached gillespite taken with Ni filtered Cu radiation in a camera of 360 mm. circumference with collimator and beam catcher designed to confine scattering of *x*-rays by air as much as possible, one observes a halo in the region corresponding to spacings 3.5 to 5.0 Å and superposed on this a diffuse line at the 3.8 Å position. This would correspond to (200), 3.82, and (004), 3.78, of the cell assigned to leached gillespite, but the absence of a line corresponding to (002), 7.55, which may be seen on precession patterns, suggests that the 3.8 line is largely due to (200) whose intensity is many times that of (004) as seen on *h*0*l* precession patterns not reproduced.

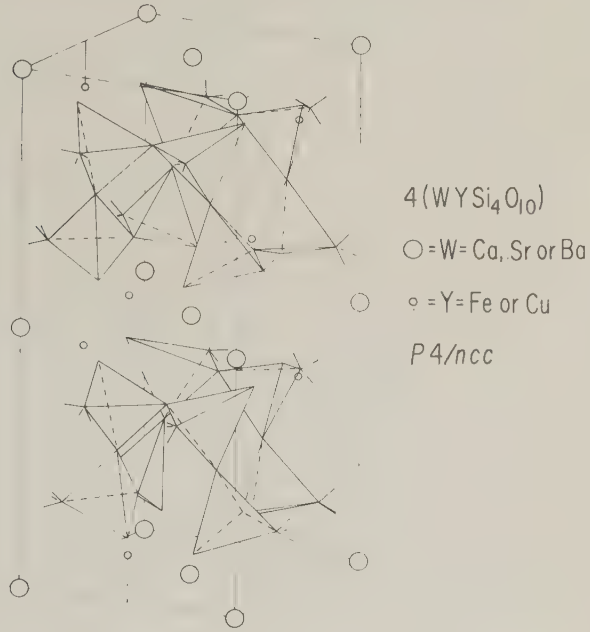

FIG. 4. Clinographic projection of the structure of gillespite and its isotypes. Two Si_4O_{10} sheets are shown within the height of one cell. The unshared corners of SiO_4 tetrahedra lie on both sides of each sheet. The Fe (or Cu) ions are at the level of these unshared corners and hence within the sheets, while the Ba (or Sr or Ca) ions are in the *n* glide planes between the sheets.

The structure of gillespite is shown in Fig. 4. The structure of leached gillespite may be derived from this by removal of all Ba and Fe and the balancing of charges by H, which requires 4/5ths of the water content reported in the leached material by Schaller (1929), giving a cell content of $H_{16}(Si_4O_{10})_4$ or $Si_{16}(OH)_{16}O_{24}$, the number of oxygens in the cell remaining unchanged. The *n* glide planes in the structure lie in $xy0$ and $xy\frac{1}{2}$. The sheets by themselves have the symmetry $P42_12$.

TABLE 3. OBSERVED AND CALCULATED F_{hk0}'S FOR GILLESPITE AND LEACHED GILLESPITE

	Gillespite		Leached Gillespite						
	F Obs.	Calc.	Calc.						Obs.
*hk*0	I	II	III	IV	V	VI	VII	VIII	IX
100	—	—	—	7	—	—	7	—	8
110	33	26	11	4	19	11	4	19	25
200	18	15	100	100	100	100	100	100	100
210	—	—	41	44	39	—	5	—	16
220	92	90	21	24	24	21	24	24	35
300	—	—	—	4	—	—	4	—	0
310	53	39	16	18	11	16	18	11	18
320	—	—	2	6	2	—	4	—	5
400	100	100	43	44	44	43	44	44	39
410	—	—	13	16	13	—	3	—	3
330	0	12	22	24	17	22	24	17	35
420	65	64	8	11	11	8	11	11	10

All values arbitrarily adjusted to make highest F in each column 100.
Dashes indicate extinction required by symmetry.
Basis for calculated F's as follows:

Gillespite, II. Corresponding to structure given by Pabst, 1943.
Leached Gillespite, III. Uncoupled sheets only.
IV. Uncoupled sheets plus H_2O in $00z$.
V. Uncoupled sheets plus H_2O in $0\frac{1}{2}z$ (and $\frac{1}{2}0z$).
VI. Coupled sheets only.
VII. Coupled sheets plus H_2O in $00z$.
VIII. Coupled sheets plus H_2O in $0\frac{1}{2}z$ (and $\frac{1}{2}0z$).

In Table 3 are given the observed and calculated structure factors for the first 12 *hk*0 planes for gillespite and leached gillespite, F's being adjusted for ease of comparison so that the highest value in each column is 100. The structure factors for leached gillespite have been calculated on several different assumptions. If the $H_{16}(Si_4O_{10})_4$ sheets retain gillespite parameters, but are not coupled to each other in any fixed manner except in orientation, the structure factors of column III result, with

(100) and (300) prohibited by the $P42_12$ symmetry of the sheets. If the sheets remain coupled as in gillespite, the criteria for $P4/ncc$ require additionally the extinction of (210), (320) and (410), column VI. As seen in column IX and Fig. 2, all of these spots are observed, though (210) and (410) with intensities much lower than those corresponding to the F's in column III. Possibly this could be accounted for by a structure in which some of the sheets remain coupled to adjacent sheets by the *n* glide in $xy0$ while many are uncoupled.

This still leaves unexplained the observation of a certain intensity of the (100) spots which can be seen in Fig. 2 superposed on the continuum streaks between the center and the very strong (200) spots. As shown in columns IV and VII of Table 2 a weak (100) reflection would arise if the remaining fifth of the water content, which is not required in the sheet structure so far described, were situated at $00z$, a likely position so far as space is concerned. The observed value of F_{320} is also in accord with this. On the other hand, water situated only in $0\frac{1}{2}z$ (and $\frac{1}{2}0z$) would not give rise to these features (columns V and VIII). Summarizing one may say that evaluation of the somewhat diffuse $hk0$ diffraction effects, for which good estimation of intensities is difficult, indicates that the silicate sheet structure of gillespite persists in the leached product but that the hydrated sheets are in part uncoupled and that there is a suggestion that the small amount of excess water is preferentially held in $00z$ locations (see Fig. 5).

The dehydration of leached gillespite was studied with care by Fairchild (Schaller, 1929). Upon heating water is lost gradually, about one third being driven off at 90° C. and some water being retained even at 400°. An attempt has been made to follow the changes attending gradual loss of water by repeated *x*-ray examination of the same flake of leached gillespite after heating to successively higher temperatures. Figs. 6, 7 and 9 show *x*-ray patterns made from the same flake that was used for the patterns of Figs. 2 and 3. They show three stages in the process. After heating to 115° and the loss of about 2/5ths of the water the dimensions of the lattice remain unchanged and the few spots still discernible are, if anything, less diffuse but only the strong (200) spots can be seen in the reproduction. The $hk0$ patterns of the same flake after heating to 185° and 405° (not reproduced) show further weakening of the pattern and after heating to 520°, at which temperature little, if any, water is still held, the "$hk0$" precession pattern is blank.

Figure 7 shows a diffraction pattern made from this flake after heating to 520° with beam normal to what had been (001), and the flake stationary at 3 cm. from the plane film. Just outside the diffuse ring suggesting "amorphous" silica one can discern four small spots conforming

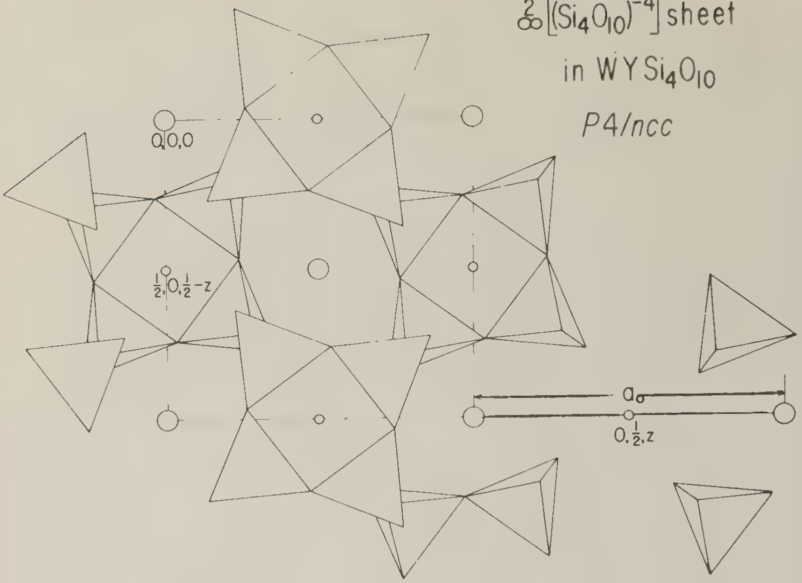
${}^2_\infty[(Si_4O_{10})^{-4}]$ sheet
in $WYSi_4O_{10}$
P4/ncc
0,0,0
$\frac{1}{2},0,\frac{1}{2}-z$
a_0
$0,\frac{1}{2},z$

FIG. 5. Structure of a single tetragonal Si_4O_{10} sheet orthographically projected onto (001). Such sheets persist in leached gillespite.

to tetragonal symmetry. From the conditions of the experiment these would be expected to be "Laue" spots. Measurement shows that they cannot be so interpreted. Rather they are 200 spots due to characteristic radiation and arise from the remnants of a single crystal because of the bending of the flake. This interpretation has been checked by a pattern taken of a stationary flake of unheated leached gillespite with beam normal to cleavage, and crystal to plane film distance 3 cm., reproduced in Fig. 8. This corresponds to an oscillation pattern for which oscillation is about axes in the plate in all azimuths and through angles of about 50°. The spots lie on hyperbolae corresponding to the higher layers of plane film rotation patterns and the entire pattern consists of spots on overlapping hyperbolae. A "Laue" pattern of leached gillespite could only be obtained by excluding characteristic radiation from the incident beam and such a pattern would be expected to consist of diffuse streaks.

Leached gillespite which has been mostly changed to "amorphous" material by heating to 520° is converted to an unoriented aggregate of cristobalite by further heating at higher temperature as shown in Fig. 9.

Attempts were made to reconstitute leached gillespite by treatment with a concentrated aqueous solution of barium and ferrous chlorides or to convert it to the isostructural barium copper silicate (Pabst, 1954).

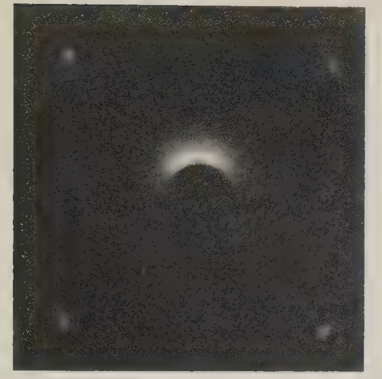

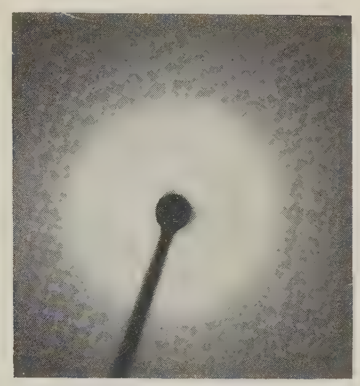

Fig. 6. (left) Leached gillespite after heating for 6 hours at 115° C.; *hk*0 precession pattern. Unfiltered Cu radiation. Exposure 12 hours. Natural size; only central part of film reproduced.

Fig. 7. (right) "Laue" pattern of leached gillespite after further heating for 14 hours at 520° C. Beam normal to cleavage, crystal to film distance 3 cm. Unfiltered Cu radiation. Exposure 12 hours. Natural size.

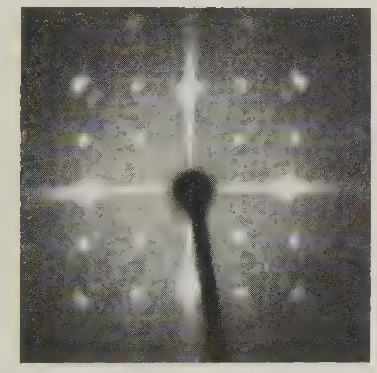

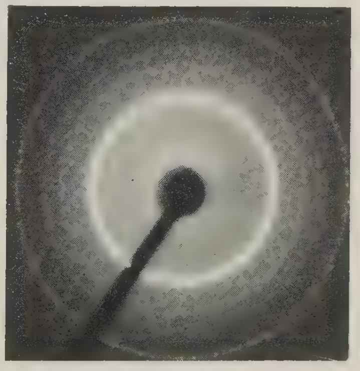

Fig. 8. (left) Pattern obtained from stationary flake of leached gillespite, beam normal to cleavage, crystal to plane film distance 3 centimeters, unfiltered Cu radiation, 35 KV, 18 MA, exposure 4 hours. Natural size. See text for explanation.

Fig. 9. (right) "Powder" pattern of leached gillespite flake after further heating for 18 hours at 780° C. Flake fixed, beam normal to cleavage, crystal to film distance 3 cm. Ni filtered Cu radiation. Exposure 4 hours. Natural size.

X-ray examination of flakes treated at room temperature for several months showed no indication of reconstitution or conversion. Treatment of fresh gillespite with concentrated solutions of copper, strontium or calcium salts produces no discernible change in color or cell dimensions that might be taken to indicate ion exchange.

ACKNOWLEDGMENT

This work was begun under a project sponsored by the Office of Naval Research and also received support from the Committee on Research of the University of California.

REFERENCES

BAILEY, EDGAR H. (1941), Skeletonized apophyllite from Crestmore and Riverside, California: *Am. Mineral.*, **26,** 565–567.

DORNBERGER-SCHIFF, K. (1957), Zur OD-Struktur (*Order-Disorder Structure*) des Purpurogallin: *Acta Cryst.*, **10,** 271–277.

MEHMEL, M. (1937), Ab- und Umbau am Biotit: *Chemie der Erde*, **11,** 307–332.

MURATA, K. J. (1943), Internal structure of silicate minerals that gelatinize with acid: *Am. Mineral.*, **28,** 545–562.

PABST, A. (1943), Crystal structure of gillespite, $BaFeSi_4O_{10}$: *Am. Mineral.*, **28,** 372–390.

PABST, A. (1954), Structure of some tetragonal sheet silicates (abstract only): *Acta Cryst.*, **7,** 630–631.

RINNE, F. (1911), Baueritisierung, ein kristallographischer Abbau dunkler Glimmer: *Ges. Wiss. Leipzig, Verhandlungen, Math.-Phys. Kl.*, **33,** 441–445.

RINNE, F. (1913), Kristallographisch-chemischer Ab- und Umbau insbesondere von Zeolithen: *Fortsch. Min.*, **3,** 159–183.

RINNE, FRIEDRICH (1924), Crystals and the Fine-Structure of Matter (translated by Walter S. Stiles): Methuen, London, ix+195 pages.

ROGERS, AUSTIN F. (1932), Sanbornite, a new barium silicate mineral from Mariposa County, California: *Am. Mineral.*, **17,** 161–172.

SCHALLER, WALDEMAR T. (1929), The properties and associated minerals of gillespite: *Am. Mineral.*, **14,** 319–322.

WYART, J. (1933), Recherches sur les zéolites: *Bull. soc. fran. min.*, **56,** 81–187.

Manuscript received March 4, 1958

THE AMERICAN MINERALOGIST, VOL. 43, SEPTEMBER-OCTOBER, 1958

NOTES AND NEWS

HOLMQUISTITE AS A RHOMBIC AMPHIBOLE

THOROLF VOGT, OTTO BASTIANSEN, AND PER SKANCKE,
Technical University of Norway, Trondheim, Norway.

A. Osann (1913) described holmquistite as a lithium-glaucophane from the island Utö, Södermanland, Sweden. Charles Palache, S. C. Davidson, and E. A. Goranson (1930) described this rare mineral from the second known locality, the Hiddenite mine, Alexander Co., North Carolina. Felix Machatschki (1953, p. 44) regarded holmquistite not as a glaucophane, but rather as an independent member of the amphibole group, and placed the mineral in the same relation to cummingtonite that spodumene has to clinoenstatite, in the pyroxene group. The excellent analysis of the end member from Utö, published by Nils Sundius (1947), gives a formula close to $Li_4Mg_6Al_4Si_{16}O_{44}(OH)_4$, with some divalent and trivalent iron. The North Carolina mineral represents a holmquistite apparently not very far from the end member. All authors regarded holmquistite as a monoclinic amphibole.

One of us (Vogt) has considered holmquistite as derived not from cummingtonite, but from anthophyllite, $Mg_{14}Si_{16}O_{44}(OH)_4$, through the couplet substitution $MgMg = LiAl$. Employing the values of ionic radii in 6-fold coordination of L. H. Ahrens (1952), Mg 0.66, Li 0.68, and Al 0.51 Å, the sums of ionic radii of this substitution are 1.32 and 1.19 respectively. This ratio (111:100) is favorable for the substitution.

The holmquistites from the two localities are relatively poor in divalent iron, giving decidedly the composition of anthophyllite and not of cummingtonite, the Li being reckoned with the Mg. Further, the extinction on 010 is reported to be near zero: Osann gives 2 3°, Sundius 0–2°, and Palache and coworkers parallel extinction or almost so. On material from Utö, kindly placed at our disposal by Professor F. E. Wickman and Dr. N. Zenzén, Riksmuseet, Stockholm, no definite deviation from parallel extinction could be found, and also no dispersion of extinction. A rhombic symmetry could, indeed, be suspected. Crystals of holmquistite with terminal faces are, by the way, unknown.

The x-ray study was performed by two of us (Bastiansen and Skancke) on holmquistite from Utö. Oscillation and Weissenberg photographs about the needle axis (c) reveal rhombic symmetry, with $c_0 = 5.29$ Å. From the Weissenberg photographs the most probable values for a_0 and b_0 at first seemed to be 9.18 and 17.75 Å respectively. The possibility of doubling of one or both of the axes had still to be considered. Oscillation diagrams around these two axes showed, indeed, that this was the case for the a-axis but not for the b-axis. From the Weissenberg diagrams around the b-axis it could further easily be seen that the $h00$ reflections occur only for h equal to 4, 8, 12 etc. The a-axis is accordingly 18.36 Å. The numerical values of the a- and b-axes were determined from the Weissenberg diagrams around the c-axis using a very small crystal fragment. The lattice constants of the rhombic unit cell were found to be the following:

$$a = 18.36\ \text{Å}\ (\pm 0.02\ \text{Å})$$
$$b = 17.75\ \text{Å}\ (\pm 0.02\ \text{Å})$$
$$c = 5.29\ \text{Å}\ (\pm 0.02\ \text{Å})$$

According to Osann, the angle $110{:}1\bar{1}0$ is 55°48′. He used material from Utö, and obviously measured cleavage angles. Palache and coworkers measured 54°39′ on crystal faces. The calculated angle, based on the lattice constants obtained in the present investigation, is 54°41½′, closely conformable to the latter statement.

The conclusion may be that the relation between the holmquistite and anthophyllite in the amphibole group corresponds to the relation between the spodumene and clinoenstatite in the pyroxene group. The lattice constants of the unit cell of these minerals are the following (three of them according to H. Strunz (1957)):

Holmquistite	$a=18.36$	$b=17.75$	$c=5.29$	
Anthophyllite	$a=18.56$	$b=18.08$	$c=5.28$	
Diff.	$+0.20$	$+0.33$	-0.01	
Spodumene	$a=9.52$	$b=8.32$	$c=5.25$	$\beta=110°28'$
Clinoenstatite	$a=9.62$	$b=8.83$	$c=5.19$	$\beta=108°21\frac{1}{2}'$
Diff.	$+0.10$	$+0.51$	-0.06	

The introduction of LiAl for MgMg in both instances involves similar changes.

BIBLIOGRAPHY

AHRENS, L. H. (1952), The use of ionization potentials Part 1. Ionic radii of the elements. *Geochim. et Cosmochim. Acta*, **2**, 155.

MACHATSCHKI, FELIX (1953), Spezielle Mineralogie, Wien.

OSANN, A. (1913), Über Holmquistit, einen Lithionglaukophan von der Insel Utö. *Sitzungsber. d. Heidelberger Akad. d. Wissensch. Math.-nat. Kl.* Abt. A, Jahrg. **1913**, 23.

PALACHE, CH., S. C. DAVIDSON, AND E. A. GORANSON (1930), The Hiddenite deposit in Alexander County, North Carolina. *Am. Mineral.*, **15**, 280.

STRUNZ, HUGO (1957), Mineralogische Tabellen 3 Ed., Leipzig.

SUNDIUS, NILS (1947), Die chemische Zusammensetzung des Holmquistits. *Geol. Fören Förhandl.*, **69**, 51.

THE AMERICAN MINERALOGIST, VOL. 43, SEPTEMBER-OCTOBER, 1958

CRANDALLITE (PSEUDOWAVELLITE) FROM GARDNER MINE RIDGE, LAWRENCE COUNTY, INDIANA*

S. S. Greenberg and W. T. Elberty, *Indiana Geological Survey and Indiana University, Bloomington, Indiana.*

Crandallite, $CaAl_3(PO_4)_2(OH)_5H_2O$, was found as a minor constituent of a brown, allophane-rich variety of hydrated halloysite (endellite) in the course of an *x*-ray investigation of clay samples from Gardner Mine Ridge, Lawrence County, Indiana (sec. 21, T. 4 N., R. 2 W.). Inasmuch as crandallite and pseudowavellite may be considered a single species (Palache, et al., 1951, p. 837), this positive identification of crandallite confirms a suggestion by Callaghan (1948, p. 34) that pseudowavellite may be present in a clay sample from Gardner Mine Ridge.

The dominant clay mineral at Gardner Mine is hydrated halloysite. Concentrations of hydrated halloysite are localized in restricted lenses and pockets stratigraphically at, or just above, the Mississippian-Pennsylvanian unconformity. A pebbly facies of the Mansfield formation overlies the clay deposits and occurs as discontinuous and irregular seams and lenses within the clay itself. The character of the sedimentary rocks beneath the clay is not known definitely, but it is probably underlain by the Mississippian Beaver Bend limestone.

The hydrated halloysite can be divided into three varieties on physical appearance:

1. Bluish-white, microgranular, nodular variety with distinct conchoidal fracture.
2. White, massive, granular variety.
3. Brown, massive, granular variety.

Callaghan (1948) described these deposits in detail.

Crandallite has been identified only in the brown, massive, hydrated halloysite. Thin section studies have not been made of this variety because of its extreme friability, and consequently the exact habit of the crandallite is not known. However, it has been shown by microscopic examination that a considerable amount of the crandallite is associated with grains of allophane, which may comprise as much as 50% of the brown variety of hydrated halloysite. Some crandallite may also be intimately mixed with the hydrated halloysite.

Grains of crandallite are composed of subparallel to radiating acicular crystals (0.05×0.001 mm.) and display a characteristic wavy extinction.

---

* Published by permission of the State Geologist, Indiana Department of Conservation, Geological Survey, Bloomington.

The grains themselves vary from elongate arcuate fragments (0.1×0.05 mm.) with well rounded edges to equidimensional clay size particles. No recognizable interference figure was obtained. Refractive indices range from 1.620–1.630±.002, and birefringence is weak.

Two grains were noted that did not have the characteristic wavy extinction of crandallite. These grains were biaxial negative with a 2V of 34°±3° as measured on a universal stage. This mineral may possibly be lewistonite or dehrnite.

The *d*-spacings from *x*-ray patterns of the Indiana crandallite correspond closely to those of McConnell's pseudowavellite (1942, p. 652). The A.S.T.M. *d*-spacing card titled "crandallite" (no. 5-0615) differs significantly from the card titled "pseudowavellite" (no. 2-0738). If crandallite and pseudowavellite are the same mineral species, then the A.S.T.M. card file is in error for one of the minerals.

Gibbsite occurs, intermixed with granular hydrated halloysite, as a crust on the nodular variety of hydrated halloysite, and may be an alteration product of the latter. The brown hydrated halloysite owes its color to iron oxides which also coat the quartz grains of the associated Mansfield sandstone. Allophane is found in both the brown and the white granular varieties of hydrated halloysite.

Two samples of allophane from Gardner Mine Ridge contained 9.51% and 10.57% P_2O_5 (Callaghan, 1948, p. 33; and White, 1953, p. 636). Callaghan (1948, p. 35) thought that the P_2O_5 in the allpohane was due to the presence of evansite. These same chemical analyses, however, show 2.86% and 2.37% CaO; thus some, if not all, of the P_2O_5 is tied up in crandallite rather than in evansite. In another sample of allophane from Gardner Mine Ridge, Ross and Kerr (1934, p. 146) found 7.15% P_2O_5 and no CaO; this allophane probably contained evansite and no crandallite. The crandallite, at least in part, is an alteration product of the evansite.

Crandallite or pseudowavellite has been described from Hesse-Nassau, Germany (Kosmann, 1869, p. 799), Silver City, Utah (Loughlin and Schaller, 1917), Amberg, Bavaria (Laubmann, 1922), Fairfield, Utah (Larsen and Shannon, 1930, p. 317), Llallagua, Bolivia (Gordon, 1944, p. 336), Thiès, French West Africa (Visse, 1952; Capdecomme, 1952, 1953; Capdecomme and Pulou, 1954), and Paraíba, Brazil (Murdoch, 1955, p. 57). The occurrence at Gardner Mine Ridge most closely resembles that at Thiès, where the deposit is believed to have originated from a phosphate rich residual soil.

At the present time a detailed investigation is in progress to describe and determine the origins of the minerals at Gardner Mine Ridge, with particular emphasis on the phosphate minerals.

The authors would like to acknowledge the many valuable suggestions made by Carl W. Beck, Professor of Mineralogy at Indiana University.

REFERENCES

Callaghan, E. (1948), Endellite deposits in Gardner Mine Ridge, Lawrence County, Indiana: *Indiana Div. Geol.* Bull. **1,** 47 p.

Capdecomme, L. (1952), Sur les phosphates alumineux de la région de Thiès (Sénégal): *Compt. Rend. Acad. Sci. Paris,* **235,** 187–189.

——— (1953), Étude mineralogique des gîtes de phosphates alumineux de la région de Thiès (Sénégal): *Compt. Rend XIX Congr. Géol. Internat. Alger* **1952,** fasc. XI, 103–117.

——— and Pulou, R. (1954), Sur la radioactivité des phosphates de la région de Thiès (Sénégal): *Compt. Rend. Acad. Sci. Paris,* **239,** 288–290.

Gordon, S. (1954), The mineralogy of the tin mines of Cerro de Llallagua, Bolivia: *Proc. Phila. Acad. Sci.,* **96,** 279–359.

Kosmann (1869), Der Apatit von Offheim und der Kalkwavelit von Dehrn und Ahlbach: *Zeit. deutsche geol. Ges.,* **21,** 795–806.

Larsen, E. S., and Shannon, E. V. (1930), The minerals of the phosphate nodules from near Fairfield, Utah: *Am. Mineral.,* **15,** 307–337.

Laubmann, H. (1922), Die Phosphat-Mineralien und Edelerden des Amberg-Auerbacher Erzkörpers: *Geogn. Jahres,* **35,** 202–203.

Loughlin, G. F., and Schaller, W. T. (1917), Crandallite, a new mineral: *Am. Jour. Sci.* **43** (**193**), 69–74.

McConnell, D. (1942), *X*-ray data on several phosphate minerals: *Am. Jour. Sci.,* **240,** 649–657.

Murhoch, J. (1955), Phosphate minerals of the Borborema pegmatites: 1-Patrimonio: *Am. Mineral.,* **40,** 50–63.

Palache, C., Berman, H., and Frondel, C. (1949), Dana's system of mineralogy, V. II: John Wiley and Sons, Inc., 1124 p.

Ross, C. S., and Kerr, P. F. (1934), Halloysite and allophane: *U. S. Geol. Surv. Prof. Paper,* **185,** 135–148.

Visse, L. D. (1952), Pseudowavellite et millisite dans les minerais phosphatés dits latéroides blancs de la région de Thiès (Sénégal): *Compt. Rend. Acad. Sci. Paris,* **234,** 1377–1378.

White, W. A. (1953), Allophanes from Lawrence County, Indiana: *Am. Mineral.,* **38,** 634–642.

THE AMERICAN MINERALOGIST, VOL. 43, SEPTEMBER-OCTOBER, 1958

RELATION OF IONIC RADIUS TO STRUCTURES OF RARE-EARTH PHOSPHATES, ARSENATES, AND VANADATES*

M. K. Carron, Mary E. Mrose, and K. J. Murata,
U. S. Geological Survey, Washington 25, D.C.

Several investigators have reported data on the crystal structures of rare-earth phosphates (Carron and others, 1958), arsenates (Strada and Schwendimann, 1934; Durif and Forrat, 1957), and vanadates (Milligan, Watt, and Rachford, 1949; Durif, 1956). For each of these groups of compounds, the boundary between the xenotime structure (zircon type, tetragonal) and other structural types is at a different element of the rare-earth group. Most of the investigators failed to note that the rare-earth elements which formed compounds other than of the xenotime type invariably produced compounds isostructural with monazite (monoclinic).

---

* Publication authorized by the Director, U. S. Geological Survey.

The purpose of this work is to assemble the available data and to correlate crystal structures of the rare-earth compounds with the ionic radii of the trivalent elements and the anions.

By wet chemical methods, we have produced rare-earth phosphates, arsenates, and vanadates that were found by *x*-ray powder diffraction patterns to be isostructural either with monazite or xenotime. In the arsenate system, we confirmed the study by Durif and Forrat (1957) who showed $SmAsO_4$ to be of the xenotime structure. They stated that $NdAsO_4$ had a different structure which, however, they did not identify. We found $NdAsO_4$ to be isostructural with monazite. In the vanadate system we also confirmed the work of Milligan, Watt, and Rachford (1949) who produced their compounds by igniting equimolecular mixtures of the rare-earth oxides and ammonium metavanadate and reported the vanadates of praseodymium through lutetium to be of the xenotime structure. Durif (1956) reported that $CeVO_4$, prepared by oxidation of "$CeVO_3$", had the xenotime structure. We also prepared $CeVO_4$ by adding a solution of ammonium metavanadate to a solution of cerous chloride and digesting the solution overnight on a steam bath. The compound, dried at 100° C., was found to be isostructural with xenotime. Neither of the investigators cited above noted that only $LaVO_4$ has the monazite structure. Carron and others (1958) have shown that in the phosphate system $TbPO_4$ ($Tb^{3+}=0.93$ Å) has the xenotime structure whereas its preceding neighbor $GdPO_4$ ($Gd^{3+}=0.97$ Å) has the monazite structure. Among the actinides, $PuPO_4$ ($Pu^{3+}=1.08$ Å) has been shown to have the monazite structure (Bjorklund, 1957). With regard to scandium, we found that $ScPO_4$, prepared in a bomb at 300° C. from solutions of $ScCl_3$ and dilute phosphoric acid, and $ScVO_4$, prepared by igniting Sc_2O_3 and V_2O_5 at 1000° C., has the xenotime structure. We also prepared a hydrated scandium arsenate from solutions of $ScCl_3$ and dilute arsenic acid which was isostructural with the metavariscite group of minerals. On ignition this compound assumed the xenotime structure.

Table 1 is a compilation of all of the anhydrous rare-earth phosphates, arsenates, and vanadates, showing the limiting elements for the monazite and xenotime structures in each system. It shows that the xenotime

TABLE 1. STRUCTURES OF RARE-EARTH AND SCANDIUM PHOSPHATES, ARSENATES AND VANADATES

Element	La	Ce	Pr	Nd	Sm	Eu	Gd	Tb	Dy	Y	Ho	Er	Tm	Yb	Lu	Sc
Ionic radius, Å (Ahrens, 1952)	1.14	1.07	1.06	1.04	1.00	0.98	0.97	0.93	0.92	0.92	0.91	0.89	0.87	0.86	0.85	0.81
PO_4	M	M	M	M	M	M	M	X	X	X	X	X	X	X	X	X
AsO_4	M	M	M	M	X	X	X	X	X	X	X	X	X	X	X	X[1]
VO_4	M	X	X	X	X	X	X	X	X	X	X	X	X	X	X	X[2]

[1] From $ScAsO_4$ which was precipitated from solution and ignited by Meeker burner.
[2] From ignition of a mixture of Sc_2O_3 and V_2O_5 for 8 hours with Meeker burner.
M = Monazite; X = Xenotime.

structure can accommodate increasingly larger cations as the size of the anion increases. There is a quantitative relationship between the radius of the largest xenotime-forming rare-earth element and the size of the anion, in the following manner (formal sixfold coordination radii from Ahrens, 1952):

	P-O	As-O	V-O
A = Oxygen-central atom distance, Å	1.75	1.86	1.99
B = Radius of the largest rare-earth element forming the xenotime structure, Å	.93(Tb^{3+})	1.00(Sm^{3+})	1.07(Ce^{3+})
A/B	1.88	1.86	1.86

The A/B ratio of 1.86 seems to specify the size limits of both the cation and anion at the xenotime-monazite structural boundary. This ratio would lead to the prediction that among orthosilicate compounds (formal Si-O distance of 1.82 Å) the largest cation radius permissible for the xenotime structure would be 0.98 Å. This predicted radius is very close to that of quadrivalent uranium (0.97 Å), and $USiO_4$, coffinite, with the xenotime structure has been synthesized recently (Hoekstra and Fuchs, 1956). Quadrivalent thorium (1.02 Å) which is only 0.04 Å larger than the predicted size forms an orthosilicate with either the monazite or xenotime structure.

Isomorphous substitution of the anions among the rare-earth phosphate, silicate, arsenate, and vanadate systems seems to be possible. However, analyses of xenotime and monazite reported in the literature (Palache and others, 1951) indicate possible replacement of only SiO_4 for PO_4. Although there are no known rare-earth arsenate or vanadate minerals, it might be well in future analyses of rare-earth phosphates and silicates to test for the possible presence of small amounts of arsenic and vanadium.

The authors wish to express thanks to Harry Rose, Jr., for numerous helpful comments and discussions.

REFERENCES

AHRENS, L. H. (1952), The use of ionization potentials. Part 1. Ionic radii of the elements: *Geochim. et Cosmochim. Acta*, **2,** 155–169.

BJORKLUND, C. W. (1957), The preparation of $Pu_2P_2O_7$ and $PuPO_4$: *Am. Chem. Soc. Jour.*, **79,** 6347–6350.

CARRON, M. K., NAESER, C. R., ROSE, H. J., JR., AND HILDEBRAND, F. A. (1958), Fractional precipitation of rare earths with phosphoric acid: *U. S. Geol. Survey Bull.* **1036-N**, 253–275.

DURIF, A. (1956), Structure et valences de $VCeO_4$: *Acta Cryst.*, **9,** p, 471.

DURIF, A., AND FORRAT, F. (1957), Sur quelques arséniates des terres rares à structure zircon: *Acad. Sci. Paris Comptes Rendus*, **245,** 1636–1638.

HOEKSTRA, H. R., AND FUCHS, L. H. (1956), Synthesis of coffinite –$USiO_4$: *Science*, **123,** 105.

Milligan, W. G., Watt, L. M., and Rachford, H. J., Jr. (1949), *X*-ray diffraction studies on heavy metal orthovanadates: *Jour. Phys. and Colloid Chem.*, **53**, No. 2, 227–234.

Palache, C., Berman, H., and Frondel, C. (1951), Dana's System of Mineralogy, 7th ed., **2**, 690, 694, New York, John Wiley and Sons, Inc.

Strada, M., and Schwendimann, G. (1934), The crystalline structure of some phosphates and arsenates of trivalent metals. II. Yttrium arsenate and yttrium phosphate: *Gazz. chim. italiana*, **64**, 662–674 (in Italian).

THE AMERICAN MINERALOGIST, VOL. 43, SEPTEMBER-OCTOBER, 1958

GOETHITE-HEMATITE RELATION—AN ORE MICROSCOPE OBSERVATION

Mihir Kumar Bose,
Geological Laboratory, Presidency College, Calcutta, India.

To the south of Chaibasa (22°33′:85°28′), Singhbhum, India, near the northern limit of the Kolhan basin, the fracture zones formed by post-Kolhan deformation, have been mineralized by a metalizing solution. The mineralization is more common in the competent sandstone than in the shale, and also along the sandstone-shale boundary. The mineralizing solution was ferriferous in the first phase and formed such minerals as limonite, goethite and specularite, these being followed by a phase of formation of the manganese minerals psilomelane, pyrolusite, and its idiomorphic form. The important textural relations are the core and rim replacement of goethite by psilomelane, and an intergrowth relation between fibrous goethite and hematite. The latter texture is described in this note.

Such a specimen of goethite on analysis shows a higher content of Fe_2O_3 (91.3%), than normal, because of the included hematite plates.*

The intergrowth has been studied on different polished surfaces with respect to the fibre axis. Goethite, the host mineral under reflecting microscope is greyish with perceptible differential adsorption in some specimens, being brighter parallel to the fibre axis. Unusual for goethite, the bireflectance is very weak but with the commoner orange internal reflection. These properties are variable since they depend on the content of adsorbed water (Ramdohr 1955). The mineral is stained brown by $SnCl_2$ ($1\frac{1}{2}$ minute). The reflectance measured in green light in air is 19.3% parallel to the fibre axis and 17.5% across. Specimens polished perpendicular to fibre axis shows no notable variation in reflecting power.

Hematite inclusions occur as continuous plates within the host. In sections with the orientation parallel to the fibre axis, the plates show an intersecting relation, with the fibre axis bisecting the acute angle (Fig. 1). Sections polished perpendicular to the fibre axis, reveal the striking parallelism of the plates. The width of the individuals depends on their inclination to the plane of section. Such plates are locally much concentrated to give a striped look to the mineral. The reflectance of the mineral in green light in air is 24%.

---

* The planes of hematitization are actually micro S-planes produced by a post-Kolhan deformation, the pattern of which is being studied in this laboratory.

The nature of the hematite plates suggests an exsolution origin for the texture, particularly because of lack of thickened intersections. (Bastin 1931). But no such exsolution pair is known (Ramdohr 1955). Closer examination of the plates under high magnification however reveals a somewhat irregular nature of the margin of the plates, which together with their continuous character suggest a replacement origin for the texture (Bastin 1931). Conversion of fibrous goethite to hematite is known to take place at a temperature of about 150° C. in a neutral medium (Smith and Kidd 1949). Association of manganiferous minerals in this case may however suggest a slightly lower pH value than neutral conditions.

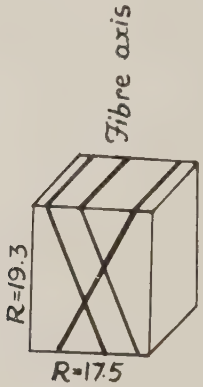

Fig. 1. Diagrammatic relation between goethite (white) and hematite plates (black).

Acknowledgment

The writer is indebted to Professor S. Ray, Department of Geology, Presidency College, for his kind help in this study.

References

Bastin, E. S., Graton, L. G. (1931), Criteria of age relations of minerals. *Econ. Geol.*, **26,** 561–610.

Ramdohr, P. (1955), Die Erzmineralien ind ihre Verwachsungen. Berlin.

Smith, F. G. and Kidd, D. J. (1949), Goethite-hematite relation in neutral and alkaline solutions under pressure. *Econ. Geol.*, **34,** 403–412.

THE AMERICAN MINERALOGIST, VOL. 43, SEPTEMBER–OCTOBER, 1958

NOTES ON THE MINERALOGY OF AN YTTRIUM-BEARING PEGMATITE BODY NEAR LAKE GEORGE, PARK COUNTY, COLORADO*

Jewell J. Glass and Harry J. Rose, Jr., *Washington 25, D. C.* and Edwin Over, *Woodland Park, Colorado*

Introduction

During a visit by Edwin Over to the Lake George pegmatite area in 1928 he discovered gadolinite, an yttrium-rich beryllium iron silicate, and collected some good crystals from a small outcrop. Inspired by a new demand for gadolinite, Over returned to the same locality in 1956. He found, as a result of road building and feldspar mining, the exposed face and waste dumps of a large vertical pegmatite body. Lumps of massive fluorite—some that weighed 600 pounds—were common in the mine dumps. Examination of these fluorite bodies revealed inclusions of several minerals found to be yttrium bearing.

The description of the fluorite masses and their associated feldspar pegmatite is based on the observations of Edwin Over, who provided the material for this study. The optical data and the mineral identifications are by Jewell J. Glass, and the spectrographic analyses were made by Harry J. Rose, Jr.

Locality

The yttrium-bearing pegmatite body is called the Teller pegmatite Lode Claim. It is in the Lake George mining district, Park County, Colorado; NE $\frac{1}{4}$, sec. 31, T. 12 S., R. 71 W. The mine workings are 0.5 mile south of Lake George on the Eleven Mile Canyon Road, and only a few hundred feet east from the South Platte river. The original workings in this pegmatite were for feldspar in 1940.

Occurrence

The yttrium-bearing deposits, apparently hydrothermal replacement of feldspar, occur as lenses of fluorite mostly in the north portion of the Teller pegmatite body which consists of a large mass of pink microcline feldspar. This pegmatite body is in an area of massive Pikes Peak granite that rises to an altitude of 8,350 feet and lies about 20 miles air line west northwest of Pikes Peak and about 4 miles nearly due west of Crystal Peak. The age of the pegmatite body is not known to the writers, but the host rock is Pikes Peak granite, whose determined age (Precambrian) is a billion years (Holmes, 1931).

---

* Publication authorized by the Director, U. S. Geological Survey.

MINERALOGY

The most abundant yttrium-bearing minerals that occur in the fluorite (some of which is itself rich in yttrium) are allanite, gadolinite, monazite, and xenotime. An unidentified, high-yttrium, cerium-earth carbonate occurs in small amounts and is being studied in detail.

Spectrographic analyses show all the lanthanides (atomic nos. 57–71) and yttrium (atomic no. 39) to be present in these minerals with the exception of promethium (atomic no. 61). The lanthanides of even atomic number (Ce, Nd, Sm, Gd, Dy, Er, Yb) are more abundant than their neighbors of odd atomic number (La, Pr, Eu, Tb, Ho, Tm, Lu) as shown in Table 1. This observation has been noted by previous investigators and is known as the rule of Oddo and Harkins (Rankama and Sahama, (1950).

Allanite (*Orthite*).—Allanite in hand specimen is glossy black, massive, in irregular lumps as large as a walnut. The allanite is brittle and has no distinct cleavage. Under the microscope the mineral is metamict. The color is smoky grayish-green. The index of refraction is $n=1.70$. Along the contact of the allanite with microcline, the allanite border is yellowish red and is partly anisotropic. The spectrographic analysis of allanite is given in Table 1.

Fluorite.—The fluorite is massive and varies from pink, pale green, and cream to deep purple. The pink and cream colored fluorite is heavy with inclusions of yttrium-bearing minerals, especially xenotime and gadolinite. The index of refraction for the fluorite ranges from 1.437 to 1.450—that is, most of this material is yttrian fluorite or yttrofluorite.

Gadolinite.—Gadolinite, an iron-beryllium-yttrium silicate, occurs as crystals as much as $1\frac{1}{2}$ inches long embedded in the fluorite. The gadolinite is greenish black; it is brittle and breaks with a conchoidal fracture. The mineral is optically positive; 2V is near 90°. The indices of refraction are: $\alpha=1.800$, $\beta=1.808$, $\gamma=1.818$. Some grains are metamict, and have lower, variable indices.

Molybdenite. —Molybdenite, a sulfide of molybdenum, occurs rarely as small foliated masses about 1 cm. across in vugs in some of the purple fluorite.

Monazite.—A reddish brown variety of monazite, cerium phosphate, that contains yttrium› is commonly associated with brick-red, earthy inclusions in the fluorite. It is assumed that these red inclusions are iron-stained residue from the alteration of gadolinite. The monazite grains are small, none of them is more than 1 mm. across. The mineral is optically biaxial positive, $2V=10°$. The indices of refraction are: $\alpha=1.786$, $\beta=1.787$, $\gamma=1.840$.

Xenotime.—Xenotime, yttrium phosphate, is disseminated unevenly but consistently through most of the fluorite, and also occurs as aggregates in allanite. No crystals have been noted but some of the grains are elongated. A few grains in one sample are 1 mm. long and about one third as wide. Most of the grains are colorless, but some are pale pink. Xenotime is uniaxial positive, $\omega=1.717$ and $\epsilon=1.816$. The spectrographic analysis of xenotime is given in Table 1.

The fine-grained, high-index carbonate in some samples may well be bastnaesite.

Association of fluorite and rare earth minerals in pegmatite bodies has been discussed by Heinrich (1948). The Teller pegmatite illustrates a reverse condition of the association common in pegmatites: the fluorite here is host to a suite of rare earth minerals.

A complex problem in geochemistry is presented here. Data are not yet sufficient for a

Table 1. Semiquantitative Spectrographic Analyses for Minor Elements in 16 Samples of Minerals from Yttrium-Bearing Pegmatite Body Near Lake George, Park County, Colorado

Analyst: Harry J. Rose, Jr.

Sample	Description	*Si*	*Al*	*Be*	*P*	*F**	*Ca*	*Fe*	*Y*	*Lu*	*Yb*
		0 in unit column means element not detected									
SpC 1	Gadolinite, massive, impure	x.	.0x	x.	0	—	.x	x.	x0.	.x	x.
SpC 2	Total ore-bearing rock	.x	.x	.0x	0	x0.	x0.	.x	x0.	.x	x.
SpC 3	Pink fluorite with xenotime	.0x	.0x	.00x	.x	x0.	x0.	.0x	x0.	.x	x.
SpC 4	Pale green fluorite	.0x	.0x	.00x	0	x0.	x0.	.0x	x.	.0x	.x
SpC 5	Purple fluorite partly pure	.0x	.x	.000x	0	x0.	x0.	.0x	.x	.00x	.0x
SpC 6	Purple fluorite ore	.x	x.	.00x	0	x0.	x0.	x.	x0.	.0x	x.
ReC 1	Gadolinite crystal	x.	.x	x.	0	—	.x	x.	x0.	.x	x.
ReC 2	Glossy black allanite	x.	x.	.00x	0	—	.x	x.	.x	0	.0x
ReC 3	Xenotime inclusions from allanite	.x	.x	.00x	x0.	—	.x	.x	x0.	.x	x.
ReC 4	Cream fluorite partly pure	.0x	.0x	.00x	0	x0.	x0.	.x	x0.	.x	x.
ReC 5	Inclusions from ReC 4	.x	.x	.00x	0	—	x0.	x.	x0.	.x	x.
ReC 6	Fluorite host of molybdenite	.x	x.	.00x	0	x0.	x0.	x.	x0.	.x	x.
ReC 7	Altered gadolinite	.x	x.	x.	0	—	.x	x.	x0.	.0x	x.
ReC 8	Red alteration products	.x	x.	x.	0	—	.x	x.	x0.	.x	x.
ReC 9	Brick-red powder, alteration	.x	.x	.00x	x.	x0.	x.	x.	x.	.x	x.
ReC 10	Fluorite with rare earth carbonate	.x	.x	.00x	0	x0.	x.	x.	x0.	.x	x.

Sample No.	*Tm*	*Er*	*Ho*	*Dy*	*Tb*	*Gd*	*Eu*	*Sm*	*Nd*	*Pr*	*Ce*	*La*	*Th*
	0 in unit column means element not detected												
SpC 1	.x	x.	.x	x.	.x	x.	.0x	.x	.x	.0x	x.	.x	.0x
SpC 2	.0x	.x	.x	.x	.0x	.x	0	.x	.x	0	x.	.x	0
SpC 3	.0x	.x	.x	.x	.0x	.x	0	.x	.x	0	x.	.x	0
SpC 4	.00x	.0x	.0x	.x	0	.0x	0	.0x	0	0	.x	.0x	0
SpC 5	.00x	.0x	.0x	.0x	0	.0x	0	.0x	0	0	.x	.0x	0
SpC 6	.0x	.x	.x	.x	.0x	.x	0	.x	.x	0	x.	.x	.0x
ReC 1	.x	x.	.0x	x.	.x	.x	.0x	.x	.x	.0x	x.	.x	.0x
ReC 2	.00x	0	.0x	.0x	0	.x	0	.x	.x	.0x	x.	.x	.x
ReC 3	.0x	x.	.x	.x	.x	.x	.0x	.x	.x	0	.x	.x	.x
ReC 4	.0x	.x	.x	.x	.0x	.x	0	.x	.x	0	.x	.x	0
ReC 5	.0x	.x	.x	.x	.0x	.x	0	.x	.x	0	x.	.x	.0x
ReC 6	.0x	.x	.x	.x	.0x	.x	.0x	.x	0	0	x.	.x	0
ReC 7	.x	.x	.x	x.	.0x	x.	0	.x	.x	0	x.	.x	.0x
ReC 8	.x	.x	.x	x.	.0x	.x	.0x	.x	.x	.0x	x.	.x	.x
ReC 9	.0x	.x	.x	.x	.0x	.x	.0x	.x	.x	.0x	x.	.x	.x
ReC 10	.0x	.x	.x	.x	.0x	.x	0	.x	.x	0	x.	.x	0

* The presence of F was determined by observing the intense yellow color of CaF in the arc during excitation. Dashes indicate the absence of the yellow color during arcing.

discussion of the geochemistry of the rare earths, nor the paragenesis of the minerals. These subjects remain for further study.

Description of Samples Used for Spectrographic Analysis in Table 1

SpC 1.—Gadolinite is massive, dark grayish green, fractured, and somewhat altered. Under the microscope the mineral is partly metamict with n = 1.78. Some areas have low birefringence with variable mean index, n = 1.80 to 1.81.

SpC 2.—Total ore-bearing fluorite rock is a mixture of fragments of pink microcline, purple, pinkish cream, gray, and pale green fluorite. The fluorite is host to several rare earth minerals.

SpC 3.—Pinkish cream fluorite, n = 1.440, contains numerous inclusions of small, high-index grains of minerals, mostly xenotime.

SpC 4.—Pale green fluorite, n = 1.440, contains few inclusions.

SpC 5.—Purple fluorite from which part of the inclusions have been removed with the Frantz separator, has the index of refraction, n = 1.437.

SpC 6.—Purple fluorite, n = 1.450, commercial ore, contains inclusions of xenotime, monazite, allanite, gadolinite, and alteration products of these minerals.

ReC 1.—Gadolinite crystal is described under mineralogy.

ReC 2.—Glossy black allanite is described under mineralogy.

ReC 3.—Xenotime, inclusions from allanite, are described under mineralogy.

ReC 4.—Cream-colored fluorite, n = 1.450, has had some inclusions removed with the Frantz separator.

ReC 5.—Inclusions from cream-colored fluorite, contain an abundance of xenotime, and some monazite.

ReC 6.—Purple fluorite, n = 1.440, contains gadolinite, monazite, and xenotime.

ReC 7.—Altered dark brown gadolinite is partly replaced by fluorite and abundant xenotime.

ReC 8.—Red dense alteration product represents a more advanced stage of alteration of gadolinite. Xenotime inclusions are less conspicuous; iron oxide, and monazite are present.

ReC 9.—Brick red powder appears to be the last stage of the alteration of gadolinite. It consists of iron oxide and monazite.

ReC 10.—Lavender colored fluorite crystals one to two centimeters in diameter contain small inclusions of an unidentified rare-earth carbonate.

References

Heinrich, E. Wm. (1948), Fluorite-rare earth mineral pegmatites of Chaffee and Fremont Counties, Colorado: *Am. Mineral.*, **33**, 64–75.

Holmes, Arthur (1931), Radioactivity and geological time, *in* Physics of the Earth—IV. Age of the Earth, pt. 4, 338: *Natl. Research Council Bull.* **80.**

Rankama, Kalervo, and Sahama, Th. G. (1950), Geochemistry. Univ. of Chicago Press, 511.

THE AMERICAN MINERALOGIST, VOL. 43, SEPTEMBER OCTOBER, 1958

EARTHY MONAZITE AT MAGNET COVE, ARKANSAS*

H. J. ROSE, JR., L. V. BLADE, AND MALCOLM ROSS,
U. S. Geological Survey, Washington 25, D. C.

Monazite is usually found as well-formed euhedral crystals ranging in size from fractions of a millimeter to several centimeters. Rare instances of massive monazite are mentioned in Dana's System of Mineralogy (Palache, Berman, and Frondel, 1951, pp. 694–695). This note reports on an unusual earthy form of this mineral.

A very irregular vein, 2 to 8 inches wide, of earthy, fine-grained, pale greenish-yellow monazite is found in the extremely weathered portion of an apatite-pyrite vein in the carbonatite of East Tufa Hill at Magnet Cove, Arkansas.

The material is too fine grained for satisfactory index measurements, but it is birefringent with a mean index of 1.81. Spectrochemical analysis indicates large amounts of cerium earths and phosphorus. From *x*-ray powder patterns the material is identified as mostly monazite with a small amount of a mineral of the plumbogummite (?) group, perhaps florencite(?), $CeAl_3(PO_4)_2(OH)_6$. Electron micrographs (Fig. 1) of the eartly monazite show irregularly shaped crystals or aggregates of crystals averaging about 0.5 micron in diameter. A few rod-shaped particles are present and may be the plumbogummite (?) mineral indicated by the *x*-ray patterns. These rod-shaped particles comprise several per cent of the sample.

This unusually fine grained monazite is believed to be a product of weathering of the rare-earth bearing apatite of the vein. Monazite has not been found as an original constituent of the vein. The proportions of the major rare-earth elements (atomic per cent) in apatite and monazite have been determined quantitatively by spectrochemical analysis as follows:

	La	Ce	Nd	Y
		(atomic per cent)		
Apatite	38	48	10	4
Monazite	44	44	10	2

The high proportions of lanthanum and cerium in both minerals are characteristic of cerium-earth minerals associated with alkalic rocks (Murata et al., 1957). Although there are variations in the relative amounts of these major rare-earth elements, the general similarity in composition indicates that apatite could have been the source for the rare earths in the earthy monazite. The monazite exhibits a slight increase in the relative amount of lanthanum, and a marked decrease in yttrium. This differentiation may be explained by the process of fractional crystallization which takes place during the formation of monazite in carbonatites. The larger ions of the cerium-earth group (atomic nos. 57–64) are preferentially accommodated in the monazite structure where a ninefold coordination of the rare-earth ion is required.

---

* Publication authorized by the Director, U. S. Geological Survey.

Another notable feature of the monazite is the absence of thorium, which was not detected by a spectrographic method sensitive to 0.1 per cent Th. Monazite derived from granitic rocks and crystalline schists invariably contains more than 3 per cent thorium, commonly 4 to 10 per cent. Monazite from another area of alkalic rocks, namely the Mountain Pass district of California, is also low in thorium according to Jaffe (1955) who reports 2 to 3 per cent in 3 samples. Therefore, a low content of thorium as well as yttrium may be characteristic of monazites from alkalic rocks. However, thorium-poor monazites have also been described from Bolivian tin veins (Gordon, 1944) and from replacement veins at pegmatite-schist contacts in Colorado (Goddard and Glass, 1940) indicating that such monazites are not restricted to alkalic rocks.

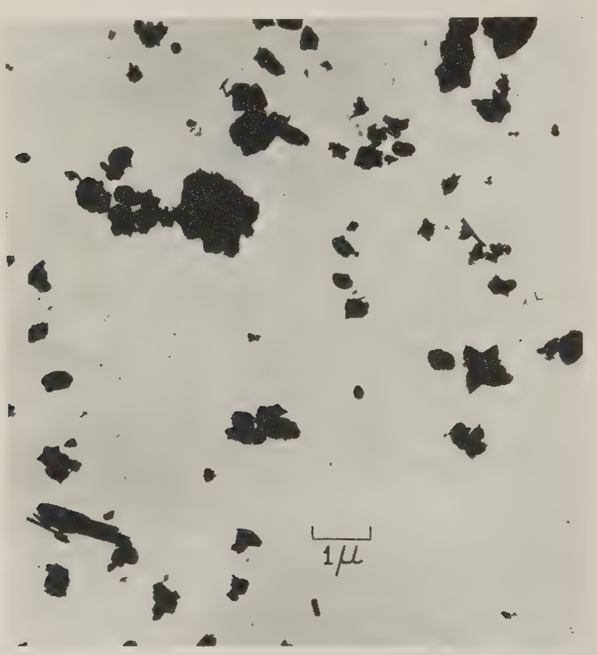

Fig. 1. Earthy monazite, Magnet Cove, Arkansas. Electron micrograph.

The authors wish to acknowledge the help of K. J. Murata and F. A. Hildebrand of the U. S. Geological Survey for helpful suggestions and x-ray identification.

References

1. Goddard, E. N., and Glass, J. J. (1940), Deposits of radioactive cerite near Jamestown, Colorado: *Am. Mineral.*, **25**, 381–404.
2. Gordon, Samuel G. (1944), The mineralogy of the tin mines of Cerro de Llallagua, Bolivia: *Acad. Nat. Sci. Philadelphia Proc.*, **96**, 279–359.
3. Jaffe, H. W. (1955), Precambrian monazite and zircon from the Mountain Pass rare-earth District, San Bernardino County, California: *Geol. Soc. America Bull.*, **66**, 1247–1256.
4. Murata, K. J., Rose, H. J., Jr., Carron, M. K., and Glass, J. J. (1957), Systematic variation of rare-earth elements in cerium-earth minerals: *Geochim. et Cosmochim. Acta*, **11**, 141–161.
5. Palache, C., Berman, H., Frondel, C. (1951), Dana's System of Mineralogy, 7th ed., v. II: John Wiley and Sons, New York.

THE AMERICAN MINERALOGIST, VOL. 43, SEPTEMBER-OCTOBER, 1958

LOW MAGNIFICATION THIN SECTION PHOTOGRAPHY

Frank W. Atchley, *Sunnyvale, California.*

Introduction

The method whereby photographs of thin sections are made by using a photographic enlarger instead of a microscope is not original, but is not widely known and is seldom used. The method has advantages which warrant further publication, so that its use will become more general.

Crooks (1938), briefly recorded the method, but did not stress its advantages. His account limited its application to plain light photographs and to use of a particular type of enlarger. This paper discusses the method in detail, lists its advantages and limitations, and describes the technique of making photographs with "crossed" polarized light, as well as with plain light.

Method

For plain light photographs no special photographic equipment or attachments are required. Only a dark room, a standard photographic enlarger, and one or more 4″×5″ sheet film holders are needed. The Leitz and other enlargers designed for roll film can be used, but they are not readily adaptable for making crossed nicol photographs. The Omega enlarger which will handle a 4″×5″ negative was found to be ideal. Most enlargers come equipped with 35 mm. negative holders made of metal. But as there is a danger of breaking the thin sections in a metal holder it is best to improvise a slide holder from cardboard, cutting the opening the size of the cover glass.

After the thin section is inserted in the enlarger, the image is projected on a large white cardboard, from a height set to give desired magnification. An image of the entire enlarged section is obtained. An open 4″×5″ sheet film holder, in which a white paper has been inserted, is placed flat upon the cardboard and moved about until the desired feature or texture in the projected image is selected. The area to be photographed is then carefully brought into focus on the white paper in the film holder. The exact position of the film holder is marked, and all lights turned off. A loaded film holder is then substituted for the open film holder and the exposure is made by turning the enlarger light on and off.

Crossed Nicol Photographs

Crossed nicol photographs are made in the same way as plain light photographs, except that the thin section must be inserted between polaroid sheets mounted at 90 degrees. This mounting of the polaroid sheets can be accomplished in several ways depending on the size and type of enlarger to be used. The writer improvised such a mount by using two gunsight lenses, obtained from Government surplus, and mounting them in folded corrugated cardboard with Scotch tape. A slide holder with permanently mounted polaroid sheets and a device for holding and rotating the thin section could be easily designed.

Exposure

Because of varying light conditions the correct exposure for different types of film is attained by trial and error, depending on the relative opacity of the thin section. A trial negative showing five different exposures can be made as follows: The loaded film holder is substituted for the empty film holder, as described. With lights off the film holder cover is opened one inch and an arbitrary time exposure made. The cover is then opened another inch and another exposure made, and so on until five exposures are completed. Each exposure is for the same time interval. For example, if a three second interval is used, the resulting negative will show exposures of 3, 6, 9, 12, and 15 seconds. The exposure producing normal contrast is used in making the final negative. It would be a simple matter to establish a calibration chart of exposure time vs. light meter readings.

Several variables are involved in setting the trial exposure interval. For example, the time required for crossed nicol exposures is usually 6–8 times that for plain light exposures. Film emulsion speed is another important factor. Longer exposures are required for higher magnifications, as with a microscope, although for a different reason. With an enlarger, longer exposures are needed as magnification increases because the distance between the light source and film is increased, causing the light intensity to decrease. Still another factor involved in judging the exposure interval is the aperture opening of the enlarging lens. It is best to open the aperture when viewing and focusing the image, and to stop down the aperture when making negatives.

Film and Developers

Modern film emulsions cover a wide range of latitudes and have been perfected for specific purposes. The applicability of these films to the present technique depends on the subject and objective in mind. However, for general use a high resolution panchromatic film (color sensitive), such a Kodak Panatomic X or Ansco Isopan, will give the best results, particularly for crossed nicols. If the subject is colorless, orthochromatic film is probably best. Emulsion speed is not particularly important, although the slower emulsions generally give a higher degree of resolution.

Any number of standard developing solutions can be used for processing the negatives, but the slower, finer grained developers, such as Kodak D-76, give better results. If strong contrast is desired, Kodak D-11 developer is satisfactory.

Advantages

The method described is ideally suited for illustrating the textures of coarse grained rocks, as low magnification permits a large area of the section to be photographed.

Microscope lenses, unless supplemented by expensive compensating oculars or auxiliary lenses, produce spherical aberration. This inherent feature of microscopes precludes low magnification photographs that are in perfect focus throughout the field of view. The use of a photographic enlarger eliminates this difficulty, for the lens system of enlargers is designed for reproduction of a flat surface. The projected image lies in a plane, and a sharp focus is effected throughout the enlarged area. There is no fuzziness in the resulting photograph and the component features in the thin section are sharply resolved.

The use of a microscope for photomicrographs presents the additional difficulty of obtaining adequate even-field illumination. Unless special equipment is used, photographs taken through a microscope almost invariably are slightly over-exposed in the center and somewhat under-exposed on the edges. This trouble is eliminated when using an enlarger; the light source is centered, and the diffusion, condensing, and enlarging system is designed for even illumination.

Petrographic microscopes in common use are not designed for magnification below 16-20×. Moreover, microscope magnification is limited to set combinations of objectives and oculars, while an enlarger makes available a continuous range of magnification from 1:1 to about 20:1, depending on the focal length of the enlarging lens used. Field diameter and exact linear magnification is obtained by placing a plastic scale in the enlarger and measuring its length in the projected image.

In addition to the advantages outlined, greater speed is possible with a photographic enlarger than with a microscope. A projected enlarged image of the entire thin section is viewed at one time and it is an easy matter to select the desired area or feature to be photographed, and since the work is done in a darkroom, an immediate check of the results is possible.

References

1. Crook, W. J. (1938), A method of photographing petrographic thin sections at low magnification: *Am. Mineral.*, **23,** 114.
2. Fairbanks, E. E. (1944), Photomicrography by combined transmitted and reflected light: *Econ. Geol.*, **39,** No. 8, 590.
3. Harbaugh, J. (1953), (Abst.) Scotch tape aids in thin section studies: *A.A.P.G.*, **37,** No. 2, p. 452.
4. Ross, C. S. (1948), Photomicrography by inclined illumination: *Am. Mineral.*, **33,** 363-365.
5. Scott, D. W. (1948), A technique for photographing through a petrographic microscopie: *Trans. AIME*, **178,** 501.
6. Sternberg, R. M., and Belding, H. F. (1942), Dry peel technique: *Jour. of Paleon.*, **16,** 135.
7. Yagoda, H. (1946), Luminescent phenomena as aids in the localization of minerals in polished section: *Econ. Geol.*, **41,** 813-820. (Notes on "contact-printing" of phosphorescent minerals on sensitized paper.)

THE AMERICAN MINERALOGIST, VOL. 43, SEPTEMBER-OCTOBER, 1958

A STAGE FOR MACRO POINT COUNTING

Donald O. Emerson,
Department of Geological Sciences
University of California, Davis, California.

Adequate sampling is the major problem in the modal analysis of the coarser-grained (3-20 mm.) and porphyritic rocks. It has been shown by several authors (e.g. Chayes, 1956, p. 93) that a standard thin section is not large enough to represent a rock with a maximum grain size of more than about 3 mm. In order to obtain a large sample area and avoid the added expense of duplicate thin sections, a technique for counting a rock slab cut from a hand specimen has been developed.

The saw cut slab is prepared for counting by grinding, etching, and staining in a manner that will make the principal minerals quickly recognizable. A mode for the rock is then determined by sampling the surface of the slab with a macro point counting stage.

The stage adapted for this purpose is shown in Fig. 1. It is a standard dual cross feed, milling table with a maximum movement in each direction of 7 inches. A spring similar to the one used on the American Optical Co. point counter stage and described by Chayes (1949) is placed so that it rides on the calibrated sleeve of the "east-west" cross feed screw. A notch filed in the sleeve will produce an audible click for each 0.1 inch of translation. The rock slab is leveled on the stage by pressing it into modeling clay. As a reference point, a small glass plate with engraved cross hairs is mounted on a movable arm so that it can be adjusted to ride over the surface of the sample. The cross hairs remain fixed as the sample translates under them. To aid in viewing the sample, a large low power lens is placed above the cross hairs. Good lighting, from a lamp not shown in the figure, is needed for rapid mineral identification. Counts can be recorded on a tabulator.

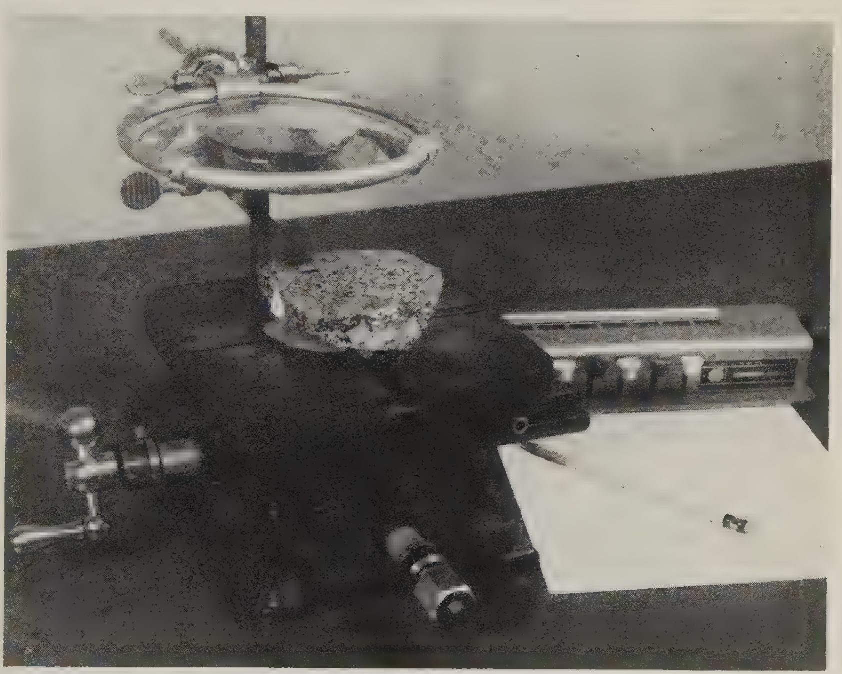

FIG. 1. Macro point counting stage.

The main advantage of macro point counting with this stage is that modes can be rapidly determined from easily prepared slabs which are large enough to be representative of the coarser-grained rocks. The principal limitation is that the items counted must be identifiable on the rock slab.

In one setting, the macro point counting stage can handle a sample area of 49 square inches or the equivalent of about 35 standard thin sections. Although very small grains are visible under the cross hairs, rocks with a maximum grain size of less than about 3 mm. are counted more conveniently and with greater detail by means of the conventional micro point counting stage. A porphyritic rock with a fine-grained groundmass lends itself to a two stage modal determination. The phenocryst to groundmass ratio is determined from slabs on the macro point counting stage, and the composition of the groundmass is determined by means of thin sections on the micro point counting stage. If the phenocrysts in the rock being studied are greater than 20 mm. and they are distinguishable in a photograph, it is even possible to obtain the phenocryst to groundmass ratio by sampling the photograph of a nearly plane surface of the outcrop with a macro point counting stage. The groundmass mineral composition can then be obtained from a saw cut slab.

To reduce the errors of identification only minerals or groups of minerals which are easily recognizable are counted. One tabulator key is used to record all the points which are minerals other than those being counted. The saw cut slab is prepared for counting by grinding, etching, and staining in a manner that will make the principal minerals quickly recognizable. Preparation of the rock slabs for several rock types is described by Jackson and Ross (1956, p. 649). After the slab is prepared, a polygonal figure is scribed just inside the edge of the rock slab. Counting is done only within this line to avoid a bias caused by one mineral occurring more frequently at the fractured edge of the sample. Traverses are made with the "east-west" cross feed which has the clicking spring and these traverses are spaced by the "north-south" cross feed which has a calibrated sleeve. The traverses can be spaced at some regular distance and if this method of counting is intended, a second clicking spring can be added to the "north-south" cross feed. The writer prefers, however, to use a stratified-random sampling pattern and eliminate biases which arise from any periodic relationship between stratification within the rock and the transverse interval. This type of sampling is described by Chayes (1956, p. 29).

As a test of the reproducibility of data obtained from macro point counting, several slabs of the McAfee adamellite from the northern Inyo Mountains of California were each counted four times. This rock is

TABLE I. DATA FROM FOUR MACRO POINT COUNTS OF A STAINED SLAB OF MCAFEE ADAMELLITE

Mineral	Mean	Standard deviation of the means	Calculated binomial standard deviation
	$\bar{x}$	$s_{\bar{x}}$	σ
Plagioclase	37.7%	1.6	1.5
K-feldspar	30.3%	1.0	1.4
Quartz	29.0%	1.3	1.4
Other	3.0%	0.6	0.5

equigranular with an average grain size of about 5 mm. and a maximum grain size of 10 mm. Plagioclase, sodium cobaltinitrite-stained microcline, quartz, and "others" were the items counted. A thousand points were counted for each determination and after each count the slab was rotated and the next count was started from a different corner. Table I shows the results of a test based on the duplicate analysis of one of these slabs. The analyses of the other slabs yielded essentially the same information.

The calculated binomial standard deviation from the equation,

$$\sigma = 100\sqrt{\frac{p(1-p)}{n}}$$

where $p=\bar{x}/100$ and $n=1000$, is seen to be a good approximation of the observed standard deviation ($s_{\bar{x}}$). Two of the observed values slightly exceed the theoretical values and two are smaller. The evidence from this slab and from five others, all of which show the same relationships, is that the counting error from this macro point counting stage is very close to binomial expectation.

These replication tests indicate that the macro point counting stage is capable of reproducible results from stained rock slabs. The relationship between macro and micro point counted modes still remains to be determined. Reliable modal mineral percentages can be determined by the macro point counting stage which permits the rapid sampling of a sufficient area of the coarser-grained and porphyritic rocks.

REFERENCES

CHAYES, FELIX (1949), A simple point counter for thin section analysis: *Am. Mineral.*, **34,** 1–11.

——— (1956), Petrographic Modal Analysis: J. Wiley and Sons, N. Y.

JACKSON, E. D., AND ROSS, D. C. (1956), A technique for modal analyses of medium- and coarse-grained (3–10 mm.) rocks: *Am. Mineral.*, **41,** 648–651.

BOOK REVIEWS

ÍNDICE ALFABÉTICO PARA EL DICCIONARIO MINERO (ESPAÑOL, FRANCÉS, ALEMÁN Y RUSO), by Alejandro Novitzky. 217 pp. quarto, Buenos Aires, 1958 (Price, $12.00; can be ordered from El Ateneo, Florida 340, Buenos Aires, Argentina, or Librería del Colegio, Alsina y Bolivar, Buenos Aires, Argentina).

When the pentalingual dictionary of which this is the index appeared in 1951 most of the reviews pointed out that for the dictionary to be generally useful such an index should be prepared. Professor Novitzky has taken these suggestions to heart and has now completed the extremely tedious and laborious task of alphabetizing the 18,000 terms originally chosen, in each of the four other languages.

The dictionary, which is still available from the sources indicated above for the index, has terms in mining, metallurgy, geology, mineralogy, petrography, and petroleum technology. Alphabetization is in English only. (For details see the review, *Am. Mineral.*, **36,** 791, 1951.)

The index has all of the terms alphabetized separately in Spanish, French, German and Russian. It is thus possible to go from any one of the five languages to any other. This means that the dictionary and index taken together are the equivalent of twenty "one-way" dictionaries (e.g., "English-Russian Geological Dictionary").

In arrangement and use these books follow the plan of other polylingual technical dictionaries-indices. To look up a word in a language other than English it is necessary to use both volumes. The word sought is found in the index, and a page-and-word reference locates the word in the dictionary. For example, to find the meaning of the German word "Schuppen" we look it up in the index and find the reference "45, 29." On page 45 the 29th word in the English column is "cabin" which is the English equivalent of the word sought. The equivalents in Spanish, French and Russian are given on the same line of the same page.

It is unfortunate that the words on each page in the dictionary are not numbered, so it is necessary to count from the top down to the word required. The reviewer finds that it does not take much longer to write the numbers of the words than just to count them (a whole column can be numbered in a little more than a minute), so if a user of the set will write in the numbers opposite the English words on a page each time he looks up a word he can have the words numbered for future use with very little extra expenditure of time.

These books should prove most useful to anyone who is interested in reading literature in the earth sciences in two or more languages other than his native tongue. They contain many terms that are not found in more general technical dictionaries and many that are not found in individual specialistic glossaries. Even when one is translating primarily from a single foreign language the Dictionary and Index can be a valuable accessory to the dictionaries and glossaries already in use.

Earl Ingerson
U. S. Geological Survey
Washington 25, D. C.

CONCISE INTERNATIONAL DICTIONARY OF MECHANICS AND GEOLOGY. English-French-German-Spanish. S. A. Cooper Philosophical Library, Inc., New York. 400 pp. $6.00.

This small dictionary has an English section of 199 pages, with equivalents given sequentially in French, German, and Spanish, and three subsequent indexes in French, German, and Spanish. Every page in the English section has its words or phrase entries numbered from top to bottom, and the alphabetical listings in the foreign indexes are referred to the appropriate page and entry number.

The compiler states in his preface, "The contents are mainly based on GENERAL MACHINE PARTS and MECHANICAL terms. It was thought advisable, however, to add varieties of COAL, IRON and STEEL, and this led naturally to the inclusion of a wide selection of ALLOYS, MINERALS and GEOLOGICAL expressions." The reviewer fails to see what is necessarily natural about such a sequence, but agrees that the selection of geological terms may have been wide but hardly broad. A quick inspection reveals the lack of inclusion of: dike, sill, strike, plunge, and igneous. Yet such rare mineral species or varietal names as jaipurite, chalcostibnite (sic), and argentic mica are included. Listed too are numerous botanical terms, especially names of trees (broad-leaved lime tree, British oak). What are these doing in a dictionary of mechanics and geology? Furthermore numerous chemical terms also have been thrown in—Chloride of potassium, carbonate of zinc, etc., and who needs a dictionary to translate them from French, German or Spanish to English?

All in all, the dictionary is neither fish nor fowl nor good red herring type, but kitchen sink type and a spotty one at that. It may be a concise dictionary of mechanics but it is sneaky to call it any kind of a dictionary of geology.

E. Wm. Heinrich
University of Michigan

NEW MINERAL NAMES

Stottite

H. Strunz, G. Söhnge, and B. H. Geier. Stottit, ein neues Germanium-Mineral, und seine Paragenes in Tsumeb. *Neues Jahrb. Mineral., Monatsh.* **1958,** No. 4, 85–96.

The mineral occurs in crystals up to 1 cm. in size. The crystals are tetragonal, dipyramidal, pseudo-octahedral with $p\{111\}$ predominant and small faces of $a\{100\}$, $c\{001\}$, $m\{110\}$, $d\{011\}$, $e\{012)$. Goniometric data are given; they give $a{:}c=1{:}0.989$. X-ray study gave a_0 7.55, c_0 7.47 Å, space group $C_{4h}{}^4-P4_2/n$ or possibly $C_{4h}{}^2-P4_2/m$. The indexed x-ray powder pattern is given; the strongest lines are 3.767 vs, 2.655 s, 1.687 ms, 2.171 m, 1.886 m, 1.672 m, 1.538 m, 1.254 m, 1.139 m, 20 other lines are given. Cleavages (100), (010) good, (001) slightly less so.

The mineral is brown with greasy luster like that of sphalerite, streak gray-white, H. 4½ (also given as 4–5), G. (pycnometer) 3.596, G (buoyancy method) 3.575; the former value is preferred. Optically anomalously biaxial, negative, 2V small, dispersion weak $r>v$; the *n*s are α 1.728 $(=\epsilon)$, β 1.737, γ 1.738 $(\omega=1.7375)$. The crust is dark brown, the center is light olive-gray to nearly colorless under the microscope.

Analysis by the Fresenius Laboratory, Wiesbaden, gave GeO_2 41.75, FeO 34.81, MgO 0.46, MnO 0.88, CaO 0.34, H_2O 21.84, sum 100.08%. This corresponds to a unit cell content of $(Fe, Mg, Mn, Ca)_{4.89}H_{7.66}Ge_{3.80}O_{16}\cdot 8H_2O$, or perhaps $4(FeH_2GeO_4\cdot 2H_2O)$ with part of the H replaced by Fe, or, if other types of bonding of H are assumed, $FeGeO_3\cdot 3H_2O$ or $FeGe(OH)_6$.

The mineral contains by far the highest germanium content of any known and is the first known germanate. It is suggested that it be classed with the nesosilicates, in view of the well-known crystallochemical relation between germanates and silicates.

Stottite occurs in Level 30 of the Tsumeb Mine, S. W. Africa, at a depth of about 1000 meters. The well-known secondary minerals of this mine have come from the surface to about 300 meters down. Recently a second zone of secondary minerals has been found at depths of 800–1000 meters, formed by the action of circulating waters on renierite and germanite. A long list of other secondary minerals is given.

The name is for Charles E Stott, geologist, General Director of the Tsumeb Mine.

Michael Fleischer

Reinerite and Unnamed Mineral

H. Strunz, G. Söhnge, and B. H. Geier, op. cit.

This paper mentions, without details, the mineral reinerite, $Zn_3(AsO_3)_2$ (zinc arsenite), occurring in the lower oxidation level, and "Mineral O," metallic, gray, probably tetragonal and structurally analogous to chalcopyrite, distinct basal cleavage, formula perhaps $CuGaS_2$, hence the first known gallium mineral, found in primary ore at Tsumeb.

M. F.

Kimzeyite

Charles Milton and Lawrence V. Blade. Preliminary note on kimzeyite, a new zirconium garnet. *Science*, v. 127, No. 3310, p. 1343 (1958).

The mineral was found as dark brown crystals about 5 mm. in diameter in calcite rock at the Kimzey Calcite Quarry, Magnet Cove, Ark. Associated minerals are monticellite, magnetite, perovskite, and apatite, which occur also as inclusions in the garnet. The latter also contains minute inclusions of sharply euhedral anhydrite.

Spectrographic analysis by Harry Bastron on 35 mg. gave SiO_2 21.4, TiO_2 5.8, ZrO_2

20.25, SnO_2 0.09, Al_2O_3 11.4, Fe_2O_3 16.45, Sc_2O_3 0.09, CaO 16.8, MgO 0.5, MnO 0.13, Cu, Ba, Sr trace, H_2O, P_2O_5, F, S, CO_2 not tested for, sum 94%. The *x*-ray pattern is that of a garnet with $a_0 = 12.46$ A. The mineral is isotropic, light brown in thin section, with *n* near 1.95.

The name is for the Kimzey family, "which has been actively associated with mineralogical developments in Magnet Cove for almost a century," notably W. J. Kimzey, his son Joe, and Lawton D. and John Kimzey.

Discussion.—Apparently a garnet with Zr distributed among tetrahedral and octahedral positions.

M. F.

Thorutite (Smirnovite)

Ya. D. Gotman and I. A. Khapaev. Thorutite—a new mineral of the group of titanates of thorium. *Zapiski Vses. Mineral. Obshch.*, v. **87**, 201–202 (1958) (in Russian).

The mineral occurs in short prismatic crystals up to 2 cm. in length and 0.5–1.0 cm. in diameter. It is black, streak pale brown, luster resinous. Translucent, dark brown, on thin edges; isotropic with *n* above 2.1 G (pycnometer) 5.82. Fracture conchoidal.

Analysis by R. L. Podval'ya and S. B. Federova gave ThO_2 54.10 (av. of 53.65 and 54.55), UO_2 1.43, UO_3 0.14, CaO 1.07, TiO_2 36.1, Fe_2O_3 1.10, Al_2O_3, Nb_2O_5 1.12, Ta_2O_5 0.08, SiO_2 0.44, H_2O 0.94, loss ignition 1.72, sum 99.74%, corresponding to $2(Th, U, Ca)O_2 \cdot 4TiO_2 \cdot H_2O$.

The mineral turns golden when heated in a closed tube and gives off water. It gave no *x*-ray lines (metamict). The pattern obtained by V. P. Butuzov when the mineral is heated at 1000° is given; 45 lines are listed of which the strongest are 3.17 (7), 1.728 (6), 1.695 (6), 1.632 (3).

The mineral occurs in a syenite massif in veins of microcline and sericitized nepheline. Associated minerals are thorite, zircon, calcite, and a little barite and galena. The locality is not given.

The name is for the composition.

Note: The same mineral is named thorutite or smirnovite (for S. S. Smirnov) by V. G. Melkov and L. Ch. Pukhal'skii, *Gosgeoltekhizdat*, 1957, 67, according to an abstract by E. M. Bonshtedt-Kupletskaya, *Zapiski Vses. Mineral. Obshch.*, **87**, 79 (1958). Not to be confused with smirnovskite.

M. F.

Lodochnikite

Ya. A. Gotman. Lodochnikite—a new mineral of the group of titanates of uranium and thorium. *Zapiski Vses. Mineralog Obshch.*, **87**, 197–200 (1958) (in Russian).

The data given are those abstracted in *Am. Mineral.*, **43**, 380 (1958), except that PbO 0.13 there given should be Pb 0.13, and CO_2 0.12 should be S 0.12%. Sp. gr. 5.88. The mineral is considered to be distinct from brannerite because (1) the content of $UO_2 + UO_3$ (51.86%) is higher, and (2) the *x*-ray pattern shows different intensities.

Discussion.—Chemically this is indistinguishable from brannerite. Although $UO_2 + UO_3$ is higher than in most analyses, there is one analysis published by George (1949) which gave $UO_2 + UO_3$ 51.76%. Furthermore, the other analyses contain CaO, Y_2O_3, etc., in amounts more than sufficient to balance the deficiency in U. The *x*-ray powder diagram differs somewhat in spacings and intensities from that given for brannerite, which checks those given in the literature. Further work, especially heating experiments under controlled conditions, is necessary to establish the validity of the mineral.

M. F.

Usigite (Usihyte)

V. G. Melkov and L. Ch. Pukhal'skii, *Gosgeoltekhizdat* 1957, 67, from an abstract by E. M. Bonshtedt-Kupletskaya, *Zapiski Vses. Mineral Obshch.*, **87**, 84 (1958).

All the data given are: Formula $R(UO_2)_2\ Si_2O_7 \cdot nH_2O$. Radiating structure, color yellow, luster vitreous, does not luminesce.

Discussion.—No excuse for this.

M. F.

DISCREDITED MINERALS

Batchelorite (= Muscovite)

D. I. Bothwell and A. A. Moss. The nature of batchelorite. *Mineralog. Mag.*, **31**, 700 (1957).

The name batchelorite was given in 1910 by Petterd (Dana's System, 6th Ed., App. III, p. 11), who gave the formula $Al_2O_3 \cdot 2SiO_2 \cdot H_2O$. A new analysis made on material from the type locality, though not a type specimen, corresponded to muscovite containing Cr_2O_3 0.3%. Optical and *x*-ray study also showed it to be muscovite.

M. F.

Barbierite (= Microcline). New Name Monalbite

Toni R. Schneider and F. Laves. Barbierit oder Monalbit? *Zeitschr. Krist.*, **109**, 241–244 (1957).

The name barbierite was given by Schaller in 1910 to monoclinic $NaAlSi_3O_8$, such as that described by Barbier and Prost (1908) (see Dana's System, App. III, p. 10). Reexamination by *x*-ray methods of the type material of Barbier and Prost from Kragero, Norway, shows it to be finely twinned microcline with about 20% of unmixed albite. The name *monalbite* is suggested for the high-temperature monoclinic modification of $NaAlSi_3O_8$, not yet found in nature.

M. F.

Hessenbergite (= Bertrandite)

Robert L. Parker and Peter Indergand. Ein neues schweizerisches Vorkommen von Bertrandit. *Schweiz. mineralog. petrog. Mitt.*, **37**, 554–558 (1957).

Crystals from St. Gotthard correspond closely to those named hessenbergite by Kenngott in 1863 (*Dana's System, 6th Ed.*, p. 1037). The name hessenbergite has priority over bertrandite, but the description was inadequate (no analysis).

M. F.

Ranite = Gonnardite

Brian Mason. Gonnardite (ranite) from Langensundfjord. *Norsk Geol. Tidsskr.*, **37**, 435–437 (1957).

Ranite was described by Paijkull in 1874 as a zeolite near thomsonite in composition (*Dana, 6th Ed.*, p. 609) from the island of Lamö (= Låven). It has been classed as a doubtful species. *X*-ray data on material from the type locality show its identity with gonnardite (Lacroix, 1896). New determinations of G. (=2.32), and of optics (α'1.513, γ'1.515) are a little higher than the corresponding figures for gonnardite. The name ranite has priority, but Mason concludes that it would be best to retain the name gonnardite. I agree.

M. F.

AMERICAN MINERALOGIST

Price Information

Back issues of the AMERICAN MINERALOGIST can be purchased at the prices given below, but certain issues as listed are available only in microtext edition. The microtext edition is on 3 x 5 inch cards, each card containing 48 pages of text material, with a heading in regular type to indicate the volume, number, pages and date. Microtext will be furnished on all orders where necessary, unless specific instructions are received to the contrary. Prices apply to both the regular and microtext editions, and postage is charged except on indexes. Agents and dealers are allowed the usual 10% discount on orders. Subscriptions for the current volume (calendar year) are available to libraries, colleges, and other organizations at $6.00, postpaid. Individuals can receive the current volume by becoming members of the Mineralogical Society of America.

Volume	Year	Price per volume	Price per issue (except special issues)
1-9	1916-1924	$3.00	$ .50
10-19	1925-1934	4.00	.50
20-28	1935-1943	6.00	.80 (monthly issue)
29-42	1944-1957	6.00	1.60 (bimonthly issue)

Microtext Edition

Vol.	No.	Year
1-5	Complete	1916-1920
7	2	1922
9	3	1924
10	3	1925
11	3	1926
25	5	1940
26	1-3, 6-9, 12	1941
27	1-12	1942
28	1-8	1943
29	1-8	1944
30	1-4, 7-8	1945
31	1-4	1946
32	1-4	1947

Special Issues

Year	Issue	Vol.	No.	Price
1925	Michigan	10	9	$1.00
1925	Harvard	10	11	1.00
1927	Harvard	12	4	1.00
1928	Harvard	13	7	1.00
1930	Harvard	15	8	1.00
1932	Harvard	17	7	1.00
1937	Palache	22	7	3.00
1938	Harvard	23	11	1.50
1945	Quartz Symposium	30	5-6	$3.00
1950	Larsen	35	9-10	2.50
1953	Hunt	38	1-2	2.00
1953	Ross-Schaller	38	11-12	3.00
1955	Kraus	40	11-12	2.00
1957	Harvard	42	11-12	2.00

Indexes

Vols. 1-20 (1916-1935) $2.00; $1.00 to members; postpaid
21-30 (1936-1945) 3.00; 2.00 to members; postpaid
31-40 (1946-1955) 5.00; 3.00 to members; postpaid

Send all orders to

MINERALOGICAL SOCIETY OF AMERICA
Earl Ingerson, Treasurer
c/o U. S. Geological Survey, Washington 25, D.C.

NEW AT WARD'S—
2" X 2" ASTRONOMY SLIDES

LX 30 Astronomy slides. A splendid set of 25 black-and-white 2″ × 2″ slides of important astronomical subjects. The photographs were taken with the largest and most powerful astronomical instruments in the world, at the Mount Wilson and Palomar Observatories, and are of the best quality under the extremely difficult conditions of this type of photography. The moon, sun, galaxies, and nebulae are all represented. The set is excellent for general science, earth science, and astronomy courses, or for personal possession and pleasure.

LX 30 Set of 25 slides $18.75

BROKEN HILL COLLECTION

The Broken Hill lode in the New South Wales desert is a classic mining district. A representative series of its ores, gangue minerals and rocks should be made available to all students of economic geology. The 23 specimens in this suite average 2″ × 2″ to 3″ × 4″ and are accompanied by a descriptive list. $74.85

All prices are list at Rochester, N.Y.

NEW WARD CATALOGS

583 Ward's Geology Catalog—The most comprehensive geology catalog ever published by Ward's. It contains a listing of mineral, rock and fossil collections; minerals, rocks and reference clay minerals in bulk or student specimens; color slides for geology (physical geology, mineralogy, paleontology, astronomy). The section on equipment for field and laboratory includes expanded listings of storage equipment, and an especially fine section on thin section equipment. There is an illustrated section on crystallographic aids including crystal models. If you are not on our mailing list to receive this catalog, write for it today.

WARD'S *NATURAL SCIENCE ESTABLISHMENT, INC.*
P.O. BOX 1712 **ROCHESTER 3, N.Y.**

GEORGE BANTA COMPANY, INC., MENASHA, WISCONSIN, U.S.A.